Erbacher, J., Mosher, D.C., Malone, M.J., et al., 2004
Proceedings of the Ocean Drilling Program, Initial Reports Volume 207

7. Site 1260[1]

Shipboard Scientific Party[2]

BACKGROUND AND OBJECTIVES

Site 1260 is located at a water depth of 2549 meters below sea level (mbsl) on the gently dipping (~1°) northwest-facing slope of Demerara Rise, which is ~380 km north of Suriname (see Fig. F1, p. 5, in Shipboard Scientific Party, this volume ("Site Survey and Underway Geophysics"). The site is located on a ridge of Paleogene sediments subcropping near the seafloor. Site 1260 is at an intermediate depth of the intended paleoceanographic depth transect across Demerara Rise. The major objectives were the following:

1. Core and log a Paleogene–Albian section to evaluate paleoceanographic and paleoclimatic changes, with emphasis on major and abrupt events during this interval that include the Eocene/Oligocene [E/O] and Paleocene/Eocene [P/E] boundaries and the Cretaceous oceanic anoxic events [OAEs]).
2. Reconstruct the history of the opening of the Equatorial Atlantic Gateway by obtaining benthic foraminifer proxy data. These data will help to understand changes in bottom water circulation over Demerara Rise during the gradual opening of the seaway.
3. Recover continuous and expanded sediment records of the Paleogene and Cretaceous in order to reconstruct short- and long-term changes in greenhouse forcing.

Seismic Stratigraphy

The seismic stratigraphy for Site 1260 is described by line GeoB215, which transects northeast–southwest, and line 207-L1S, which crosses orthogonal to line GeoB215 (Figs. F1, F2). A nearby industry multi-

F1. Seismic line GeoB215, p. 40.

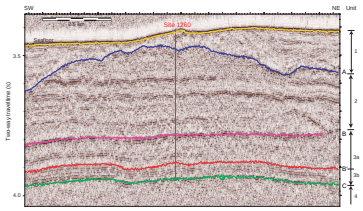

F2. Seismic line 207-L1S, p. 41.

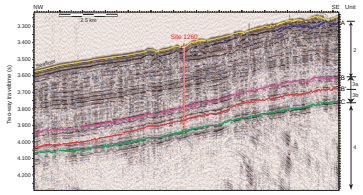

[1]Examples of how to reference the whole or part of this volume.
[2]Shipboard Scientific Party addresses.

Ms 207IR-107

channel seismic line (C2211) passes nearly parallel to line 207-L1S ~1.7 km to the southwest (Fig. F3).

Seismic Unit 1 lies between the seafloor and Reflection "A." It is very thin or absent at the drill site, as Reflector A forms the top of a ridge of seismic Unit 2. This ridge is presumably a remnant from early Miocene erosion. To the southwest and northeast of this ridge, seismic Unit 1 comprises a series of low-amplitude coherent reflections that onlap this ridge and are unconformable against the seafloor.

Between Reflectors A and "B" lies seismic Unit 2. It is 365 ms thick (two-way traveltime) at this location, calculated to be ~315 meters below seafloor (mbsf) using velocity data from downhole logs, a checkshot survey, and laboratory-measured compressional (*P*)-wave velocities on core samples. The topmost sequence in this seismic unit consists of contorted reflectors that pinch out against the seafloor within 1.5 km downslope, which may represent a slumped interval. Below this interval, Unit 2 is characterized by a sequence of crenulated but coherent reflection horizons separated by transparent or incoherent intervals. In the downslope direction, these reflections are reasonably flatlying, dipping slightly less than the angle of the seafloor.

Reflector B is a double-wavelet reflection on line GeoB215 (Fig. F1) of high amplitude relative to events above and below. It is laterally coherent both downslope and alongslope but slightly crenulated, like the reflections above. Seismic Unit 3, between Reflector B (365 ms subbottom) and Reflector "C" (522 ms subbottom), is a ~170-m-thick flatlying sequence that dips 1.5° to the north-northwest. This unit is divided into two subunits. Subunit 3a is an acoustically transparent zone between Reflectors B and "B′." Subunit 3a is ~100 ms thick (87 m). The basal subunit (Subunit 3b) lies between Horizons B′ and "C" (464–522 ms subbottom [~392–485 mbsf]). It is defined on the basis of a series of strong parallel coherent reflections that are laterally contiguous and correlate to the black shale interval at the previous sites. Horizon C forms a regional unconformity that separates the Upper Cretaceous black shales and younger sediments from Albian and older synrift sediments (seismic Unit 4).

On industry profile C2211 (Fig. F3), seismic Unit 4 is clearly defined. Immediately beneath the drill site, reflectors of Unit 4 form a small syncline or basin fill sequence resulting from horst and graben faulting. At this site, Horizon C appears as a disconformity. South of the drill site, this basin is clearly truncated by a fault, with adjacent tilted beds truncating against the Horizon C in an angular unconformity. Further in board, another normal fault separates these tilted beds from a flatlying sequence. This fault is probably a growth fault that apparently propagates to the modern seafloor.

F3. Multichannel seismic reflection line C2211, p. 42.

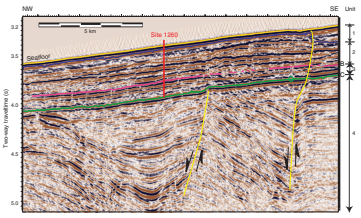

OPERATIONS

Transit from Site 1259 to Barbados to Site 1260

We departed Site 1259 at 0300 hr on 4 February 2003 and headed toward Barbados for a medical evacuation. After a prearranged rendezvous with a helicopter ~20 nmi southwest of Barbados, we proceeded to Site 1260, arriving at 0430 hr on 7 February. The 727.0-nmi transit required 73.5 hr at an average speed of 9.9 kt. After positioning the ship over the site's coordinates, thrusters and hydrophones were lowered and a beacon deployed at 0619 hr on 7 February.

Hole 1260A

A standard rotary core barrel (RCB) bottom-hole assembly was assembled and lowered to the seafloor, and Hole 1260A was spudded at 1115 hr on 7 February. The first core recovered 0.81 m of sediment. With ship heave approaching 3 m, Core 1R was assumed to be a "punch core" (i.e., equivalent to an advanced piston core mudline), and the seafloor depth was determined to be 2560.0 meters below rig floor (mbrf) (2548.8 mbsl), the official water depth for the site. However, in Hole 1260B, the driller felt bottom at 2553 mbrf, the same seafloor depth determined during logging of Hole 1260B. If these second two Hole 1260B measurements are correct, then the seafloor depth at Site 1260 is 2541.8 mbsl.

Hole 1260A was cored from 0.0 to 491.9 mbsf, taking 54 cores (recovery = 79.6%) (Table T1). Site 1260 drilling had the Pollution Prevention and Safety Panel approval to penetrate to either 535 mbsf or the bottom of the black shales, whichever was reached first. We stopped drilling in Hole 1260A at 491.9 mbsf when we reached Albian age sediments, although it was not clear at the time if we had reached the bottom of the black shale facies. This decision was made in preference for exploring the depth limit of the black shales in Hole 1260B, which was the hole to be logged. In preparation for abandonment, Hole 1260A was displaced with 150 bbl of sepiolite mud. The bit was then pulled clear of the seafloor at 0735 hr on 9 February, officially ending Hole 1260A.

T1. Coring summary, p. 81.

Hole 1260B

The ship was offset 50 m southwest of Hole 1260A, and Hole 1260B was spudded at 0845 hr on 9 February. RCB coring advanced to 509 mbsf without incident and stopped when coring times increased dramatically. We interpreted the increase in coring times to mean we had exited the black shale facies, which turned out to be a change to well-cemented silty claystone. The recovery rate in Hole 1260B was 88.2% (Table T1). The hole was swept with 30 bbl of sepiolite mud, and a wiper trip was performed, noting 6 m of fill on bottom. The hole was circulated with twice its volume of seawater, and the bit was released. The hole was displaced with 158 bbl of mud and the pipe pulled to 96 mbsf in preparation for logging.

Three logging tool strings were deployed in Hole 1260B. The triple combination (triple combo) tool string was run from 516 mbsf to the seafloor in two passes. The Schlumberger tools on the triple combo tool string were then deactivated, and the Lamont-Doherty Earth Observatory (LDEO) Multi-Sensor Spectral Gamma Ray Tool (MGT) was run in two passes. The second tool string, the Formation MicroScanner (FMS)-sonic, was deployed and run in two passes from 516 mbsf to the base of the pipe. The final logging run was a checkshot survey conducted with the Well Seismic Tool (WST), which collected clean data at 14 stations. After completion of logging operations, the drill string was pulled to the ship, clearing the rotary table at 0000 hr on 13 February, ending operations in Hole 1260B.

LITHOSTRATIGRAPHY

Site 1260 represents an intermediate water depth site (current water depth = 2548.8 mbsl) of the Leg 207 Demerara Rise depth transect. Re-

covery of the cored interval (862.2 m) averaged 83% over the two holes (1260A and 1260B). A maximum depth of 509 mbsf was reached in Hole 1260B.

Similar to the other Demerara sites cored during Leg 207, five lithostratigraphic units were recognized at Site 1260 (Table **T2;** Fig. **F4**). The oldest unit recovered is Unit V (Albian) and is dominated by silty quartz claystone to calcareous claystone with opaque minerals and quartz interbedded with well-cemented limestones. The overlying Unit IV (Coniacian–Cenomanian) is composed of interbedded laminated organic-rich claystones and laminated limestones. The three youngest units (Campanian–Pleistocene) are pelagic and primarily composed of pervasively bioturbated nannofossil chalk or ooze. They are distinguished based on their clay, microfossil, and zeolite content. Unit III is relatively clay rich, with abundant zeolites. Unit II is relatively carbonate rich and is dominated by calcareous nannofossils and planktonic foraminifers and its lower part contains abundant siliceous microfossils. Unit I is carbonate poor and is composed of nannofossils, foraminifers, quartz, and glauconite in a clay matrix. The sediments recovered at Site 1260 include the records of several critical events including the P/E and K/T boundaries (see **"Biostratigraphy,"** p. 11). Hiatuses correspond to the absence of middle and upper Oligocene, middle Eocene, lower Campanian, and upper Albian sediments.

T2. Lithostratigraphic units, p. 84.

F4. Carbonate and TOC, p. 43.

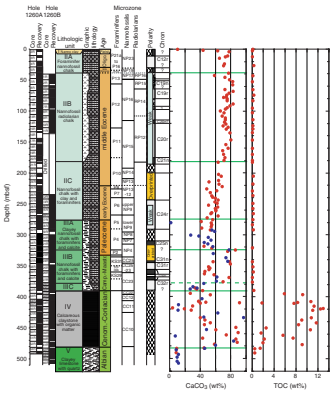

Unit I

Interval: 207-1260A-1R-1, 0 cm, through 2R-1, 10 cm
Depth: Hole 1260A: 0–1.10 mbsf (0–1.10 meters composite depth [mcd])
Thickness: 1.10 m
Age: Pleistocene
Lithology: nannofossil clay

Unit I was recovered only in Hole 1260A. It consists of dark greenish gray clay with 10 wt% carbonate. The top of the unit, immediately below the sediment/water interface, is an olive-brown sandy clay. There is a sharp color change to gray clay at 8 cm that likely represents a redox boundary. It overlies a 2-cm-thick glauconite-rich (20%) interval. Calcareous nannofossils are the main biogenic component in Unit I (20%). Planktonic foraminifers are common at the top of the unit, becoming increasingly rare downhole. The siliceous biogenic component consists of diatoms and a few radiolarians and is found primarily in the olive-brown layer. No bioturbation is observed, but its absence is likely an artifact of drilling disturbance.

The main mineral phases include glauconite (~5%), quartz (15%), and clay. Disseminated pyrite is present in the sediments (<3%). The boundary with Unit II is placed at the base of a white planktonic foraminifer–rich horizon at Section 207-1260A-2R-1, 10 cm.

Unit II

Intervals: 207-1260A-2R-1, 10 cm, through 30R-7, 74 cm; and 207-1260B-1R-1, 0 cm, through 17R-7, 69 cm
Depths: Hole 1260A: 1.10–276.74 mbsf; and Hole 1260B: 40.20–279.84 mbsf
Thickness: 275.64 m (Hole 1260A)
Age: early Oligocene–early Eocene

Lithology: foraminifer and nannofossil ooze and chalk, nannofossil and radiolarian chalk, nannofossil chalk with foraminifers and radiolarians, and nannofossil chalk with clay and foraminifers

Unit II consists of light greenish gray to greenish gray ooze and chalk with 50–80 wt% carbonate. The ooze is restricted to the upper 3 m of the unit. Bioturbation is pervasive and *Zoophycos* and *Planolites* traces are common. *Chondrites* are also abundant in the upper part of this unit. The upper contact of Unit II coincides with the base of the foraminifer-rich layer of Unit I. The base of Unit II is gradational and is placed at a clay bed that forms part of the P/E boundary interval. Unit II is divided into three subunits based on clay and biogenic silica content. The contact between Subunits IIA and IIB is placed at a sharp color change, whereas the contact between Subunits IIB and IIC is gradational.

Subunit IIA

Interval: 207-1260A-2R-1, 10 cm, through 5R-CC, 12 cm
Depth: Hole 1260A: 1.10–36.03 mbsf
Thickness: 34.93 m
Age: early Oligocene
Lithology: foraminifer and nannofossil ooze and foraminifer and nannofossil chalk

Subunit IIA consists of light greenish gray nannofossil ooze with foraminifers and clay to light greenish gray foraminifer and nannofossil chalk (Fig. **F5A**). The top of the Subunit IIA is placed at the base of a planktonic foraminifer–rich bed of Unit I. The carbonate content of Subunit IIA is ~70 wt% and is relatively uniform throughout the sequence. Calcareous nannofossils are the major biogenic component of this subunit. Planktonic foraminifers are rare in the upper part and gradually increase in abundance from the middle to the base of the subunit. Fish debris and calcispheres are also present. Bioturbation is pervasive with *Chondrites, Planolites,* and *Zoophycos* identified. Dark material often fills the burrows. Several gradational redox color changes from light yellowish brown to light greenish gray occur in the upper part of the subunit (Sections 207-1260A-2R-1 and 2R-2 [1.10–3 mbsf]). Clay is relatively abundant (~20%) in the upper portion of the subunit and rare in the lower portion. Few zeolites and disseminated pyrite are present throughout the subunit. Uniformly inclined burrow mottles and grain fabric suggest a slump deposit of Oligocene sediment in the lower part of the subunit. The contact with Subunit IIB is a sharp color change that corresponds to an increase in siliceous microfossils (Fig. **F5B**).

F5. Representative lithologies, Units II and III, p. 44.

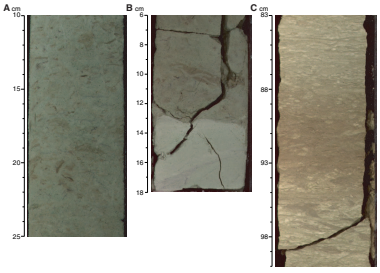

Subunit IIB

Intervals: 207-1260A-5R-CC, 12 cm, through 20R-3, 78 cm; and 207-1260B-1R-1, 0 cm, through 11R-CC, 25 cm
Depths: Hole 1260A: 36.03–176.58 mbsf; and Hole 1260B: 40.20–135.61 mbsf
Thickness: 140.55 m (Hole 1260A)
Age: middle Eocene
Lithology: nannofossil and radiolarian chalk and nannofossil chalk with foraminifers and radiolarians

Subunit IIB is composed of a light greenish gray calcareous biogenic (50% nannofossils) chalk containing common to abundant radiolarians (25%–30%). It is characterized by high carbonate content (70 wt%). The top and bottom boundaries of the unit are placed at the first and last consistent occurrence of siliceous microfossils in smear slides. The upper limit also coincides with a sharp color and lithologic change (Fig. F5B).

Planktonic foraminifers are rare in the top part of Subunit IIB and become increasingly abundant in Core 207-1260A-7R (20%). Diatoms and siliceous sponge spicules are common throughout. Bioturbation (*Planolites, Zoophycos,* and *Chondrites*) is moderate to pervasive. Burrows are often filled with black material, but white foraminifer-rich (45%) sands are found within some *Planolites* traces.

Mottles in the top part of the subunit (light greenish gray to pale olive) are due to pervasive bioturbation. Subtle dark–light color alternations on a scale of 20–30 cm with gradational mottled contacts are observed. At the base of the subunit, early diagenetic, millimeter-scale horizontal dark bands are present over a 20-cm interval but show no microfacies variation in smear slides. Chert as nodules and as bands with chalk inclusions also appear in the lower part of the subunit (Section 207-1260A-15R-3). Rare pyrite, both disseminated and concentrated in burrows, is found throughout Subunit IIB.

Subunit IIC

Intervals: 207-1260A-20R-3, 78 cm, through 30R-7, 74 cm; and 207-1260B-12R-1, 0 cm, through 17R-7, 69 cm
Depths: Hole 1260A: 176.58–276.74 mbsf; and Hole 1260B: 235.00–279.84 mbsf
Thickness: 100.16 m (Hole 1260A)
Age: middle Eocene–early Eocene
Lithology: nannofossil chalk with clay and foraminifers

Subunit IIC consists of light greenish gray nannofossil chalk with clay and foraminifers with lower carbonate content (60 wt%) than the rest of Unit II. The upper boundary of the subunit is gradational and placed at the last consistent occurrence of radiolarians in smear slides. The base of the subunit coincides with the clay-rich layer of the P/E boundary interval. In Hole 1260B, the top of Subunit IIC was not recovered. Calcareous nannofossils represent the major component (50%), with estimates of planktonic foraminifer abundances fluctuating between 10% and 35% (from smear slide description). Bioturbation is pervasive to moderate, with discrete *Planolites* and *Zoophycos*.

Distinct cyclic color changes between light olive brownish gray bands (10 cm thick) and light greenish gray sediments over a scale of 10–50 cm occur in the upper part of the subunit (Fig. F5C). Brown material fills burrows in the darker intervals, and some of these burrows are surrounded by green redox halos. At the base of the Subunit IIC, gradational dark green-gray to light greenish gray alternations are observed on a scale of 10–20 cm. Light greenish gray intervals are rich in calcareous microfossils and calcite, whereas dark brownish and greenish gray layers have higher clay and zeolite content.

Dark green chert is present in the upper part of Subunit IIC. Estimated abundance of zeolite ranges from 5% in the upper part of the subunit to 15% in the middle part. Pyrite is rare (<2%) throughout. Clay content increases downward through the subunit (20%–30%). Di-

agenetic calcite is also more common at the base of the subunit (10%–20%) than elsewhere in Unit II.

Unit III

Intervals: 207-1260A-30R-7, 74 cm, through 42R-CC, 15 cm; and 207-1260B-17R-7, 69 cm, through 30R-CC, 8 cm
Depths: Hole 1260A: 276.74–390.65 mbsf; and Hole 1260B: 279.84–390.83 mbsf
Thickness: 113.91 mbsf (Hole 1260A)
Age: late Paleocene–early Campanian
Lithology: nannofossil chalk with foraminifers to calcareous claystone

Unit III is composed of nannofossil chalk, clayey nannofossil chalk, and claystone with nannofossils. Planktonic foraminifers, calcite debris (both biogenic and diagenetic), and zeolites are minor to major constituents in portions of the unit. Dominant colors are shades of greenish gray, although reddish hues are prominent for several meters above and below the K/T boundary. There are distinct to subtle alternations on a decimeter scale between light and dark intervals throughout Unit III. Unit III has higher clay content than Unit II, but the transition is gradational. The contact is placed at the base of a distinct 20-cm-thick laminated greenish gray clay layer that corresponds to the biostratigraphically recognized P/E boundary (see **"Biostratigraphy,"** p. 11). Unit III is distinguished from Unit IV by its pervasively bioturbated fabric and low levels of organic carbon. The base of Unit III is placed at the first downhole occurrence of laminated strata. Unit III is subdivided into three subunits based on differences in the abundance of foraminifers and carbonate content. This unit contains an apparently complete sequence leading up to the P/E boundary and the record of the K/T boundary event, including an apparent ejecta layer (Fig. **F6**).

Subunit IIIA

Intervals: 207-1260A-30R-7, 74 cm, through 35R-5, 93 cm; and 207-1260B-17R-7, 69 cm, through 22R-3, 145 cm
Depths: Hole 1260A: 276.74–324.03 mbsf; and Hole 1260B: 279.84–324.55 mbsf
Thickness: 47.29 mbsf (Hole 1260A)
Age: late Paleocene–early Paleocene
Lithology: nannofossil chalk with foraminifers and calcite to clayey nannofossil chalk with foraminifers and calcite

Subunit IIIA consists of light greenish gray to greenish gray, mottled nannofossil chalk with foraminifers and calcite to clayey nannofossil chalk with foraminifers and calcite. Olive hues are present in the lower 2–4 m of the subunit. Carbonate contents are generally between 40 and 60 wt% (Fig. **F4**). Zeolites, quartz, calcispheres, and/or pyrite commonly compose a small percentage of identified grains. Fish debris was observed in trace amounts in several samples. Subtle to distinct alternations between light (relatively carbonate rich) and dark (relatively clay rich) color bands occur on a decimeter scale. Burrow mottling is pervasive, and discrete traces assigned to *Zoophycos* (Fig. **F7A**), *Planolites,* and *Chondrites* are common.

F6. Lithology transitions at P/E and K/T boundaries, p. 45.

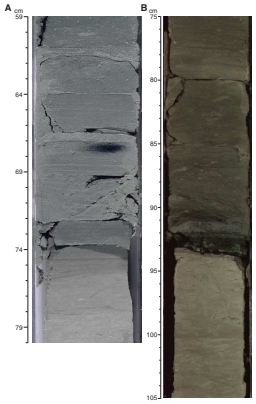

F7. Representative lithologies, Unit III, p. 46.

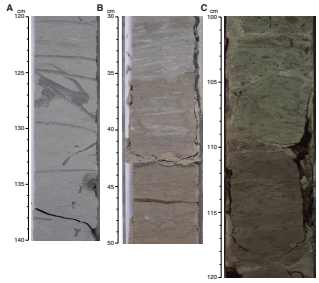

Subunit IIIA is distinguished from Subunit IIIB by its generally lower and more uniform carbonate content and its lower abundance of foraminifers. The contact is placed at the top of the first downhole occurrence of light greenish gray relatively well indurated nannofossil chalk with foraminifers.

Subunit IIIB

Intervals: 207-1260A-35R-5, 93 cm, through 41R-3, 125 cm; and 207-1260B-22R-3, 145 cm, through 28R-2, 145 cm
Depths: Hole 1260A: 324.03–379.59 mbsf; and Hole 1260B: 324.55–379.85 mbsf
Thickness: 55.56 mbsf (Hole 1260A)
Age: late Paleocene–late Campanian
Lithology: nannofossil chalk with foraminifers and calcite to clayey nannofossil chalk with foraminifers and calcite

Lithostratigraphic Subunit IIIB consists of light greenish gray to greenish gray chalk with clay to clayey chalk, although olive and reddish hues are common in the interval near the K/T boundary (see below) (Fig. **F7B**). Carbonate content varies from 40 to 80 wt% (Fig. **F4**), and this variation seems to follow light (carbonate rich) and dark (carbonate poor) color alternations (Fig. **F7C**) through most of the subunit. Carbonate constituents include subequal proportions of nannofossils, foraminifers, and calcareous debris. Bioturbation is pervasive with *Zoophycos, Planolites,* and *Chondrites* traces identified. The darker intervals often exhibit a subhorizontal fabric that may result from the orientation of burrows, compaction, primary lamination, or some combination of these three. Pyrite and clay increase in abundance in the lower half of the subunit. Rare barite nodules that range from a few millimeters to a centimeter in diameter are observed in the lower part of the subunit.

The top of Subunit IIIB is placed at the first downhole occurrence of relatively well indurated light-colored nannofossil chalk with foraminifers, which seems to represent the downcore initiation of pronounced alternations in carbonate content. The base of Subunit IIIB is placed at a marked increase in clay content apparent from smear slide description that corresponds to a dominance of dark greenish gray colors and approximates the level where planktonic foraminifers disappear from washed residues (see **"Biostratigraphy,"** p. 11).

An excellent record across the K/T boundary appears to be present in Subunit IIIB. The ejecta layer was best recovered in Hole 1260A, but the entire K/T interval was better recovered in Hole 1260B. Approximately 3.5 m below the boundary, the color of the Maastrichtian chalks shifts gradationally from greenish gray to dark yellowish brown, but the color returns to greenish gray ~0.5 m below the boundary. The boundary is placed at a 1.5-cm-thick graded bed composed of light green spherules (Fig. **F6B**). Spherules decrease in size from ~1 mm in diameter at the base of the layer to ~0.25 mm in diameter at the top. The spherule bed sits on a ~3-mm-thick gray fine-grained homogeneous layer. There are impressions of spherules on the upper surface of this gray layer. A massive green clay lies above the spherule bed, but it was disturbed by drilling in both holes at this site. About 5 cm above the spherule bed, there are burrow mottles up to 0.5 cm across and sediment color becomes progressively lighter and more mottled over the subjacent 20 cm, suggesting increased carbonate content and return to background pelagic

deposition. About 30 cm above the boundary, there is a ~30-cm-thick yellowish brown interval, which grades back to a greenish gray color.

Subunit IIIC

Intervals: 207-1260A-41R-3, 125 cm, through 42R-CC, 15 cm; and 207-1260B-28R-2, 145 cm, through 30R-CC, 8 cm
Depths: Hole 1260A: 379.59–390.65 mbsf; and Hole 1260B: 379.85–390.83 mbsf
Thickness: 11.06 mbsf
Age: early Campanian
Lithology: nannofossil chalk with foraminifers and calcite to clayey nannofossil chalk with foraminifers and calcite

Lithostratigraphic Subunit IIIC consists of claystone with foraminifers and nannofossils to clayey nannofossil chalk. Pyrite is common and barite is present as millimeter- to centimeter-sized nodules. Light–dark alternations with a 20- to 50-cm spacing represent changes in the relative abundance of clay and carbonate (Fig. F7C). Bioturbation is heavy to pervasive, but darker intervals often have a subhorizontal fabric. *Zoophycos, Planolites,* and *Chondrites* traces are present.

This subunit is distinguished from Subunit IIIB by its higher clay content. The transition is gradational and is placed where relatively dark claystone intervals are more abundant than the relatively light clayey chalk intervals. This level approximately coincides with the disappearance of planktonic foraminifers (see "Biostratigraphy," p. 11), suggesting the relative increase in clay content downcore results in part from the dissolution of the calcareous components. Subunit IIIC is distinguished from Unit IV by the presence of burrows and low organic carbon content. The lower contact is placed at the first downhole occurrence of laminated dark olive-gray calcareous claystone (Fig. F8A).

F8. Representative lithologies, Unit IV, p. 47.

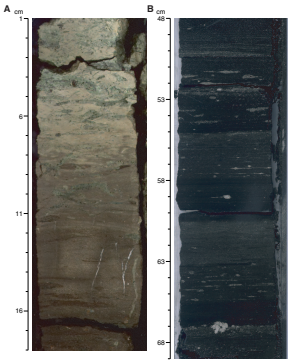

Unit IV

Intervals: 207-1260A-42R-CC, 15 cm, through 53R-2, 42 cm; and 207-1260B-30R-CC, 8 cm, through 42R-1, 129 cm
Depths: Hole 1260A: 390.65–483.30 mbsf; and Hole 1260B: 390.32–483.60 mbsf
Thickness: 93.28 mbsf
Age: Coniacian–Cenomanian
Lithology: calcareous claystone with organic matter, clayey chalk with organic matter, and limestone

Unit IV ranges from black, finely laminated calcareous claystone with organic matter (Fig. F8B) to laminated clayey chalks with foraminifers and organic matter and clayey foraminifer micritic limestones (Fig. F8C). The top of Unit IV is defined by the shift from bioturbated greenish gray claystone of Unit IIIC above to laminated claystones with high organic carbon contents below (Fig. F8A). The transition is gradational over ~20 cm in Hole 1260A and is characterized by a greenish gray clay with abundant glauconite, pyrite, and quartz (interval 207-1260A-42R-CC, 1–18 cm). Contacts between the major lithologies in the unit are gradational over a centimeter to decimeter scale and from light–dark color cycles that are typical for Unit IV. Color shifts correspond to significant changes in carbonate (higher in light intervals) and total organic carbon (TOC) (higher in dark intervals) content (Fig. F4), and there

is a trend toward increasing carbonate content. Some intervals of Unit IV have a considerable zeolitic component (intervals 207-1260A-45R-2, 46 cm, and 46R-5, 30 cm). Phosphatic fecal pellets, fish remains, and inoceramids are present throughout the unit (Fig. F8B), as are white millimeter-scale calcite layers composed entirely of foraminifers filled with sparry calcite (Figs. F8C, F9B).

The lower portion of Unit IV (intervals 207-1260A-52R-CC, 13–22 cm, and 207-1260B-41R-5, 1–18 cm) contains massive coarse-grained decimeter-scale beds with sharp, possibly erosive, bases. These layers are primarily composed of large shell fragments, glauconite, and subangular quartz grains (Fig. F9A). Some of this lithology is found in burrows projecting up to 50 cm into the underlying laminated claystone. These beds are similar to lithologies found at the top of the black organic-rich claystones at Sites 1257, 1258, 1259, and 1261 and seem to correspond to a distinctive natural gamma ray (NGR) and magnetic susceptibility peak (see "Physical Properties," p. 30). They may represent mass flow deposits or a period of very low sedimentation and slightly higher oxygen levels, allowing for the observed bioturbation.

F9. Typical lithologies, Units IV and V, p. 49.

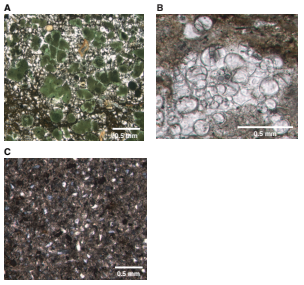

Unit V

Intervals: 207-1260A-53R-2, 42 cm, through 54R-CC, 12 cm; and 207-1260B-42R-1, 129 cm, through 46R-CC, 37 cm
Depths: Hole 1260A: 483.30–491.90 mbsf; and Hole 1260B: 483.60–507.37 mbsf
Thickness: 23.77
Age: early–late Albian
Lithology: clayey limestone with quartz and calcareous claystone with quartz

Unit V consists of dark greenish gray silty limestones and silty calcareous claystones. The top is placed at the base of the lowest debris flow deposit in Unit IV. Unit V extends to the bottom of the hole. The limestones of Unit V display a mottled fabric but are otherwise homogeneous with no discrete burrows evident. No bedding features are discernable in the claystones, but rare white mottles (~1 mm diameter) filled with subangular quartz are present. Clay content in the claystones is estimated to be as high as 80% in smear slides, with silt-sized calcite and subangular quartz making up the remaining fraction (Fig. F9C). The claystone contains occasional pyrite nodules, and both lithologies have disseminated pyrite and rare shell debris. Some woody carbonaceous debris, often ringed with pyrite, is present in the claystones.

Summary

The oldest unit recovered at Site 1260 is Albian in age and is assigned to Unit V in the lithostratigraphic classification. It is relatively homogeneous and consists of clayey limestones with quartz and quartz silty calcareous claystone. Rare ichnofossils, pelagic microfossils, shell fragments, and fish debris are present. Terrigenous input into the basin resulted in clay-rich intervals containing subangular quartz, woody debris, and inorganic calcite. Common pyrite in the unit suggests a relatively low oxygen content of the bottom water and/or early diagenesis in pore waters. Based on these observations, Unit V appears to reflect sedimentation in a synrift proximal shallow-marine environment with high sedimentation rates.

Unit IV is Turonian–Cenomanian in age. It is an interval with high (up to 14 wt%) TOC concentrations. Rock-Eval results indicate that the organic carbon is primarily of marine origin (see "Organic Geochemistry," p. 25). The dominant lithologies in this unit are dark laminated calcareous claystone and relatively light laminated limestone. Debris flow deposits, wood fragments, and quartz grains are found at the base of the unit. The carbonate-rich deposits contain more microfossils than the organic-rich clay. This unit was likely deposited in a deeper marine environment than Unit V, and the carbonate–clay alternations may be related to fluctuations in seawater oxygen content and carbonate and organic carbon productivity, winnowing, or variations in deposition and redeposition processes. Phosphatic fecal pellets, fish remains, and inoceramids are present. The high percentage of zeolite suggests original biosiliceous fauna.

Unit III is late Paleocene–early Campanian in age and is a clayey nannofossil chalk with a wide range of carbonate content and low percentage of TOC. The lower contact is distinct and corresponds to a 20-cm-thick coarse glauconite-rich level that overlies the laminated dark calcareous claystones of Unit IV. The upper boundary is gradational and is placed at the base of the gray clay layer at the P/E boundary. Unlike Units IV and V, Unit III is pervasively bioturbated, suggesting higher benthic oxygen levels. A deepening of the calcite compensation depth (CCD) or less corrosive pore waters is suggested by better foraminifer preservation upsection. Light (carbonate rich) and dark (clay rich) cyclic color alternations indicate variations in a combination of factors (i.e., productivity, deposition, preservation, and diagenetic alteration).

The K/T and P/E boundaries are well preserved in Holes 1260A and 1260B. The K/T boundary and ejecta layer (1.5 cm thick in Hole 1260A) are present in Subunit IIIB. Sediments are reddish within a meter on either side of the K/T boundary, but immediately above and below the boundary, the sediments return to a greenish gray pelagic clayey chalk. The P/E boundary represents the boundary between Units III and II and is composed of laminated clays on either side of a distinct color change. A decrease in carbonate content at the event and evidence of reduced oxygen and benthic activity is likely related to a shoaling of the CCD (Dickens, 2000).

Unit II is early Eocene–Oligocene in age and consists of pelagic nannofossil chalk with foraminifers. Relative to Unit III, Unit II has a high carbonate content. Unit II is subdivided into three subunits based on clay content and biosiliceous abundance. Subunit IIB contains radiolarians, siliceous sponge spicules, and diatoms, whereas Subunits IIA and IIC are relatively rich in calcareous microfossils. Subunit IIC also contains more clay and zeolite than Subunits IIA and IIB. Subtle light–dark color alternations on a scale of 10–50 cm throughout Unit II are regular enough to suggest periodic forcing. A slump deposit ~13 m thick composed of pelagic Oligocene sediments is present in the upper part of Unit II. The upper Pleistocene veneer, (i.e., Unit I) is primarily composed of clay with glauconite, nannofossils, and foraminifers, indicating that this is presently a site with minimal sediment accumulation.

BIOSTRATIGRAPHY

The two holes at Site 1260 yielded primarily Eocene–mid-Cretaceous marine sediments that contain planktonic foraminifers, calcareous nannofossils, and radiolarians in abundances and states of preservation

that vary widely with lithology and sediment induration. Shipboard examination of these microfossil groups in core catcher samples and additional samples in the cores permitted zonal or stage assignments to be made for the entire sequence. Datum levels are summarized in Figure **F10** and in Tables **T3, T4, T5, T6, T7,** and **T8.**

A thin (10 cm) veneer of Pleistocene ooze at the top of the section overlies ~35 m of lower Oligocene calcareous ooze. The Oligocene interval from Cores 207-1260A-2R to 5R shows complicated ages, in part inverted by extensive reworking and slumping. A middle Eocene nannofossil radiolarian chalk from Cores 207-1260A-6R to 20R contains abundant and well-preserved radiolarians. Planktonic foraminifers are poorly preserved from Cores 207-1260A-11R to 23R because of dissolution. The P/E boundary is in Sections 207-1260A-30R-7 and 207-1260B-17R-7.

The K/T boundary ejecta layer (~1.8 cm thick) is recognized in Sections 207-1260A-36R-4 and 207-1260B-23R-3. The late Maastrichtian nannofossil *Micula murus* was identified immediately below the ejecta horizon; overlying strata contain the Danian planktonic foraminifers from Zone Pα.

A distinctive condensed glauconite-rich horizon visible in Core 207-1260A-42R separates the Campanian chalk from the ~93-m-thick black shales below (lithostratigraphic Unit IV) that compose the lower part of OAEs 3 and 2. Site 1260 provides a nearly continuous Coniacian–Cenomanian black shale record. Calcareous microfossils are generally present throughout the black shales, and foraminifers range in preservation from very poor to glassy. Clayey quartz siltstones of lithostratigraphic Unit V are early Albian in age, and microfossils are rare.

Calcareous Nannofossils

The two holes drilled at Site 1260 obtained primarily middle Eocene–early Albian deposits under a thin veneer of Pleistocene and slumped sediments of early Oligocene age. These contain, apart from the Turonian–Albian interval, generally common to abundant calcareous nannofossils of moderate to good preservation. The observations made allow for zonal or stage assignments that are summarized in Figure **F10** and Tables **T3** and **T7.** Core catcher samples were examined for all holes and supplemented as necessary by samples in the cores to further refinement of the zonal assignments. In the more detailed description to follow, the assemblages and ages pertain to Hole 1260A unless noted otherwise.

Sample 207-1260A-1R-CC contains a Pleistocene nannofossil assemblage (Zone NN21 of the Martini, 1971 scheme) including *Gephyrocapsa oceanica, Emiliania huxleyi,* and *Pontosphaera indooceanica*. Samples 207-1260A-2R-CC to 4R-CC are of early Oligocene age (Zones NP23–NP21) as indicated by the presence of *Sphenolithus distentus, Reticulofenestra umbilica, Reticulofenestra hillae, Discoaster tani, Isthmolithus recurvus,* and *Sphenolithus predistentus*. Samples 207-1260A-2R-CC, 3R-CC, and 4R-CC are assigned to Zone NP23, but intervening Samples 3R-2, 25 cm, to 3R-3, 25 cm, produce an older NP21 Zonal assignment. These partly inverted ages indicate some major slumping.

Sample 207-1260A-5R-CC contains an upper Eocene assemblage (Zone NP19/NP20) that includes *Sphenolithus pseudoradians, Discoaster barbadiensis, Discoaster saipanensis*, and *D. tani*. *Chiasmolithus grandis, Chiasmolithus solitus,* and *R. umbilica* in Sample 207-1260A-6R-CC are of late middle Eocene age (Zone NP17). The subjacent Samples 207-1260A-

F10. Planktonic foraminifer, calcareous nannofossil, and radiolarian biozonation, p. 50.

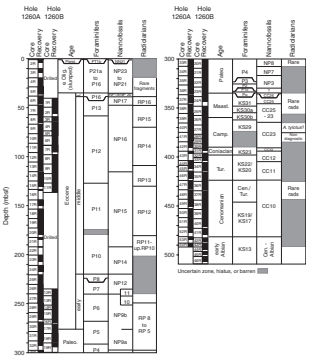

T3. Calcareous nannofossils, p. 85.

T4. Planktonic foraminifers, Hole 1260A, p. 86.

T5. Planktonic foraminifer datums, p. 87.

T6. Radiolarian datums, p. 88.

T7. Datum levels, ages, and preservation of samples, p. 89.

T8. Planktonic foraminifers, Hole 1260B, p. 90.

7R-CC to 13R-CC have a middle Eocene age (NP16), yielding *C. grandis, Sphenolithus furcatus, R. umbilica, Discoaster lodoensis, Ericsonia formosa*, and *Sphenolithus radians*. Based on the presence of *C. grandis, Nannotetrina fulgens,* and *Chiasmolithus gigas,* Samples 207-1260A-14R-CC to 21R-2, 71 cm, have been assigned a middle Eocene age (Zone NP15). The underlying Samples 207-1260A-22R-CC to 23R-CC are of early middle Eocene age (Zone NP14) based on the presence of *Discoaster sublodoensis* and *Rhabdosphaera inflata*. Sample 207-1260A-24R-CC contains *D. barbadiensis, D. sublodoensis, D. lodoensis,* and *S. radians* and is thus of earliest middle Eocene age (Zone NP14).

Samples 207-1260A-25R-CC to 26R-CC yielded *Sphenolithus conspicuus, E. formosa,* and *S. radians,* giving an early Eocene age (Zone NP12). Abundant *Neochiastozygus junctus* and *Zygrhablithus bijugatus* and the absence of *Fasciculithus* spp. in Samples 207-1260A-27R-CC to 207-1260B-29R-CC support an earliest Eocene age above the P/E boundary (upper part of Zone NP9). An assemblage with common *Fasciculithus* spp. and *Discoaster multiradiatus* in Samples 207-1260A-30R-CC to 32R-CC assigns this interval a latest Paleocene age (NP9 lower part). A nannofossil assemblage consisting of *Discoaster mohleri, Heliolithus riedelii,* and *Fasciculithus tympaniformis* in the absence of *D. multiradiatus* characterizes Sample 207-1260A-33R-CC as late Paleocene in age (Zone NP8). A late Paleocene age (Zone NP7) is also assigned to Samples 207-1260A-34R-CC based on the presence of *Chiasmolithus consuetus* and *Ellipsolithus macellus* along with common *D. mohleri*. *Ellipsolithus macellus,* however, is absent in Sample 207-1260A-35R-CC, but *Cruciplacolithus primus* and *Cruciplacolithus tenuis* (up to 10 µm long) denote Zone NP3.

Samples 207-1260A-36R-CC to 37R-CC contain a rich nannoflora of late Maastrichtian age, including *M. murus* (Zones CC25–CC26). Samples 207-1260A-38R-CC to 39-CC yield a nannofossil assemblage of Maastrichtian age (Zones CC25–CC23 of the Sissingh, 1977 scheme) including *Reinhardtites levis, Ceratolithus aculeus,* and *Arkhangelskiella cymbiformis*. Samples 207-1260A-40R-CC to 41R-CC contain an early Maastrichtian to late Campanian assemblage (Zone CC23), including *Uniplanarius trifidum, R. levis, A. cymbiformis,* and *Uniplanarius sissinghi*.

The bottom of subjacent Samples 207-1260A-42-CC to 43R-2, 109–111 cm, yielded *Eprolithus octopetalus, Quadrum gartneri,* and *Eiffellithus eximius,* allowing a Turonian age assignment (Zone CC12). Samples 207-1260A-44-CC to 46R-CC have an early Turonian age (Zone CC11), indicated by the co-occurrence of *E. eximius* and *E. octopetalus*. The underlying succession from Samples 207-1260A-47R-7, 0–4 cm, to 52R-CC is of Cenomanian–latest Albian age (Zone CC10) since *Eiffellithus turriseiffelii* and *Axopodorhabdus albianus* are present. A section of Albian age was encountered in Samples 207-1260A-53R-CC to 54R-CC (bottom of hole). *Eiffellithus* spp. is absent, whereas *Prediscosphaera columnata, Rhagodiscus angustus, Microstaurus chiastus, Eprolithus floralis, Eprolithus apertior, Radiolithus planus,* and occasional *Watznauria britannica* and *Heliolithus trabeculatus* range downhole.

Planktonic Foraminifers

Planktonic foraminifer biostratigraphy at Site 1260 was based upon a combination of core catchers and samples taken in every section in Hole 1260A and selected sections in Hole 1260B. Zonal assignments are summarized in Figure **F10** and Tables **T4, T5,** and **T8.** Pleistocene planktonic foraminifer Subzone PT1b through lower Albian Zone KS13 were

identified in Hole 1260A. Significant breaks in the biozonation occur in the middle Oligocene–Pleistocene, the middle Eocene–upper Eocene, the lower/middle Eocene boundary, and the Coniacian–Campanian. A significant hiatus may also occur around the Albian/Cenomanian boundary. Planktonic foraminifers are present in nearly all samples but vary widely in preservation and abundance. Preservation is best in clay-rich parts of the Albian–Coniacian sequence, although foraminifers are difficult to extract and completely clean in the "black shales." Many samples from the black shales required three or more washing/drying cycles as well as heating in a mixture of Calgon and peroxide to produce large numbers of identifiable specimens. Foraminifers in the light-colored bands in the organic-rich claystones are frequently filled with calcite spar. Good preservation is found in the Pleistocene, Oligocene, and middle–upper Eocene section, whereas preservation is mostly moderate or poor in the chalk of the lower Eocene, Paleocene, and Campanian–Maastrichtian sequence. Some clay-rich chalks in the Paleocene and Maastrichtian contain outwardly well-preserved foraminifers that are filled with bladelike crystals of calcite. Foraminifers in the lower Danian (Zones P3–Pα) are strongly fragmented and recrystallized.

Sample 207-1260A-1R-1, 0–2 cm, contains a mixture of Pleistocene or Holocene planktonic foraminifers such as *Orbulina universa, Globigerinoides sacculifer, Globorotalia truncatulinoides, Globorotalia menardii,* and *Globigerinoides ruber.*

Yellow and green calcareous ooze between Samples 207-1260A-2R-CC and 4R-CC contains a lower Oligocene section complicated by extensive reworking or slumping. Sample 207-1260A-2R-CC includes typical species of late early Oligocene age, including *Globigerina angulosuturalis*. This species is absent from the rest of the Oligocene section, and the presence of *Pseudohastigerina* spp. in all sections between Samples 207-1260A-3R-1, 50–54 cm, and 4R-2, 50–54 cm, suggests lowermost Oligocene Zone P18. However, Sample 207-1260A-3R-2, 50–54 cm, contains a diverse upper Eocene foraminifer assemblage with *Turborotalia cunialensis* and *Hantkenina alabamensis,* indicating Zone P16. Age reversals between Oligocene Zones P18, P19, and P20 were noted in Core 207-1260A-4R and suggest that the Oligocene sequence is not in original stratigraphic order. The absence of distinctive Oligocene species in the Eocene assemblage from Sample 207-1260A-3R-2, 50–54 cm, suggests reworking may be the result of slumps rather than winnowing. However, the foraminifer markers for Oligocene Zones P20, P19, and P18 are all last occurrences (LOs), which make it hard to distinguish wholesale slumping from reworking of distinctive species. Indeed, the absence of large-scale reworking of Eocene species of calcareous nannofossils into Oligocene assemblages (see **"Calcareous Nannofossils,"** p. 12) suggests that although there may have been extensive redeposition of older sediments into the Oligocene this need not always have been produced by slumping.

Sample 207-1260A-5R-CC contains a well-preserved upper Eocene foraminifer fauna with *Subbotina gortani, H. alabamensis, Turborotalia pomeroli,* and *Turborotalia cerroazulensis*. The upper Eocene sequence must be very thin in Hole 1260A because Sample 207-1260A-6R-1, 50–54 cm, contains a middle Eocene foraminifer fauna from Zone P13. Common species in Zone P13 include *Orbulinoides beckmanni, T. cerroazulensis, Morozovella spinulosa, Globigerinatheka rubriformis, Acarinina rohri,* and *Catapsydrax africana*. Specimens of *O. beckmanni* in Core 207-1260A-6R have a final chamber that envelops at least half of the test and includes large nearly spherical forms. There has been much confu-

sion over the definition of *O. beckmanni;* Saito (1962) chose his holotype from an assemblage containing nearly perfectly spherical forms, but he selected a type specimen more closely resembling a large example of *Globigerinatheka kugleri* than the spherical forms that most workers have described as *O. beckmanni.* Hence, if we follow the type specimen to define the Zone P13 interval, the zone extends downward to Sample 207-1260A-8R-1, 50–54 cm, at which point *O. beckmanni* mainly consists of large specimens that closely resemble the holotype with three nearly equally sized chambers in the final whorl and relatively deep sutures between the chambers.

An expanded record of middle Eocene Zones P12–P10 is present between Samples 207-1260A-8R-2, 50–54 cm, and 24R-CC. Samples from Zones P12 and P11 are very rich in well-preserved radiolarians, which in some cases hinder observations of foraminiferal zone species. Zone P12 has been recognized between Samples 207-1260A-8R-2, 50–54 cm, and 14R-CC. Foraminifer assemblages are dominated by *A. rohri, Acarinina bullbrooki, M. spinulosa, T. pomeroli,* and *G. kugleri. Guembelitrioides nuttali* has its LO near the middle of Zone P12 in Sample 207-1260A-10R-CC. Zone P11 is recognized by the LO of *Morozovella aragonensis* in Sample 207-1260A-15R-1, 50–54 cm. In addition, Zone P11 faunas include *G. kugleri, A. rohri, Igorina broedermanni, M. spinulosa, Subbotina boweri, Turborotalia possagnoensis,* and *Globigerinatheka index*. The Zone P10/P11 boundary is difficult to distinguish precisely owing to the rare occurrence of *G. kugleri.* Single specimens of globigerinathikids are found in Samples 207-1260A-20R-CC and 21R-CC, and these resemble *G. index* with a single aperture and incised sutures. We draw the Zone P9/P10 contact between Samples 207-1260A-19R-CC and 20R-CC based upon the lowest common occurrence of globigerinathikids. Poor preservation also prevents us from clearly delineating this boundary in the core catchers, so, in contrast to the rest of the cored sequence, we do not attempt a refined estimate of the boundary location using samples from in the adjacent sections. The base of Zone P10 is approximated in Sample 207-1260A-24R-CC based upon the first occurrence (FO) of *G. nuttali*. Other species characteristic of Zone P10 include *Acarinina aspensis, Acarinina pentacamerata, M. aragonensis,* and *Globigerina lozanoi*. Unlike Site 1258, we do not find clavigerinellids in our samples from Zone P10, but we did find "*Hastigerina" bolivariana* in Sample 207-1260A-23R-CC.

An unconformity evidently separates Cores 207-1260A-24R (Zone P10) from Sample 207-1260A-25R-1, 50–54 cm (Zone P8). Zone P8 is between Samples 207-1260A-25R-1, 50–54 cm, and 25R-4, 50–54 cm, and is characterized by *M. aragonensis, G. lozanoi, Acarinina quetra, Acarinina soldadoensis,* and *I. broedermanni*. Zone P7 has a similar foraminifer fauna but includes *Morozovella formosa* and *Globigerina praecentralis* between Samples 207-1260A-25R-5, 50–54 cm, and 26R-CC.

The evolution of *M. aragonensis* with six chambers in the last whorl from *Morozovella lensiformis* with four or five chambers in the last whorl was used to recognize the Zone P6/P7 boundary in Sample 207-1260A-27R-1, 50–54 cm. The FO of *M. formosa* could not be determined precisely owing to extremely poor preservation in most of Core 207-1260A-27R, but specimens of *M. formosa* with six chambers in the last whorl were observed in Sample 207-1260A-27R-3, 50–54 cm, suggesting that this sample belongs to Subzone P6b. Large specimens of *Chiloguembelina wilcoxensis* and *Morozovella gracilis* were observed from the top of Core 207-1260A-27R to Sample 207-1260A-29R-CC along with typical species in Subzone P6a, such as *Acarinina wilcoxensis, Morozovella subbotinae, Morozovella marginodentata,* and *Morozovella aequa*.

The top of Zone P5 is observed in Sample 207-1260A-30R-1, 50–54 cm, at the last appearance of *Morozovella acuta, Morozovella velascoensis,* and *Morozovella occlusa*. This sample also contains inflated specimens of *Pseudohastigerina wilcoxensis* as well as *M. subbotinae* and *A. soldadoensis*. The P/E boundary appears at 74 cm in Section 207-1260A-30R-7 and 69 cm in Section 207-1260B-17R-7. Samples 207-1260A-30R-6, 50–54 cm, and 30R-8, 50–54 cm, span the boundary and contain very poorly preserved foraminifers. We are not able to identify any representatives of the excursion fauna of planktonic foraminifers that are characteristic of the Paleocene–Eocene Thermal Maximum. However, Sample 207-1260A-30R-CC contains the benthic foraminifer *Aragonia velascoensis,* a species that became extinct at the P/E boundary. The LO of *Globanomalina pseudomenardii* (total range marker for Zone P4) occurs between Samples 207-1260A-32R-1, 50–53 cm, and 32R-3, 45–48 cm, and defines the lower limit of Zone P5.

Zone P4 is characterized by abundant *M. velascoensis, A. soldadoensis, Igorina albeari, Subbotina velascoensis,* and *Subbotina triangularis*. The bottom of Zone P4 is found between Samples 207-1260A-35R-5, 50–54 cm, and 35R-6, 50–54 cm, based upon the first appearance of *Acarinina coalingensis* and *Acarinina subspherica,* which are known to make their initial appearance at the same time as the zone marker *G. pseudomenardii*. Sample 207-1260A-35R-5, 50–54 cm, contains abundant benthic foraminifers and a dissolved planktonic foraminifer assemblage that includes reworked Cretaceous species such as *Globotruncana arca* and *Heterohelix globulosa*. The underlying strata in Samples 207-1260A-35R-6, 50–54 cm, and 35R-7, 18–22 cm, include highly recrystallized and overgrown foraminifers such as *Morozovella angulata, Morozovella praeangulata,* and *Parasubbotina varianta* that suggest Subzone P3a.

The lower Danian is in a highly condensed interval in Cores 207-1260A-35R and 36R. Samples 207-1260A-35R-CC to 36R-3, 28–29 cm, contain species typical of Zone P2, including *Praemurica uncinata, M. praeangulata, Parasubbotina pseudobulloides,* and *Subbotina triloculinoides*. In contrast, Sample 207-1260A-36R-4, 0–1 cm, represents Subzone P1c, as it contains *Praemurica pseudoinconstans, Praemurica inconstans,* and *Praemurica taurica*. Sample 207-1260A-36R-4, 80–81 cm, includes extremely small specimens of *Woodringina claytonensis, Guembelitria cretacea, Eoglobigerina eobulloides,* and *Parvularugoglobigerina eugubina* that distinguish Zone Pα. The K/T boundary is believed to occur in interval 207-1260A-36R-4, 93 cm, based upon a spherule bed at this level.

The Maastrichtian sequence extends between Samples 207-1260A-36R-CC and 38R-CC. Assemblages belonging to Zone KS31 (defined by the total range of *Abathomphalus mayaroensis*) are present between Samples 207-1260A-36R-CC and 38R-1, 49–52 cm. Accompanying species include *Gansserina gansseri, Rosita contusa, Rugoglobigerina rugosa, Rugoglobigerina rotundata,* and *Pseudoguembelina palpebra*. Subzone KS30a (the *Raceiguembilina fructicosa*/*R. contusa* Zone) is identified in Samples 207-1260A-38R-2, 49–53 cm, to 38R-6, 49–52 cm. Species typical of Subzone KS30a include *R. contusa, Abathomphalus intermedius,* and *Globotruncana aegyptiaca* in addition to those taxa in Zone KS31. Subzone KS30b (the *G. gansseri* Zone) is suggested in Sample 207-1260A-38R-CC by the absence of *R. contusa*. The other marker for Subzone KS30a, *R. fructicosa,* is very rare in the Maastrichtian in Site 1260 and is not considered a reliable datum marker on Demerara Rise. Samples 207-1260A-39R-CC to 41R-CC are difficult to assign to a zone with confidence. However, the absence of *G. gansseri* and the presence of *G. aegyptiaca* suggests these samples belong to Campanian Zone KS29. Common spe-

cies include *Rosita plummerae, Rosita fornicata, Rugotruncana subcircumnodifer, Globotruncanita stuartiformis,* and *Globotruncana linneana*. Samples 207-1260A-41R-CC to 42R-4, 0–1 cm, are barren of planktonic foraminifers.

A distinctive glauconitic-rich interval separates the green calcareous claystone of Sample 207-1260A-42R-4, 0–1 cm, from the brown claystone of Sample 207-1260A-42R-CC. The presence of *Marginotruncana pseudolinneana, Dicarinella hagni, Archaeoglobigerina cretacea,* and *Hastigerinoides watersi* from the base of Section 207-1260A-43R-2 suggests a Coniacian age for the assemblage (Zone KS23). Sample 207-1260A-42R-CC and several dark-colored shales in Core 207-1260A-43R yield well-preserved glassy foraminifers that were not age diagnostic and included *Hedbergella delrioensis, Whiteinella baltica, H. globulosa,* and *Heterohelix moremani*. Similar non–age diagnostic assemblages were present in Cores 207-1260A-44R, 45R, and 46R. Sample 207-1260A-46R-CC was the only sample in the black shale sequence that yielded no foraminifers at all.

The location of the Cenomanian/Turonian (C/T) boundary can be only approximated on the basis of planktonic foraminifers. The C/T boundary may lie above Sample 207-1260A-47R-7, 0–2 cm, since this sample contains *Globigerinoides caseyi,* a species that we have observed only in samples of Cenomanian age from other sites on Demerara Rise. The first distinctive Cenomanian species are found in Sample 207-1260A-49R-2, 42–44 cm, where *Rotalipora globotruncanoides* is present together with *H. delrioensis* and *Hedbergella planispira*. Preservation of foraminifers in Cores 207-1260A-48R and 49R is generally very poor because the shells are filled with calcite spar and cemented together with blocky calcite. In contrast, samples in Cores 207-1260A-50R and 51R are mostly well preserved with glassy shells. Specimens of *R. globotruncanoides* and *Rotalipora appenninica* were intermittent between Samples 207-1260A-50R-CC and 52R-2, 99–100 cm, and provide our lowest definite occurrence of Cenomanian assemblages at Site 1260. Well-preserved foraminifers including *H. delrioensis, H. moremani, H. planispira,* and *Globigerinelloides* spp. were present between Samples 207-1260A-52R-3, 115–116 cm, and 52R-CC. These samples are consistent with either a Cenomanian or a late Albian age.

The interval between Samples 207-1260A-52R-1, 115–117 cm, and 54R-CC contains a sparse fauna with *Ticinella primula, Globigerinelloides bentonensis,* benthic foraminifers, and ostracodes that represent lower Albian Zone KS13. Ticinellids are present continuously between Samples 207-1260B-41R-CC and 45R-CC. Sample 207-1260B-46R-CC is barren of planktonic foraminifers but contains a similar benthic foraminifer and ostracode assemblage to that observed in the overlying Albian samples.

Radiolarians

Core catcher samples were processed and examined systematically for radiolarians from Hole 1260A. Identifiable radiolarians are present mainly in the middle Eocene interval, and the observations allow for zonal assignments summarized in Figure **F10** and Table **T6.** The highest sample to yield age-diagnostic radiolarians, Sample 207-1260A-6R-CC, is assigned to Zone RP16 based on the co-occurrence of *Podocyrtis goetheana* (marker species of the base of Zone RP16) and *Sethochyrtis triconiscus* (which last occurs in the middle part of Zone RP16).

Samples 207-1260A-7R-CC and 8R-CC are assigned to Zone RP15 based on abundant *Podocyrtis chalara*. As *Podocyrtis mitra* is abundant in Sample 207-1260A-9R-CC, whereas *P. chalara* is absent, the boundary between Zones RP15 and RP14 is placed in Core 207-1260A-9R. Abundant *P. mitra* in Samples 207-1260A-9R-CC through 12R-CC allows their assignment to Zone RP14.

The marker species of Zone RP13 (*Podocyrtis ampla*) is abundant in Samples 207-1260A-13R-CC and 14R-CC. As abundant specimens of *Podocyrtis phyxis* are present in Sample 207-1260A-15R-CC, the boundary between Zones RP13 and RP12 is placed in Core 207-1260A-15R. Although the marker species of the base of Zone RP12 (*Eusyringium lagena*) is observed only in Sample 207-1260A-16R-CC, Samples 207-1260A-16R-CC to 19R-CC are all assigned to Zone RP12 based on abundant *Thyrsocyrtis triacantha, Podocyrtis diamesa,* and *Theocotyle conica*. Rare specimens of *T. triacantha* are observed in Section 207-1260A-20R-4 (top) together with abundant specimens of *Thyrsocyrtis tensa, Thyrsocyrtis robusta,* and *Dictyoprora mongolfieri,* which allows assignment of this sample to the lowermost part of Zone RP12 or to RP11. Therefore, the boundary between Zones RP12 and RP11 is tentatively placed in Core 207-1260A-20R. Based on *T. robusta* and *T. tensa* in Samples 207-1260A-21R-2, 71–76 cm, and 22R-CC, this interval is regarded as a part of Zone RP11 or upper Zone RP10. Cores 207-1260A-29R through 32R may be assigned to Zones RP5–RP8, based on the presence of species *Buryella tetradica*. Radiolarians are common and relatively well preserved again at the Campanian interval. The genera *Amphipyndax* and *Dictyomitra* dominate the assemblage of Sample 207-1260A-40R-CC. Possible *Amphipyndax tylotus* in this sample may argue for a late Campanian or younger age.

PALEOMAGNETISM

Shore-based paleomagnetic analyses of minicores from the combined holes at Site 1260 resolved a high-resolution record of Chrons C18r–C21r from the middle Eocene. A lower-resolution identification was possible for Chrons C31r–C29 from the Campanian to Maastrichtian and Chrons C26n–C23n from the late Paleocene to early Eocene.

Shipboard and Shore-Based Procedures and Data Filters

Details are given in **"Paleomagnetism,"** p. 16, in the "Explanatory Notes" chapter of the standard shipboard analysis using the pass-through cryogenic magnetometer, of the filtering and polarity interpretation procedures of this shipboard data, and of the shore-based progressive demagnetization of discrete minicores. Measurements were made at 5-cm intervals using the shipboard pass-through cryogenic magnetometer on archive halves of cores longer than 15 cm. Sections were measured at natural remanent magnetization and at 10- and 15-mT alternating-field (AF) demagnetization steps (Table **T9**). The 10-mT step appeared to be effective in removing extraneous overprints induced by the drilling process. The Cenomanian–Coniacian black shale intervals displayed magnetizations near the background noise level of the shipboard cryogenic magnetometer. These shales are known to have been deposited during the Long Normal Polarity Cretaceous Superchron C34n. As at the other Leg 207 sites, we decided to leave the ma-

T9. Shipboard cryogenic magnetometer analyses, p. 91.

jority of the black shale cores intact rather than partially demagnetize the sediments without prospects of obtaining useful shipboard information. However, the basal facies of clayey limestone of early Albian age underwent the routine analysis procedure.

The generalized stratigraphy of sediment facies, biostratigraphic ages, and magnetization characteristics of Site 1260 from the shipboard pass-through cryogenic magnetometer are summarized in Figure **F11.** Shipboard identification of polarity zones through nearly half of the succession was not possible because of weak magnetization near the noise limit of the cryogenic magnetometer or because of secondary overprints associated with reddish coloration that could not be removed by shipboard AF demagnetization. Less than 20% of the shipboard measurements at 15 mT for Hole 1260A remained after the filtering procedures. Therefore, we drill pressed a suite of oriented paleomagnetic cylinders from every second section (3-m spacing) of Hole 1260B spanning the Campanian–middle Eocene and the lower Albian. Additional minicores from Hole 1260A covered the lower portion of the middle Eocene stratigraphic interval that was not recovered in Hole 1260B. These minicores underwent combined progressive AF (5 mT) and thermal demagnetization at the magnetically shielded facility at the University of Munich, Germany. The magnetic polarity of each minicore was interpreted from an examination of the movement of its magnetic vector during progressive demagnetization (see **"Paleomagnetism,"** p. 16, in the "Explanatory Notes" chapter) (Table **T10**). These shore-based measurements enabled resolution of removed and characteristic components of magnetization and significantly modified the tentative shipboard polarity interpretations from all facies (Fig. **F12**).

F11. Shipboard paleomagnetic data, p. 51.

T10. Polarity and characteristic directions, p. 92.

F12. Shore-based magnetostratigraphy, p. 52.

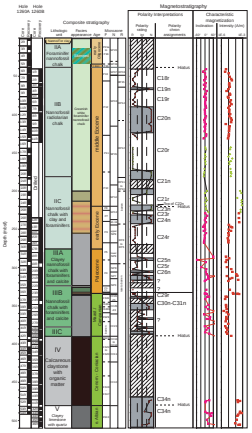

Paleomagnetic Behavior and Interpretations of Magnetostratigraphy

Late (Priabonian) Eocene–Early (Rupelian) Oligocene

A pronounced downward decrease in both magnetic intensity and susceptibility of the foraminifer nannofossil chalk was observed from the yellowish colored chalk in the uppermost meters (~10^{-2} A/m after 15-mT demagnetization) to the greenish white chalk at 25 mbsf (~10^{-5} A/m) (Fig. **F11**). This phenomenon is postulated to be a rock magnetic response to a progressive dissolution of magnetic oxides associated with the observed redox diagenetic trend (e.g., oxidized in the upper meters but reduced iron minerals below). However, we believe that those magnetic minerals responsible for the paleomagnetic polarity record are not significantly affected by this dissolution. We will analyze the rock magnetism from these facies of varying coloration to determine the magnetic minerals responsible for this decrease.

A series of slumps at 20–45 mbsf has redeposited upper Eocene–lower Oligocene greenish white foraminifer nannofossil chalk. These sediments display "polarity zones" of clusters of negative and positive inclination samples. It is unknown whether this apparent polarity record was acquired before (i.e., fixed in the sediment mass prior to downslope transport) or during the slumping episodes. In theory, one could distinguish between these alternatives by performing a paleomagnetic "fold test" in the future, in which one compares the characteristic magnetic directions from discrete samples taken from strata with different tilt magnitudes and orientations from within the slump.

Lower and Middle Eocene

The upper portion of the middle Eocene (~40–185 mbsf) is primarily greenish white foraminifer nannofossil chalk. Magnetic intensity of these sediments after 15-mT AF demagnetization were very low, generally in the range of 10^{-5}–10^{-4} A/m, and a large number of measurements were below the background noise level of 3×10^{-5} A/m (Fig. F11). Progressive thermal demagnetization of minicores from the two holes yielded a well-defined polarity pattern identical to Chrons C21n–C18r, as expected from the paleontological ages.

The polarity pattern assigned to Chrons C20n and C20r has one caveat in that it may contain artifacts introduced during the minicore drill-pressing process in this weakly magnetized soft–pliable chalk facies. We assigned polarity to each individual minicore on the basis of observed magnetic declination rotations and intensity changes during the progressive demagnetization. The majority of the characteristic declinations (after initial AF and thermal demagnetization steps) from Cores 207-1260B-9R and 10R and a significant number of those from Cores 207-1260A-18R and 19R are within 30° of a 180° direction and display horizontal to very low angle inclinations. In Ocean Drilling Program (ODP) coordinates, this corresponds to a magnetic vector directed along the axis of each minicore. It is common for ODP cores to have a downward magnetic overprint introduced during the main drilling process, and we are suspicious that this clustering of characteristic declinations near 180° direction might be an analogous artifact produced during the minicoring for this particularly soft chalk. However, an alternative explanation is a statistical coincidence in alignment of the rotated cores, and perhaps the sediment in each core did not experience any significant relative rotation among identified blocks. The apparent uniformity of the assigned polarity for the succession of minicores, as individually interpreted from declination and intensity behaviors during demagnetization, and the excellent apparent correlation of the polarity pattern with the expected biostratigraphic ages and relative widths of Chrons C21r–C18r support this alternative explanation, thereby implying that the polarity pattern is reliable.

The lower portion of the middle Eocene to the uppermost lower Eocene (~200–245 mbsf) is a reddish brown carbonate chalk with a relatively high magnetic intensity and susceptibility (Fig. F11). Applying a 10-mT demagnetization step reduced the magnetic intensity to less than half and removed a steep positive inclination that probably represents drilling-induced overprints. After this initial change, the magnetization of the reddish colored sediments displayed no significant difference in the intensity and inclination upon applying a 15-mT AF demagnetization and displayed a consistent positive inclination averaging 20° (Fig. F11). Thermal demagnetization of minicores was very effective in removing this AF-resistant overprint. The resulting polarity pattern is assigned to the lower portion of Chron C21n through the uppermost portion of Chron C22n (Fig. F12). Biostratigraphy indicates a hiatus spanning foraminifer Zone P9 and nannofossil Zone NP13 in the uppermost part of Section 207-1260A-25R-1, thereby causing an apparent juxtaposition of the normal polarity zones from uppermost Chron C22n (top of this section) and that of lower Chron C23n (lower sections).

The underlying lower Eocene clayey chalk is generally characterized by relatively weak intensity (~10^{-5}–10^{-4} A/m) and low susceptibility (Fig. F11). The paleomagnetism of the minicores yielded a pattern of

polarity zones that matches Chron C24r through Chron C23n (lower portion).

Paleocene

The upper Paleocene clayey nannofossil chalk is similar in its weak magnetic characteristics to that from the lowermost Eocene. The magnetostratigraphy was resolved from minicores. The polarity pattern and biostratigraphic constraints from the upper Paleocene match the lower portion of Chrons C26n–C24r. Apparent rapid polarity changes, coupled with apparent biostratigraphic gaps among foraminifer and nannofossil datums, preclude an unambiguous chron assignment to the minicore results from the lower Paleocene.

Campanian–Maastrichtian

The uppermost Maastrichtian reddish brown chalk displayed a normal polarity overprint that resisted shipboard AF demagnetization. Thermal demagnetization of minicores from this facies was effective in revealing the reversed polarity of Chron C29r.

The underlying Campanian–Maastrichtian white to greenish white chalk had weak magnetizations that generally approached the background noise level of the Munich cryogenic magnetometer upon heating >200°C. Very few minicores yielded reliable characteristic directions, and the polarity assignments of some intervals are uncertain (Fig. F12). The broad biostratigraphic constraints are inadequate to make assignments of polarity chrons to the strata older than Chron C31n.

Albian

The Albian quartz siltstone is characterized by relatively high intensity (~10^{-4}–10^{-3} A/m after 15-mT AF demagnetization) and high susceptibility. Application of 10-mT AF demagnetization removes a secondary component that was probably acquired during the drilling process. Applying an additional 15-mT AF step does not affect the remanent directions of the 10-mT step, which averaged +30° in inclination. Progressive thermal demagnetization of several minicores yielded normal polarity behaviors with well defined characteristic directions, but these inclinations are uniformly positive. The implied mean paleolatitude is ~15–20°N, which is slightly north of the present 9°–10° latitude of this site, is in conflict with paleogeographic reconstructions that project Site 1260 to have been near or south of the paleoequator during the mid-Cretaceous (C. Scotese, pers. comm., 2002). We suggest that the mid-Cretaceous reconstructions of the position of this portion of the South American margin requires further refinement in the paleolatitude constraints. In summary, Site 1260 yielded preliminary magnetostratigraphic patterns which, when combined with the shipboard paleontological constraints, can be unambiguously correlated to the biomagnetic polarity timescale for the late Paleocene–middle Eocene.

COMPOSITE DEPTHS

Coring at Site 1260 extended to a total depth of 507 mbsf. Moderate to poor core recovery in specific intervals between Holes 1260A and 1260B resulted in three discrete intervals suitable for constructing com-

posite sections. These intervals cover 65% of the cored interval at Site 1260. Magnetic susceptibility and gamma ray attenuation (GRA) bulk density were collected with the multisensor track (MST) at 2.5-cm intervals on all whole-core sections from Hole 1260A and 1260B. Natural gamma ray (NGR) data were collected at 7.5-cm intervals on all whole cores from Hole 1260A and from Cores 207-1260B-1R and 2R and from Section 12R-3 to the base of Hole 1260B. To maintain a reasonable processing rate in the core laboratory, NGR data were collected at 15-cm resolution from the top of Core 207-1260B-3R to the base of Section 12R-2, an interval that showed little structure in the NGR record in Hole 1260A. Noncontact resistivity (NCR) data were collected at 2.5-cm intervals from the top of Core 207-1260A-1R through Section 27R-3 and from the top of Core 207-1260B-1R through Section 12R-2 (see **"Physical Properties,"** p. 33, in the "Explanatory Notes" chapter for a discussion of problems associated with the calibration and accuracy of NCR data). Spectral reflectance data were collected at 2.5-cm intervals on all split cores. Spectral reflectance and GRA bulk density were the primary data sets used to correlate between holes in the middle Eocene section at Site 1260 (~38–133 mcd). From the lower Eocene to the top of the Cretaceous black shale sequence (~230–395 mcd), magnetic susceptibility was the primary data set used to correlate between holes. Within the black shales (~418–484 mcd), NGR and bulk density data provided the most reliable core-to-core comparisons.

Composite Section

The depth offsets that compose the composite section for Holes 1260A and 1260B are given in Table **T11.** In the middle Eocene interval (38–133 mcd), the GRA bulk density data and the color reflectance data provide an excellent record that seems to reflect the cyclic variation in carbonate and silica content. These data, combined with the good RCB recovery in Holes 1260A and 1260B, allowed the construction of a nearly continuous composite section in this interval. One core gap (near 57 mcd) was not bridged. The spectral reflectance ratio (680/430 nm) data used to construct the composite section over this interval are presented in Figure **F13.**

In the interval from the lower Eocene to the top of the Cretaceous black shales (230–395 mcd), core recovery was excellent and definitive hole-to-hole correlations were possible throughout the section using magnetic susceptibility data. The alignment of cores in Holes 1260A and 1260B, however, resulted in numerous core gaps that could not be bridged, making it impossible to construct a continuous section through the interval (Fig. **F14**). The absolute depth of composite section in this interval cannot be accurately determined because some coring gaps were not spanned and the cores in this interval cannot be definitely tied to the sections above and below.

The quasi-periodic variability of the claystone and chalks/limestone composing the black shales resulted in strong signal-to-noise ratios in both the GRA bulk density and NGR data sets (Fig. **F15**). These data sets, combined with good RCB recovery over a significant portion of the black shale interval, allowed for the construction of a nearly continuous composite section from 418 to 484 mcd. Only one core gap could not be bridged (between Cores 207-1260A-47R and 48R [436 mcd]) in this interval. Poor recovery from 394 to 418 mcd precluded the construction of a composite section in this interval of the Cretaceous black shales.

T11. Composite depth offsets, p. 95.

F13. Composite and spliced spectral reflectance, p. 54.

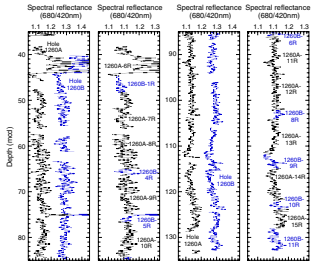

F14. Composite and spliced magnetic susceptibility, p. 55.

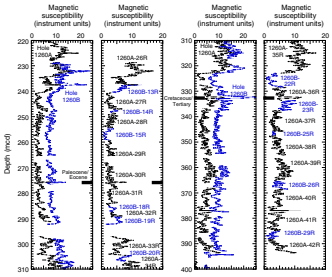

F15. Composite and spliced GRA bulk density, p. 56.

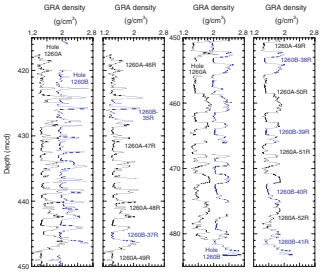

The periodic variability in the middle Eocene color reflectance and GRA bulk density data at Site 1260 will provide a good basis for postcruise cyclostratigraphic studies. Age control is excellent, with well-defined paleomagnetic datums in the section (e.g., Chrons C19n and C20n) (see "Paleomagnetism," p. 18). Preliminary investigation suggests the dominant periodicities of the magnetic susceptibility data are Milankovitch in nature.

Splice Record

Following construction of the composite depth section at Site 1260, three discrete splice records were assembled for the aligned cores in the intervals 38–133, 229–394, and 418–484 mcd (Table T12; Figs. F13, F14, F15). As discussed above, the middle Eocene (38–133 mcd) and black shale (418–484 mcd) splices are nearly continuous. The lower Eocene–Campanian splice (229–394 mcd) is discontinuous in nature but still provides a good record for most centimeter- to decimeter-scale studies and high-resolution centimeter-scale studies over shorter intervals. Figure F16 provides a qualitative estimate of the confidence of the core-to-core correlations and the resultant splices between cores in Holes 1260A and 1260B.

When utilizing these splices as sampling guides, it is advisable to overlap a few decimeters from different holes to accommodate anticipated postcruise revisions to the composite depth scale. The reason for this approach is that distortion of the cored sequence can lead to stretching or compression of sedimentary features. Because much of the distortion occurs in individual cores on depth scales of <9 m, it was not possible to align every feature in the MST and color reflectance records. However, at crossover points along the splice, care was taken to align highly identifiable features from cores in each hole. Postcruise work will establish a detailed correlation between holes by establishing a revised meters composite depth (rmcd) scale that allows differential stretching and squeezing within cores.

SEDIMENTATION RATES

Age-Depth Model

An age-depth model of Site 1260 was established by combining all available biostratigraphic and magnetostratigraphic datums of Hole 1260A (Fig. F17). The diagram was constructed by plotting highest and lowest possible ages for selected paleontological samples examined shipboard against the depth of those samples (Table T13). In addition, the age and depth of magnetic reversals recognized shipboard (Table T14) are also plotted.

The biostratigraphic resolution is limited in parts of the succession by moderate to poor preservation and/or the absence of certain taxa. In particular, the Turonian–Albian interval was difficult to date by means of shipboard samples. Interpretation of paleomagnetic data was ambiguous throughout much of Site 1260, resulting in reliable magnetostratigraphic datums (boundaries between periods of reversed and normal polarity) only for the middle Eocene and the Maastrichtian–early Campanian intervals (Table T14). The remainder of the recovered succession (the Coniacian–Albian) did not allow a magnetostratigraphic age as-

T12. Splice tie points, p. 96.

F16. Magnetic susceptibility data, p. 57.

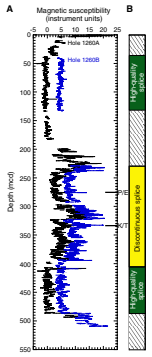

F17. Age-depth plot, p. 58.

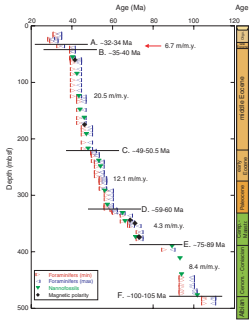

T13. Planktonic foraminiferal and calcareous nannofossil datums, p. 97.

T14. Magnetostratigraphic datums, p. 99.

signment because of the presence of the Long Normal Polarity Superchron C34n (~38 m.y.).

Sedimentation Rates

Linear sedimentation rates (LSRs) in Hole 1260A varied between 4.3 and 20.5 m/m.y. (Table T15). These rates are typical for pelagic chalks, which characterize the early Oligocene–Campanian interval (lithostratigraphic Units II and III) (see "Lithostratigraphy," p. 3). Hiatuses separate the section into five intervals, each with approximately constant sedimentation rates (Fig. F17). The Neogene, comprising only 1 m of the section, is not included in this tally. In addition, sedimentation rates were not calculated for the early Oligocene (Biozones P21a–P19 [1–28.8 mbsf]) because of significant reworking, which resulted in age inversions. The five intervals of approximately uniform sedimentation rates are the following:

1. Late Eocene (Biozone P16 [28.8–38.2 mbsf]): LSR = ~6.7 m/m.y.
2. Middle Eocene–early middle Eocene (Biozones P13–P10 [38.2–220.7 mbsf]): LSR = ~20.5 m/m.y.
3. Early Eocene–late Paleocene (Biozones P8–P4 [220.7–324.6 mbsf]): LSR = ~12.1 m/m.y.
4. Late Paleocene–late Campanian (Biozones P3a–KS28 [324.6–384.5 mbsf]): LSR = ~4.3 m/m.y.
5. Coniacian–Cenomanian (Biozone KS23–KS19–KS16 [384.5–491.41 mbsf; base of Hole 1260A]): LSR = ~8.4 m/m.y.

Mass accumulation rates (MARs) were calculated from LSRs and average dry bulk density data. For these five intervals (see "Physical Properties," p. 30) (Table T15), MAR calculations may allow for better assessment of the sedimentation processes because the influence of sediment compaction has been taken into account. Middle Eocene–late Paleocene MARs were relatively high and stable with values of 2.1 g/cm²/k.y., the highest values calculated at this site. Early Eocene–late Paleocene values are 1.6 g/cm²/k.y. Rates of 0.7 and 0.8 g/cm²/k.y. were observed for the Maastrichtian–Campanian and Coniacian–Cenomanian intervals, respectively.

Hiatuses

With current stratigraphic resolution, the succession seems to reflect intervals of approximately constant sedimentation separated by six distinct hiatuses, periods of slow deposition, erosional events, or a combination thereof (see letters A–F in Fig. F17). Each of these hiatuses comprises at least 1 m.y., based on biostratigraphic dating (see "Biostratigraphy," p. 11). Hiatus A spans ~2 m.y. (early Oligocene; Biozone P18), Hiatus B spans ~5 m.y. (late Eocene–middle Eocene; Biozones P14–P15), Hiatus C spans ~1.5 m.y. (early Eocene; Biozone P9), Hiatus D spans ~1 m.y. (late Paleocene; Biozone P3b), Hiatus E spans ~14 m.y. (early Campanian–Coniacian), and Hiatus F spans ~5 m.y. (late Albian).

T15. LSRs and MARs, p. 100.

ORGANIC GEOCHEMISTRY

Concentrations of calcium carbonate and TOC were determined on sediments from Holes 1260A and 1260B. Organic matter atomic carbon/nitrogen (C/N) ratios and Rock-Eval pyrolysis analyses were employed to assess the type of organic matter contained in the sediments. Routine monitoring of interstitial gas contents was performed for drilling safety, and possible microbial activity was assessed from headspace gas contents of Hole 1260A.

Inorganic and Organic Carbon Concentrations

Concentrations of inorganic carbon vary from virtually 0 to 11.6 wt% in sediments at Site 1260 (Table T16). These concentrations are equivalent to 0.1 to 96 wt% $CaCO_3$, assuming that all of the carbonate is calcite or aragonite. Carbonate concentrations of the five lithostratigraphic units (see "Lithostratigraphy," p. 3) generally decrease with greater depth. However, black shales in Unit IV still contain ~50 wt% carbonate, largely because calcite laminae are interspersed in this laminated unit.

TOC concentrations of sediments at Site 1260 have a wide range. Most of the sediments of lithostratigraphic Units I–III contain <0.1 wt% TOC (Table T16). In marked contrast, the black shales in Unit IV have TOC concentrations that average 7.2 wt% and reach as high as 13.9 wt%. A piece of carbonized wood was found in this unit; its TOC value is 55.9 wt% (Sample 207-1260B-39R-7, 29–30 cm). Unit V (calcareous siltstones) has TOC values that cluster at ~0.5 wt%, which is nearly twice that of the average deep-sea value of 0.3 wt% compiled by McIver (1975) from Deep Sea Drilling Project Legs 1–33, and this unit is therefore relatively rich in organic matter.

T16. Inorganic and organic carbon and total nitrogen, p. 101.

Organic Matter Source Characterization

Atomic $C_{organic}/ N_{total}$ ratios were employed to help identify the origins of the organic matter of Site 1260 sediments. Most of the C/N values in organic carbon–lean Units I–III are low (Table T16) and are below the range typical of fresh algal organic matter (4–10) (Meyers, 1997). These values are probably an artifact of the low TOC concentrations combined with the tendency of clay minerals to absorb ammonium ions generated during degradation of organic matter (Müller, 1977). Values of other samples are artificially elevated because their low amounts of C and N are near the limits of detection of the shipboard elemental analyzer.

The C/N ratios of the black shales in Unit IV average 33, which is a value usually considered typical of land-plant organic matter but that is also common to Cretaceous black shales (Meyers, 1997). A plot of hydrogen index (HI) and oxygen index (OI) values (Fig. F18) indicates that the black shales in Unit IV contain Type II (algal) organic matter that is thermally immature and relatively well preserved (Espitalié et al., 1977; Peters, 1986). The generally low T_{max} values of this unit (Table T17) confirm the thermal immaturity. Consequently, the elevated C/N values that mimic those of land-derived organic matter are likely to be the result of partial alteration of marine organic matter. A probable scenario is that nitrogen-rich components are preferentially degraded dur-

F18. Rock-Eval van Krevelen–type diagram, p. 59.

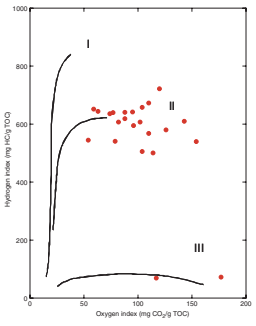

T17. Rock-Eval pyrolysis analyses, p. 104.

ing sinking of organic matter to the seafloor, thereby elevating the C/N ratio of the surviving organic matter (Twichell et al., 2002).

The C/N value of the carbonized wood in Sample 207-1260B-39R-7, 29–30 cm, is 81, which clearly identifies the organic matter of this sample as land-plant woody tissue (Meyers et al., 1995). A number of C/N values between 40 and 60 in the lower half of Units IV and V (Table T16) suggests some fraction of land-plant debris in these sequences.

Based on its low HI values (Table T17), organic matter in the lower Albian siltstones of Unit V is composed of Type III kerogen (Fig. F18). This type of kerogen appears to represent a mixture of degraded marine organic matter and detrital land-derived organic matter at Site 1260.

Interstitial Gas Contents

Sediments at Site 1260 have fairly low interstitial gas concentrations. Neither gas voids nor other evidence of gas release from cores was observed. A faint odor of hydrogen sulfide was noticeable in cores from the black shales in lithostratigraphic Unit IV (391–484 mbsf), but the natural gas analyzer, which has a sensitivity of ~1 ppmv, did not detect this gas in headspace samples.

Headspace gas results from routine safety monitoring and the special microbial gas study are similar (Fig. F19). Methane (C_1) first appears in the routine monitoring results at 273 mbsf. Concentrations increase to reach a broad maximum between 393 and 474 mbsf before decreasing with greater depth in the core. High methane/ethane (C_1/C_2) ratios and the absence of measurable amounts of higher molecular weight volatile hydrocarbons indicate that the origin of the methane is biogenic and not thermogenic (Table T18). A biogenic origin is also supported by the disappearance of interstitial sulfate at the same subbottom depth where methane concentrations begin to rise (see "Inorganic Geochemistry," p. 26); interstitial sulfate generally inhibits microbial methanogenesis (Claypool and Kvenvolden, 1983).

Interstitial gas concentrations and compositions were found to relate to lithology; concentrations consistently increase and abruptly peak in the black shales. The possible relation between sediment organic matter contents and gas concentrations was investigated by measuring the TOC concentrations of the headspace sediment samples from Holes 1259A, 1260A, and 1260B. A rough correspondence exists between higher TOC and larger gas concentrations (Fig. F20). Marked excursions from a simple linear relation suggest that organic matter quality, and not simply quantity, affect gas generation from the black shales. Moreover, dramatic changes in methane concentrations at lithologic boundaries (Fig. F19) suggest either that gas does not freely migrate from its origin in the black shales or that it migrates and is being quickly generated from the organic matter in this unit so that elevated concentrations are maintained.

F19. Headspace gas and microbial methane, p. 60.

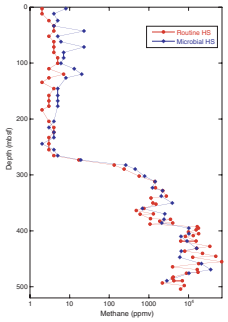

T18. Headspace analysis of gases, p. 105.

F20. TOC vs. interstitial methane, p. 61.

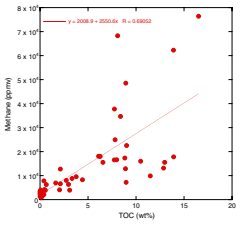

INORGANIC GEOCHEMISTRY

Interstitial water from 28 samples at Site 1260 were collected: 25 from Hole 1260A (0.58–490.50 mbsf) and 3 from Hole 1260B (451.36–508.58 mbsf). The samples from both holes were taken to constitute a single depth profile. However, slight differences in lithology may cause minor breaks in concentration-depth gradients of some chemical pa-

rameters. An incomplete data set exists for Sample 207-1260A-33R-1, 0–12 cm, because of low pore water yield (Table T19).

Alkalinity, chloride, ammonium, and silica were determined by the standard shipboard procedures (see "Inorganic Geochemistry," p. 31, in the "Explanatory Notes" chapter). The major ions Na, K, Mg, and Ca were analyzed by inductively coupled plasma–atomic emission spectroscopy (ICP-AES) after 50-fold sample dilution with deionized water. The minor components Li, B, Si, Fe, Mn, and Sr were determined by ICP-AES from 10-fold diluted interstitial water samples. From the minor component dilution, we determined sulfate as total sulfur by ICP-AES. Details of the methods, including the emission lines used for analysis, are given in "Inorganic Geochemistry," p. 31, in the "Explanatory Notes" chapter. Results of the chemical analyses are presented in Table T19 and in Figure F21.

T19. Pore water analyses, p. 107.

F21. Pore water chemical profiles, p. 62.

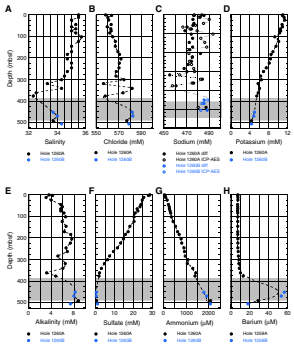

Black Shales as a Diagenesis Bioreactor

Interstitial water chemistry at Site 1260 is dominated by the black shales and associated organic matter–rich sediments. These sediments are of Cenomanian–Coniacian age (lithostratigraphic Unit IV [~390–475 mbsf]). Sulfate concentrations approach zero at the top of lithostratigraphic Unit IV (see Fig. F21F), and the gradient from the top of Unit III to the sediment/water interface is almost linear. These observations suggest the following:

1. Almost 100 m.y. after Unit IV was deposited, the organic matter–rich sediments continue to provide a suitable substrate for ongoing microbial activity.
2. Sulfate reduction is of minor importance at shallower depth intervals.
3. The resulting downhole profile is controlled by the existence of one major stratigraphic sink (Unit IV) and simple compensatory downward diffusion from the sediment/seawater interface in the absence of the accumulation of significant sediments younger than middle Eocene age (Fig. F10).

The modest departure from linearity in the sulfate concentration profile seen below ~250 mbsf may indicate sulfate reduction by the oxidation of methane. This interpretation is consistent with the sharp uphole decrease in methane concentrations recorded across the transition from lithostratigraphic Units IV–III. The two samples that we collected from the quartz siltstones of Albian age at the base of the site (lithostratigraphic Unit V) suggest that the black shale sequence may also be supplied by the diffusion of sulfate from below (Fig. F21F), as is the case at Site 1257.

At Site 1260, we detected no odor of hydrogen sulfide during core-splitting procedures on the catwalk, in contrast to Site 1257. Occasionally, however, an H_2S smell was detected from interstitial water whole rounds taken from lithostratigraphic Unit III during the routine scraping that is undertaken to remove contaminated material prior to squeezing. It is possible that pyrite formation in Unit III sediments is triggered by hydrogen sulfide diffusion upward from the Unit IV sediments, which are most likely Fe limited. Shore-based sulfur isotopic studies will help to test this hypothesis.

The reducing character of the sedimentary column is also seen in elevated Mn and Fe concentrations (Fig. F21O, F21P). At Site 1260, our

first sample (Sample 207-1260A-1R-1, 58–63 cm) was taken at a very shallow depth (0.58 mbsf) and captures the Fe and Mn concentration maxima (Fe = >50 µM and Mn = >10 µM, respectively) associated with organic matter respiration in the thin veneer of Holocene sediments that drape the outer Demerara Rise. The Fe profile shows broad secondary peaks between ~50 and 200 mbsf, but an obvious relationship with sediment color is absent. Very low Fe concentrations are attained in lithostratigraphic Unit III (clayey chalks of Campanian–Paleocene age) (**"Lithostratigraphy,"** p. 3).

With the exception of one questionable data point in our Fe profile (Fig. **F21O**), only very low pore water concentrations of the redox-sensitive metals are attained from lithostratigraphic Unit IV (Mn = <1 and Fe = 5 µM). The same is true of Unit V. A similar association between organic matter–rich sediments and low interstitial water concentrations of Mn and Fe was observed at the previous sites. Our favored working hypothesis for this observation is that these redox-sensitive metals were completely remobilized during or shortly after the host organic matter–rich units were deposited, implying conditions of severe synsedimentary oxygen depletion. Alternatively, the low pore water Mn concentrations observed in Units IV and V reflect the formation of Mn-rich carbonate phases (e.g., ankerite/rhodochrosite). Shore-based chemical analysis of the interstitial water "squeeze cakes" will provide a definitive test of these two competing hypotheses.

Sulfate depletion in pore water samples is accompanied by increases in ammonium (Fig. **F21G**), which is consistent with organic matter consumption. Ammonium concentrations decrease almost linearly from the deepest sample toward the sediment/seawater interface. The modest departure between this linear ammonium profile and the dissolved sulfate profile in lithostratigraphic Units III and IV is consistent with the hypothesis that sulfate reduction in Unit III proceeds by methane oxidation.

The complete absence of sulfate in Unit IV at Site 1260 most probably promotes the same two phenomena inferred from the data sets obtained at Sites 1257–1259: (1) mobilization of Ba and (2) formation of dolomite.

Background concentrations of Ba at Site 1260 are unrealistically high, implying an analytical baseline problem, but the form of the downhole pore water Ba profile, together with sedimentological evidence, indicates Ba mobilization from near the base of the black shale sequence. Authigenic barite crystals of millimeter to centimeter scale are frequently observed in the overlying Upper Cretaceous chalks (lithostratigraphic Unit III) (see **"Lithostratigraphy,"** p. 3). Similar sedimentological and mineralogical relationships are reported elsewhere (Brumsack, 1986; Torres et al., 1996).

The downhole interstitial water concentration profile for Mg is nearly linear from the sediment/water interface to the base of the drill hole at Site 1260. In contrast, the downhole interstitial water profile for Ca is nonlinear. Ca concentrations peak (~1.6 times seawater values) at ~200 mbsf, fall to lower values (~1.3 times seawater) near the base of lithostratigraphic Unit III, and then increase slightly to the base of the black shales (~1.4 times seawater) (Fig. **F21I**). At Sites 1257 and 1258, we interpreted a downhole decrease in dissolved Mg concentration in terms of dolomite formation in the sulfate reduction zone in the black shale sequence (Unit IV). Unfortunately, the gap in our sampling between ~375 and 450 mbsf does not allow us to determine whether the same is true at Site 1260.

The nonlinearity of the Ca profile from the base of Unit III to the sediment/water interface indicates carbonate diagenesis in sediments of Late Cretaceous and Paleogene age as deduced from associated trends in alkalinity (Fig. F21E). The alkalinity and Ca concentration depth profiles show a particularly pronounced structure in lithostratigraphic Unit III (clayey chalks of Campanian–Paleocene age). This general association between these interstitial water chemistry parameters and sediment $CaCO_3$ content (see Fig. F4) is similar to that seen at Site 1258 and implies some local control by ongoing carbonate dissolution and reprecipitation reactions. On the other hand, the downhole dissolved Sr and ammonium profiles, which are widely thought to be sensitive proxies for recrystallization of biogenic carbonate and organogenic bicarbonate, show minimal local control. Instead, we see near-linear downhole increases in both parameters, indicating sources at depth and simple diffusion to the sediment/water interface (Fig. F21J). One interpretation of the decoupled behavior between these parameters (Ca and alkalinity vs. Sr and ammonium) is that carbonate diagenesis in the Upper Cretaceous chalks (Unit III) is dominated by calcite precipitation fed by chemical diffusion from below rather than dissolution or in situ recrystallization. In fact, the form of the Sr pore water depth profile (Fig. F21J) suggests that the main locus of carbonate recrystallization most likely lies below the strata that we drilled at Site 1260. We interpret the simple diffusion-dominated Sr and ammonium profiles to reflect minimal accumulation of sediments younger than middle Eocene age (see Fig. F10). Similar findings have been reported from Blake Nose, where Eocene-age sediments crop out at the seafloor (Rudnicki et al., 2001). Average linear pore water Sr depth gradients (~2 µM/m) are lower than those seen at Sites 1257 and 1259 (~5 and ~3 µM/m, respectively) and those at Site 1258 (~1 µM/m) and in the range of many Deep Sea Drilling Project/ODP sites (Rudnicki et al., 2001).

Dissolved silica concentrations at Site 1260 are relatively high from ~40 to 300 mbsf and thus do not correspond to the abundance of biogenic Si as recorded in the lithostratigraphy at the site (Fig. F4). As is the case at other Leg 207 sites, the clay-rich Paleoecene and Albian sediments both above and below the black shale sequence appear to serve as a sink for K (Fig. F21D). In fact, significant parallels exist between the K and Mg profiles at Site 1260. This observation suggests that clays may act as an important sink for Mg at the site.

Low Salinity/Chlorinity Anomalies

Two relatively low salinity and Cl concentration anomalies occur in lithostratigraphic Unit III at Site 1260. The first anomaly occurs at ~318 mbsf, and the second one occurs at ~375 mbsf (Fig. F21A, F21B). These anomalies are in contrast to our findings at Sites 1257 and 1259, where we infer the presence of a brine in the black shale sequence of lithostratigraphic Unit IV but in remarkable accordance with the Cl profile above the black shale sequence at Site 1258 (see Fig. F20B, p. 67, in the "Site 1258" chapter). Both of the low Cl concentration anomalies at Site 1260 are paralleled by Na, and the average Na/Cl ratio at the site is 0.84, which is very close to the International Association for the Physical Sciences of the Ocean (IAPSO) seawater value of 0.86. The two Cl minima (<560 mM) indicate near-seawater concentrations, which is a small (<4%) freshening relative to the highest Cl concentrations measured at the site. At Site 1258, the Cl anomalies in lithostratigraphic Unit III implied a similar degree of freshening but overall absolute Cl concentra-

tions are significantly lower (less than seawater) than at Site 1260 (see Fig. F20B, p. 67, in the "Site 1258" chapter). Furthermore, at Site 1258, a much larger interstitial water Cl anomaly is seen below the black shale sequence (~17% freshening relative to seawater). Unfortunately, the two samples that we collected from the Albian quartz claystones at the base of the site (lithostratigraphic Unit V) do not lie far enough below Unit IV to determine whether the same is true at Site 1260 (Fig. F21B). Taken alone, the modest Cl anomalies seen in Figure F21 would not invite extensive comment, but the parallels between the pore water Cl profiles at Sites 1260 and 1258 are striking. Significant concentrations of CH_4 in headspace gas analyses (>50,000 ppmv) (see "Organic Geochemistry," p. 25) are consistent with the anomalies having been caused by dissociation of gas hydrates (see "Inorganic Geochemistry," p. 26, in the "Site 1258" chapter). Alternative explanations for the Cl anomalies are clay dehydration reactions and dilution by meteoric water. The former possibility seems unlikely given the lithologies encountered, but the latter possibility cannot be excluded even though the nearest landmass is located >300 km away. Li pore water concentrations show significant elevation at Site 1260 (Fig. F21L), suggesting that the association between high Li concentrations and the brines of the black shale sequence at Site 1257 may be coincidental, but the cause of these significant Li anomalies remains enigmatic.

In summary, the interstitial water chemistry profiles from Site 1260 primarily reflect ongoing organic matter diagenesis in the black shales and carbonate diagenesis. In sharp contrast to our findings at Sites 1257, 1259, and 1261 where lithostratigraphic Unit IV appears to act as an aquifer for fluids of relatively high salinity, we observe relatively low salinity and chlorinity anomalies in lithostratigraphic Unit III at Site 1260 that are strikingly parallel in form to those observed at Site 1258. We hypothesize that these anomalies are caused by either gas hydrate dissociation or dilution by meteoric water.

PHYSICAL PROPERTIES

Physical property measurements at Site 1260 were conducted on whole cores, split cores, and discrete samples. Whole-core measurements, conducted with the MST include GRA bulk density, magnetic susceptibility, and NGR. Compressional (*P*)-wave velocity was measured in the transverse direction on split cores at intervals of 50 cm and along both transverse and longitudinal directions on cube samples taken at a frequency of one per core in Hole 1260B. Moisture and Density (MAD) properties were determined on discrete samples at a frequency of one per section from Hole 1260A to the depth of the Cretaceous black shale sequence. MAD measurements in the black shale sequence were performed on samples from Hole 1260B at a frequency of one per core. Sampling for MAD was minimal across critical intervals. A full description of the various measurement techniques can be found in "Physical Properties," p. 33, in the "Explanatory Notes" chapter.

Density and Porosity

MAD measurements at Site 1260 include bulk density, porosity, grain density, water content, and void ratio (Table T20). Bulk density was determined on whole-core sections using the MST (GRA density) and on discrete samples. GRA tends to underestimate the bulk density in RCB

T20. MAD properties of discrete samples, p. 108.

cores because the core material does not completely fill the inner diameter of the liner. At this site, the average difference between GRA and discrete sample density is 0.12 g/cm³. Despite this offset, the downcore bulk density trends derived by the two methods are essentially the same (Fig. F22).

Three distinct downhole trends are seen in the MAD profile (Fig. F23). Between 0 and 37 mbsf (0–37 mcd) (lithostratigraphic Unit I and Subunit IIA), bulk density decreases slightly from 1.8 to 1.6 g/cm³ and porosity increases from 50% to 60%. Grain density values are highly variable and increase marginally with depth. This interval is a mass-failure deposit (see "Biostratigraphy," p. 11, and "Lithostratigraphy," p. 3).

The boundary between Subunits IIA and IIB coincides with a step decrease in bulk density from 1.6 to 1.4 g/cm³ and an increase in porosity from 60% to 68%. Between 37 and ~380 mcd, bulk density increases linearly from 1.65 to 1.8 g/cm³ and porosity decreases from 70% to 40%. Average grain density (2.7 g/cm³) remains constant throughout the interval. These downhole trends are typical of normally consolidated sediments. In Subunit IIB, from 37 to 175 mcd, MAD data (especially grain density) are characterized by high variability, reflecting frequent variations in carbonate content and radiolarian abundance. Variability is low in Subunit IIC, with nearly constant grain density and no deviation of bulk density and porosity values from their respective downhole trends. At ~276 mcd, just above the P/E boundary, the general trend is perturbed by a drop in bulk density and an increase in porosity similar to that found at the other sites over this interval, but of lower magnitude. In Subunits IIIA and IIIB from 276 to 390 mcd, variability in bulk density and porosity increases, reflecting frequent cyclic variations in color and hardness of the sediment.

The transition to Unit IV corresponds to the largest change in the MAD depth profile. Bulk density drops from 2 to 1.7 g/cm³ and grain density from ~2.6 to ~2.2 g/cm³, whereas porosity increases from 40% to 60%. Based upon the limited MAD data in this unit, variability in bulk density and porosity values is extremely high, reflecting cyclic changes in lithology between claystone and limestone. In Unit V, MAD values are nearly constant with depth, with an average bulk density of 2.1 g/cm³, an average grain density of 2.7 g/cm³, and an average porosity of 30%.

Acoustic Velocity

P-wave velocity was measured on split cores using the modified Hamilton Frame apparatus. In addition, measurements of transverse (x- and y-direction) and longitudinal (z-direction) velocity were conducted on cube samples from Hole 1260B (Table T21).

Acoustic velocities tend to increase downhole, with peaks at overconsolidated or lithified intervals (Fig. F24). The general depth trend correlates directly with bulk density and inversely with porosity. Between 0 and 37 mcd (Unit I and Subunit IIA), in *P*-wave velocity increases sharply from ~1500 to ~1800 m/s. A drop in *P*-wave velocity magnitude to ~1500 m/s marks the transition to Subunit IIB. From 37 to 276 mcd (Subunits IIB and IIC), *P*-wave velocity increases linearly from ~1500 to ~1980 m/s, reflecting the normal consolidation trend seen in the bulk density and porosity data. Beginning at the depth of the P/E boundary (276 mcd) and throughout Subunit IIIA, velocity de-

F22. Discrete and MST-GRA bulk density, p. 64.

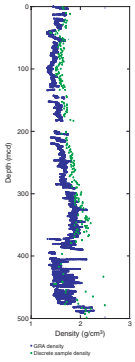

F23. Bulk density, grain density, and porosity, p. 65.

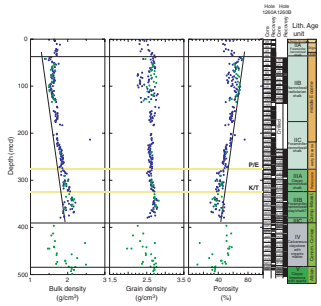

T21. Velocity measurements, p. 112.

F24. Bulk density and velocity, p. 66.

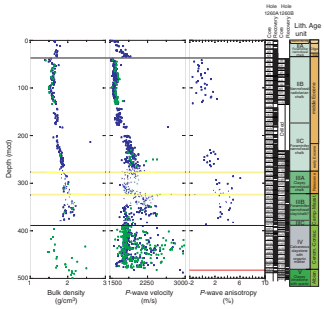

creases slightly with depth. Cyclic variations in velocity ranging between 1800 and 2000 m/s correspond to color changes in the unit between dark and light intervals, respectively.

The K/T boundary at 329 mcd marks a major offset in *P*-wave velocity values. Similar offsets are not seen in bulk density or porosity profiles. Throughout Subunits IIIB and IIIC (379–390 mcd), the variations in *P*-wave velocity continue, reflecting cyclic lithologic alternations between dark clay-rich intervals and light-colored cemented intervals.

In Unit IV (black shale sequence), velocity values in the organic-rich shales are nearly constant with depth, averaging 1800 m/s, whereas the cemented limestone velocities vary between 2100 and >3000 m/s (Fig. F25).

Velocity is isotropic from 0 to ~150 mcd, with <1% difference between longitudinal and transverse directions. Below ~150 mcd, the sediment develops a small degree of *P*-wave velocity anisotropy with higher velocities in the transverse direction. The development of anisotropy correlates with an increase in clay content. The higher clay content allows the development of a preferred orientation, perpendicular to overburden pressure, in sediment grain fabric and hence to different velocities in the transverse and longitudinal direction.

F25. *P*-wave velocity and MST data, p. 67.

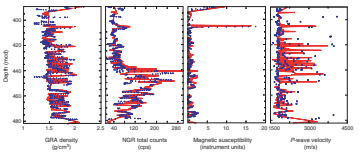

Whole-Core Multisensor Track

MST data from the two holes at Site 1260 have similar trends throughout the defined lithostratigraphic units once mbsf has been translated into mcd (see "Composite Depths," p. 21). Unit I and Subunit IIA are characterized by moderately high NGR emissions (~10 cps) and a low magnetic susceptibility signature (~2–5; magnetic susceptibility values are reported here as raw instrument units. See "Physical Properties," p. 33, in the "Explanatory Notes" chapter for conversion of this data to SI units). Both NGR emission and magnetic susceptibility decline to values close to background in Subunit IIB.

In Subunit IIC, NGR and magnetic susceptibility depth profiles are characterized by a pronounced peak at ~240 mcd. The P/E boundary is recorded as a spike in both NGR emissions and magnetic susceptibility measurements at ~276 mcd and also as a sharp decrease in the carbonate record (Figs. F26, F4).

Between 276 and 323 mcd (Subunit IIIA), magnetic susceptibility and NGR emissions gradually increase, reaching a maximum at 323 mcd before a significant drop coincident with the K/T boundary. In Subunits IIIB and IIIC, the NGR data increase linearly with depth whereas the magnetic susceptibility profile is characterized by cyclic variations.

The laminated shales of Unit IV show a high degree of variation in GRA density and NGR emissions, similar to those observed in *P*-wave velocity (Fig. F25). Susceptibility remains low through the laminated shale sequence relative to the overlying sediment, increasing in variability and magnitude after the transition into Unit V. Density generally increases with depth in Unit IV. Alternation of organic-rich layers and highly lithified and cemented layers is responsible for the scatter in the GRA, NGR, and *P*-wave velocity data throughout Unit IV. NGR emissions peak at ~440 mcd, reaching values as high as 280 cps (Fig. F25), which is probably a result of uranium enrichment in the organic-rich intervals.

F26. MST data with lithostratigraphic units, p. 68.

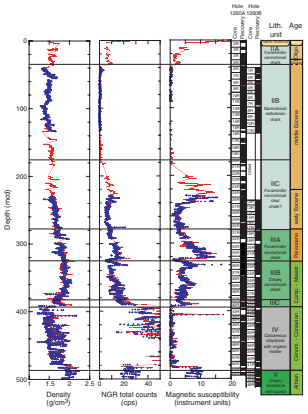

DOWNHOLE LOGGING

Following completion of RCB coring operations in Hole 1260B, the hole was conditioned with a wiper trip and pumped with sepiolite mud. The drill pipe was set at 90 mbsf for all passes except the first, when it was pulled to 80 mbsf. The following three tool strings were run:

1. The triple combo) with the Lamont-Doherty Earth Observatory Temperature/Acceleration/Pressure (TAP) tool and MGT;
2. The FMS-sonic tool string; and
3. The WST for a checkshot survey (see "Downhole Logging," p. 39, in the "Explanatory Notes" chapter for further tool specifications).

The wireline heave compensator (WHC) was used on all passes, with heave varying between 1.3 and 2.0 m throughout the operation. The first tool string run was the triple combo, which was successfully lowered to the bottom of the hole at 515 mbsf logging depth (drillers depth = 509 mbsf). Two full logging-uphole passes were made with the triple combo, the first to seafloor. Following this run, control of the wireline passed to the downhole measurements laboratory and the MGT was powered up and stabilized. Two full passes (the bottom of the hole was reached on both passes) were made with the MGT. The second tool string, the FMS-sonic, was successfully run to the bottom of the hole. Two full passes were at maximum FMS recommended speed (548.6 m/hr). The WST was the final tool string. It was run successfully to the bottom of the hole and acquired a total of 14 checkshot stations at ~30-m spacing.

In summary, three tool strings were run during the logging operation, with seven separate logging passes. All passes were from total depth into the pipe, providing a logged section of 425 m (Fig. F27). The wireline depth to seafloor was set at 2553 mbrf, determined from the step increase in gamma ray counts found at the sediment/seafloor interface, recorded on the first pass of the triple combo. The official ODP depth to seafloor was 2560 mbrf. Thus, there is a 7-m offset between the core and logging depths. In all of the chapter diagrams, the core recovery and lithostratigraphic units have not been depth shifted, giving an apparent 7-m depth mismatch.

Data Quality

Borehole diameter can affect the response of some tools, for example the Hostile Environment Litho-Density Tool (HLDT) and Accelerator Porosity Sonde (APS), so the size and shape of the borehole are important when interpreting the quality of logging data. The caliper logs from the triple combo (one per pass) and the FMS-sonic (two per pass) tool strings provide information on the borehole size (Fig. F28). The borehole conditions as indicated by the caliper logs were excellent. From the pipe (90 mbsf) down to 450 mbsf, the hole diameter varies little, from 450 to 485 mbsf the hole widens out and then narrows again, and below 485 mbsf it remains constant, punctuated only by a few washouts/breakouts. Everywhere, the borehole diameter is less than the maximum extension of the FMS-sonic calipers (15.5 in; 39.4 cm). Because of excellent borehole conditions and successful heave compensation, the processed FMS data are good throughout the logged formation. Caliper data from both the FMS-sonic and triple combo tool

F27. Summary of logging runs, p. 69.

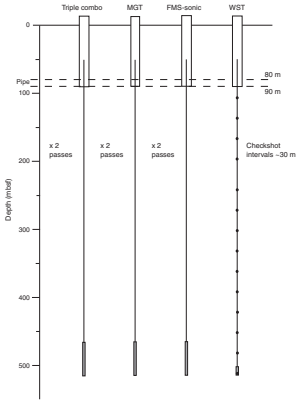

F28. Borehole caliper logs, p. 70.

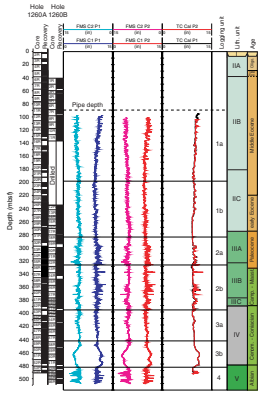

strings indicate hole enlargements at ~9.5-m intervals from 100 to 250 mbsf (Fig. F28) and from 300 to 430 mbsf. These data indicate borehole enlargement due to incomplete active heave compensation of the drill pipe, which is exacerbated during drill pipe addition and core barrel recovery and reload. Any time-series analyses on logging data from tools susceptible to borehole diameter effects that show cycles corresponding to 9- to 10-m or 5-m wavelengths (where short cores were taken) should be treated with caution.

Data from the triple combo tool string are good, with excellent repeatability and only minor (<1 m) depth mismatches between passes. Gamma ray data from the Hostile Environment Gamma Ray Sonde (HNGS), MGT, and Scintillation Gamma Ray Tool (SGT) are also well matched in depth and magnitude, making depth matching the MGT and FMS-sonic logging runs to the first pass of the triple combo tool string straightforward.

Core physical property data provide a rapid method for visualization of the core-log correlation (Fig. F29). Drilling ahead with selective coring resulted in a lack of core data from Hole 1260B, which has been supplemented with core data from Hole 1260A. The core density and porosity data from the index property measurements are close to logging values. Small offsets may be related to unloading effects in the cores. Core velocities, measured directly on the core with the modified Hamilton Frame, are less than the logging values. This observation is interpreted to result from either sampling (removal from in situ conditions) and/or an overestimation of formation velocities by the Long Spacing Sonic (LSS) logging tool (see **"Checkshot Survey and Synthetic Seismogram,"** p. 37). Core gamma ray values underestimate the logging values. The depth match between logging mbsf and core data are excellent when the core depths are corrected (7-m downhole shift).

Logging Stratigraphy

Four logging units have been defined for Hole 1260B.

Unit 1 (base of pipe [80 mbsf]–285 mbsf)

Unit 1 is characterized by a downhole increase in density (covarying with porosity) and velocity logs (Fig. F30). The porosity and gamma ray logs display cyclicity. This logging unit is further divided into two subunits.

Subunit 1a (80–199 mbsf)

Density (porosity covarying) and velocity increase steadily downhole through this subunit (Fig. F30) and show only small-scale fluctuations. Porosity decreases downhole, as expected, and displays high-amplitude cyclicity. The high-resolution MGT gamma ray log also displays cyclicity through this subunit. The increase in density is manifest in the borehole caliper logs as a gradual narrowing of the borehole. The density gradient likely results from normal consolidation as there is no concomitant increase in carbonate content (see **"Organic Geochemistry,"** p. 25) or clay content (see the gamma ray spectrum on Fig. F31). The base of this subunit is marked by a short-lived peak in resistivity, density, and velocity (Fig. F30). The FMS images indicate a 13.5-m-thick region of higher resistivity, containing 15 distinct high-resistance bands varying from ≥1 to ~20 cm thick (Fig. F32). The photoelectric effect (PEF) log indicates a peak in carbonate levels through this interval but

F29. Core vs. logging physical properties, p. 71.

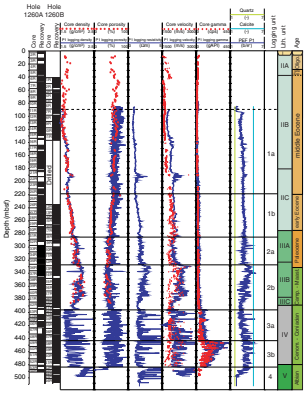

F30. Geophysical logs, p. 72.

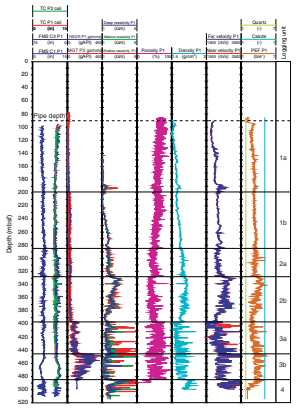

F31. High-resolution MGT logs, p. 73.

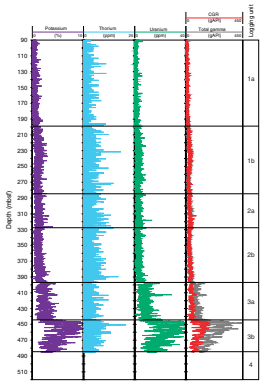

with increased amplitude variation between high and low carbonate levels. Core was only recovered from the topmost part of this interval and indicates chert nodules (see "Lithostratigraphy," p. 3). Based on the core and logging descriptions, this interval appears to be a carbonate-cemented zone with layers of chert or carbonate and chert nodules. The logging Subunit 1a/1b boundary is equivalent to the change from lithostratigraphic Subunits IIB/IIC.

Subunit 1b (199–285 mbsf)

Density (porosity covarying) and velocity continue to increase downhole to the bottom of the unit (Fig. F30). Gamma ray counts increase across the top of Subunit 1b and continue rising to ~240 mbsf, when they begin to fall (Fig. F31). Resistivity stays low in the top part of the unit but begins to increase from 230 mbsf to the bottom of the subunit (Fig. F30). Porosity and gamma ray logs display cyclicity down to the submeter scale. The change in density appears to follow a normal consolidation line, showing little correlation with changes in carbonate (see "Organic Geochemistry," p. 25) or clay content.

Unit 2 (285–397 mbsf)

The top of Unit 2 is best seen as a peak in the gamma ray log and a step in the porosity log (Fig. F30). This change is close to the P/E boundary (see "Biostratigraphy," p. 11) and the change from lithostratigraphic Units II to III (see "Lithostratigraphy," p. 3). Resistivity, density, and velocity values all show increased amplitude fluctuations throughout this unit (Fig. F30), clearly distinguishing it from Unit 1. Porosity and gamma ray logs have well-developed cyclicity. The logging unit is further subdivided into two subunits.

Subunit 2a (285–328 mbsf)

Gamma ray counts, resistivity, density (covarying porosity), and velocity values all gradually increase downhole in Subunit 2a (Figs. F30, F31). Porosity and gamma ray logs display well-developed cyclicity, which is also observed in both FMS dynamic and static images (Fig. F33). The variability of the logs in this subunit presumably reflects concomitant fluctuations in depositional processes (see "Lithostratigraphy," p. 3). Density continues to increase along what appears to be a normal consolidation line (Fig. F30). The base of the subunit is marked by a peak–trough couplet seen in all the logs. The subunit lower boundary correlates with the lithostratigraphic Subunit IIIA/IIIB boundary (see "Lithostratigraphy," p. 3).

Subunit 2b (328–397 mbsf)

Resistivity, density, and velocity values increase rapidly from the top boundary of Subunit 2b, with a concomitant decrease in porosity and gamma ray counts. There is a marked peak in porosity, a trough in resistivity, density, and velocity, and a low resistivity region in the FMS imagery at 339 mbsf (Fig. F34), correlating with the location of the K/T boundary. Below the K/T boundary, resistivity decreases gradually downhole. Density and velocity fluctuate about a relatively constant average, punctuated by a small increase between 370 and 378 mbsf, before dropping off rapidly in the lowest 12 m of the subunit (Fig. F30). Porosity and gamma ray values increase continuously downhole, still displaying cyclicity down to the submeter scale (Figs. F30, F31). Resistivity, density, and velocity all show increased amplitude fluctuations compared with Subunit 2a above. The increase in resistivity, density,

F32. FMS images, p. 74.

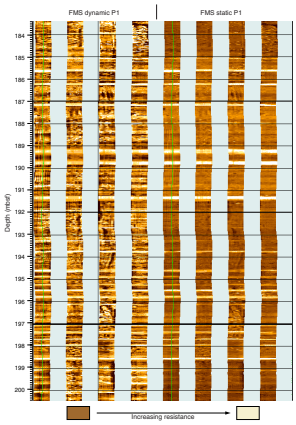

F33. Cyclic variations in sedimentation, p. 75.

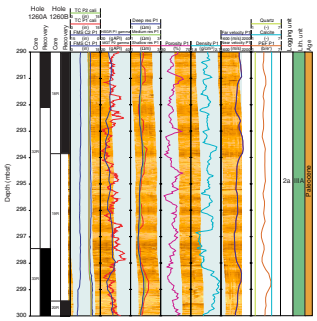

F34. Logging and FMS imagery, p. 76.

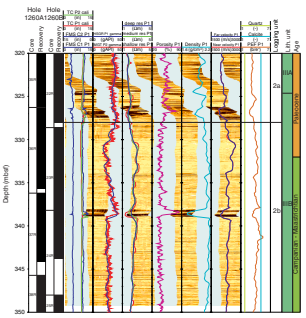

and velocity are linked to a higher carbonate content than in the subunit above (see "Organic Geochemistry," p. 25), which is also indicated by the PEF log (Fig. F30). The base of this subunit correlates with the base of lithostratigraphic Subunit IIIC (see "Lithostratigraphy," p. 3).

Unit 3 (397–485 mbsf)

Logging Unit 3 is characterized by a large increase in gamma ray and porosity log values, with a concomitant decrease in the density and velocity (Fig. F30). The gamma ray spectrum (Fig. F31) reveals the source of increased gamma ray emission to be dominantly uranium (organic matter), with some contribution from potassium (clay). The high organic content indicated by the uranium contribution to the gamma ray spectrum is corroborated by correlation of logging Unit 3 with lithostratigraphic Unit IV (calcareous claystone with organic matter) (see "Lithostratigraphy," p. 3, and "Organic Geochemistry," p. 25). Large-amplitude fluctuations are observed in all the logs and are interpreted to result from periodic cemented layers, giving peaks in density (troughs in porosity), resistivity, and velocity, and are highlighted in Figure F35. The PEF log indicates that the layers are calcite cemented (calcite photoelectron absorption cross-section index [*Pe*] = 5.08 b/e$^-$) (Fig. F33). Unit 3 is further subdivided into two subunits (Figs. F30, F31, F35).

Subunit 3a (397–445.5 mbsf)

Subunit 3a is characterized by lower total counts and lower-amplitude fluctuations in the gamma ray logs (Figs. F31, F35). The converse is observed especially in the resistivity, density, and velocity logs (Figs. F30, F35).

Subunit 3b (445.5–485 mbsf)

The top of the subunit is marked by a large increase in the amplitude of gamma ray fluctuations and in the overall counts, which subsequently fall continuously to the base of the unit (Figs. F30, F32, F35). Average resistivity and velocity values drop marginally (Figs. F30, F35), whereas density shows a small increase downhole as does the PEF log (Figs. F30, F35), indicating an increased carbonate content that is corroborated by geochemical analyses (see "Organic Geochemistry," p. 25).

Unit 4 (485 mbsf–total depth [515 mbsf])

The top of Unit 4 is defined by a sharp increase in resistivity, density (porosity covarying), and velocity (Figs. F30, F35). Resistivity, density, and velocity then decrease (as does the PEF log), indicating decreasing carbonate content. The FMS images highlight 10 prominent high-resistivity cemented layers, the thickest being 0.4 m. Gamma ray counts are still high, reflecting the high clay content (see "Lithostratigraphy," p. 3). This unit correlates with lithostratigraphic Unit V (see "Lithostratigraphy," p. 3).

Discussion

Excellent hole conditions (mostly just beyond bit size) combined with good heave compensation led to the acquisition of high-quality

F35. Stratigraphy of the black shales, p. 77.

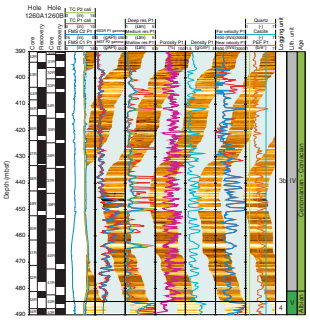

logging data. For the most part, the logging units described above correlate well with the designated lithostratigraphic units (see "Lithostratigraphy," p. 3).

Total Organic Carbon

The continuous data derived from the logs through the black shale interval (logging Unit 3) provide the opportunity for estimation of the TOC content in this unit. The result is only approximate because the shale porosity is assumed to equate to that of the sediments above and values for some densities (e.g., organic matter) that are not well constrained are also assumed. Following Rider (1996), the following three equations are used to calculate the TOC:

$$\phi_{fl} = (\rho_{bk} - \rho_{ma})/(\rho_{fl} - \rho_{ma}),$$

$$\phi_{om} = (\rho_{bs} - \rho_{bk})/(\rho_{om} - \rho_{ma}), \text{ and}$$

$$\text{TOC (wt\%)} = [(0.85 \times \rho_{om} \times \phi_{om})/(\rho_{om} \times \phi_{om}) + \rho_{ma}(1 - \phi_{om} - \phi_{fl})] \times 100\%,$$

where

- ρ_{bk} = density of the background sediment from the density log (1.938 g/cm³).
- ρ_{bs} = density of the black shale interval from the density log.
- ρ_{om} = density of the organic matter (assumed) (1.15 g/cm³).
- ρ_{ma} = density of the matrix (grain density) averaged from five MAD measurements (2.441 g/cm³).
- ρ_{fl} = density of seawater (1.05 g/cm³).
- ϕ_{fl} = water-filled porosity.
- ϕ_{om} = volume fraction of organic matter.

The results are plotted along with values measured on core samples from Holes 1260A and 1260B (see "Organic Geochemistry," p. 25) and are shown in Figure F36. The core depths have been depth shifted but are not depth matched to the logs. The results are good in terms of the magnitudes of TOC.

F36. Core vs. logging-derived TOC, p. 78.

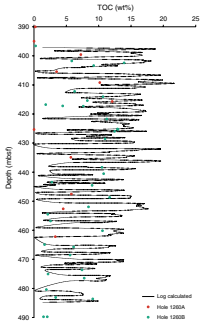

Checkshot Survey and Synthetic Seismograms

A checkshot survey was conducted during logging operations in Hole 1260B, and 14 stations were collected, using a series of stacked shots at 30-m intervals up the borehole (Fig. F27). The checkshot survey provides a direct measure of acoustic traveltime (Table T22) and thus formation velocity. Conversion of these traveltimes to interval velocities allows checkshot data to calibrate the velocity log. For most checkshot locations, the logging velocity is higher than the measured interval velocity by ~100 m/s. To compute a synthetic seismogram, formation density and velocity profiles are needed. Wireline logging provided density and velocity logs from the bottom of the hole up to pipe depth (90 mbsf). The wireline velocity data were corrected by –100 m/s. Density and velocity data for the remainder of the formation, above the pipe, were obtained from MAD property (bulk density) and Hamilton Frame (PWS3 velocity) measurements (see "Physical Properties," p. 30). Core velocities were also corrected for in situ temperature and

T22. Checkshot data and velocities, p. 113.

pressure. Downhole impedance was calculated from velocity × density, and the impedance contrast between successive layers gave the reflection coefficient series (Fig. **F37**). An idealized Ormsby wavelet was convolved with the reflection coefficient series to generate the synthetic seismogram (Fig. **F38**). The synthetic seismogram matches accurately to the seismic data, which allowed Reflectors A, B, B′, and C to be accurately identified. Reflector C represents the base of the black shales, unconformably overlying the middle–late Albian synrift sediments. Reflector B′ ties to the top of the black shale sequence (397 mbsf), and Relector B matches the density and velocity step at 330 mbsf just below the logging Subunit 2a/2b boundary, equivalent to lithostratigraphic Subunits IIIA and IIIB (see **"Lithostratigraphy,"** p. 3). Reflector A correlates with the middle–upper Eocene hiatus (see **"Biostratigraphy,"** p. 11), equivalent to the lithostratigraphic Subunit IIA/IIB boundary (see **"Lithostratigraphy,"** p. 3).

F37. Density, velocity, impedance, and reflection profiles, p. 79.

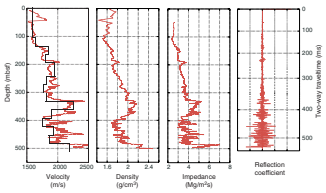

F38. Seismic line M49-4-GeoB215, p. 80.

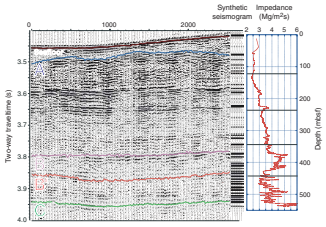

REFERENCES

Brumsack, H.-J., 1986. The inorganic geochemistry of Cretaceous black shales (DSDP Leg 41) in comparison to modern upwelling sediments from the Gulf of California. *In* Summerhayes, C.P., and Shackleton, N.J. (Eds.), *North Atlantic Palaeoceanography.* Geol. Soc. Spec. Publ., 21:447–462.

Claypool, G.E., and Kvenvolden, K.A., 1983. Methane and other hydrocarbon gases in marine sediment. *Annu. Rev. Earth Planet. Sci.,* 11:299–327.

Dickens, G.R., 2000. Methane oxidation during the Late Palaeocene Thermal Maximum. *Bull. Soc. Geol. Fr.,* 171:37–49.

Espitalié, J., Laporte, J.L., Madec, M., Marquis, F., Leplat, P., Paulet, J., and Boutefeu, A., 1977. Méthode rapide de caractérisation des roches mères, de leur potentiel pétrolier et de leur degré d'évolution. *Rev. Inst. Fr. Pet.,* 32:23–42.

Martini, E., 1971. Standard Tertiary and Quaternary calcareous nannoplankton zonation. *In* Farinacci, A. (Ed.), *Proc. 2nd Int. Conf. Planktonic Microfossils Roma:* Rome (Ed. Tecnosci.), 2:739–785.

McIver, R.D., 1975. Hydrocarbon occurrences from JOIDES Deep Sea Drilling Project. *Proc. Ninth Petrol. Congr.,* 269–280.

Meyers, P.A., 1997. Organic geochemical proxies of paleoceanographic, paleolimnologic, and paleoclimatic processes. *Org. Geochem.,* 27:213–250.

Meyers, P.A., Leenheer, M.J., and Bourbonniere, R.A., 1995. Diagenesis of vascular plant organic matter components during burial in lake sediments. *Aquatic Geochem.,* 1:35–42.

Müller, P.J., 1977. C/N ratios in Pacific deep sea sediments: effect of inorganic ammonium and organic nitrogen compounds sorbed by clays. *Geochim. Cosmochim. Acta,* 41:765–776.

Peters, K.E., 1986. Guidelines for evaluating petroleum source rock using programmed pyrolysis. *AAPG Bull.,* 70:318–329.

Rider, M.H., 1996. *The Geological Interpretation of Well Logs* (2nd ed.): Caithness (Whittles Publishing).

Rudnicki, M.D., Wilson, P.A., and Anderson, W.T., 2001. Numerical models of diagenesis, sediment properties and pore fluid chemistry on a paleoceanographic transect: Blake Nose, Ocean Drilling Program Leg 171B. *Paleoceanography,* 16:561–573.

Saito, T., 1962. Eocene planktonic foraminifera from Hahajima (Hillsborough Island). *Trans. Proc. Paleontol. Soc. Jpn.,* 45:209–225.

Sissingh, W., 1977. Biostratigraphy of Cretaceous calcareous nannoplankton. *Geol. Mijnbouw,* 56:37–65.

Torres, M.E., Brumsack, H.-J., Bohrmann, G., and Emeis, K.C., 1996. Barite fronts in continental margin sediments: a new look at barium remobilization in the zone of sulfate reduction and formation of heavy barites in diagenetic fronts. *Chem. Geol.,* 127:125–139.

Twichell, S.C., Meyers, P.A., and Diester-Haass, L., 2002. Significance of high C/N ratios in organic-carbon-rich Neogene sediments under the Benguela Current upwelling system. *Org. Geochem.,* 33:715–722.

Figure F1. Seismic line GeoB215 over Site 1260. See Figure F1, p. 5, in Shipboard Scientific Party, this volume ("Seismic Stratigraphy and Underway Geophysics") for a location map for this line. Subunit 3a is the zone between Reflections B and B′; Subunit 3b lies between Horizons B′ and C.

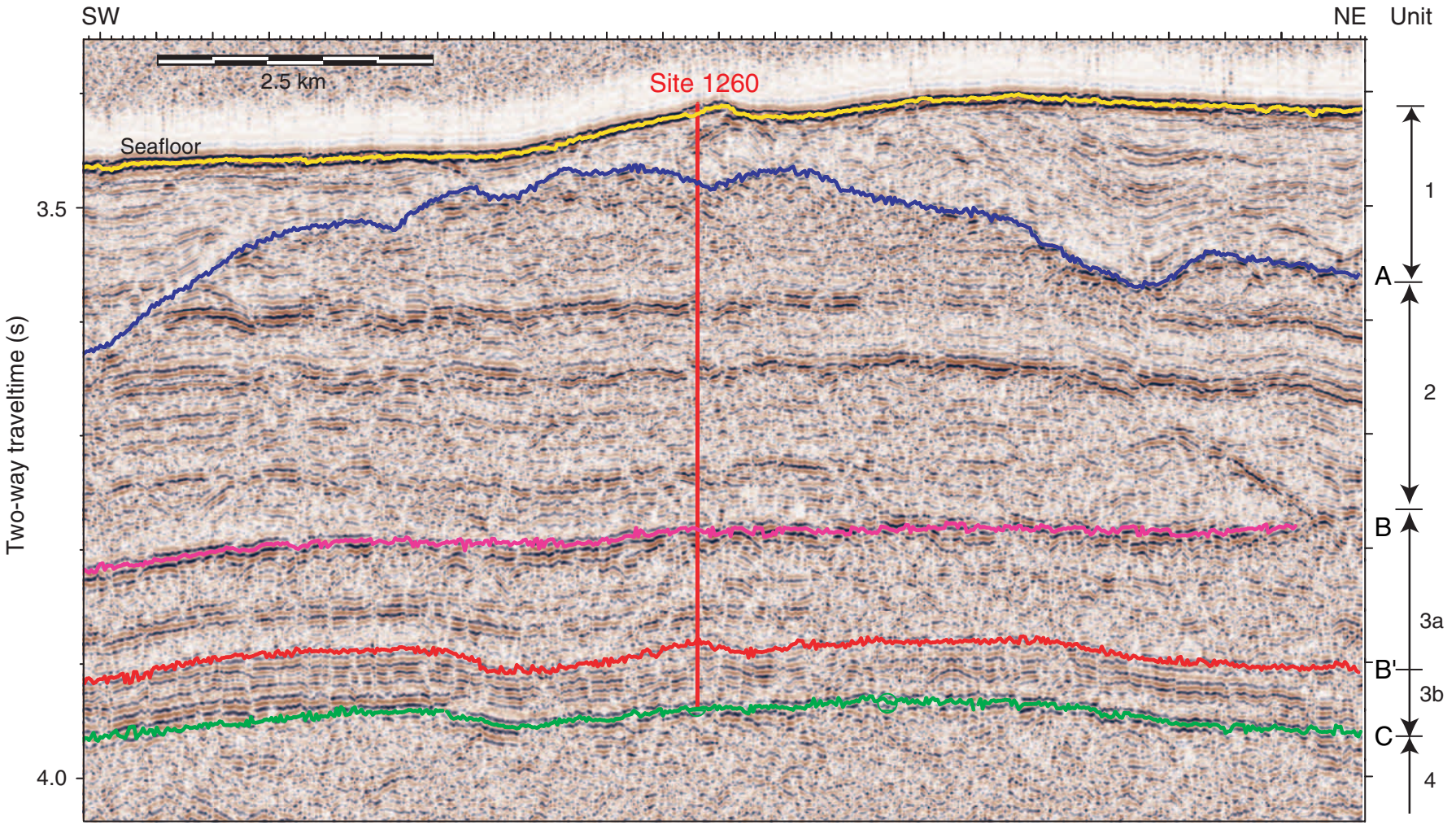

Figure F2. Seismic line 207-L1S at Site 1260. See Figure F1, p. 5, in Shipboard Scientific Party, this volume ("Seismic Stratigraphy and Underway Geophysics") for a location map for this line.

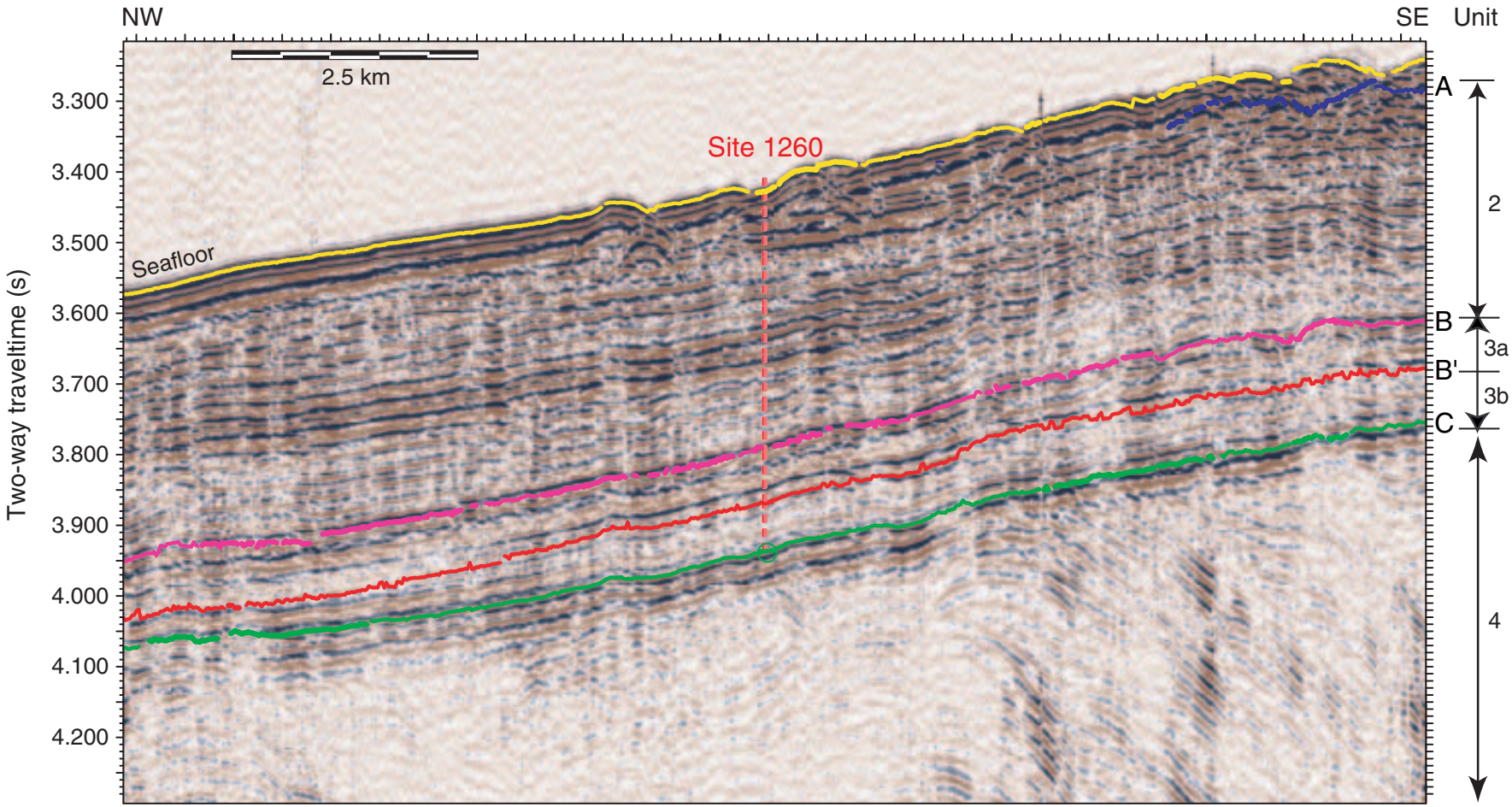

Figure F3. Industry multichannel seismic reflection line C2211 passing 1.7 km east of Site 1260. See Figure F1, p. 5, in Shipboard Scientific Party, this volume ("Seismic Stratigraphy and Underway Geophysics") for a location map for this line. The site location is projected onto the line at the point of closest passing.

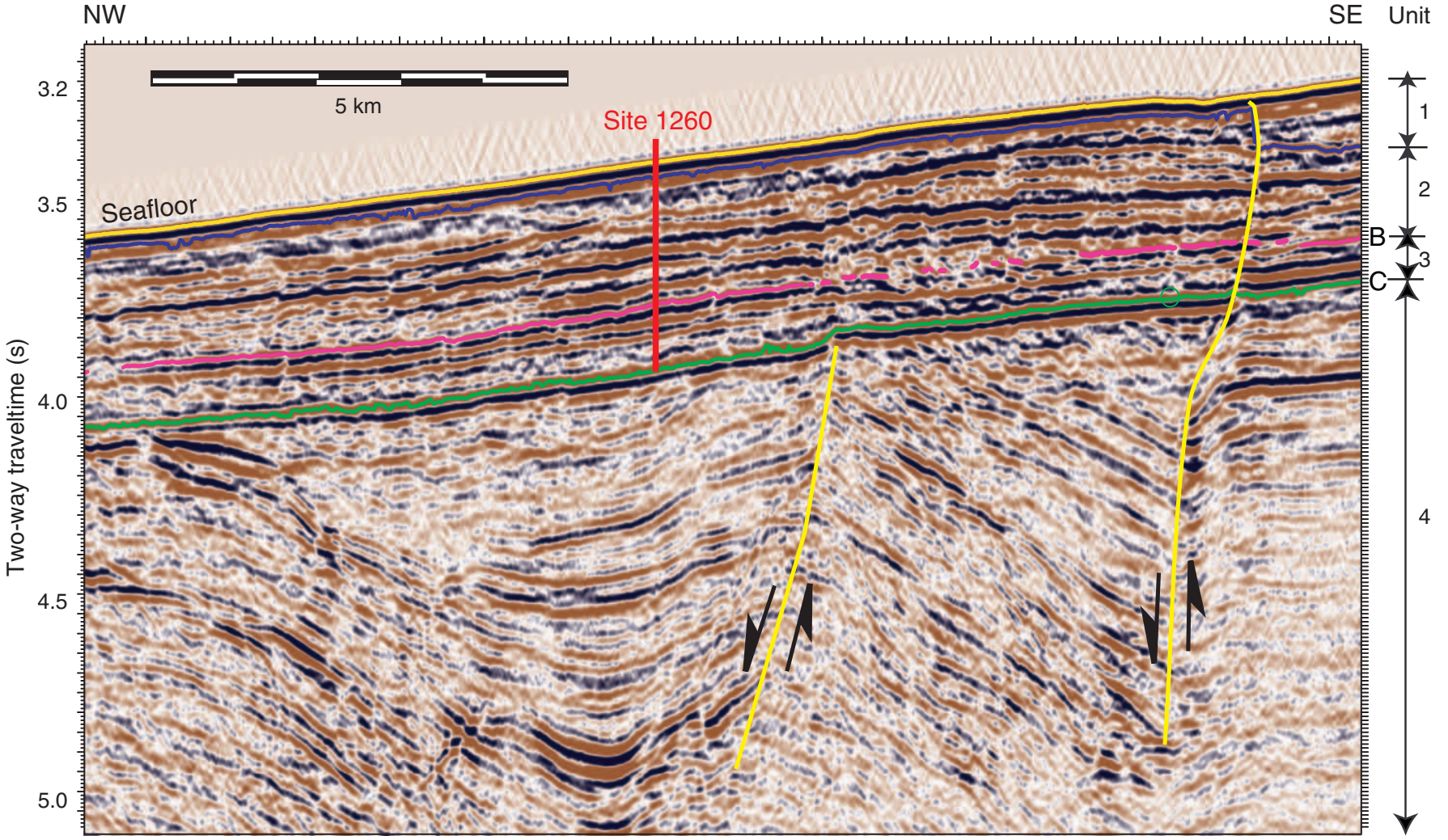

Figure F4. Comparison of core recovery, lithostratigraphic units, biostratigraphic units, paleomagnetic chrons, weight percent carbonate, and total organic carbon (TOC) at Site 1260.

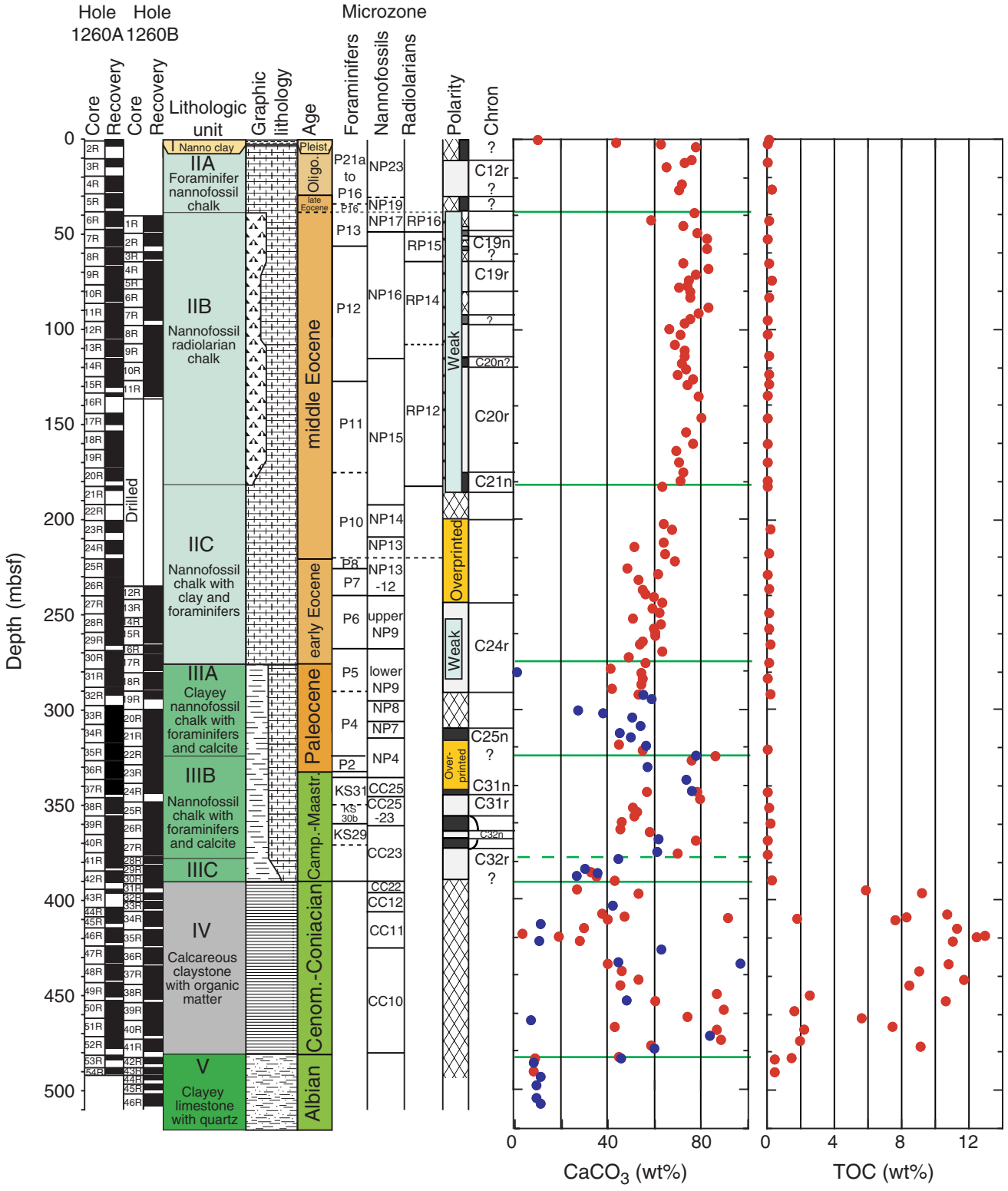

Figure F5. Close-up photographs of representative lithologies from Units II and III at Site 1260. **A.** Subunit IIA pervasively bioturbated foraminifers nannofossils chalk (interval 207-1260A-4R-2, 10–25 cm). **B.** Contact between Subunit IIA (foraminifers nannofossils chalk) and IIB (radiolarian nannofossils chalk) at a distinct color change (interval 207-1260A-5R-CC, 6–18 cm). **C.** Subunit IIC, with subtle color alternations (interval 207-1260A-24R-4, 83–100 cm).

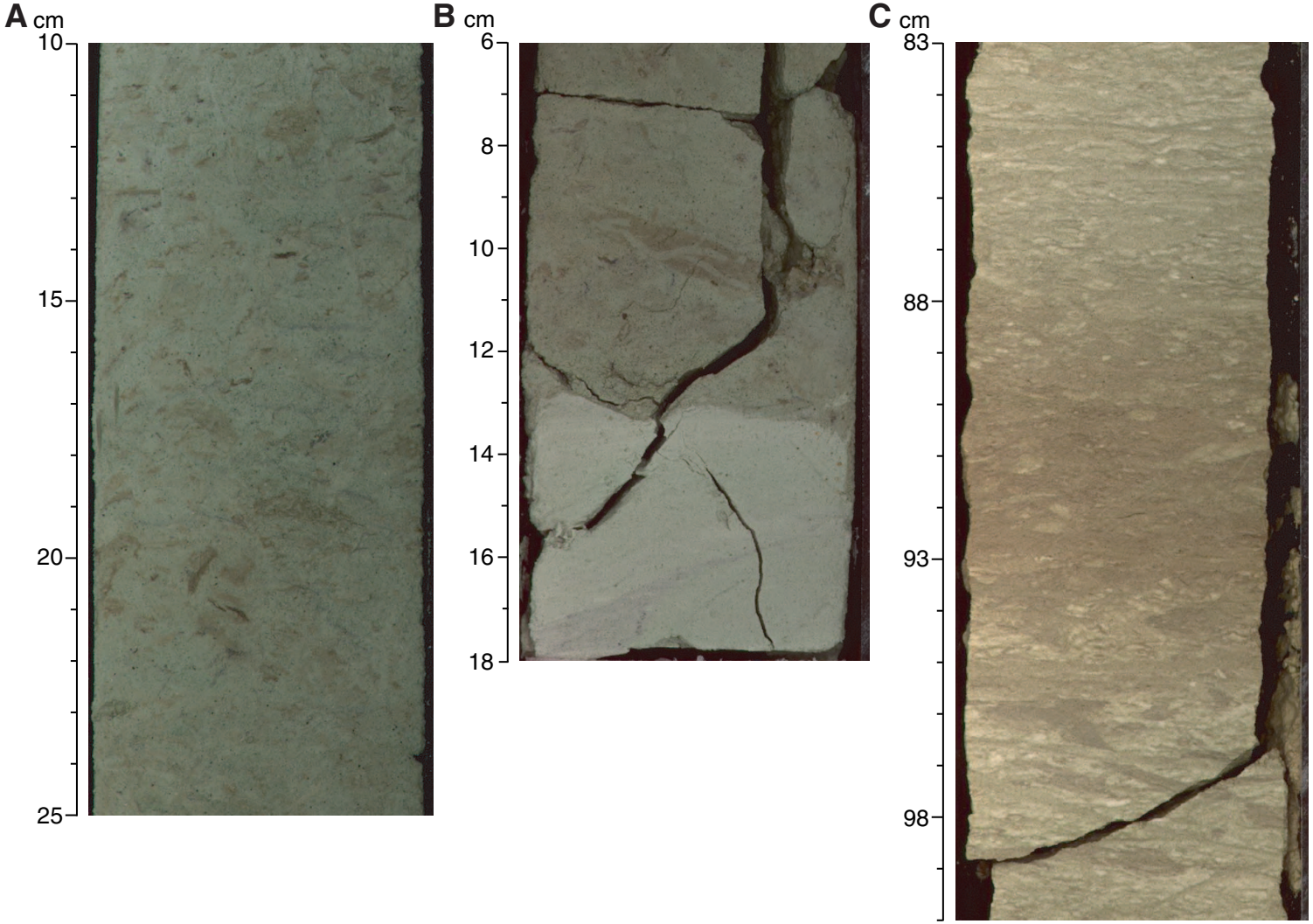

Figure F6. Close-up photographs of lithostratigraphic transitions at the P/E and K/T boundaries. **A.** P/E boundary with laminated clays and a distinct color change (interval 207-1260A-30R-7, 59–80 cm). **B.** K/T boundary, with nannofossil claystone below the spherule ejecta layer, which is overlain by greenish gray clay (interval 207-1260A-36R-4, 75–105 cm).

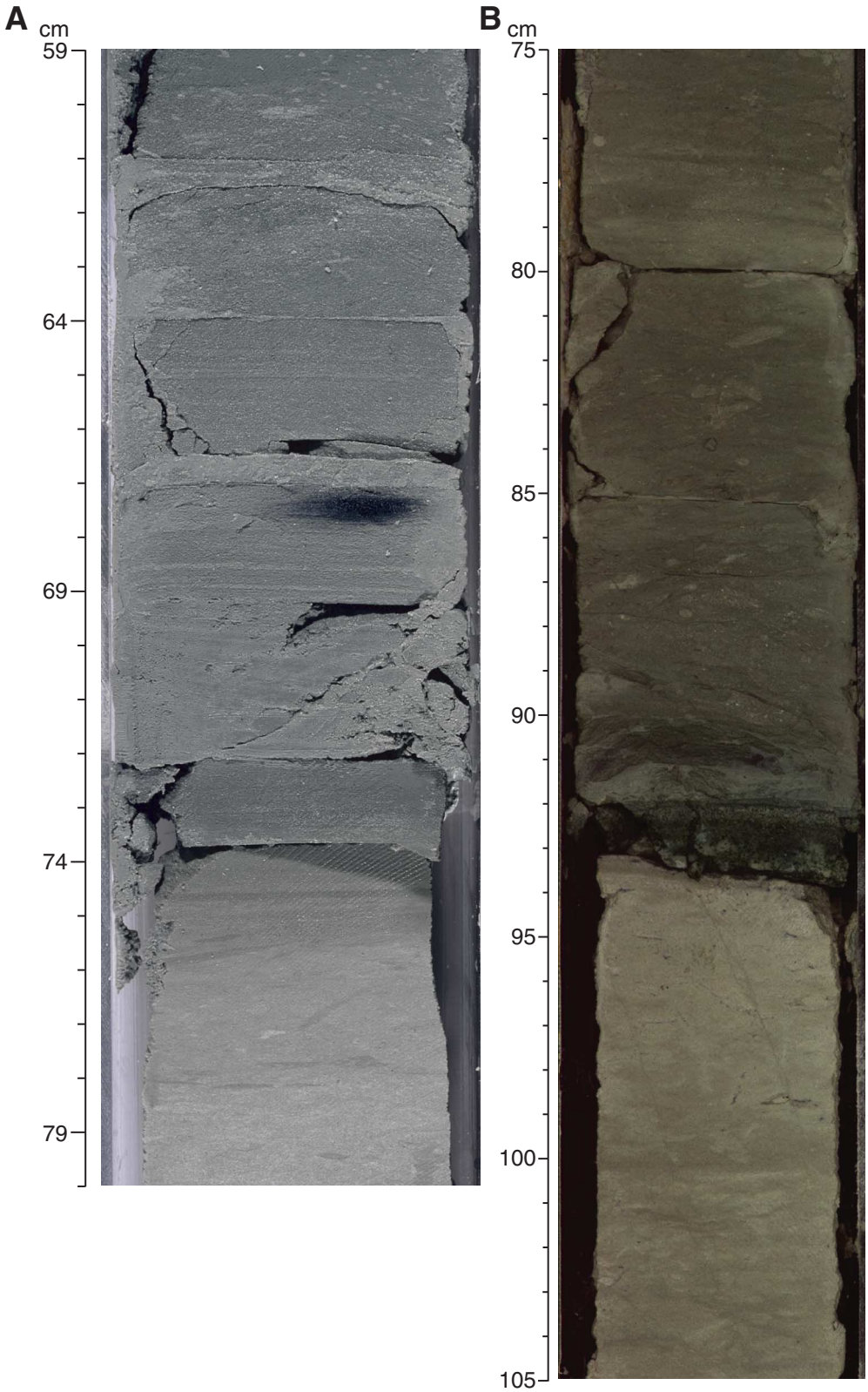

Figure F7. Close-up photographs of lithologies from Unit III. **A.** Subunit IIIA, consisting of clayey nannofossils chalk with *Zoophycos* and pyrite (interval 207-1260A-31R-3, 120–140 cm). **B.** Subunit IIIB with yellowish brown color mottles above the K/T boundary (interval 207-1260A-36R-4, 30–50 cm). **C.** Color alternations of Subunit IIIC with increasing clay content (interval 207-1260A-41R-5, 100–120 cm).

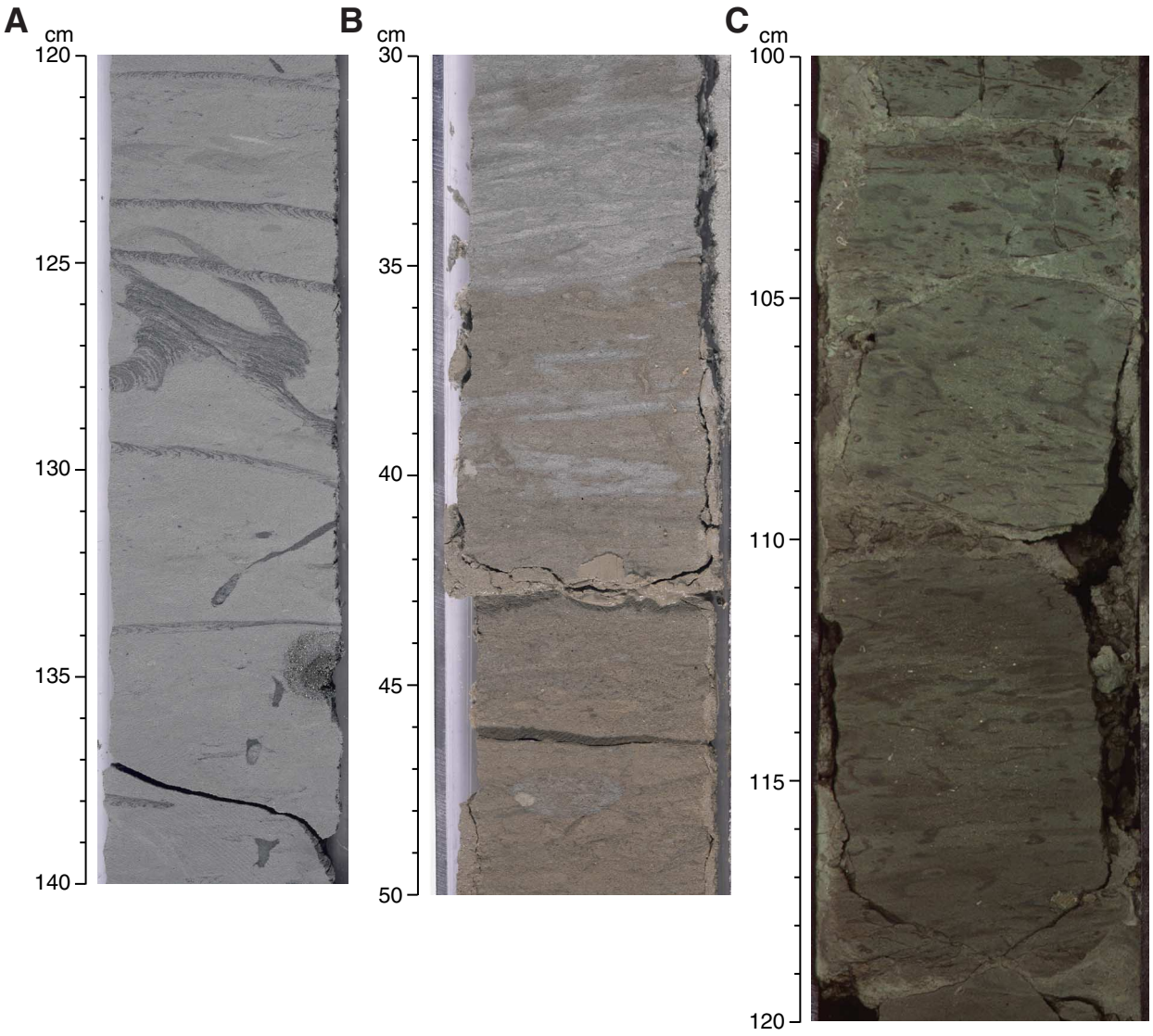

Figure F8. Close-up photographs of representative lithologies from Unit IV at Site 1260. **A.** Boundary between Subunit IIIC and Unit IV, where a coarse-grained glauconite-rich layer sits on laminated brown clays with high TOC content (interval 207-1260-42R-CC, 1–18 cm). **B.** Typical calcareous claystone of Unit IV with organic matter and phosphatic stringers, fish debris, and fecal pellets (interval 207-1260A-46R-6, 48–69 cm). (Continued on next page.)

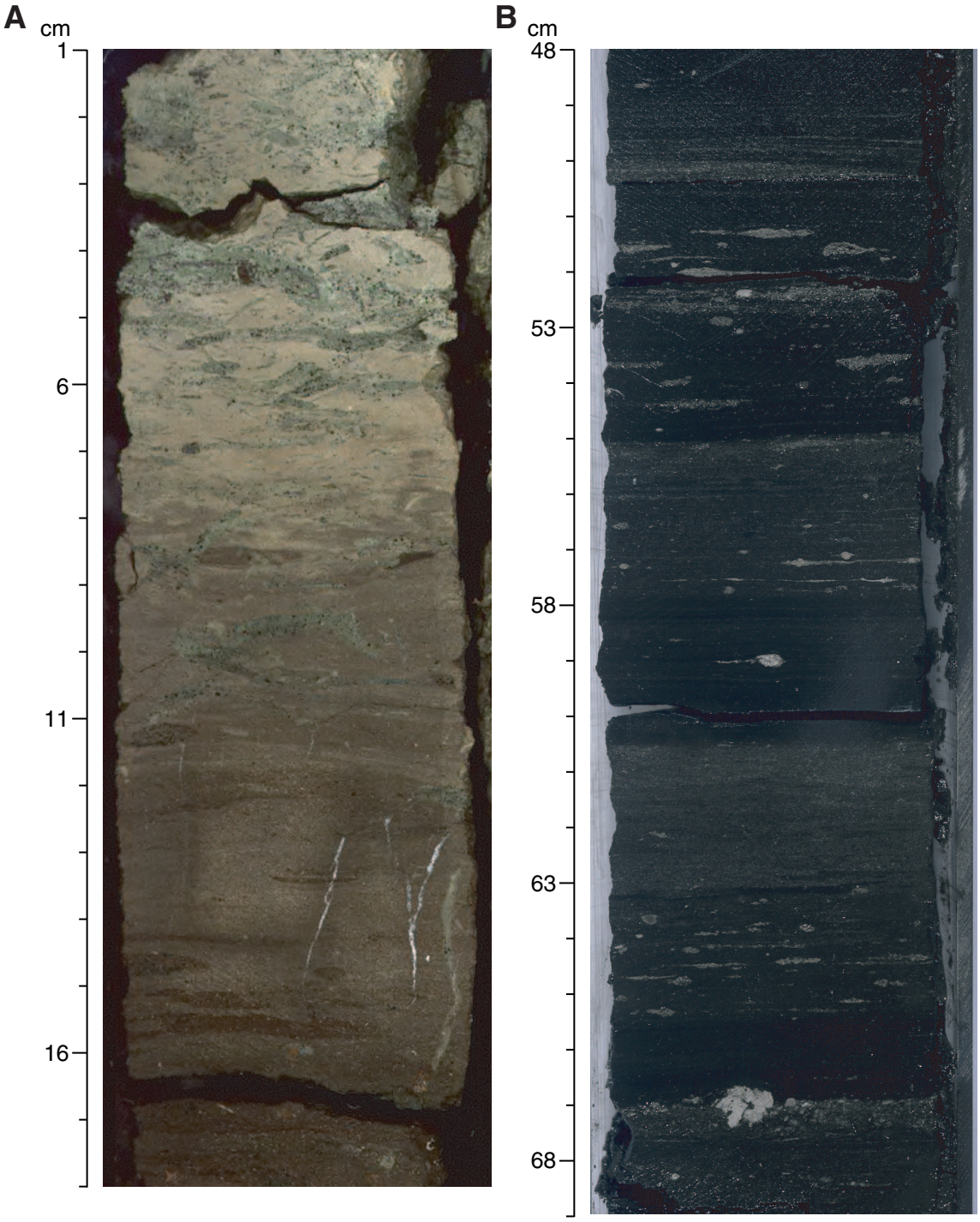

Figure F8 (continued). C. Limestone layers made up of cemented foraminifer sands interbedded with the organic-rich claystones from the lower portion of Unit IV (interval 207-1260A-48R-4, 47–67 cm).

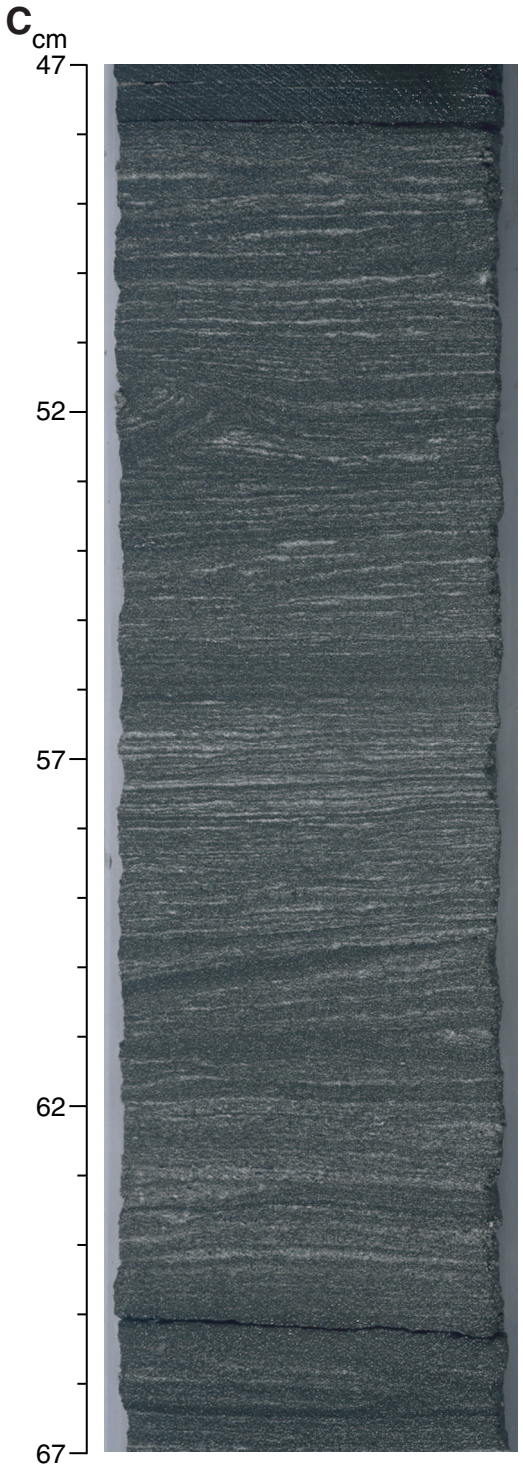

Figure F9. Photomicrographs showing typical lithologies of Unit IV and V. **A.** Thin section of a coarse glauconite-rich horizon (Sample **207-1260B-34R-1, 1–4 cm;** field of view = 2.5 mm). **B.** One of the foraminifer calcite cemented sands as seen in Figure **F8C,** p. 48, (Sample **207-1260B-37R-5, 108–111 cm;** field of view = 1.25 mm). **C.** Typical calcareous claystone with quartz of Unit V (Sample **207-1260B-42R-2, 10–12 cm;** field of view = 2.5 mm; cross-polarized light).

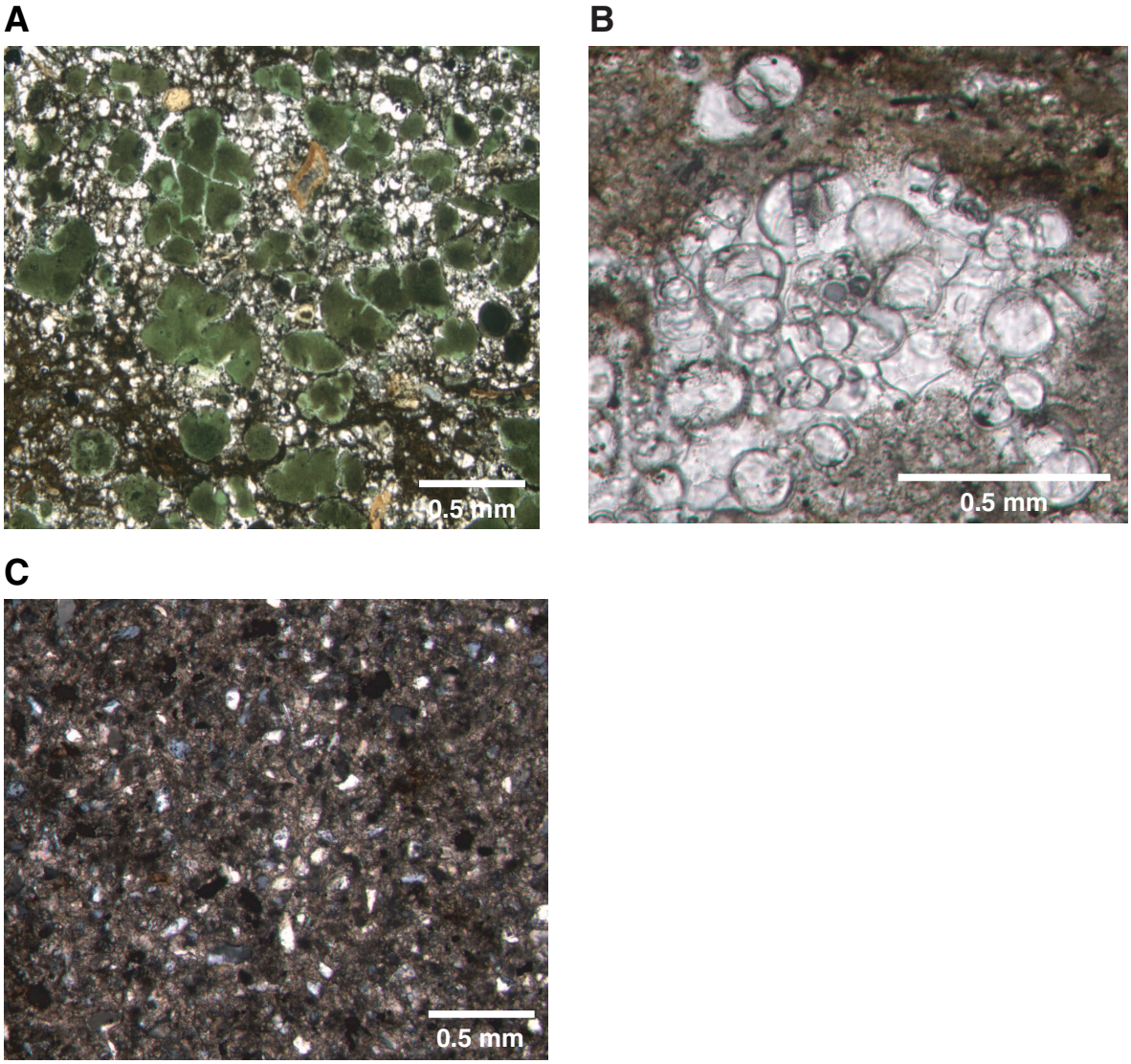

Figure F10. Planktonic foraminifer, calcareous nannofossil, and radiolarian biozonation of Site 1260.

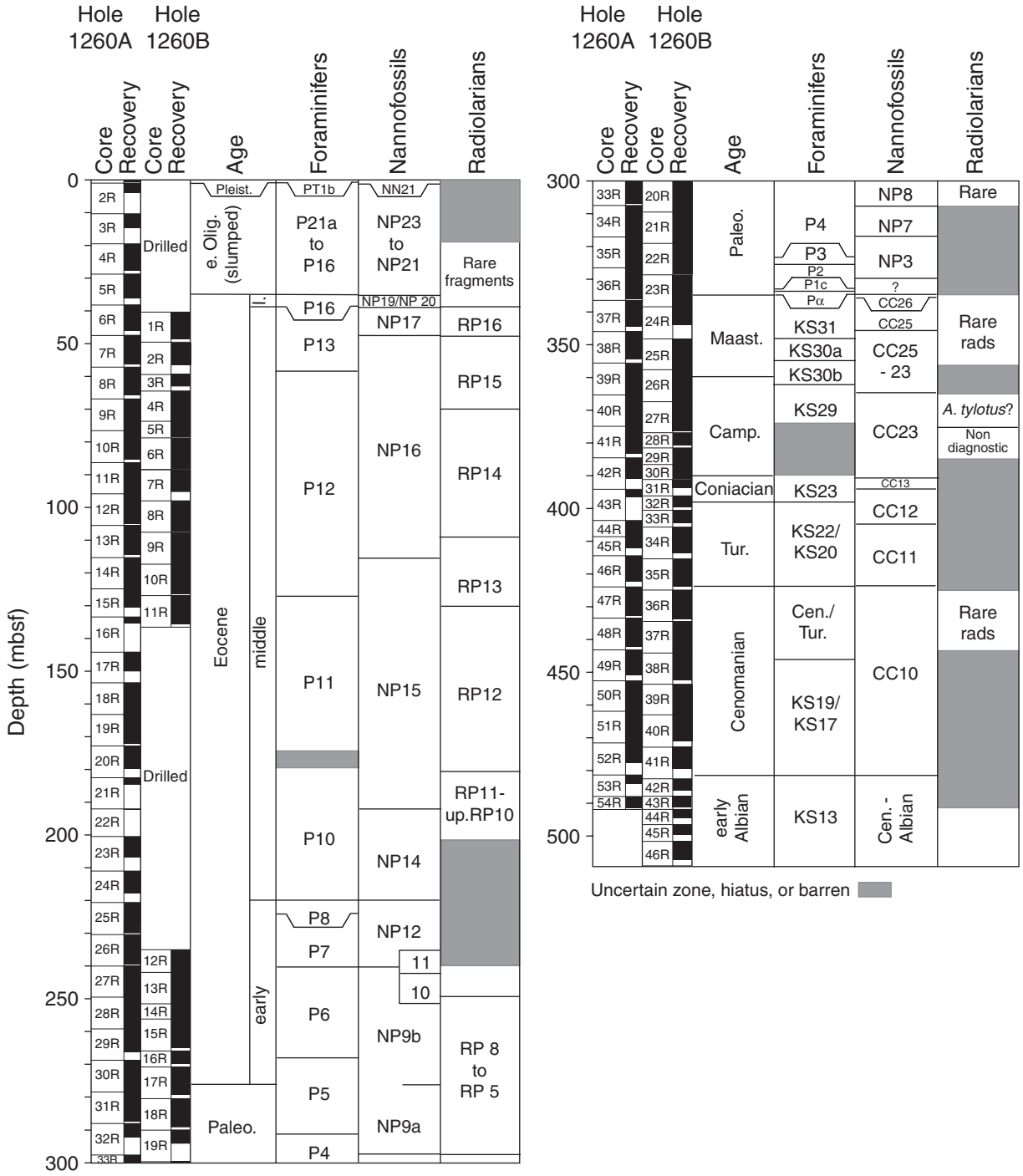

Figure F11. Shipboard paleomagnetic data and initial interpretations of inclination clusters in the Cretaceous–Oligocene of Holes 1260A and 1260B. Visual color variations in the sediment succession generally correspond to changes in magnetic properties and are displayed as an exaggerated schematic column to the right of the shipboard lithostratigraphic units. The paleomagnetic data from the holes have been compared using the composite depth offsets, which rarely exceeded a relative displacement of 4 m at this site. Magnetic inclinations are from intact blocks (excluding measurements within 5 cm of the end of each blocks) after 15-mT demagnetization. The inclination data exclude measurements near the background noise limit of the cryogenic magnetometer (~3×10^{-5} A/m), therefore measurements with intensities <5×10^{-5} A/m are not considered reliable. In addition, the upper 20 cm of each core that commonly displays spurious high-intensity magnetization or downhole contamination and the upper 5 cm of each section that is influenced by magnetization carried by the blue-colored end cap are excluded. The displayed inclinations are either 3-point running means (closed circles), 2-point means (open circles), or single-level data (open triangles) (from the central portion of blocks between 10 and 15 cm long, or from isolated levels within a larger block in which the adjacent measurements were <5×10^{-5} A/m). The magnetic intensity column includes NRM (small orange dots = 21-point running mean) and after the 15-mT demagnetization (small black dots, large blue dots = 101-point log-mean average). Magnetic susceptibility obtained using a magnetic susceptibility core logger (MSCL) is shown by green dots in the right most column. Shipboard assignment of polarity zones were based on clusters of magnetic inclinations from intact blocks (to right of polarity zone column), as delimited by the thin lines. Zones of positive inclinations (originally considered to be normal polarity zones) = black or medium gray, if reliability is less certain; negative or mixed inclinations (originally considered to be reversed polarity zones) = white or light gray, if reliability is less certain. Uncertain inclination characteristics or gaps in data coverage = cross hatched. The shipboard interpretations of polarity zones were not always supported by analyses of magnetic characteristics during progressive thermal demagnetization of minicores (Fig. **F12,** p. 52). F = foraminifers, N = nannofossils, R = radiolarians. (This figure is available in an **oversized format.**)

Figure F12. Magnetostratigraphy and characteristic directions of Albian and Campanian–middle Eocene of Holes 1260A and 1260B based on shore-based analysis of minicores. The minicore data from the two holes have been merged using composite depth scales from each hole. Polarity ratings are graded according to reliability and number of vectors utilized in the characteristic direction. R = reliable reversed polarity, INT = indeterminate, N = reliable normal polarity) (relative placement of other points indicates degree of precision or uncertainty). Methods of polarity interpretation, polarity ratings, and derivation of characteristic inclinations and intensities are in **"Paleomagnetism,"** p. 16, in the "Explanatory Notes" chapter. Polarity zones are assigned according to clusters of individual polarity interpretations. Normal polarity zones = dark gray; reversed polarity zones = white; uncertain polarity or gaps in data coverage = cross hatched. Assignments of polarity chrons are based on the polarity zone pattern and the constraints from microfossil biostratigraphy. Biozones: F = foraminifer, N = nannofossil, R = radiolarian. (**Figure shown on next page.**)

Figure F12 (continued). (Caption shown on previous page.)

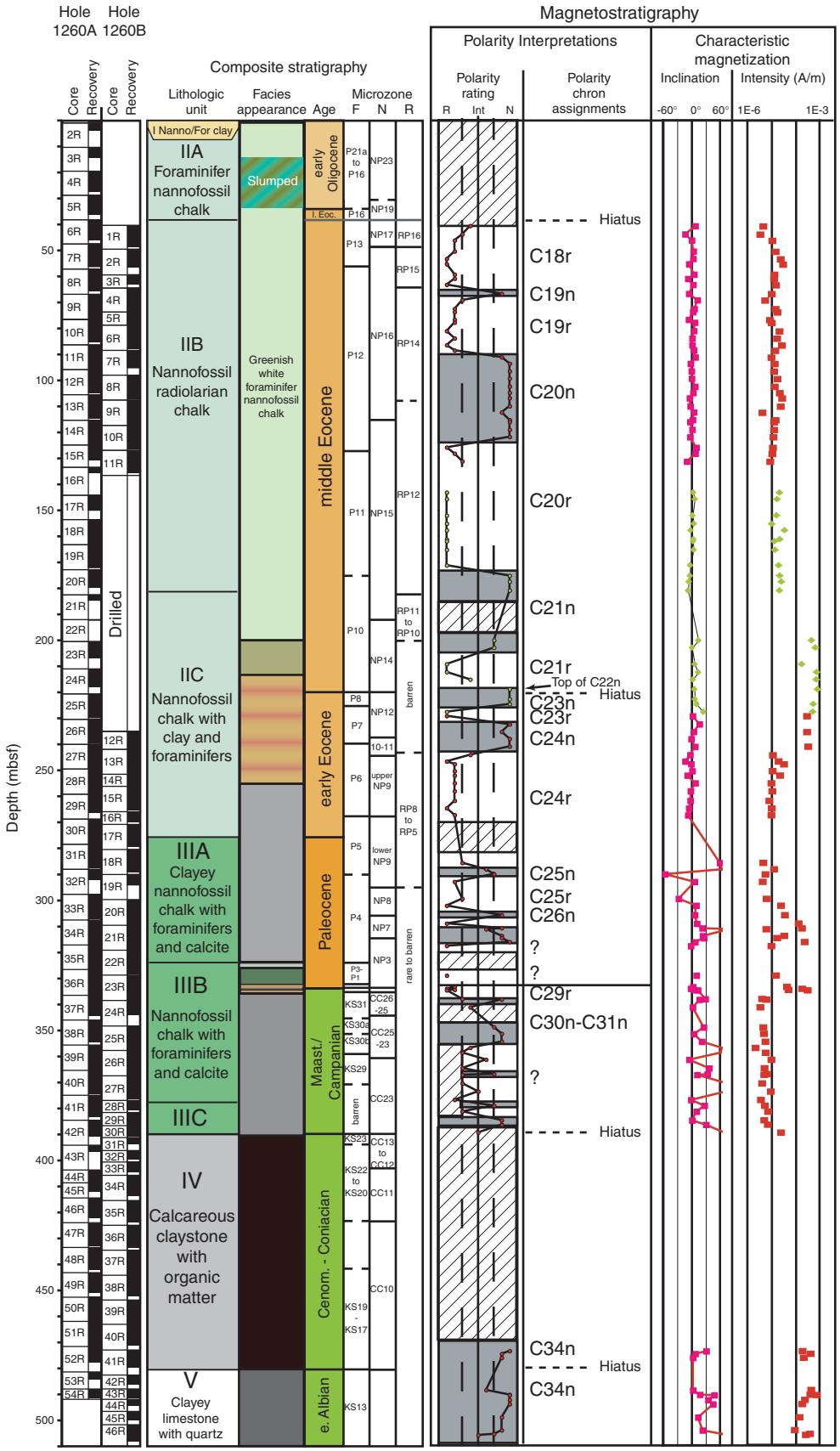

Figure F13. Composite and spliced spectral reflectance ratio (680/430 nm) for the middle Eocene section of Holes 1260A (black) and 1260B (blue). The composite data from Hole 1260B are offset by a constant (0.15 units) for illustration purposes. All data sets are smoothed with a 9-point Gaussian filter.

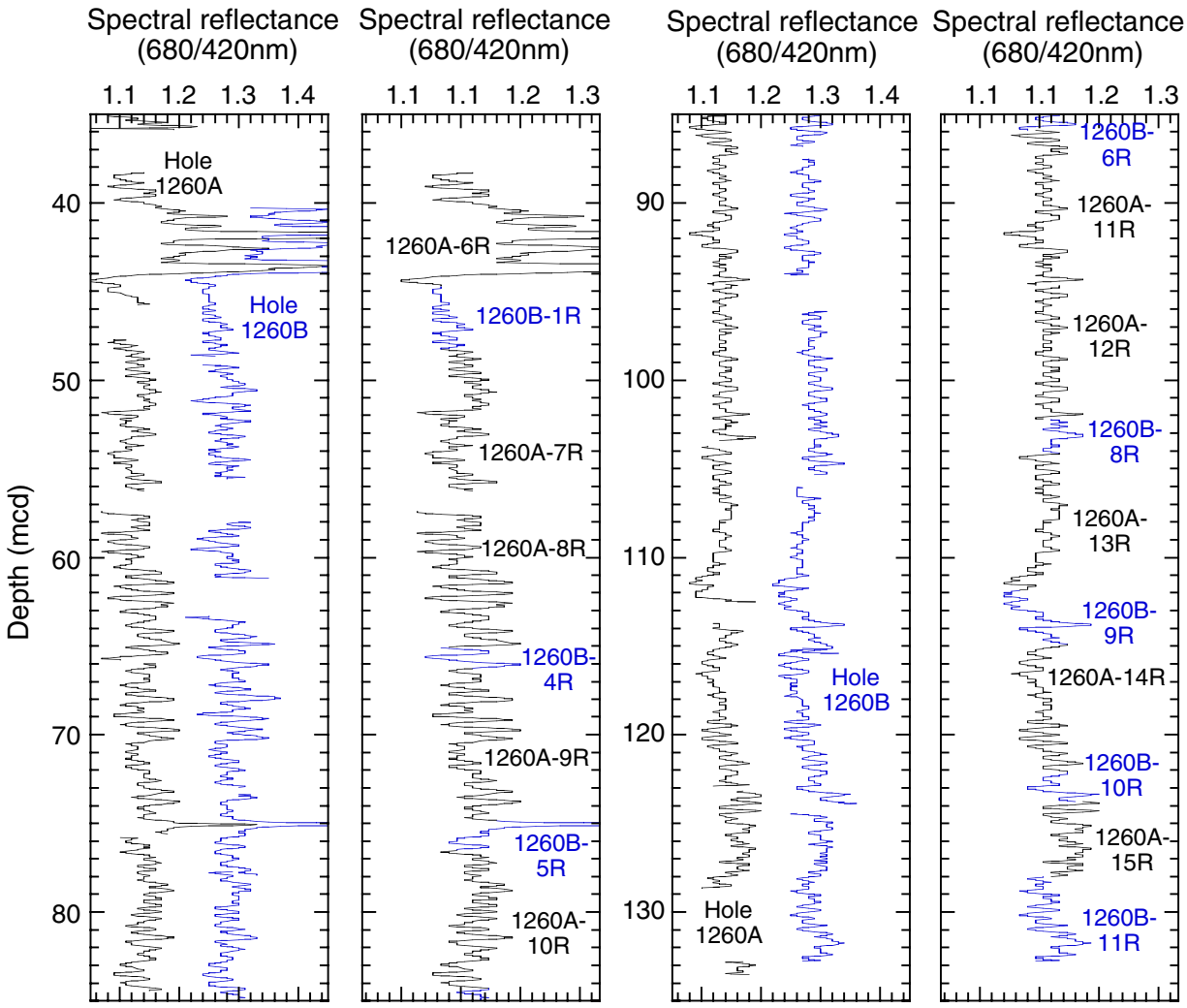

Figure F14. Composite and spliced magnetic susceptibility data for the lower Eocene–Campanian section of Holes 1260A (black) and 1260B (blue). The composite data from Hole 1260B are offset by a constant (5 units) for illustration purposes. All data sets are smoothed with a 9-point Gaussian filter.

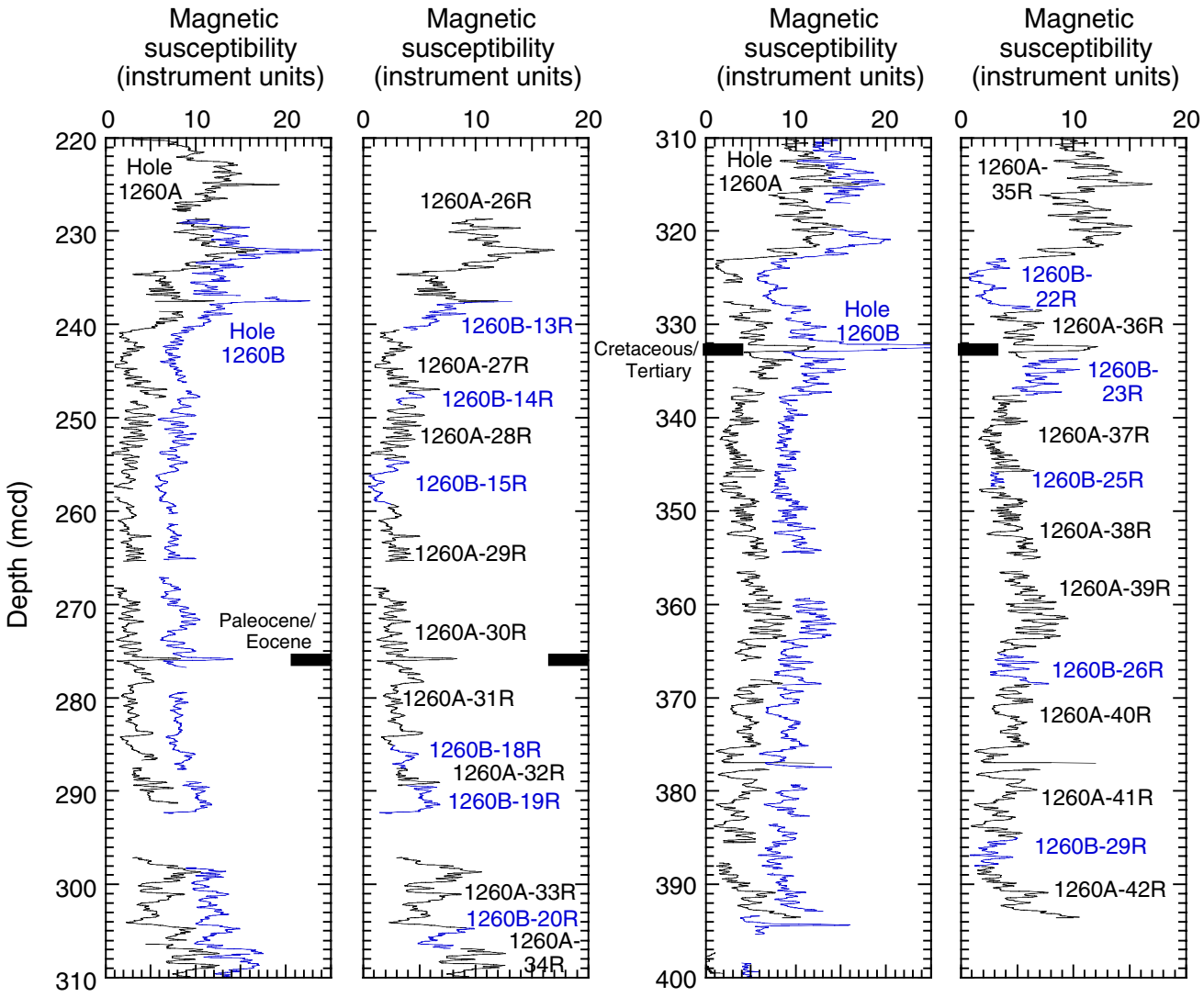

Figure F15. Composite and spliced gamma ray attenuation (GRA) bulk density data for the black shale sequence of Holes 1260A (black) and 1260B (blue). The composite data from Hole 1260B are offset by a constant (0.4 units) for illustration purposes. All data sets are smoothed with a 9-point Gaussian filter.

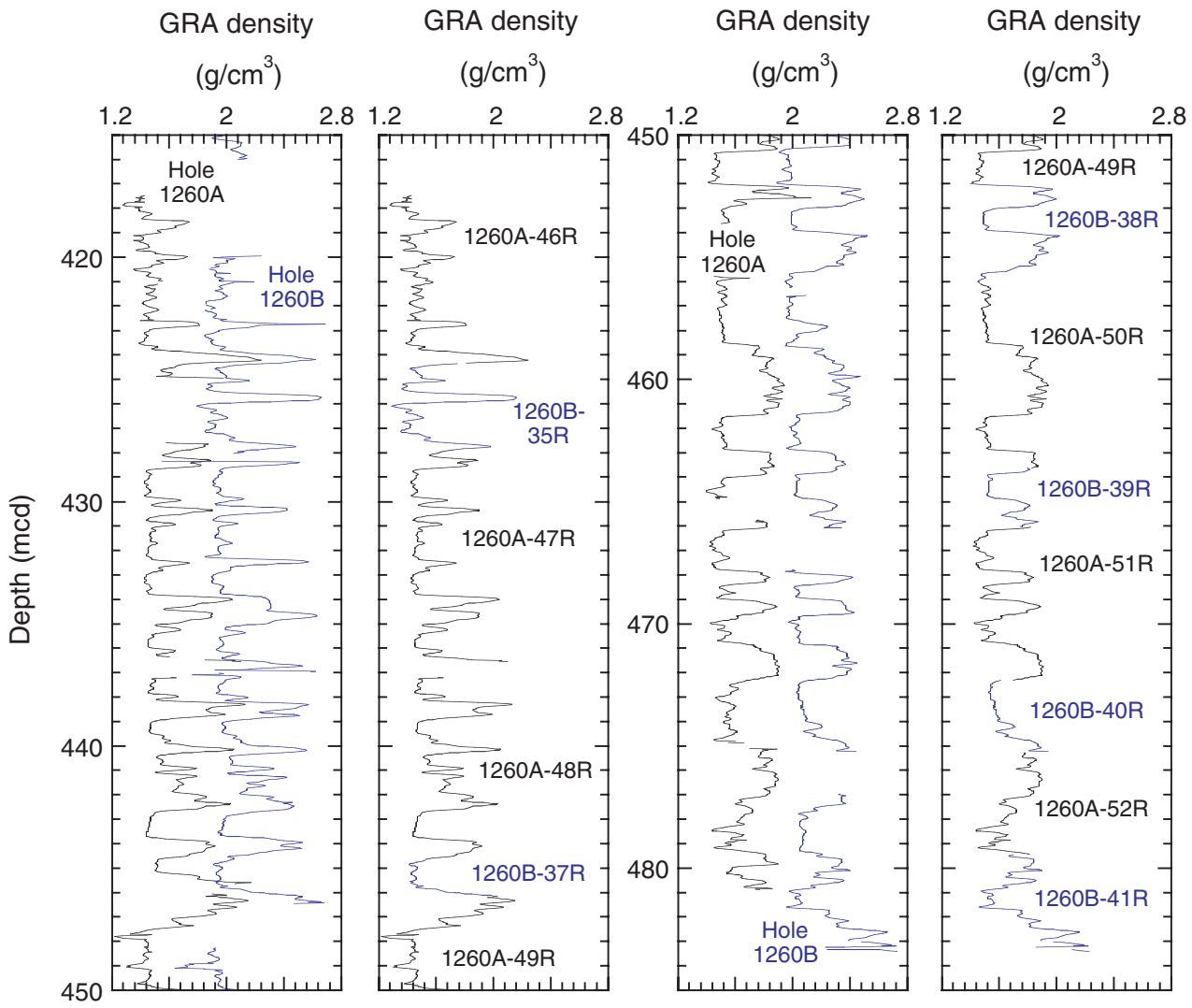

Figure F16. Magnetic susceptibility data plotted along with a qualitative estimate of the confidence of the core-to-core correlations between holes at Site 1260. **A.** Magnetic susceptibility data for Holes 1260A (black) and 1260B (blue). The composite data from Hole 1260B are offset by a constant (5 units) for illustration purposes. All data sets are smoothed with a 9-point Gaussian filter. **B.** Green indicates intervals with definitive hole-to-hole correlations and a high-quality splice (i.e., most core gaps spanned). Yellow indicates intervals where good core-to-core correlations could be made (i.e., a one-to-one match of signals between holes) but definitive depth positions could not be established because core gaps could not be spanned. The diagonal line pattern indicates intervals where hole-to-hole correlations could not be made (primarily a result of only one hole in that interval). P/E = Paleocene/Eocene boundary, K/T = Cretaceous/Tertiary boundary.

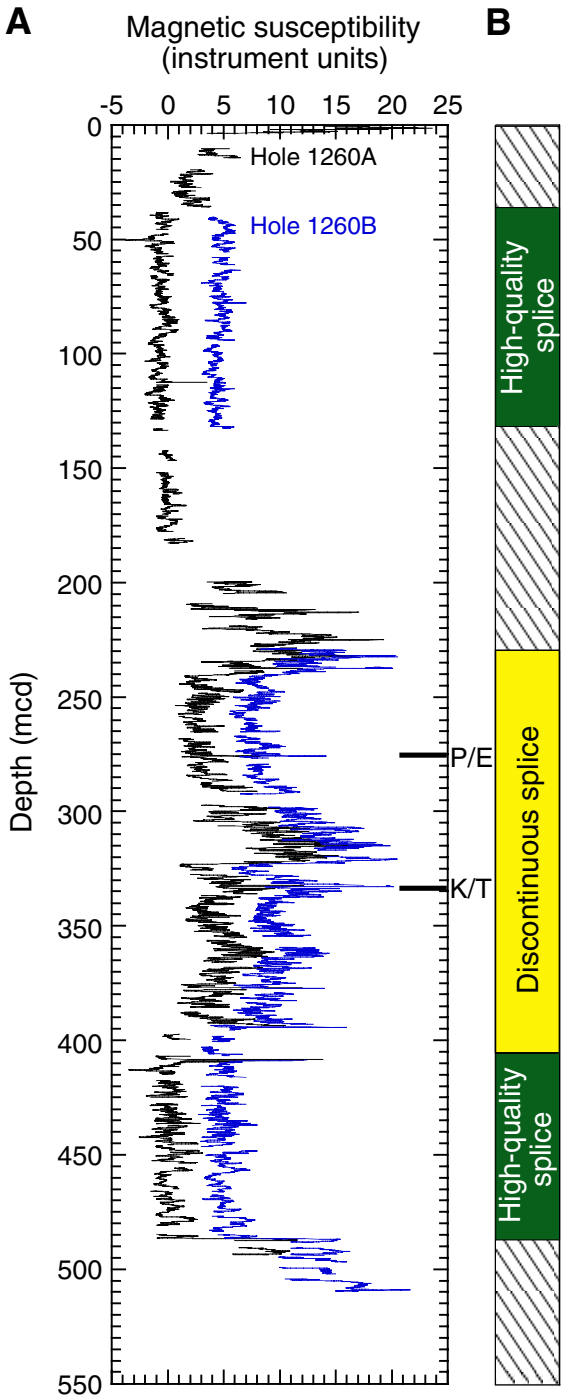

Figure F17. Age-depth plot combining available biostratigraphic and magnetostratigraphic data from Hole 1260A. LSRs for intervals of apparently constant sedimentation rate and the approximate age ranges of the hiatuses (letters A–F) separating each of them are shown.

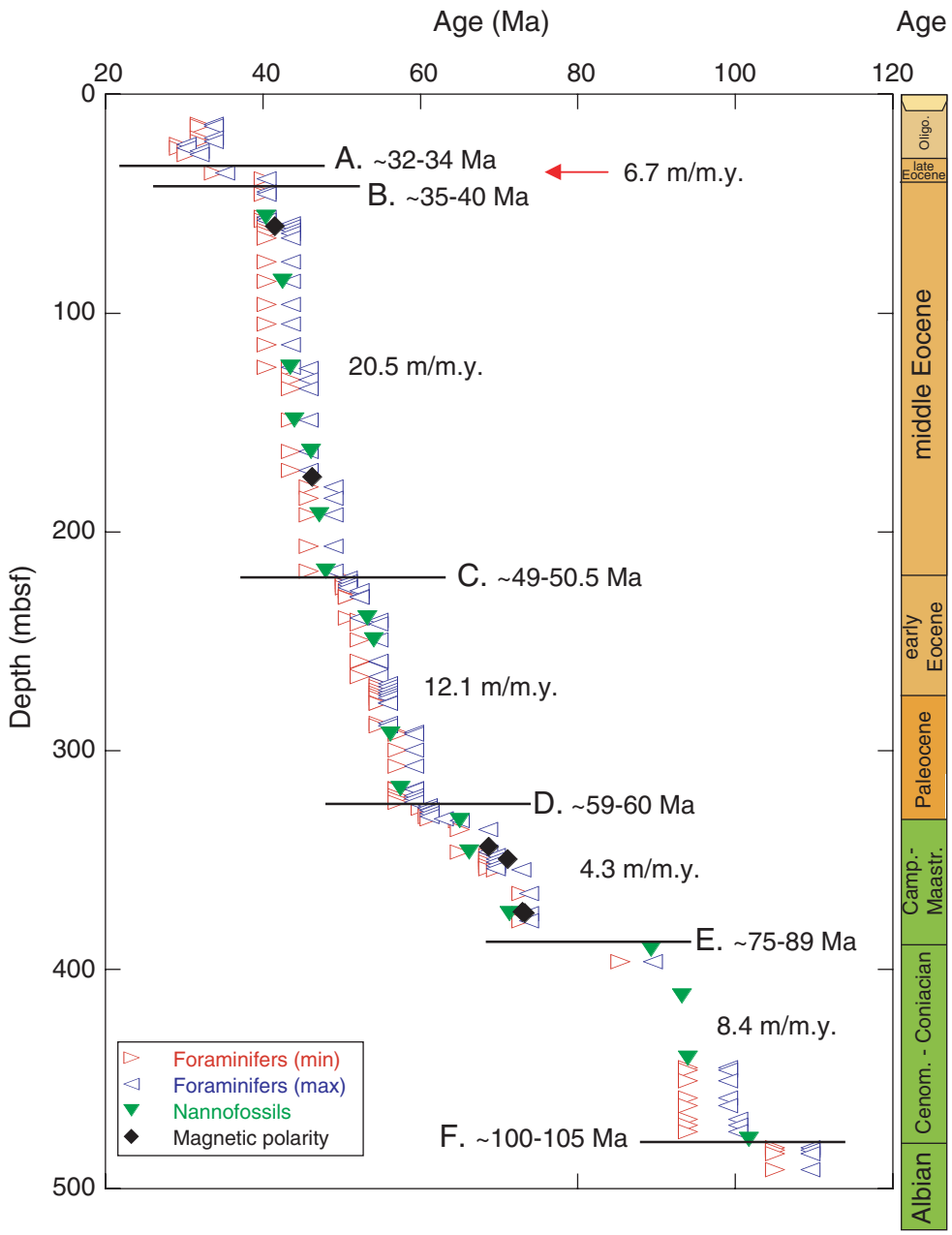

Figure F18. Rock-Eval van Krevelen-type diagram for samples from Units IV and V in Holes 1260A and 1260B. Organic matter appears to be predominantly Type II algal material (Unit IV) and Type III degraded material (Unit V). TOC = total organic carbon.

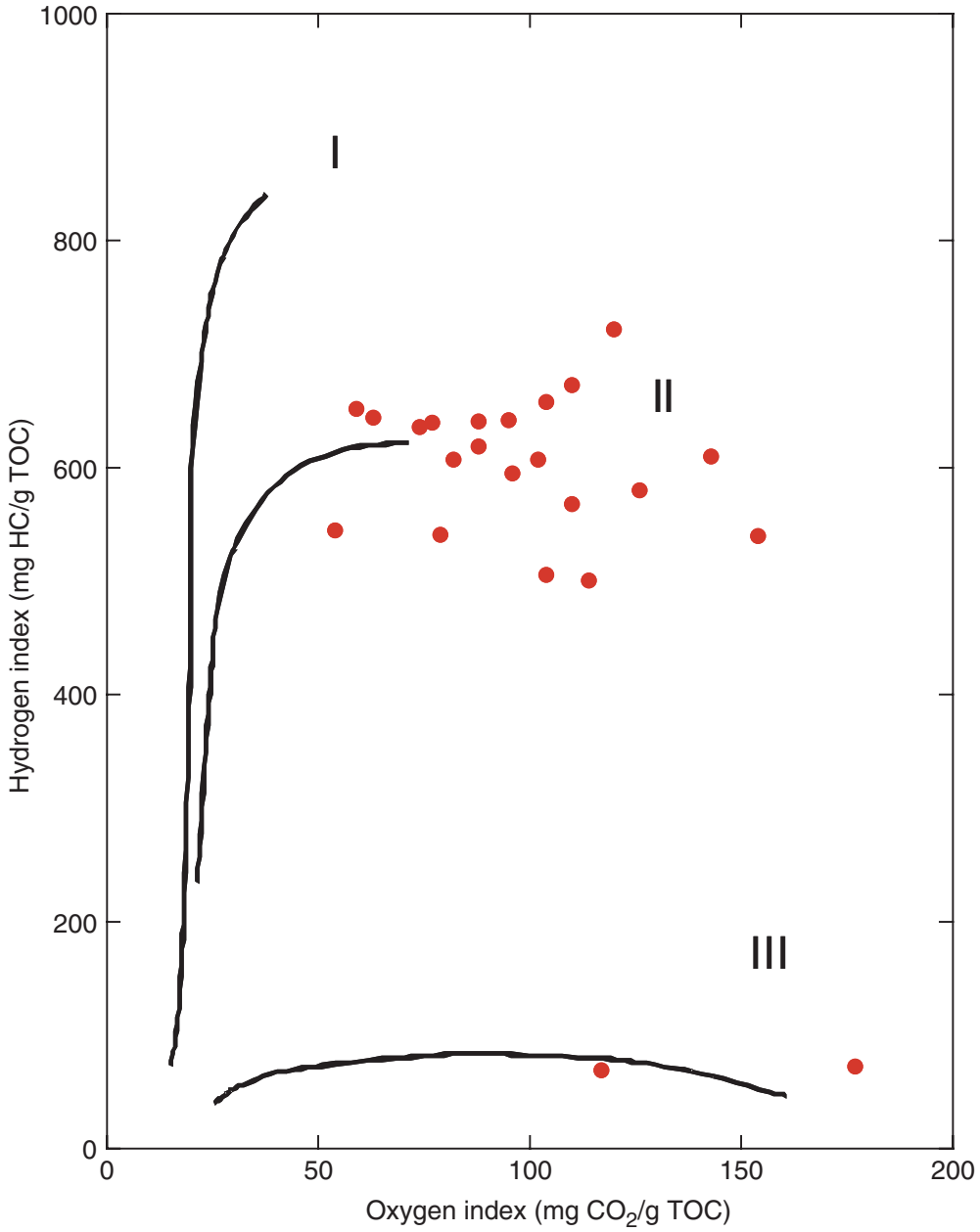

Figure F19. Comparison of concentrations of routine headspace gas analyses (HS) and microbial methane in sediments of Holes 1260A and 1260B.

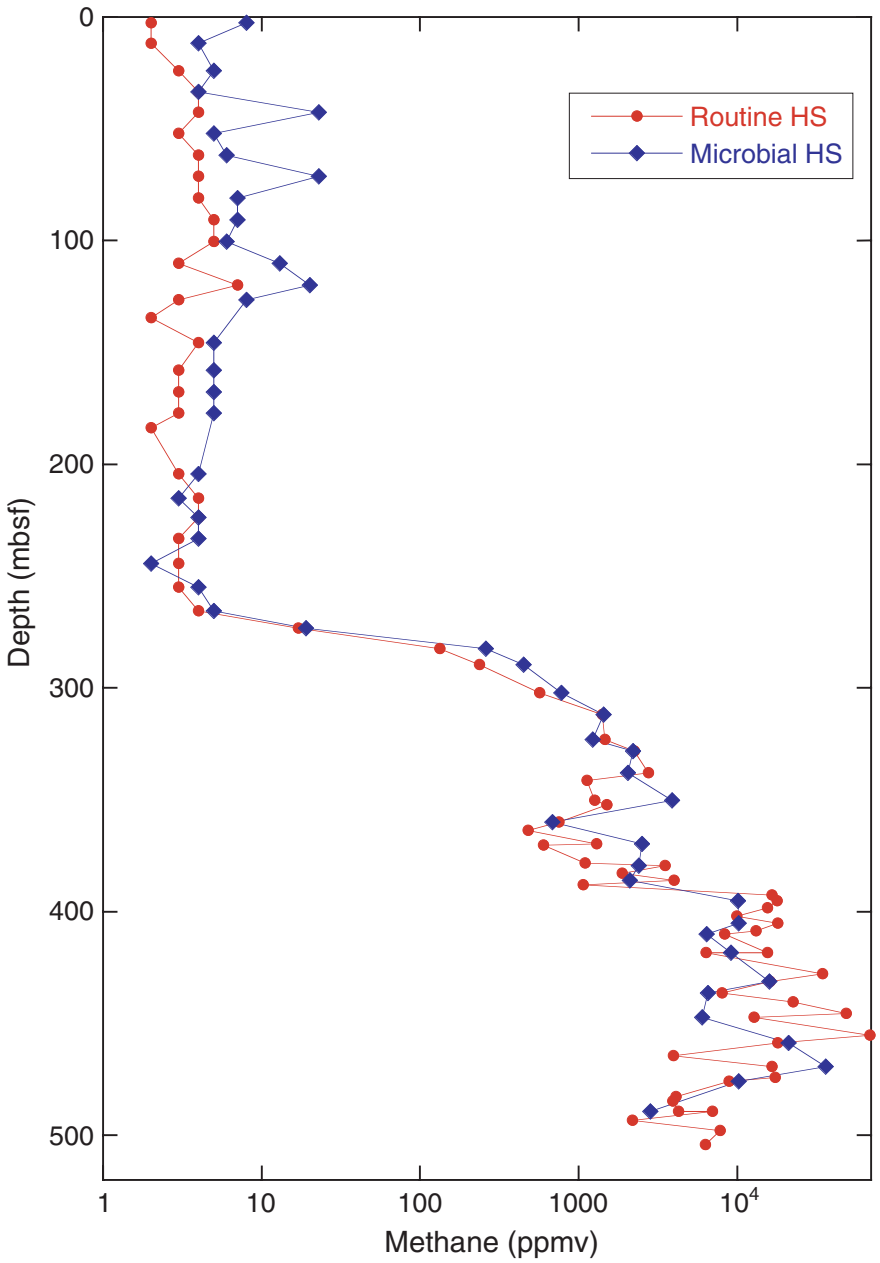

Figure F20. Comparison of total organic carbon (TOC) and methane concentrations in headspace samples from Holes 1259A, 1260A, and 1260B.

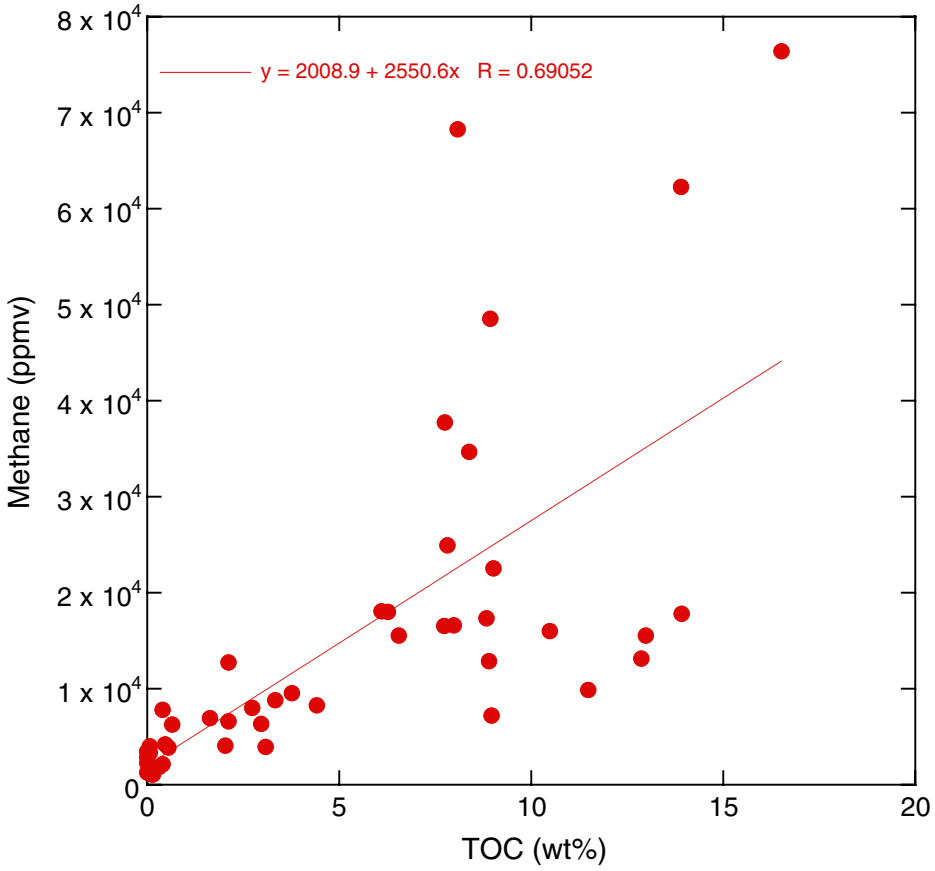

Figure F21. Profiles of chemical constituents in interstitial water at Site 1260. **A.** Salinity. **B.** Chloride. **C.** Sodium. **D.** Potassium. **E.** Alkalinity. **F.** Sulfate. **G.** Ammonium. **H.** Barium. (Continued on next page.)

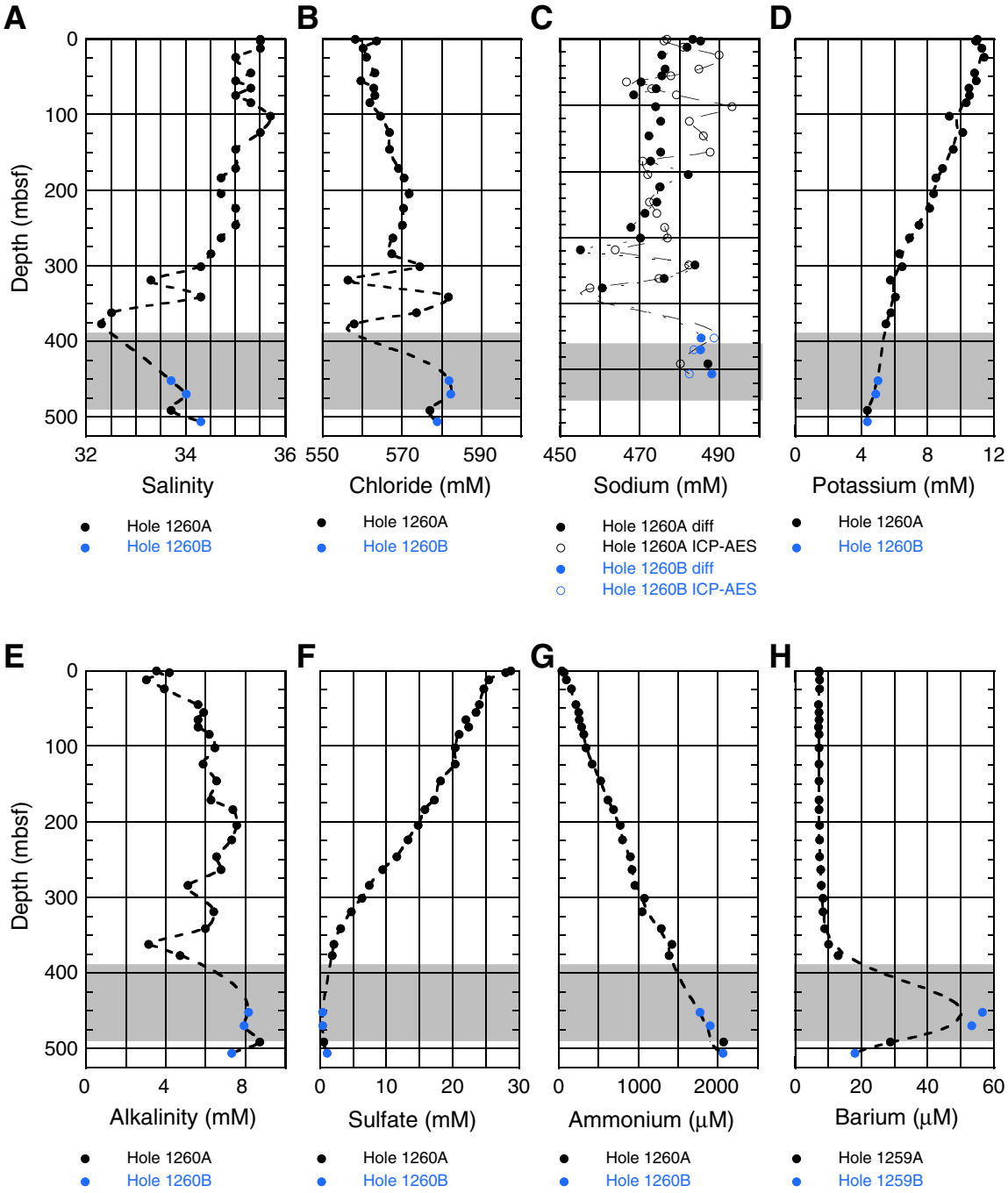

Figure F21 (continued). **I.** Calcium. **J.** Strontium. **K.** Magnesium. **L.** Lithium. **M.** Boron. **N.** Silica. **O.** Iron. **P.** Manganese. diff = calculated by difference, ICP-AES = inductively coupled plasma–atomic emission spectroscopy. "?" denotes a questionable data point. Gray bar shows Unit IV, the black shale sequence.

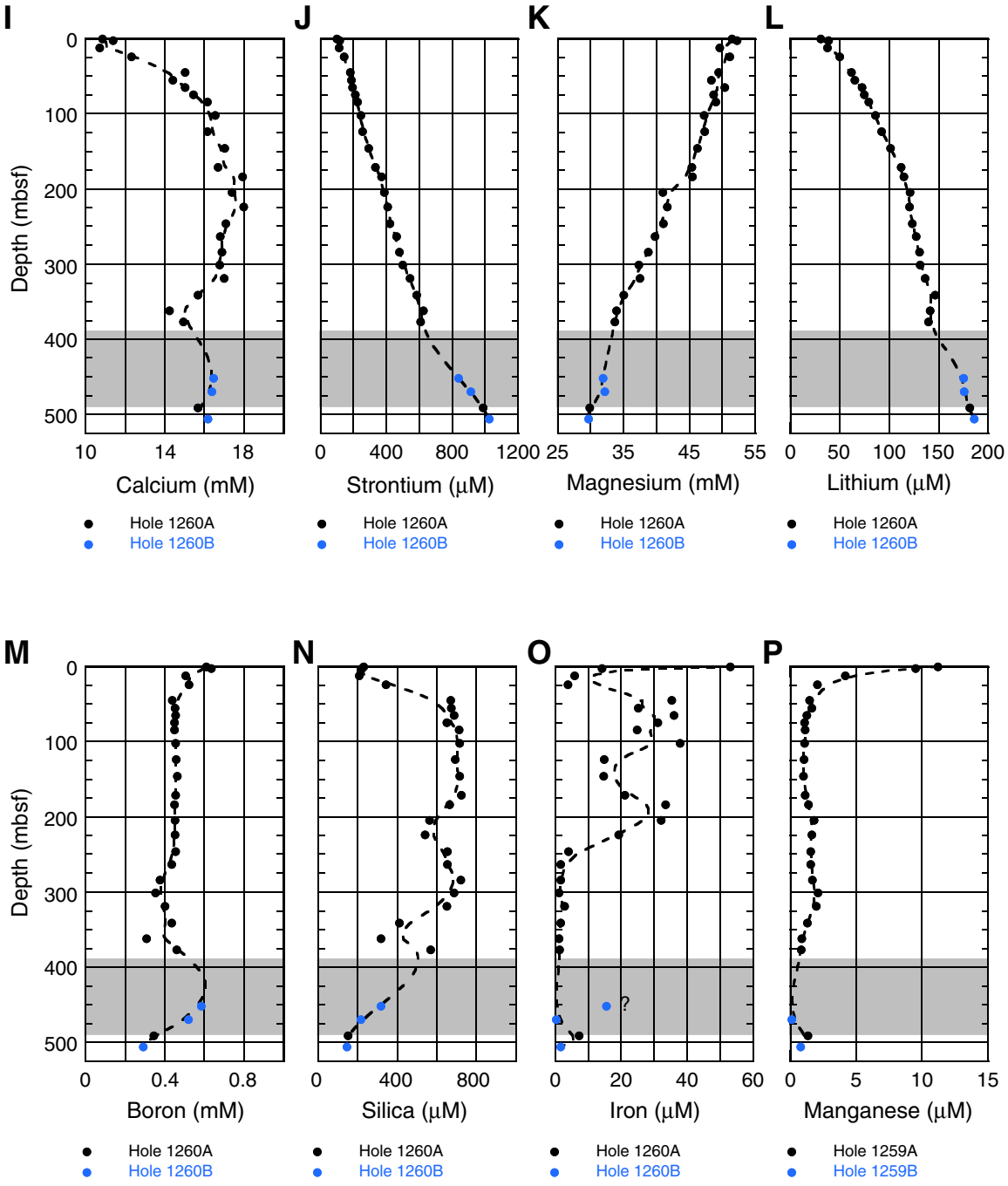

Figure F22. Discrete (green) and MST gamma ray attenuation (GRA) bulk density in Hole 1260A.

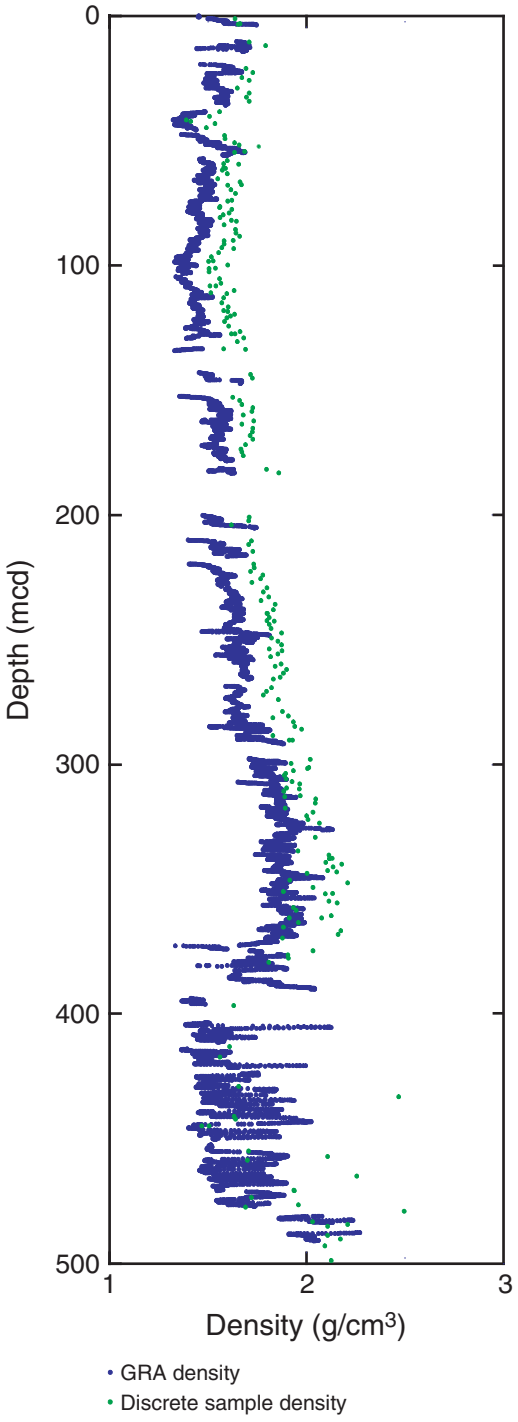

Figure F23. Bulk density, grain density, and porosity of discrete samples at Site 1260. Blue = Hole 1260A, green = Hole 1260B. P/E = Paleocene/Eocene boundary, K/T = Cretaceous/Tertiary boundary.

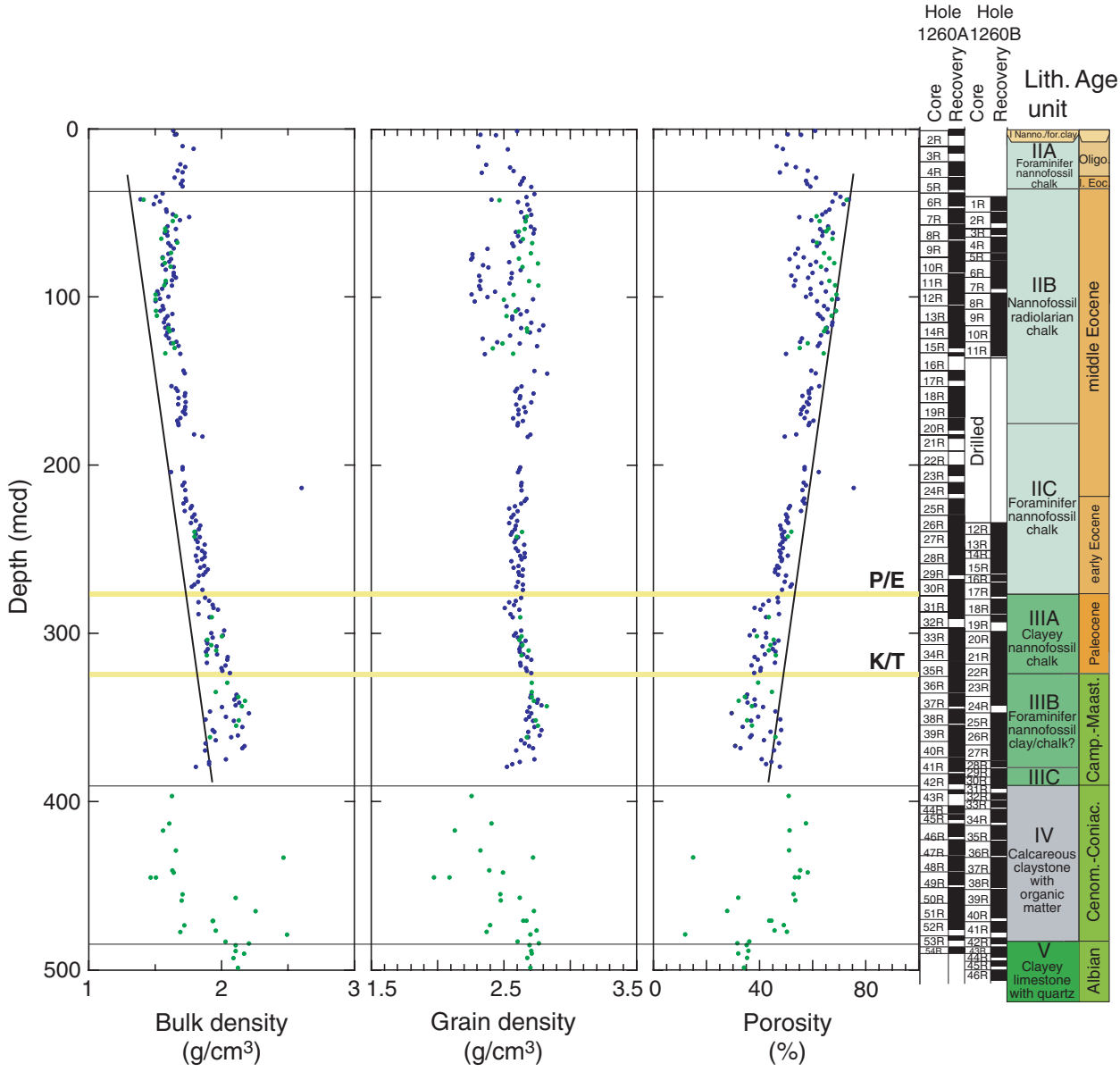

Figure F24. Bulk density and *P*-wave velocity measurements from split cores at Site 1260. *P*-wave anisotropy was measured on 8-cm³ samples from Hole 1260B. For anisotropy calculations see **"Physical Properties,"** p. 33, in the "Explanatory Notes," chapter. Blue = Hole 1260A, green = Hole 1260B.

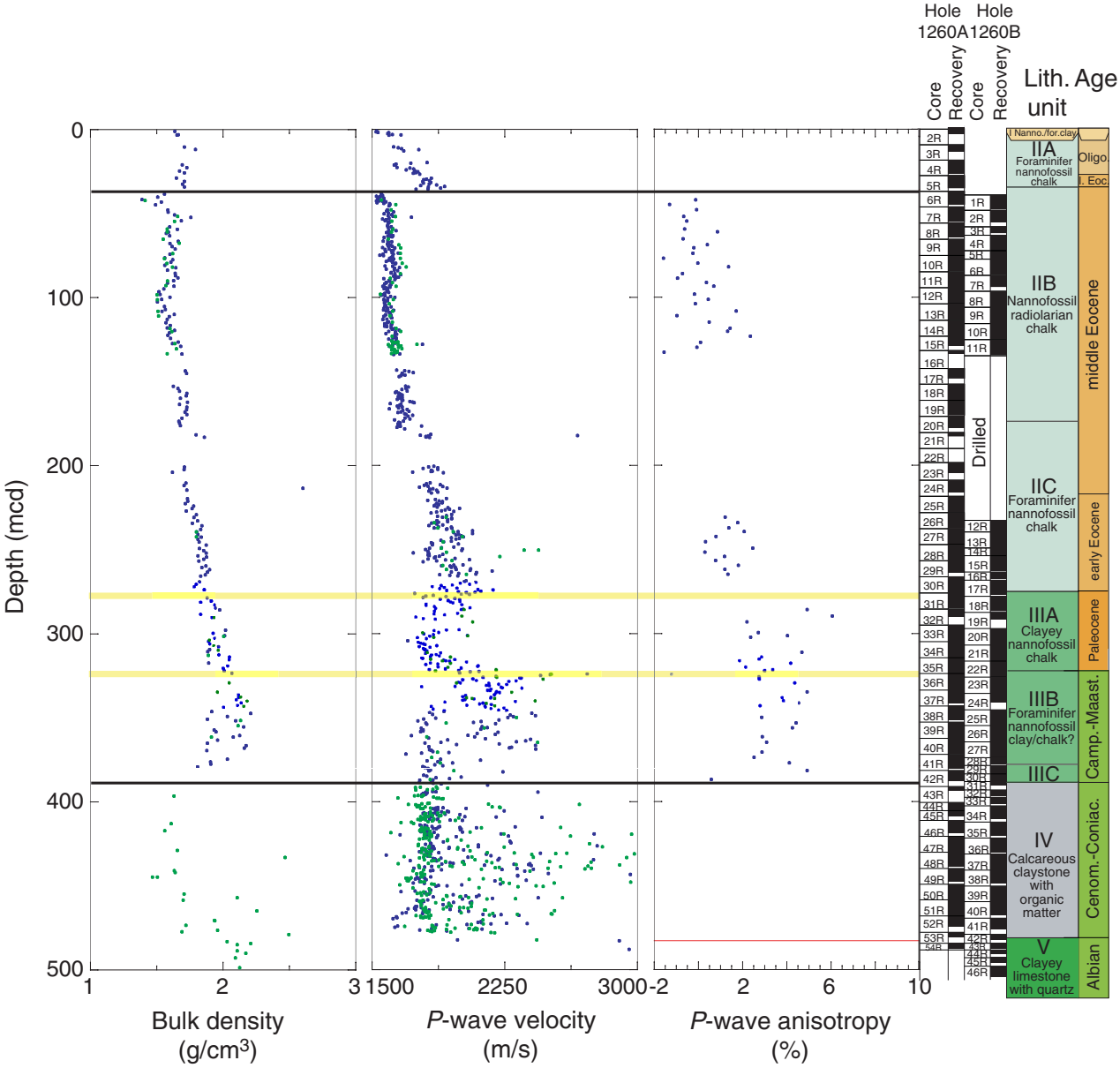

Figure F25. *P*-wave velocity and MST data from Holes 1260A (red) and 1260B (blue) through the black shale sequence of lithostratigraphic Unit IV. GRA = gamma ray attenuation, NGR = natural gamma radiation.

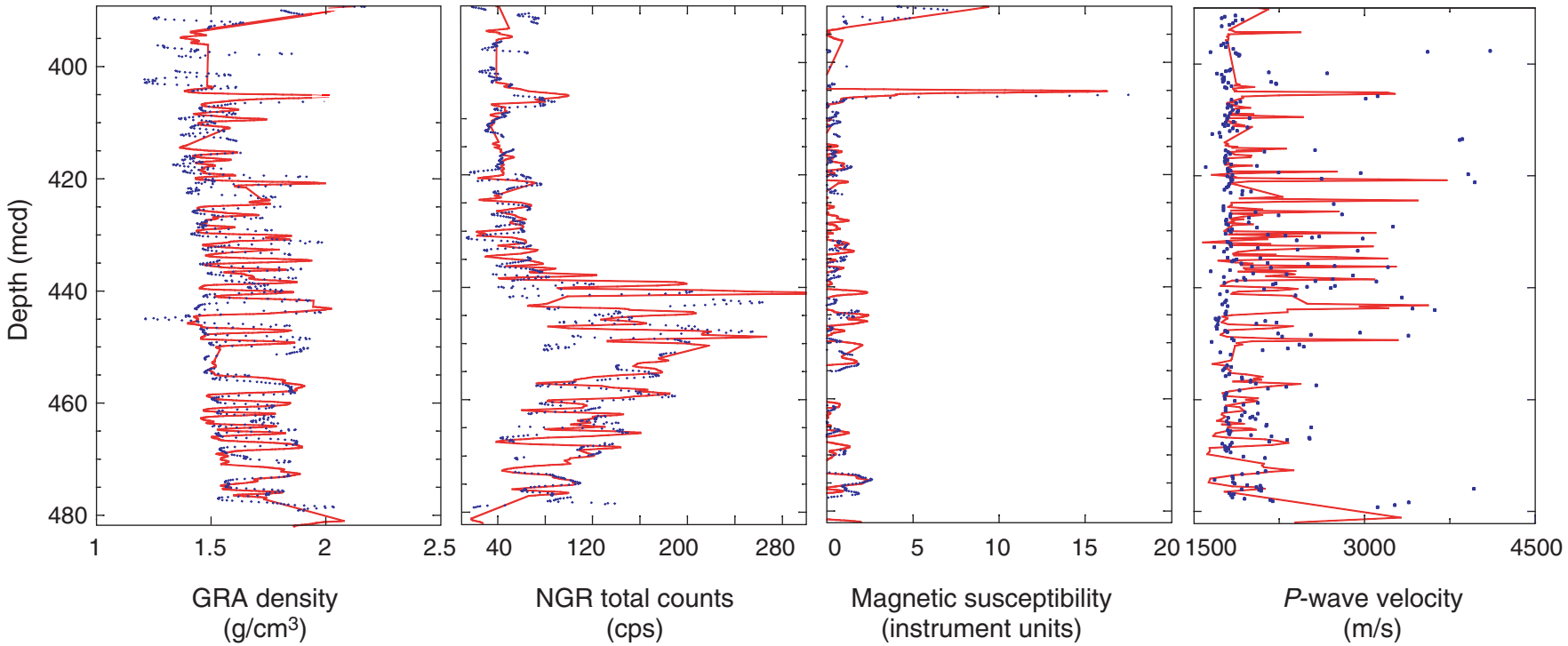

Figure F26. MST data with lithostratigraphic units from Holes 1260A (red) and 1260B (blue). Data have been smoothed using a 75-cm moving window. NGR = natural gamma radiation.

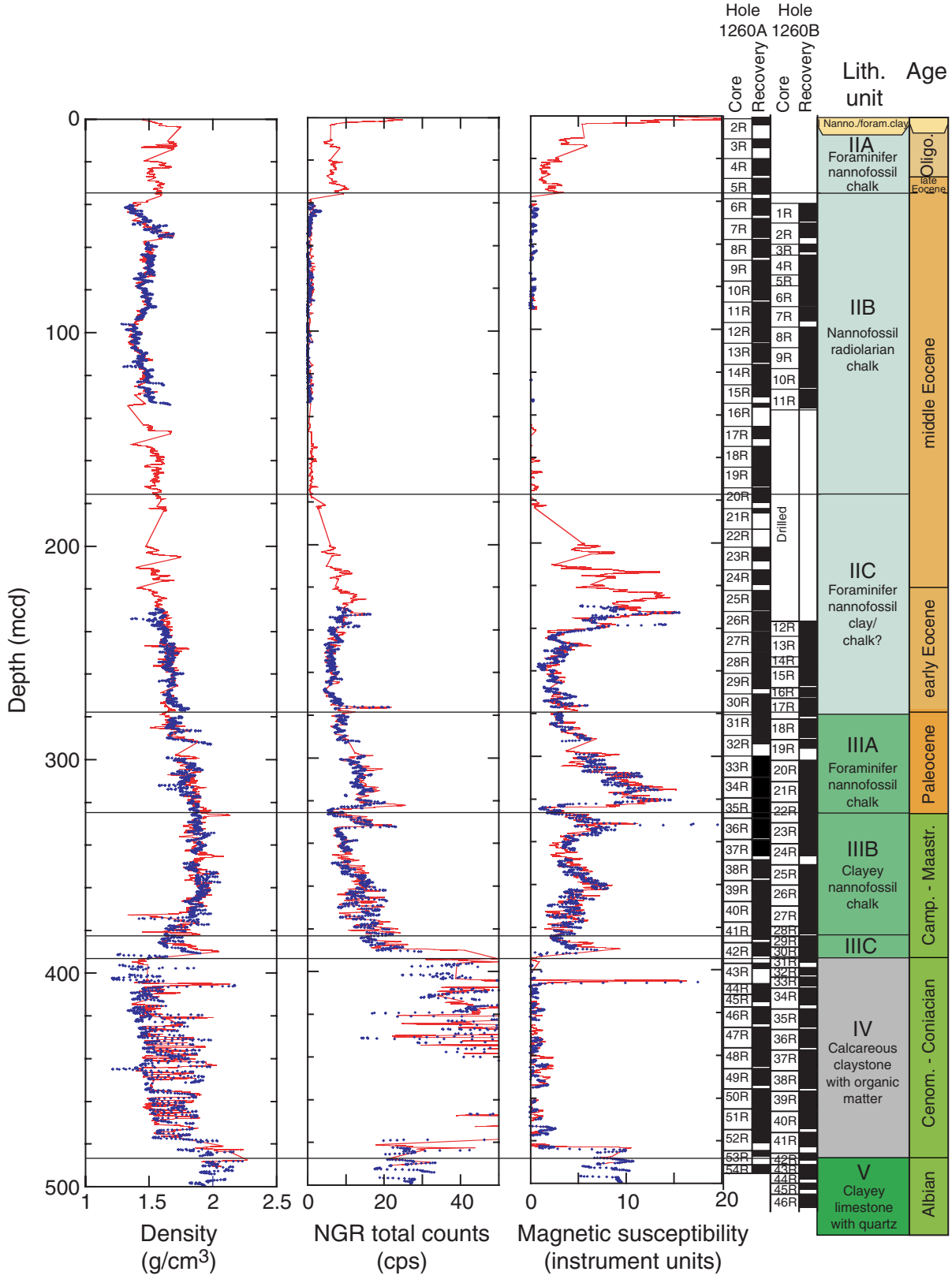

Figure F27. Summary of the logging runs undertaken in Hole 1260B. MGT = Multi-Sensor Spectral Gamma Ray Tool, FMS = Formation MicroScanner, WST = Well Seismic Tool.

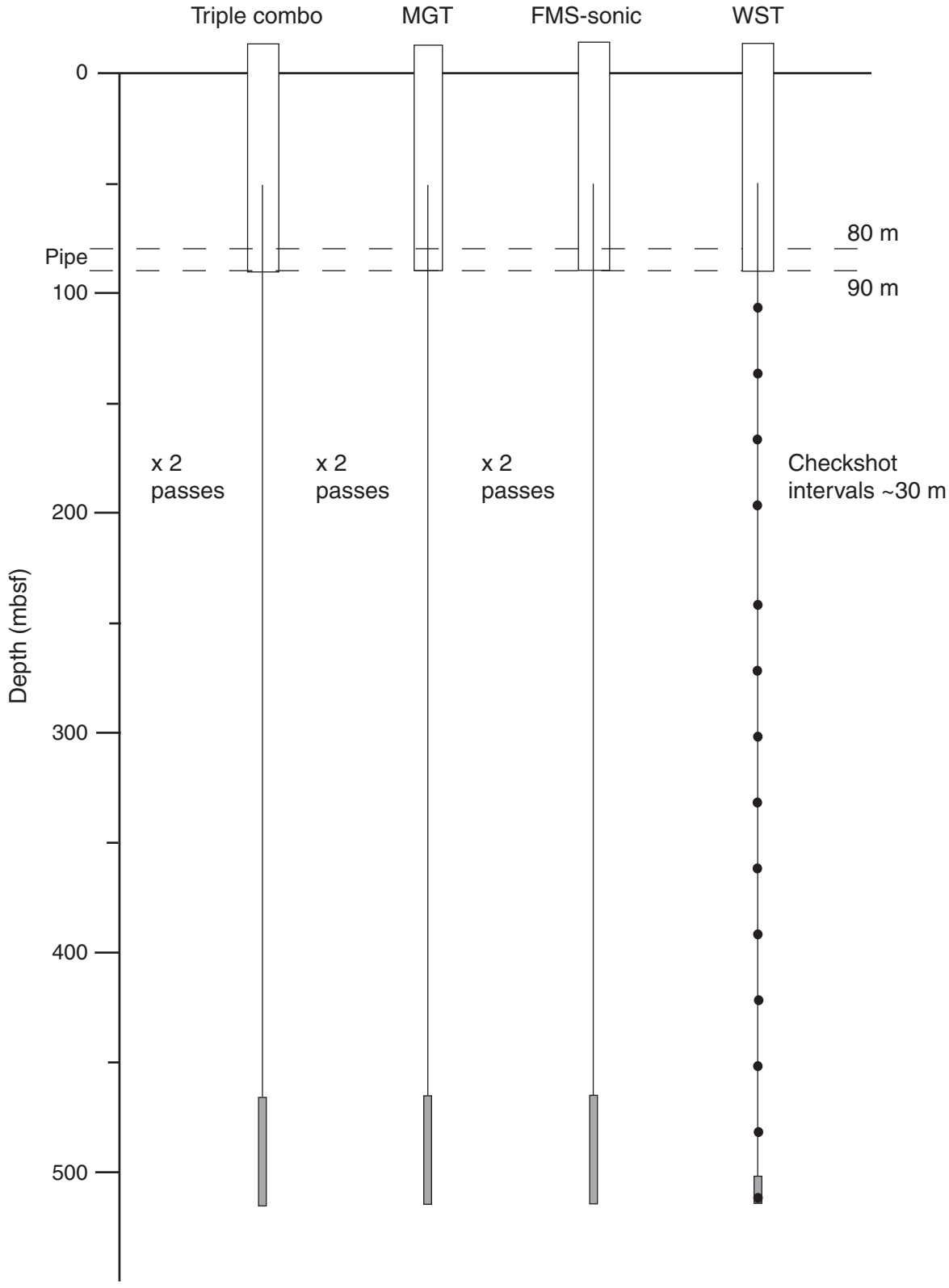

Figure F28. Borehole caliper logs from two passes of the triple combination (TC) and Formation MicroScanner (FMS)-sonic tool strings.

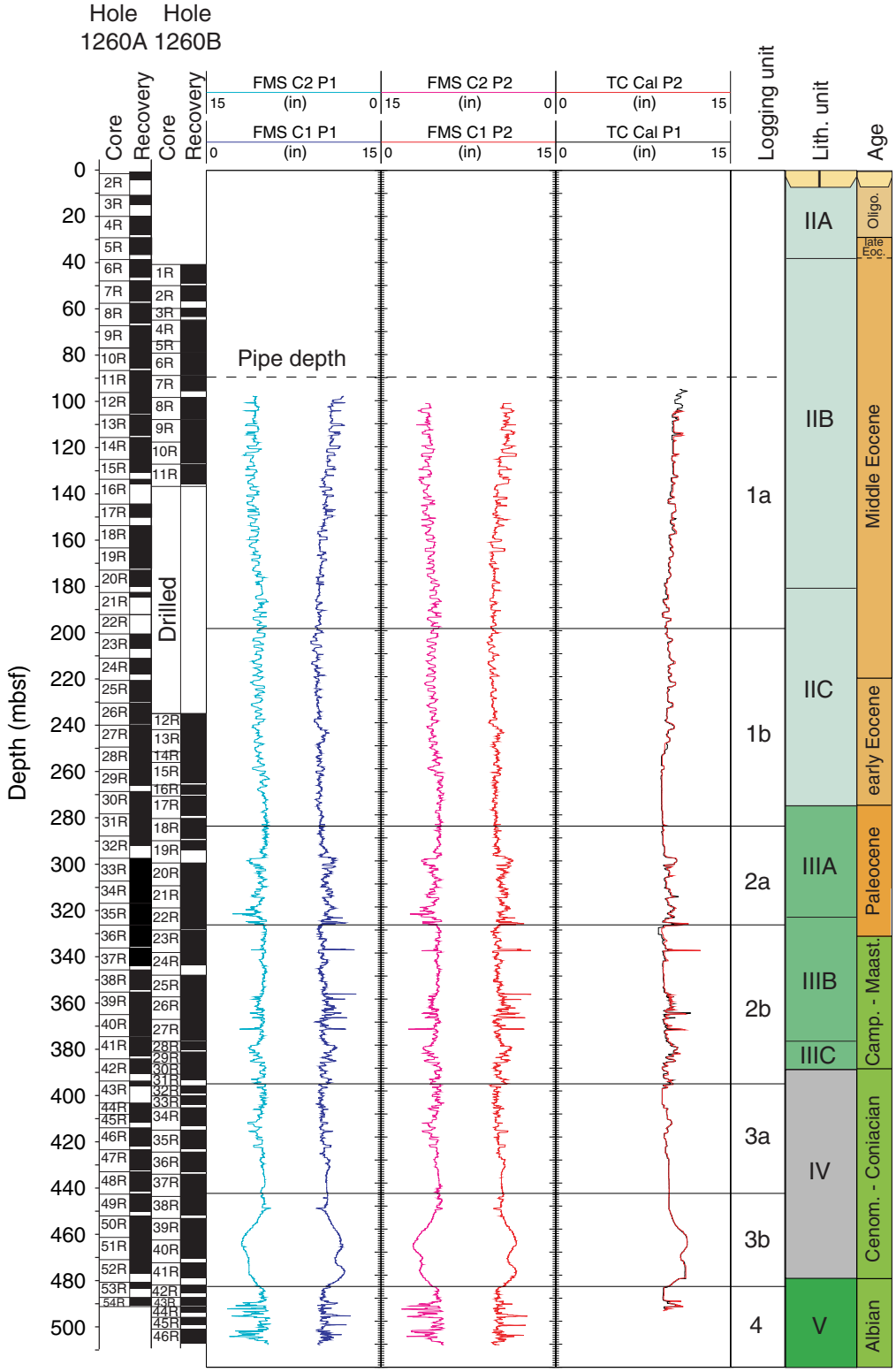

Figure F29. Geophysical logs from Hole 1260B and equivalent core physical properties (MST and MAD) from Holes 1260A and 1260B. PEF = photoelectric effect.

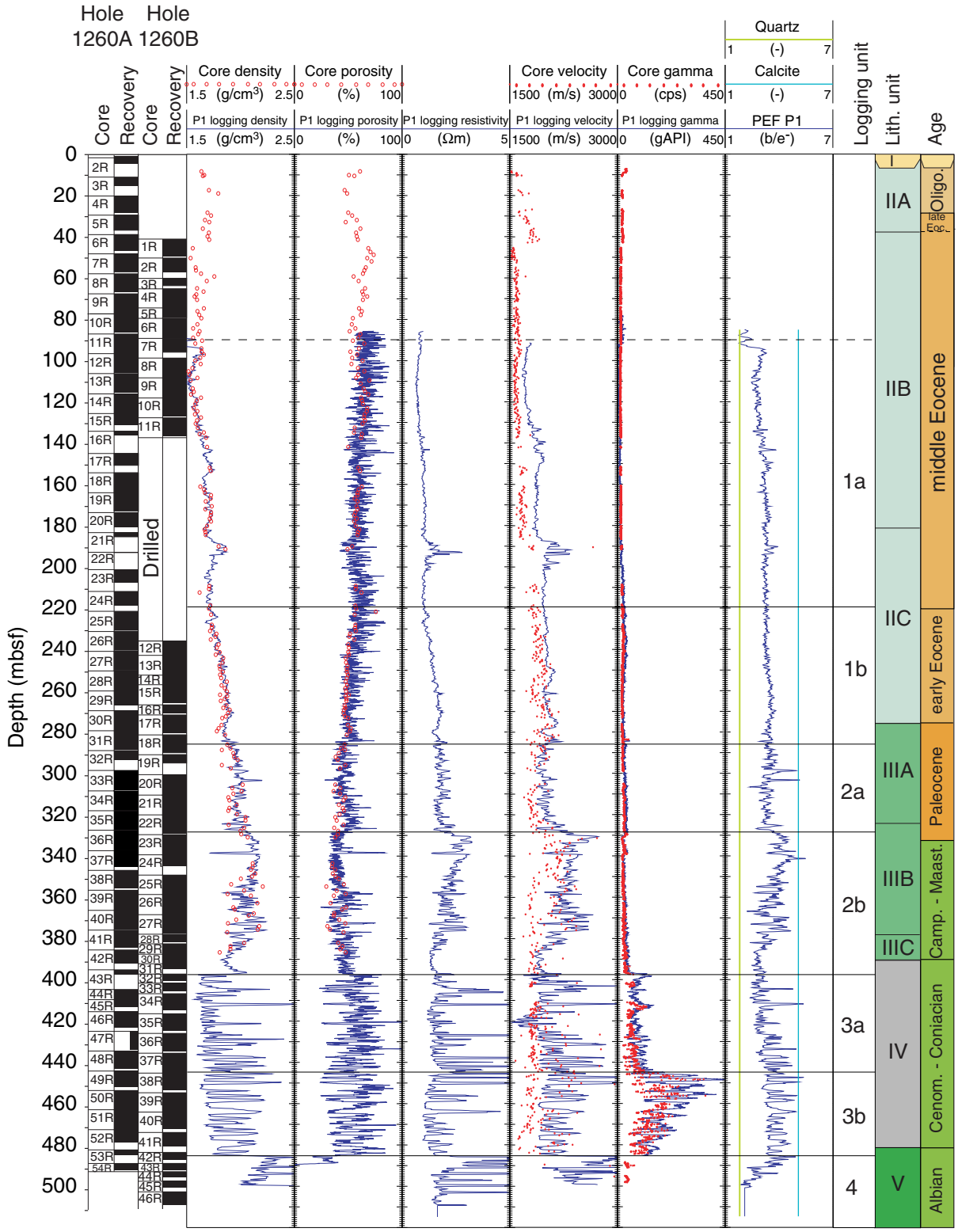

Figure F30. Geophysical logs, caliper data, and logging units, Hole 1260B. TC = triple combination, FMS = Formation MicroScanner, MGT = Multi-Sensor Spectral Gamma Ray tool, HSGR = HNGS Standard (total) Gamma Ray, PEF = photoelectric effect.

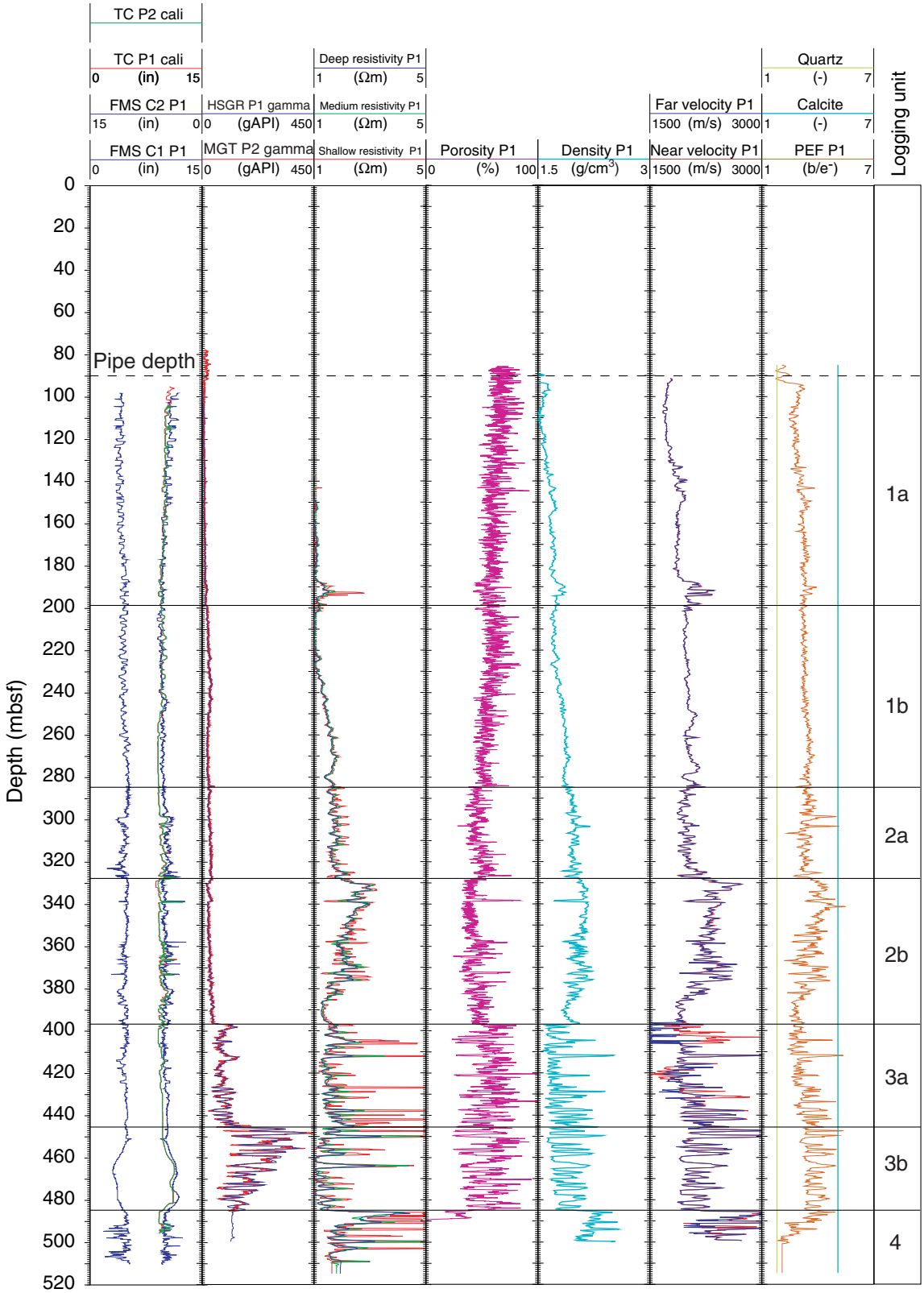

Figure F31. High-resolution MGT gamma ray logs from Hole 1260B. CGR = computed gamma ray.

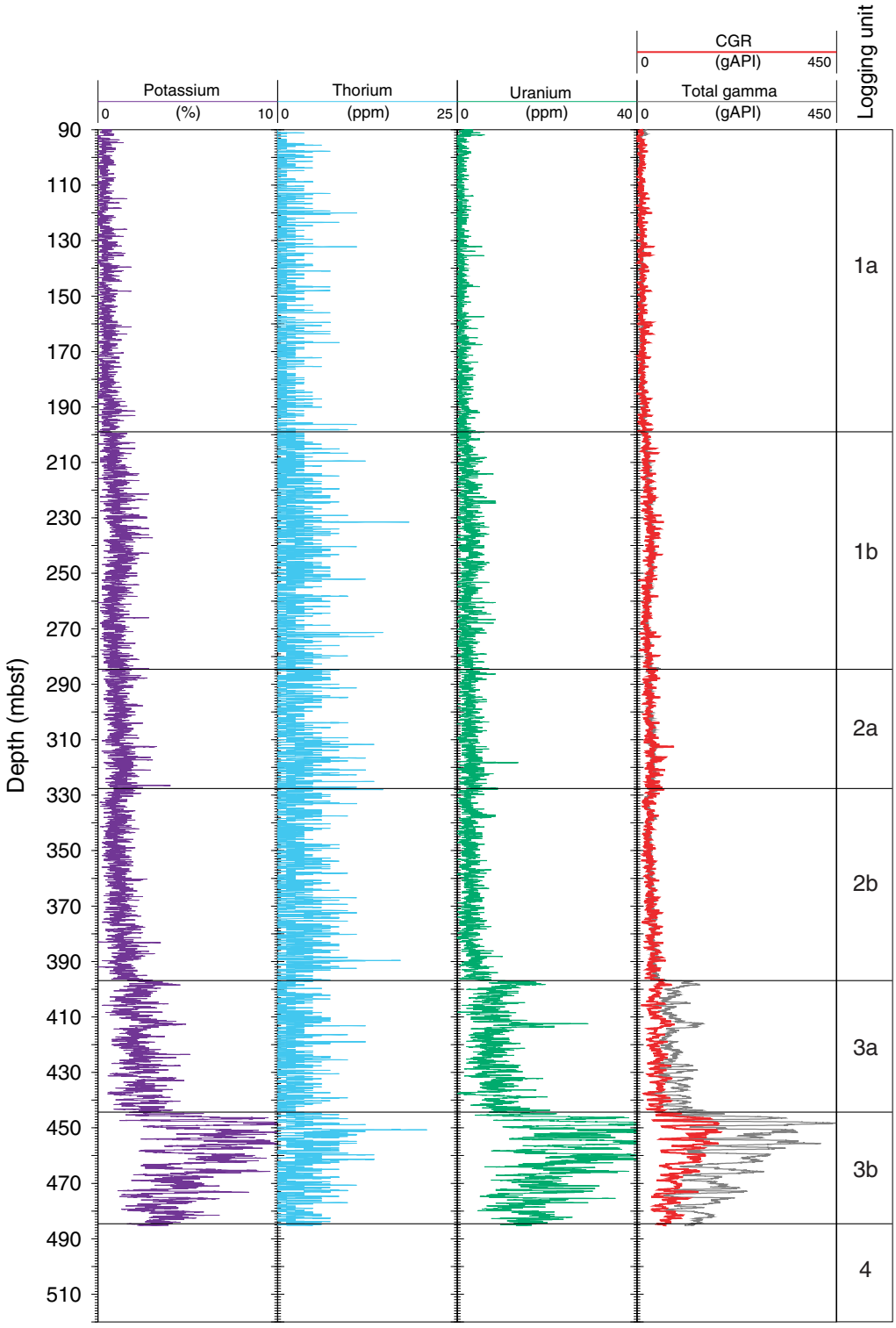

Figure F32. FMS pass 1 images, showing the region of high-resistivity (lighter color) and the high-resistance bands (180–202 mbsf) in Hole 1260B.

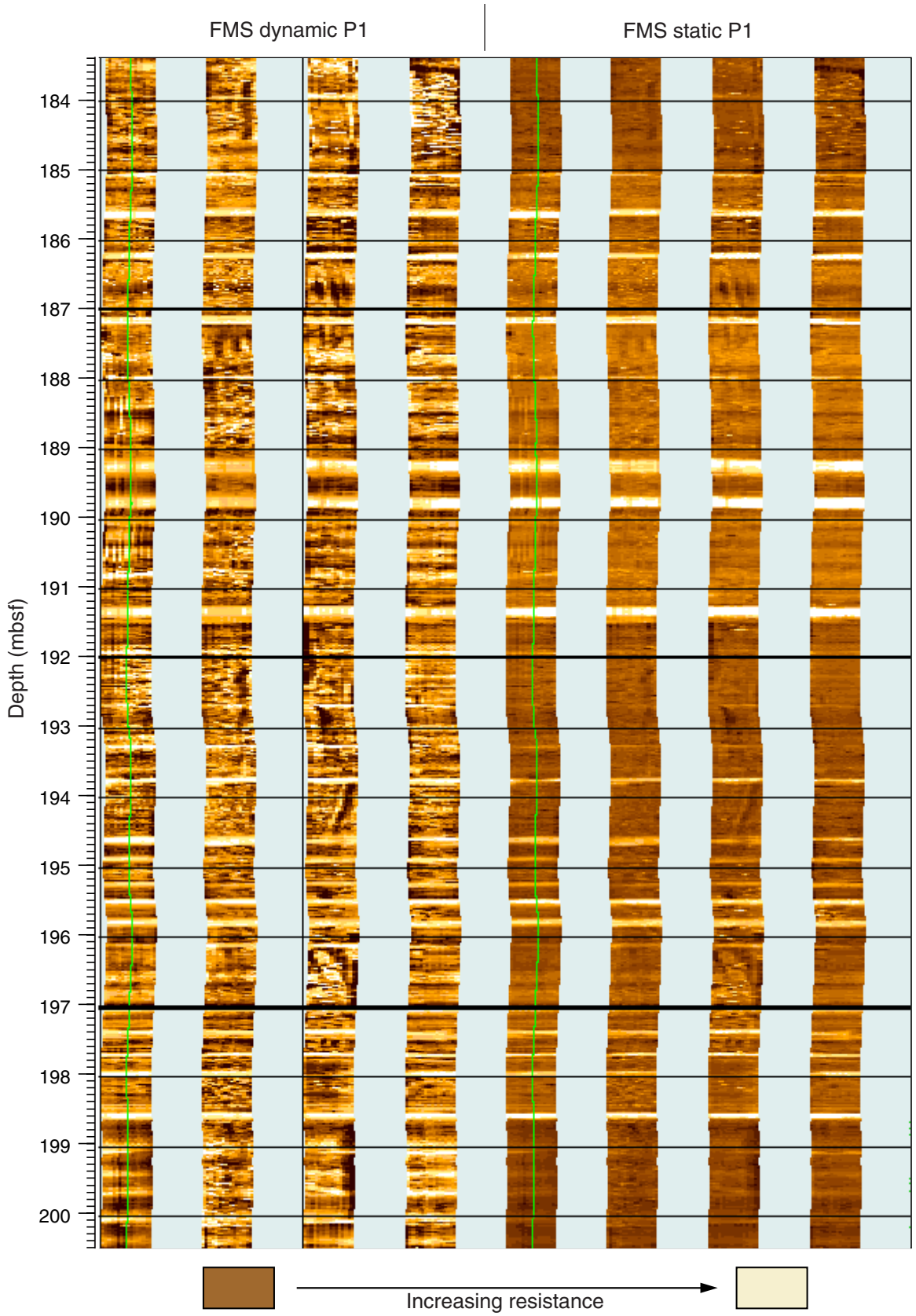

Figure F33. Cyclic variations in sedimentation highlighted by wireline physical property and Formation MicroScanner (FMS) imagery from an interval through logging Subunit 2a in Hole 1260B. TC = triple combination, PEF = photoelectric effect.

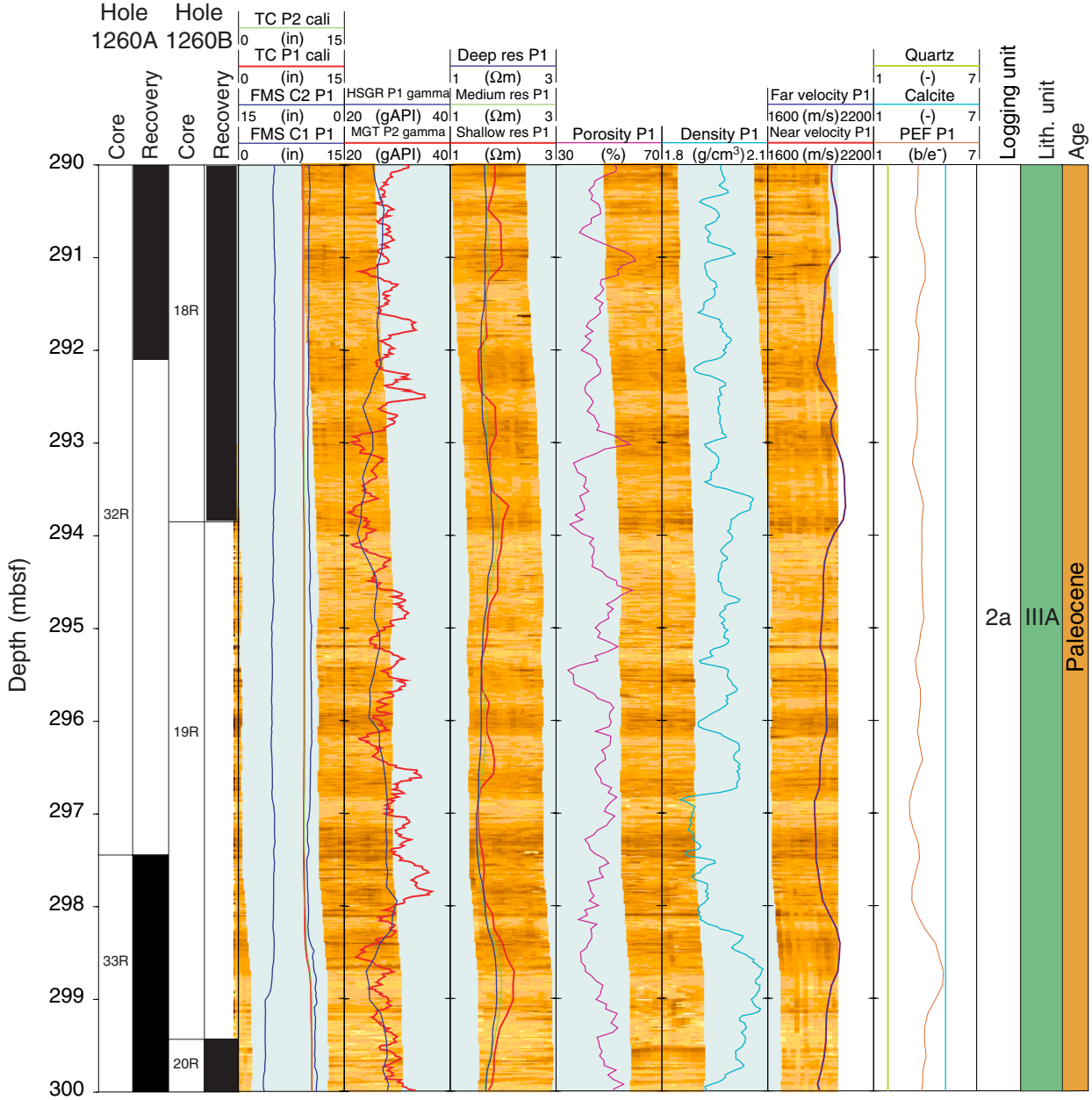

Figure F34. Logging and Formation MicroScanner (FMS) imagery showing the Subunit 2a/2b boundary and the K/T boundary at 338–339 mbsf. (Note the 7-m depth offset between the logging depths and the core lithostratigraphic units.) TC = triple combination, PEF = photoelectric effect.

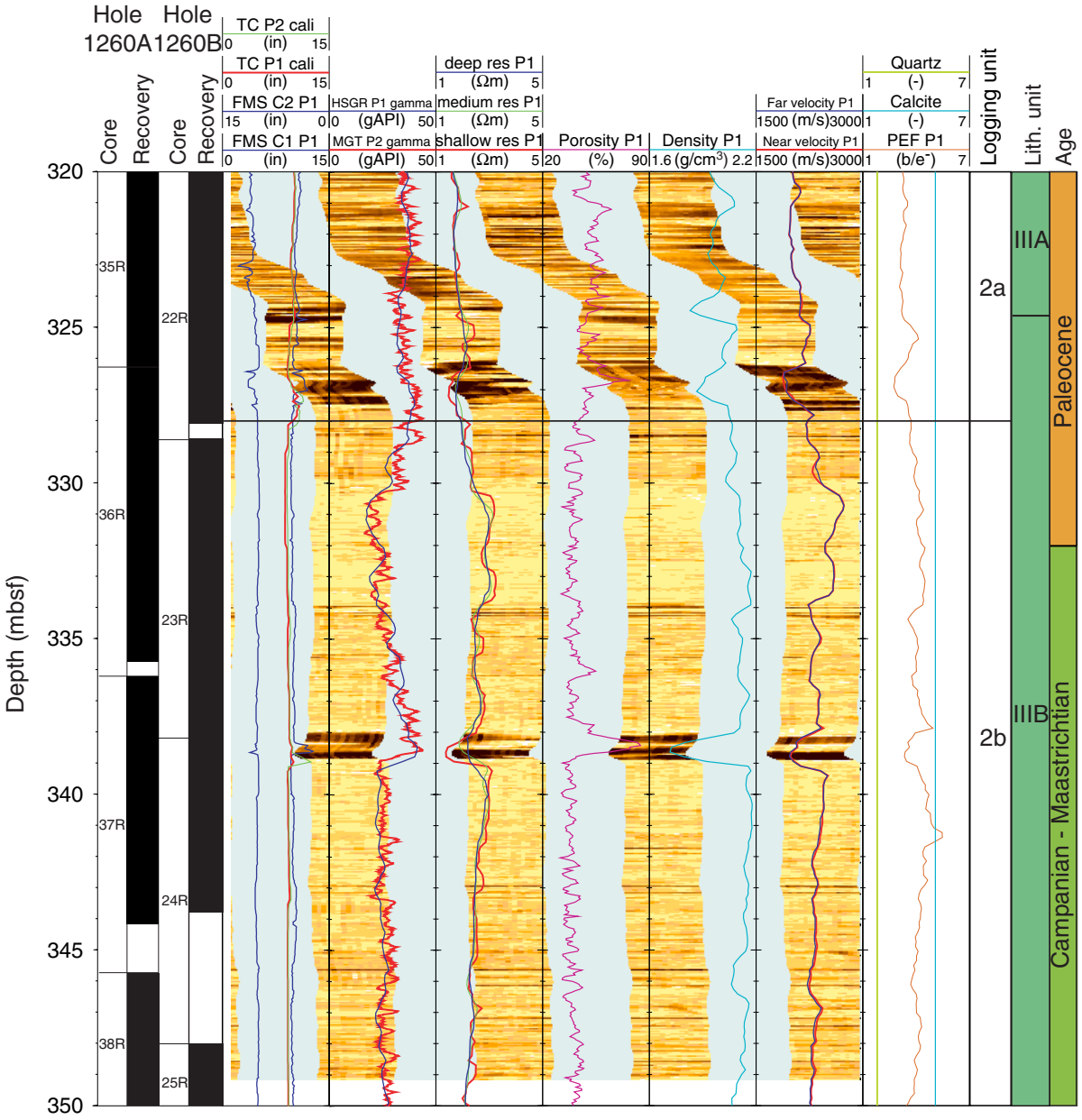

Figure F35. Stratigraphy of the black shale interval revealed by Formation MicroScanner (FMS)-sonic images and wireline-measured physical properties from logging Unit 3 in Hole 1260B. TC = triple combination, PEF = photoelectric effect.

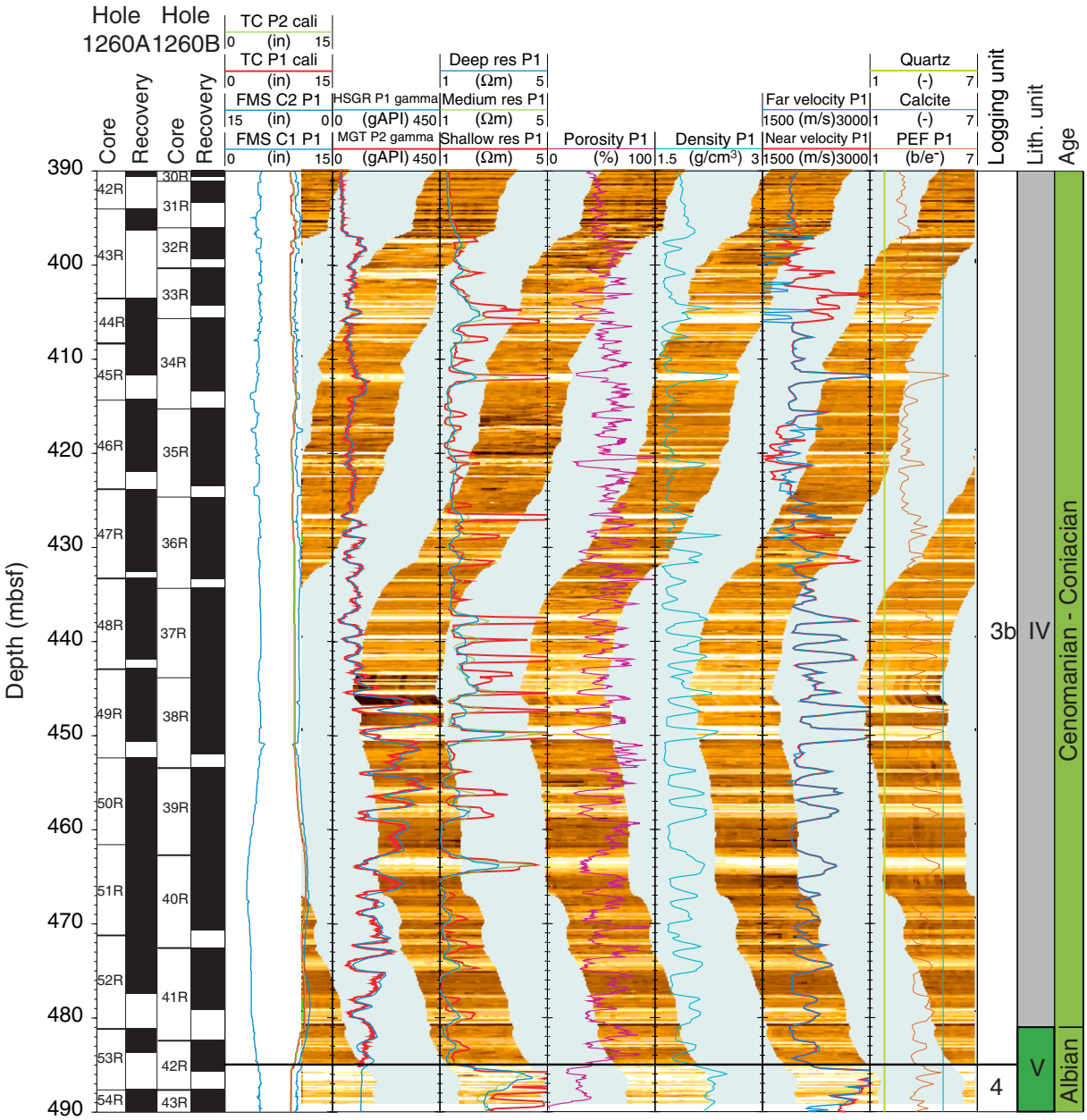

Figure F36. Comparison of core-measured total organic carbon (TOC) in Holes 1260A and 1260B and log-calculated TOC values in Hole 1260B through the black shale interval.

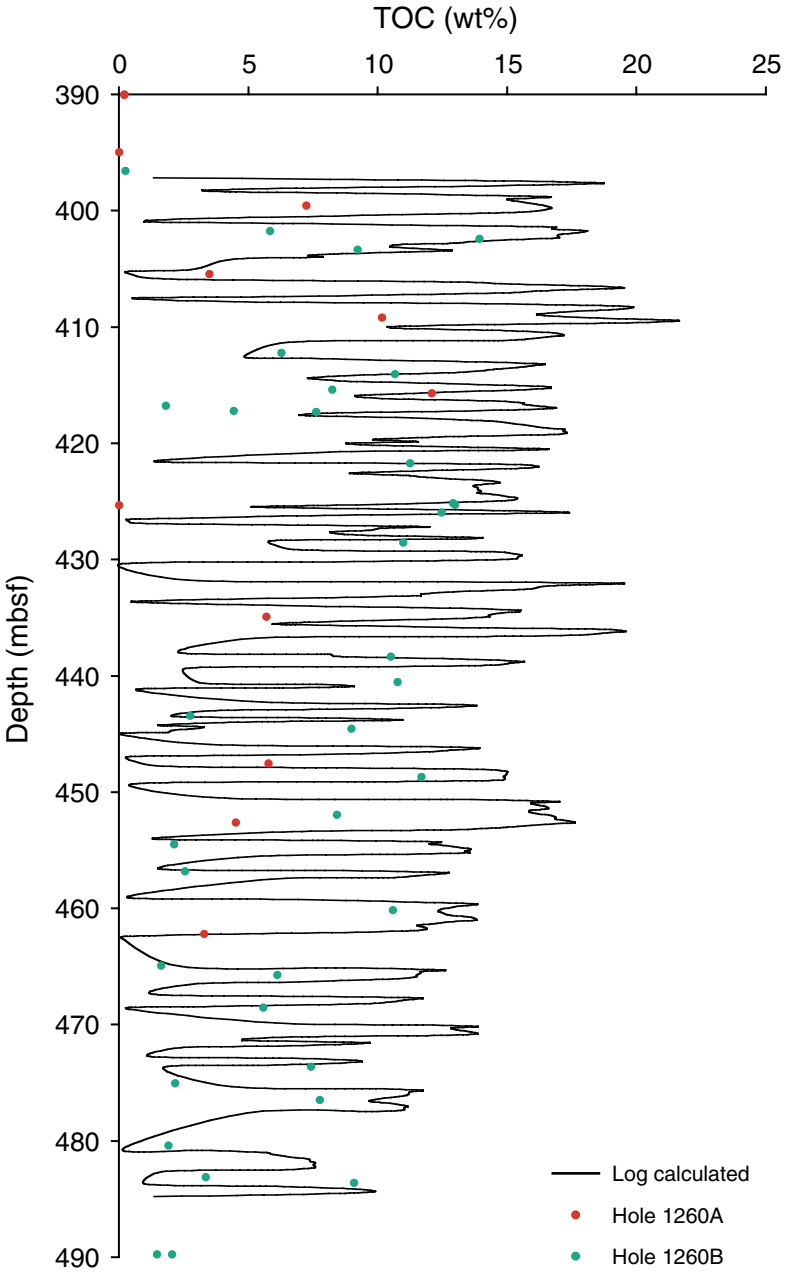

Figure F37. Formation density, velocity, impedance, and reflection coefficient series profiles obtained from downhole logging and core physical property measurements from Hole 1260B. The black line on the velocity plot represents interval velocities derived from the checkshot survey (Table T22, p. 113).

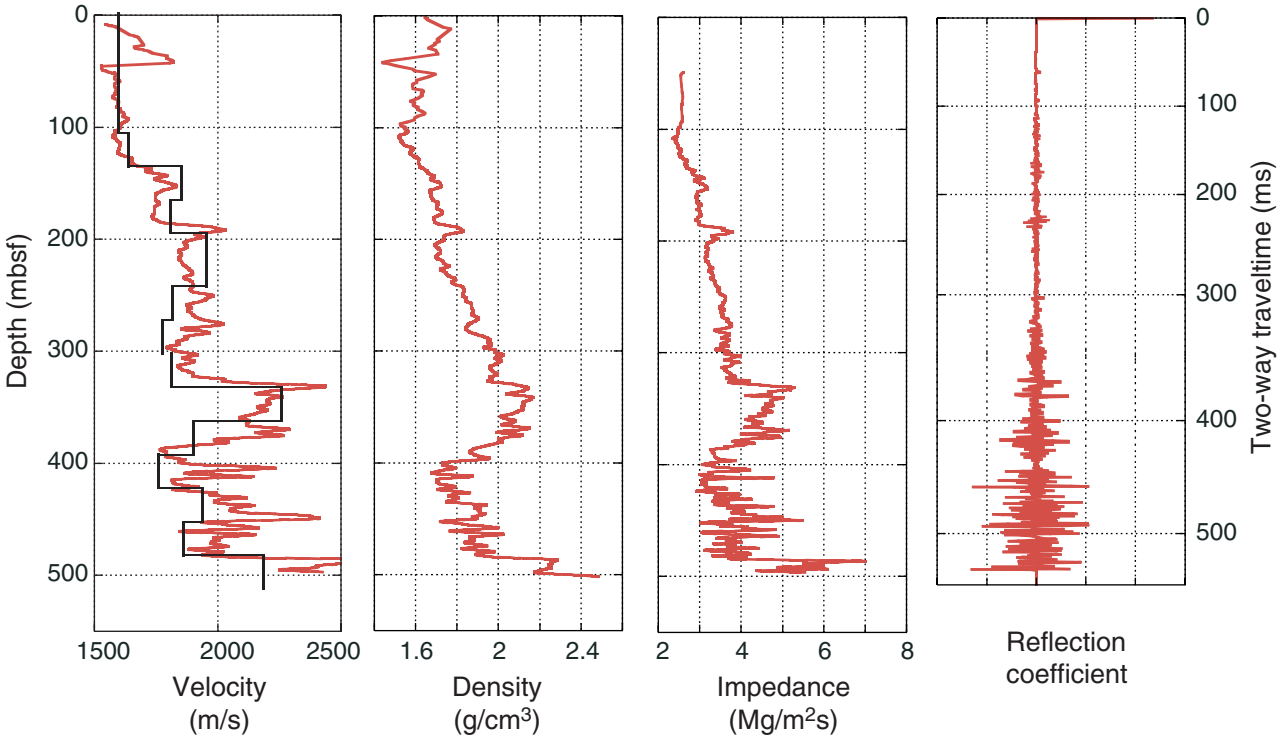

Figure F38. Part of seismic line M49-4-GeoB215 showing the core-defined reflectors, the calculated synthetic seismogram, and impedance profile (derived from the density and velocity data) from Hole 1260B.

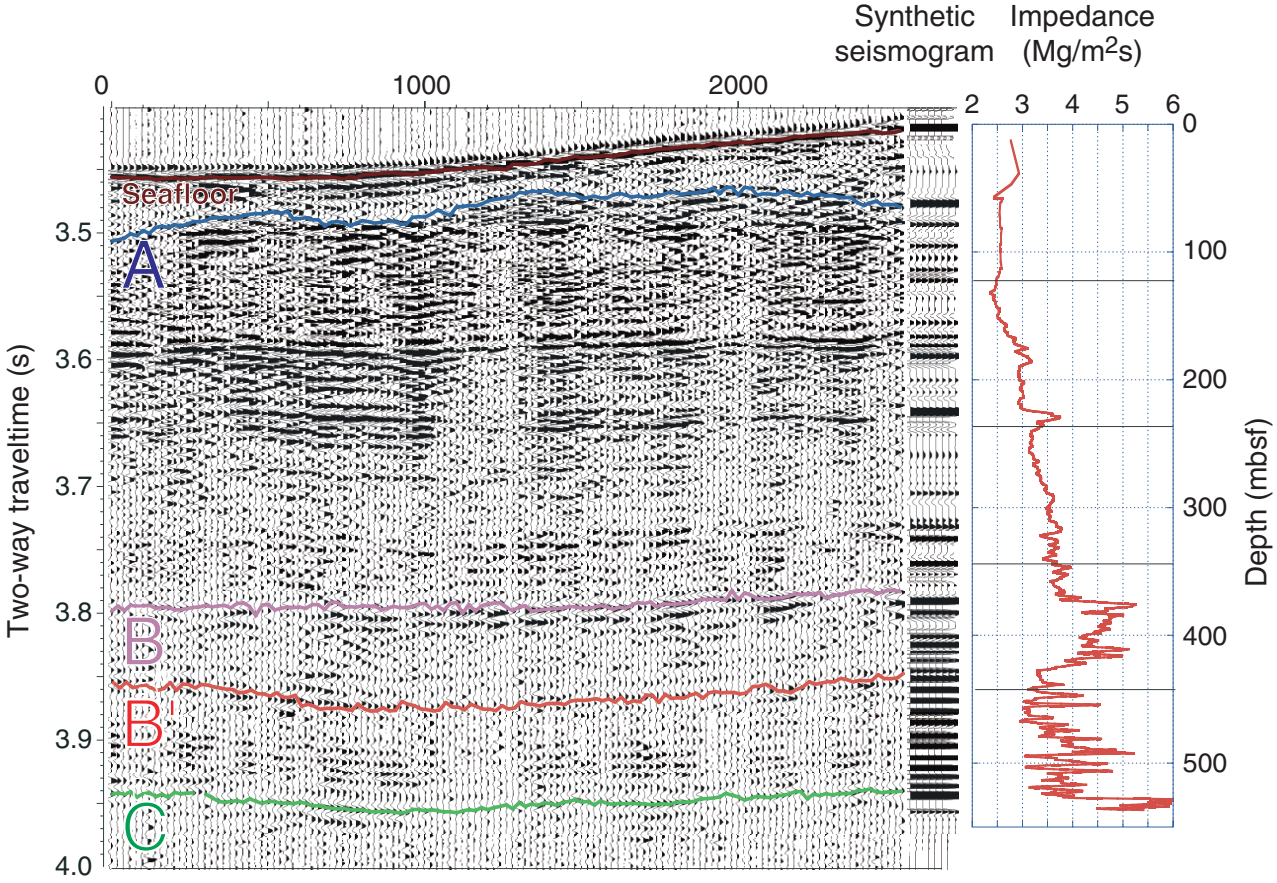

Table T1. Coring summary, Site 1260. (See table notes. Continued on next two pages.)

Hole 1260A
Latitude: 9°15.9485′N
Longitude: 54°32.6327′W
Time on site: 139.50 (0430 hr, 7 Feb–0000 hr, 13 Feb 2003)
Time on hole: 51.08 (0430 hr, 7 Feb–0735 hr, 9 Feb 2003)
Seafloor (drill pipe measurement from rig floor, mbrf): 2560.0
Distance between rig floor and sea level (m): 11.2
Water depth (drill pipe measurement from sea level, m): 2548.8
Total depth (drill pipe measurement from rig floor, mbrf): 3051.9
Total penetration (meters below seafloor, mbsf): 491.9
Total length of cored section (m): 491.9
Total core recovered (m): 391.6
Core recovery (%): 79.61
Total number of cores: 54
Total number of drilled intervals: 0

Hole 1260B
Latitude: 9°15.9307′N
Longitude: 54°32.6518′W
Time on hole: 88.42 (0735 hr, 9 Feb–0000 hr, 13 Feb 2003)
Seafloor (drill pipe measurement from rig floor, mbrf): 2560.0
Distance between rig floor and sea level (m): 11.2
Water depth (drill pipe measurement from sea level, m): 2548.80
Total depth (drill pipe measurement from rig floor, mbrf): 3069.0
Total penetration (meters below seafloor, mbsf): 509.0
Total length of cored section (m): 370.3
Total length of drilled intervals (m): 138.7
Total core recovered (m): 326.49
Core recovery (%): 88.2
Total number of cores: 46
Total number of drilled intervals: 2

Core	Date (Feb 2003)	Local time (hr)	Depth (mbsf) Top	Depth (mbsf) Bottom	Length (m) Cored	Length (m) Recovered	Recovery (%)	Remarks
207-1260A-								
1R	7	1145	0.0	1.0	1.0	0.81	81.0	
2R	7	1235	1.0	10.3	9.3	2.91	31.3	
3R	7	1325	10.3	19.5	9.2	4.31	46.9	AHC on
4R	7	1405	19.5	28.8	9.3	8.16	87.7	AHC on
5R	7	1440	28.8	38.2	9.4	7.35	78.2	AHC on
6R	7	1510	38.2	47.5	9.3	7.71	82.9	
7R	7	1545	47.5	57.2	9.7	8.74	90.1	
8R	7	1615	57.2	66.9	9.7	8.56	88.3	
9R	7	1645	66.9	76.6	9.7	9.76	100.6	
10R	7	1715	76.6	86.3	9.7	8.90	91.8	
11R	7	1750	86.3	95.9	9.6	9.90	103.1	
12R	7	1820	95.9	105.6	9.7	9.13	94.1	
13R	7	1850	105.6	115.3	9.7	9.13	94.1	
14R	7	1920	115.3	124.9	9.6	9.54	99.4	
15R	7	1950	124.9	134.5	9.6	5.77	60.1	
16R	7	2020	134.5	144.2	9.7	0.99	10.2	
17R	7	2050	144.2	153.5	9.3	4.70	50.5	
18R	7	2120	153.5	163.2	9.7	9.87	101.8	
19R	7	2150	163.2	172.8	9.6	8.82	91.9	
20R	7	2220	172.8	182.5	9.7	7.02	72.4	
21R	7	2250	182.5	192.1	9.6	2.21	23.0	
22R	7	2325	192.1	201.4	9.3	0.05	0.5	
23R	8	0005	201.4	211.1	9.7	5.30	54.6	
24R	8	0040	211.1	220.7	9.6	6.88	71.7	
25R	8	0115	220.7	230.3	9.6	9.24	96.3	
26R	8	0150	230.3	240.0	9.7	9.33	96.2	
27R	8	0230	240.0	249.6	9.6	9.52	99.2	
28R	8	0320	249.6	259.2	9.6	9.81	102.2	
29R	8	0400	259.2	268.9	9.7	7.11	73.3	
30R	8	0445	268.9	278.5	9.6	9.69	100.9	
31R	8	0545	278.5	288.2	9.7	9.24	95.3	
32R	8	0635	288.2	297.8	9.6	4.18	43.5	
33R	8	0730	297.8	307.4	9.6	9.24	96.3	
34R	8	0815	307.4	317.1	9.7	9.92	102.3	

Table T1 (continued).

Core	Date (Feb 2003)	Local time (hr)	Depth (mbsf) Top	Depth (mbsf) Bottom	Length (m) Cored	Length (m) Recovered	Recovery (%)	Remarks
35R	8	0900	317.1	326.7	9.6	9.93	103.4	
36R	8	0945	326.7	336.4	9.7	9.42	97.1	K/T boundary recovered
37R	8	1025	336.4	346.0	9.6	10.01	104.3	
38R	8	1105	346.0	355.6	9.6	8.53	88.9	
39R	8	1155	355.6	365.3	9.7	10.03	103.4	
40R	8	1240	365.3	374.9	9.6	9.31	97.0	
41R	8	1340	374.9	384.5	9.6	8.37	87.2	
42R	8	1435	384.5	394.1	9.6	6.28	65.4	
43R	8	1525	394.1	403.7	9.6	2.52	26.3	
44R	8	1715	403.7	408.7	5.0	4.98	99.6	
45R	8	1820	408.7	414.3	5.6	3.33	59.5	
46R	8	1935	414.3	423.9	9.6	7.80	81.3	
47R	8	2045	423.9	433.5	9.6	9.10	94.8	
48R	8	2200	433.5	443.1	9.6	8.79	91.6	
49R	8	2310	443.1	452.7	9.6	7.90	82.3	
50R	9	0005	452.7	462.0	9.3	9.46	101.7	
51R	9	0100	462.0	471.6	9.6	9.57	99.7	
52R	9	0230	471.6	481.3	9.7	6.16	63.5	
53R	9	0415	481.3	487.9	6.6	2.80	42.4	
54R	9	0530	487.9	491.9	4.0	3.51	87.8	
			Cored totals:		491.9	391.60	79.6	
207-1260B-								
			*****Drilled from 0.0 to 40.2 mbsf*****					
1R	9	1040	40.2	49.7	9.5	8.63	90.8	
2R	9	1115	49.7	59.4	9.7	6.74	69.5	
3R	9	1150	59.4	64.4	5.0	3.58	71.6	
4R	9	1220	64.4	73.8	9.4	9.82	104.5	
5R	9	1250	73.8	78.8	5.0	4.83	96.6	
6R	9	1320	78.8	88.4	9.6	9.28	96.7	
7R	9	1350	88.4	98.0	9.6	6.83	71.2	
8R	9	1420	98.0	107.6	9.6	9.48	98.8	
9R	9	1450	107.6	117.2	9.6	9.68	100.8	
10R	9	1520	117.2	126.9	9.7	9.13	94.1	
11R	9	1550	126.9	136.5	9.6	8.71	90.7	
			*****Drilled from 136.5 to 235.0 mbsf*****					AHC on
12R	9	1935	235.0	242.0	7.0	8.54	122.0	
13R	9	2015	242.0	251.6	9.6	9.55	99.5	
14R	9	2050	251.6	256.2	4.6	4.84	105.2	
15R	9	2130	256.2	265.9	9.7	8.81	90.8	
16R	9	2205	265.9	270.9	5.0	4.04	80.8	
17R	9	2300	270.9	280.5	9.6	9.96	103.8	
18R	9	2345	280.5	290.1	9.6	8.63	89.9	
19R	10	0110	290.1	299.8	9.7	3.89	40.1	
20R	10	0210	299.8	309.4	9.6	9.57	99.7	
21R	10	0300	309.4	319.1	9.7	9.84	101.4	
22R	10	0340	319.1	328.7	9.6	9.46	98.5	
23R	10	0425	328.7	338.4	9.7	9.95	102.6	K/T boundary recovered
24R	10	0505	338.4	348.0	9.6	5.71	59.5	
25R	10	0550	348.0	357.7	9.7	9.85	101.6	
26R	10	0635	357.7	367.3	9.6	9.62	100.2	
27R	10	0725	367.3	376.9	9.6	8.99	93.7	
28R	10	0810	376.9	381.5	4.6	3.82	83.0	
29R	10	0855	381.5	386.5	5.0	5.09	101.8	
30R	10	0945	386.5	391.1	4.6	4.36	94.8	
31R	10	1025	391.1	396.1	5.0	2.35	47.0	
32R	10	1110	396.1	400.7	4.6	2.56	55.7	
33R	10	1205	400.7	405.7	5.0	3.83	76.6	
34R	10	1325	405.7	415.3	9.6	7.97	83.0	AHC on
35R	10	1445	415.3	424.9	9.6	8.41	87.6	
36R	10	1550	424.9	434.5	9.6	8.80	91.7	
37R	10	1710	434.5	444.1	9.6	9.94	103.5	
38R	10	1820	444.1	453.7	9.6	8.29	86.4	
39R	10	1915	453.7	463.1	9.4	9.90	105.3	
40R	10	2020	463.1	472.7	9.6	7.91	82.4	
41R	10	2145	472.7	482.3	9.6	6.77	70.5	
42R	11	0005	482.3	487.9	5.6	3.61	64.5	
43R	11	0135	487.9	491.9	4.0	3.40	85.0	
44R	11	0340	491.9	496.5	4.6	2.48	53.9	

Table T1 (continued).

Core	Date (Feb 2003)	Local time (hr)	Depth (mbsf) Top	Depth (mbsf) Bottom	Length (m) Cored	Length (m) Recovered	Recovery (%)	Remarks
45R	11	0515	496.5	501.5	5.0	3.17	63.4	
46R	11	0700	501.5	509.0	7.5	5.87	78.3	
				Cored totals:	370.3	326.49	88.2	
				Drilled total:	138.7			
				Total:	509.0			

Notes: AHC = active heave compensator. K/T = Cretaceous/Tertiary.

Table T2. Lithostratigraphic units and subunits, Site 1260.

Unit/ Subunit	Hole, core, section, interval (cm)	Depth (mbsf)	Thickness (mbsf)	Age	Lithology
	207-				
I	1260A-1R-1, 0, through 2R-1, 10 *	0–1.10	1.10	Pleistocene	Nannofossils clay
IIA	1260A-2R-1, 10, through 5R-CC, 12 *	1.10–36.03	34.93	early Oligocene	Foraminifers and nannofossils ooze; foraminifers and nannofossils chalk
IIB	1260A-5R-CC, 12, through 20R-3, 78 1260B-1R-1, 0 through 11R-CC, 25	36.03–176.58 40.2–>135.61	140.55 >95.41	middle Eocene	Nannofossils and radiolarian chalk; nannofossils chalk with foraminifers and radiolarian
IIC	1260A-20R-3, 78, through 30R-7, 74 <1260B-12R-1, 0, through 17R-7, 69	176.58–276.74 <235–279.84	100.16 >44.84	middle Eocene–early Eocene	Nannofossils chalk with clay and foraminifers
IIIA	1260A-30R-7, 74, through 35R-5, 93 1260B-17R-7, 69, through 22R-3, 145	276.74–324.03 279.84–323.55	47.29 43.71	Paleocene	Nannofossils chalk with foraminifers and calcite; clayey nannofossils chalk with foraminifers and calcite
IIIB	1260A-35R-5, 93, through 41R-3, 125 1260B-22R-3, 145, through 28R-2, 145	324.03–379.15 323.55–379.85	55.12 56.30	Maastrichtian–late Campanian	Nannofossils chalk with foraminifers and calcite; clayey nannofossils chalk with foraminifers and calcite
IIIC	1260A-41R-3, 125, through 42R-CC, 15 1260B-28R-2, 145, through 30R-CC, 8	379.15–390.65 379.85–390.83	11.50 10.98	early Campanian	Nannofossils chalk with foraminifers and calcite; clayey nannofossils chalk with foraminifers and calcite
IV	1260A-42R-CC, 15, through 53R-2, 42 1260B-30R-CC, 8, through 42R-2, 1	390.65–483.22 390.83–483.59	92.57 92.76	Santonian–middle Cenomanian	Calcareous claystone with organic matter; clayey chalk with organic matter; limestone
V	1260A-53R-2, 42, through 54R-CC, 2 1260B-42R-2, 1, through 46R-CC, 32	483.22–491.90 483.59–507.37	8.68 23.78	middle–late Albian	Clayey limestone with quartz; calcareous claystone with quartz

Note: * = not recovered from Hole 1260B.

Table T3. Datum levels for calcareous nannofossils, Site 1260.

Core, section, interval (cm)	Depth (mbsf) Top	Depth (mbsf) Bottom	Depth (mcd) Top	Depth (mcd) Bottom	Datum	Species	Zone	Age	Age (Ma)
207-1260A-									
1R-CC, 12–18	0.75	3.85	0.75	3.85	B	*Emiliania huxleyi*	NN21	late Pleistocene	0.3
2R-CC, 8–14		3.85		3.85	Slumps; no datums given		NP 23/21 mixed	early Oligocene	
3R-CC, 13–18		14.51		14.51	Slumps; no datums given		NP 23/21 mixed	early Oligocene	
4R-CC, 0–5	27.50		27.50		Slumps; no datums given E/O boundary is in 5R-5		NP 23/21 mixed	early Oligocene	
5R-CC, 19–24					T	*Cribrocentrum reticulatum*	NP 20	late Eocene	34.9
5R-CC, 19–24	27.50	36.10	27.50	36.10	B	*Dictyoccocites bisectus*	NP17	middle Eocene	38.5
7R-CC, 0–5	36.10	45.79	36.10	45.79	T	*Chiasmolithus solitus*	NP16	middle Eocene	40.4
10R-CC, 8–13	45.79	56.19	45.79	56.29	B	*Reticulofenestra umbilicus*	NP16	middle Eocene	42.5
14R-CC, 19–24	85.45	96.15	84.55	94.77	T	*Nannotetrina fulgens*	NP15	middle Eocene	43.5
17R-CC, 13–19	114.67	124.79	112.69	123.11	T	*Chiasmolithus gigas*	NP15	middle Eocene	44.0
18R-CC, 11–17	134.50	148.84	132.69	147.03	B	*Chiasmolithus gigas*	NP15	middle Eocene	46.1
22R-CC, 0–5	163.31	171.95	161.50	170.14	T	*Discoaster sublodoensis*	NP14	middle Eocene	47.2
24R-CC, 13–18	184.61	192.10	182.80	190.29	B	*Discoaster sublodoensis*	NP14	middle Eocene	48.0
26R-CC, 10–15	217.93	229.89	216.12	228.08	B	*Sphenolithus radians*	NP11	early Eocene	53.3
27R-CC, 9–15	239.50	249.46	237.69	247.95	T	*Fasciculithus* sp.	NP9	early Eocene	54.1
30R-7, 72	239.50	249.46	237.69	247.95	X	*Zygrhablithus bijugatus/fasciculiths* (= PETM)	NP9	Eocene/Paleocene boundary	55.0
32R-CC, 22–25	276.72		275.95		B	*Discoaster multiradiatus*	NP9	late Paleocene	56.2
34R-CC, 20–22	292.35	307.01	291.58	306.24	B	*Discoaster mohleri*	NP7	late Eocene	57.5
36R-4, 92–92	317.30	327.00	316.22	325.92	T	Cretaceous taxa	NP1	K/T Boundary	65.0
37R-CC, 24–27	332.12		332.84		B	*Micula murus*	CC26	late Maastrichtian	66.2
40R-CC, 17–22	346.38	354.50	346.63	355.24	T	*Uniplanarius trifidum*	CC23	late Campanian	71.3
42R-CC, 20–22	365.38	374.56	366.12	377.22	B	*Marthasterites furcatus*	CC12	late Turonian	89.3
45R-CC, 21–27	390.70	396.47	393.82	399.59	B	*Eprolithus eptapetalus*	CC11	Turonian	93.2
48R-5, 146–150	411.97	422.05	415.09	425.12	T	*Axopodorhabdus albianus*	CC10a	late Cenomanian	94.0
52R-CC, 7–11	432.13	440.64	435.72	444.23	B	*Eiffellithus turriseiffelii*	NC10a	late Albian	101.7
53R-2, 129–130	477.63	484.09	481.04	487.50					
207-1260B-									
3R-CC, 15–19	56.41	62.86	55.74	61.36	T	*Chiasmolithus solitus*	NP16	middle Eocene	40.4
5R-CC, 9–14	78.58	88.03	78.05	86.85	B	*Reticulofenestra umbilicus*	NP16	middle Eocene	42.5
10R-CC, 17–22	117.23	126.28	115.57	124.12	T	*Nannotetrina fulgens*	NP15	middle Eocene	43.5
11R-CC, 9–17	126.28	135.45	124.12	132.89	T	*Chiasmolithus gigas*	NP15	middle Eocene	44.0
12R-CC, 19–24	243.49	251.51	237.16	246.45	X	*Tribrachiatus contortus/T. orthostylus*	NP11	early Eocene	53.4
13R-CC, 19–24	251.51	256.39	246.45	251.78	B	*Tribrachiatus bramlettei*	NP10	early Eocene	53.9
17R-7, 69–69	279.84	279.84	275.97	275.97	X	*Zygrhablithus bijugatus/fasciculiths* (= PETM)	NP9	Eocene/Paleocene boundary	55.0
19R-CC, 26–32	293.93	309.31	292.71	307.63	B	*Discoaster multiradiatus*	NP9	late Paleocene	56.2
21R-CC, 16–22	319.22	328.50	317.19	329.05	B	*Discoaster mohleri*	NP7	late Eocene	57.5
23R-3, 83–83	332.33	332.33			T	Cretaceous taxa	NP1	K/T Boundary	65.0
24R-CC, 3–8	344.06	357.80	344.56	354.66	B	*Micula murus*	CC26	late Maastrichtian	66.2
26R-CC, 11–16	357.80	367.27	354.66	368.83	T	*Uniplanarius trifidum*	CC23	late Campanian	71.3
31R-CC, 21–24	393.42	412.69	395.63	415.39	B	*Marthasterites furcatus*	CC12	late Turonian	89.3
34R-CC, 0–5	423.56	433.69	428.10	437.04	B	*Eprolithus eptapetalus*	CC11	Turonian	93.2
43R-CC, 0–6	491.18	494.33	493.86	497.01	B	*Eiffellithus turriseiffelii*	NC10a	late Albian	101.7

Note: B = bottom, T = top, E/O = Eocene/Oligocene, X = crossover in relative abundance, K/T = Cretaceous/Tertiary. PETM = Paleocene/Eocene Thermal Maximum.

Table T4. Distribution of planktonic foraminifers, Hole 1260A. (This table is available in an **oversized format.**)

Table T5. Datum levels for planktonic foraminifers, Site 1260.

Core, section, interval (cm)	Depth (mbsf)		Depth (mcd)		Datum	Species	Zone	Age	Age (Ma)
	Top	Bottom	Top	Bottom					
207-1260A-									
1R-CC, 12–18	0.75	3.58	0.75	3.58	B	*Globorotalia truncatulinoides*	PT1	Holocene–Pleistocene	1.9
2R-CC, 8–14	3.85	10.80	3.85	10.80	B	*Globigerina angulisuturalis*	P21a	early Oligocene	29.4
5R-CC, 19–24	27.50	36.10	27.50	36.10	T	*Hantkenina* spp.*	P16	late Eocene	33.7
6R-1, 50–54	36.10	38.70	36.10	38.70	T	*Orbulinoides beckmanni*	P13	middle Eocene	40.1
8R-1, 50–54	57.70	59.20	57.80	59.3	B	*Orbulinoides beckmanni*	P13	middle Eocene	40.5
15R-1, 50–54	124.79	125.40	123.11	123.59	T	*Morozovella aragonensis*	P11	middle Eocene	43.6
19R-CC, 0–7	171.95	179.62	170.14	177.81	B	*Globigerinatheka* spp.	P11	middle Eocene	45.8
24R-CC, 13–18	217.93	221.20	216.12	219.39	B	*Guembelitrioides nuttali**	P10	middle Eocene	49.0
25R-5, 50–54	225.70	227.00	223.89	225.19	T	*Morozovella formosa*	P7	early Eocene	50.8
26R-CC, 10–15	239.50	240.50	237.69	238.99	B	*Morozovella aragonensis*	P7	early Eocene	52.3
30R-1, 50–54	269.40	270.82	268.63	270.05	B	*Morozovella velascoensis* group	P5	early Eocene	54.7
32R-3, 45–48	290.14	291.65	289.37	290.88	T	*Globanomalina pseudomenardii*	P4	late Paleocene	55.9
35R-3, 50–54	320.60	322.10	319.52	321.02	B	*Globanomalina pseudomenardii*	P4	late Paleocene	59.2
35R-7, 18–22	326.28	327.00	325.2	325.92	B	*Morozovella angulata*	P3a	late Paleocene	61.0
36R-3, 28–29	329.98	331.20	330.7	331.92	B	*Praemurica uncinata*	P2	early Paleocene	61.2
36R-4, 80–81	331.20	332.00	331.92	332.72	T	*Parvularugoglobigerina eugubina**	Pα	early Paleocene	64.7–64.9
36R-CC, 6–9	332.00	336.09	332.72	336.81	T	*Abathomphalus mayaroensis*	KS31	Maastrichtian	65.0
38R-1, 49–52	346.49	347.99	347.23	348.73	B	*Abathomphalus mayaroensis*	KS31	Maastrichtian	68.6
38R-6, 49–52	353.99	354.50	354.73	355.24	B	*Contusotruncana contusa*	KS30a	Maastrichtian	69.6
38R-CC, 5–8	354.50	365.38	355.24	366.12	B	*Gansserina gansseri*	KS30b	late Campanian–Maastrichtian	72.8
49R-2, 42–44	441.64	444.95	445.23	447.82	T	*Rotalipora* spp.*	KS19–KS17	Cenomanian	94.0
207-1260B-									
4R-CC, 0–5	74.17	78.58	73.00	78.05	B	*Orbulinoides beckmanni*	P13	middle Eocene	40.5
10R-CC, 17–22	117.23	126.28	115.57	124.12	T	*Morozovella aragonensis*	P11	middle Eocene	43.6
11R-CC, 9–17	135.45	243.49	132.89	237.16	B	*Morozovella aragonensis**	P11	middle Eocene	52.3
17R-CC, 16–21	269.89	280.81	265.27	276.94	T	*Morozovella velascoensis* group	P5	late Paleocene	54.7
20R-CC, 14–20	293.93	309.31	292.71	307.63	T	*Globanomalina pseudomenardii*	P4	late Paleocene	55.9
21R-CC, 16–22	319.22	328.50	317.19	329.05	B	*Globanomalina pseudomenardii*	P4	late Paleocene	59.2
22R-CC, 17–23	328.50	338.56	329.05	339.06	B	*Praemurica uncinata*	P2	early Paleocene	61.2
23R-CC, 28–34	328.50	338.56	329.05	339.06	T	*Abathomphalus mayaroensis*	KS31	Maastrichtian	65.0
25R-CC, 13–18	357.80	367.27	354.66	368.83	B	*Racemiguembelina fructicosa*	KS30a	Maastrichtian	69.6

Notes: Top and bottom depth values refer to the range of possible depth in the core within which the datum is believed to fall. B = bottom, T = top. * = datums that probably reflect incomplete ranges of the foraminiferal marker species.

Table T6. Datum levels for radiolarians, Site 1260.

Core, section, interval (cm)	Depth (mbsf)	Depth (mcd)	Datum	Species	Zone	Age	Age (Ma)
207-1260A-							
6R-CC, 0–5	45.79	45.79	B	*Podocyrtis goetheana*	RP16	middle Eocene	~38.8
8R-CC, 0–5	65.71	65.81	EVOL	*Podocyrtis chalara*	RP15	middle Eocene	~39.5
12R-CC, 15–22	104.96	103.58	EVOL	*Podocyrtis mitra*	RP14	middle Eocene	~42.8
15R-CC, 6–12	130.56	128.75	EVOL	*Podocyrtis ampla*	RP13	middle Eocene	44.5
16R-1, 0–3	134.50	132.69	B	*Eusyringium lagena*	RP12	middle Eocene	~49.0
19R-CC, 0–7	171.95	170.14	EVOL	*Thyrsocyrtis triacantha*	RP12	middle Eocene	~49.0
22R-CC, 0–5	192.10	190.29	FO	*Thyrsocyrtis robusta*	RP10	middle Eocene	~47.5
32R-CC, 22–25	292.35	291.58	B	*Buryella tetradica*	RP5	late Paleocene	~60.9

Note: B = bottom, EVOL = evolutionary transition between species, FO = first occurrence.

Table T7. Datum levels, ages, and preservation of samples for calcareous nannofossils, Site 1260.

Core, section, interval (cm)	Depth (mbsf)	Zone	Age	Preservation	Group abundance
207-1260A-					
1R-CC, 12–18	0.75	NN21	Pleistocene	G	C
2R-CC, 8–14	3.85	NP23	early Oligocene	G	C
3R-CC, 13–18	14.51	NP23	early Oligocene	G	C
4R-CC, 0–5	27.50	NP23	early Oligocene	G	C
5R-CC, 19–24	36.10	NP19/20	late Eocene	G	C
6R-CC, 0–5	45.79	NP17	middle Eocene	G	C
7R-CC, 0–5	56.19	NN16	middle Eocene	G	C
8R-CC, 0–5	65.71	NN16	middle Eocene	M	C
9R-CC, 0–5	76.61	NN16	middle Eocene	M	C
10R-CC, 8–13	85.45	NN16	middle Eocene	M	C
11R-CC, 11–16	96.15	NN16	middle Eocene	M	C
12R-CC, 15–22	104.96	NN16	middle Eocene	M	C
13R-CC, 15–21	114.67	NN16	middle Eocene	G	C
14R-CC, 19–24	124.79	NP15	middle Eocene	G	C
15R-CC, 6–12	130.56	NP15	middle Eocene	M	C
16R-1, 0–3	134.50	NP15	middle Eocene	M	C
17R-CC, 13–19	148.84	NP15	middle Eocene	M	C
18R-CC, 11–17	163.31	NP15	middle Eocene	M	C
19R-CC, 0–7	171.95	NP15	middle Eocene	M	C
20R-CC, 0–4	179.62	NP15	middle Eocene	M	C
21R-2, 71–76	184.61	NP15	middle Eocene	M	C
22R-CC, 0–5	192.10	NP14	middle Eocene	M	C
23R-CC, 6–10	206.66	NP14	middle Eocene	M	C
24R-CC, 13–18	217.93	NP14	middle Eocene	M	C
25R-CC, 16–21	229.89	NP12	early Eocene	M	C
26R-CC, 10–15	239.50	NP12	early Eocene	G	C
27R-CC, 9–15	249.46	NP 9b	early Eocene	G	C
28R-CC, 18–24	259.35	NP 9b	early Eocene	G	C
29R-1, 0–1	259.20	NP 9b	early Eocene		
29R-CC, 0–3	266.16	NP 9b	early Eocene	G	C
30R-CC, 0–4	278.35	NP 9a	Paleocene	G	C
31R-CC, 16–23	287.67	NP 9a	Paleocene	G	C
32R-CC, 22–25	292.35	NP 9a	Paleocene	G	C
33R-CC, 16–19	307.01	NP 8	Paleocene	G	C
34R-CC, 20–22	317.30	NP 7	Paleocene	G	C
35R-CC, 34–37	327.00	NP 3	Paleocene	M	C
36R-CC, 6–9	336.09	CC26	Maastrichtian	G	C
37R-CC, 24–27	346.38	CC25	Maastrichtian	G	C
38R-CC, 5–8	354.50	CC25	Maastrichtian	G	C
39R-CC, 0–5	365.38	CC25	Maastrichtian	M	C
40R-CC, 17–22	374.56	CC23	Campanian	M	C
41R-2, 147–150	377.87				
41R-CC, 0–7	382.96	CC23	Campanian	M	C
42R-4, 0–5	389.00				
42R-CC, 20–22	390.70	CC12	Turonian	M	R
43R-2, 109–111	396.47	CC12	Turonian	M	F
44R-CC, 12–18	408.62	CC11	Turonian	M	F
45R-CC, 21–27	411.97	CC11	Turonian	M	C
46R-CC, 12–17	422.05	CC11	Turonian	M	F
47R-7, 0–4	432.13	CC10	Turonian	G	C
48R-5, 146–150	440.64	CC10	Cenomanian	G	C
49R-CC, 0–7	450.82	CC10	Cenomanian	G	C
50R-CC, 16–21	462.11	CC10	Cenomanian	M	C
51R-CC, 24–29	471.52	CC10	Cenomanian	M	C
52R-CC, 7–11	477.63	CC10	Cenomanian	M	C
53R-2, 129–130	484.09	NC8c	Albian	P	F
54R-CC, 6–11	491.36	NC8a	Albian	P	F
207-1260B-					
1R-CC, 11–15	48.79	NP17	middle Eocene	G	C
2R-CC, 14–17	56.41	NP16	middle Eocene	G	C
3R-CC, 15–19	62.86	NP16	middle Eocene	G	C
4R-CC, 0–5	74.17	NP16	middle Eocene	G	C
5R-CC, 9–14	78.58	NP16	middle Eocene	G	C
6R-CC, 0–5	88.03	NP16	middle Eocene	G	C
7R-CC, 0–5	95.10	NP16	middle Eocene	G	C
8R-CC, 7–12	107.43	NP16	middle Eocene	G	C
9R-CC, 8–13	117.23	NP16	middle Eocene	G	C
10R-CC, 17–22	126.28	NP16	middle Eocene	G	C
11R-CC, 9–17	135.45	NP16	middle Eocene	G	C
12R-CC, 19–24	243.49	NP11	early Eocene	G	C
13R-CC, 19–23	251.51	NP10	early Eocene	G	C
14R-CC, 8–13	256.39	NP 9	early Eocene	G	C
15R-CC, 0–7	264.94	NP 9	early Eocene	G	C
16R-CC, 0–5	269.89	NP 9	early Eocene	P	F
17R-CC, 16–21	280.81	NP 9	Paleocene	G	C
18R-CC, 11–17	289.07	NP 9	Paleocene	G	C
19R-CC, 26–32	293.93	NP 9	Paleocene	G	C
20R-CC, 14–20	309.31	NP 8	Paleocene	G	C
21R-CC, 16–22	319.22	NP 7	Paleocene	G	C
22R-CC, 17–23	328.50	NN 4	Paleocene	G	C
23R-CC, 28–34	338.56	CC26	Maastrichtian	G	C
24R-CC, 3–8	344.06	CC25	Maastrichtian	G	C
25R-CC, 13–18	357.80	CC25	Maastrichtian	G	C
26R-CC, 11–16	367.27	CC23	Campanian	M	C
27R-CC, 19–24	376.24	CC23	Campanian	M	C
28R-CC, 20–24	380.68	CC23	Campanian	M	C
29R-CC, 9–12	386.56	CC23	Campanian	M	C
30R-3, 124–125	390.74	CC23	Campanian	M	C
31R-CC, 21–24	393.42	CC13	Coniacian	G	C
34R-5, 99–100	412.69	CC11	Turonian	G	C
35R-CC, 0–5	423.56	CC11	Turonian	M	F
36R-6, 129–130	433.69	CC10	Cenomanian	M	F
38R-CC, 5–10	452.34	CC10	Cenomanian	M	F
39R-CC, 14–19	463.55	CC10	Cenomanian	M	F
40R-CC, 21–26	470.96	CC10	Cenomanian	M	F
41R-CC, 0–8	479.30	CC10	Cenomanian	M	F
42R-CC, 0–4	485.66	NC8a	Albian	M	F
43R-CC, 0–6	491.18	NC8a	Albian	M	F
44R-CC, 15–20	494.33	NC8a	Albian	P	F
45R-CC, 0–6	499.52	NC8a	Albian	P	F
46R-4, 103–105	507.03	NC8a	Albian	P	F

Notes: Preservation: G = good, M = moderate, P = poor. Abundance: C = common, F = few, R = rare.

Table T8. Distribution of planktonic foraminifers, Hole 1260B. (This table is available in an **oversized format.**)

Table T9. Shipboard cryogenic magnetometer analyses, Site 1260.

Section, cores	Approximate age range	Demagnetization
207-1260A-		
2R–42R	Oligocene–Campanian	NRM; 10 and 15 mT
207-1260B-		
1R–30R	Oligocene–Campanian	NRM; 10 and 15 mT
41R–46R	Albian	NRM; 10 and 15 mT

Note: NRM = natural remanent magnetization.

Table T10. Characteristic directions of minicores, Holes 1260A and 1260B. (See table notes. Continued on next two pages.)

Core, section, interval (cm)	PMAG code	Depth (mcd)	Polarity			Chron/ subchron	Declination (°)	Inclination (°)	Intensity (mA/m)	MAD (°)	N	Temperature steps used in least square analysis (°C)									
			Label	Code								1	2	3	4	5	6	7	8	9	10
207-1260A-																					
17R-1, 86	171.086	143.25	R	–4		C20r	70.2	3.4	2.16E–02	2.9	5	200	250	300	350	400	Org	Tied			
17R-3, 43	173.043	145.82	R	–4			26.9	6.7	1.72E–02	3.4	4	250	300	350	400	Org	Tied				
18R-1, 42	181.042	152.11	R	–4			283.5	2.1	1.59E–02	2.8	5	200	250	300	350	400	Org	Tied			
18R-3, 61	183.061	155.30	R	–4			206.8	4.8	1.03E–02	4.5	5	200	250	300	350	400	Org	Tied			
18R-5, 15	185.015	157.84	R	–4			320.0	–2.0	3.48E–02	1.7	5	200	250	300	350	400	Org	Tied			
18R-7, 63	187.063	161.32	R	–4			338.0	4.0	2.24E–02	1.7	5	200	250	300	350	400	Org	Tied			
19R-1, 61	191.061	162.01	R	–4			217.3	2.9	1.32E–02	2.0	5	200	250	300	350	400	Org	Tied			
19R-3, 95	193.095	165.34	R	–4			175.4	4.4	1.38E–02	3.9	4	250	300	350	400	Org	Tied				
20R-1, 30	201.030	171.29	R	–4			124.1	–3.0	1.98E–02	3.0	5	200	250	300	350	400	Org	Tied			
20R-3, 130	203.130	175.29	N	4		C21n	74.2	–3.6	2.22E–02	5.3	6	150	200	250	300	350	400	Org	Tied		
20R-5, 62	205.062	177.61	N	4			69.8	–6.0	2.53E–02	2.5	5	200	250	300	350	400	Org	Tied			
21R-1, 28	211.028	180.98	N	4			193.4	–7.2	2.17E–02	2.3	5	200	250	300	350	400	Org	Tied			
23R-1, 58	231.058	200.17	NPP	2			291.4	14.2	4.62E–01	1.8	5	200	250	300	350	400	Org	Tied			
23R-3, 43	233.043	203.02	NPP	2			204.9	1.1	6.62E–01	1.1	5	200	250	300	350	400	Org	Tied			
24R-1, 6	241.006	209.35	R	–4		C21r	169.6	6.5	1.77E–01	1.1	5	200	250	300	350	400	Org	Tied			
24R-3, 35	243.035	212.44	R	–4			54.0	13.6	7.51E–01	2.2	4	250	300	350	400	Org	Tied				
24R-5, 31	245.031	215.29	R?	–1			109.3	2.5	7.32E–01	3.4	4	250	300	350	400	Org	Tied				
						Hiatus															
25R-1, 12	251.012	219.01	N	4		C22n	37.9	5.8	8.22E–01	1.5	5	200	250	300	350	400	Org	Tied			
25R-3, 91	253.091	222.80	N	4		C23n	335.3	6.9	2.88E+00	1.0	6	150	200	250	300	350	400	Org	Tied		
25R-5, 5	255.005	224.74	N	4			81.3	10.5	5.53E–01	2.6	4	250	300	350	400	Org	Tied				
25R-7, 32	257.032	227.71	R	–4		C23r	195.5	24.5	5.21E–01	1.1	4	250	300	350	400	Org	Tied				
207-1260B-																					
1R-1, 48	11.048	40.68	R?	–1			276.6	7.7	4.38E–03	5.3	4	50	50	150	150	Org	Tied				
1R-3, 66	13.066	43.86	RPP	–2		C18r	267.3	–13.4	3.37E–03	3.4	2	240	240	Org	Tied						
1R-5, 4	15.004	46.24	RP	–3			115.8	0.5	1.04E–02	5.8	4	270	300	350	350	Org	Tied				
2R-1, 140	21.140	50.43	RP	–3			256.4	4.0	1.43E–02	3.9	2	300	350	Org	Tied						
2R-3, 131	23.131	53.34	R	–4			151.9	3.5	2.37E–02	1.3	5	200	240	270	300	350	Org	Tied			
2R-5, 33	25.033	55.36	R	–4			140.0	–5.3	2.97E–02	1.4	5	200	240	270	300	350	Org	Tied			
3R-1, 141	31.141	59.31	RP	–3			3.6	5.4	1.28E–02	3.8	5	200	240	270	300	350	Org	Tied			
3R-3, 57	33.057	60.97	RP	–3			106.6	–7.3	1.23E–02	3.2	3	270	300	350	Org	Tied					
4R-1, 15	41.015	63.38	R	–4			30.8	3.2	1.48E–02	2.2	4	200	270	300	350	Org	Tied				
4R-3, 61	43.061	66.84	NP	3		C19n	76.0	–5.4	9.93E–03	8.1	8	150	200	240	270	270	300	350	350	Org	Tied
4R-5, 3	45.003	69.26	RPP	–2		C19r	194.3	12.2	5.29E–03	6.3	6	270	270	300	300	350	350	Org	Tied		
4R-7, 40	47.040	72.63	RP	–3			6.4	5.9	1.43E–02	3.6	3	270	300	350	Org	Tied					
5R-1, 64	51.064	73.91	RP	–3			23.1	2.8	1.70E–02	3.2	5	200	240	270	300	350	Org	Tied			
5R-3, 60	53.060	76.87	RP	–3			158.3	–5.7	8.44E–03	5.0	8	200	200	240	240	270	270	300	350	Org	Tied
6R-1, 43	61.043	78.05	RP	–3			210.6	6.7	9.91E–03	4.7	7	200	240	270	300	300	350	350	Org	Tied	
6R-3, 68	63.068	81.30	R	–4			232.1	4.8	2.10E–02	2.1	5	200	240	270	300	350	Org	Tied			
6R-5, 50	65.050	84.12	RP	–3			287.4	1.3	1.66E–02	1.4	3	270	300	350	Org	Tied					
6R-7, 66	67.066	86.78	R	–4			337.2	1.3	2.66E–02	1.1	5	200	240	270	300	350	Org	Tied			
7R-1, 132	71.132	88.75	RP	–3			301.3	5.1	1.41E–02	3.9	6	150	200	240	270	300	350	Org	Tied		
7R-3, 100	73.100	91.43	NP	3		C20n	122.0	8.1	9.55E–03	4.1	6	150	200	240	270	300	350	Org	Tied		
7R-5, 44	75.044	93.87	N	4			82.6	–1.8	1.33E–02	2.9	5	150	240	270	300	350	Org	Tied			
8R-1, 68	81.068	96.70	N	4			0.0	0.1	1.24E–02	3.3	4	200	240	300	350	Org	Tied				
8R-3, 51	83.051	99.53	N	4			343.7	0.3	1.71E–02	3.1	6	50	150	200	270	300	350	Org	Tied		
8R-5, 56	85.056	102.58	N	4			334.0	7.5	1.32E–02	1.9	3	240	300	350	Org	Tied					

Table T10 (continued).

Core, section, interval (cm)	PMAG code	Depth (mcd)	Polarity			Chron/ subchron	Declination (°)	Inclination (°)	Intensity (mA/m)	MAD (°)	*N*	Temperature steps used in least square analysis (°C)									
			Label	Code								1	2	3	4	5	6	7	8	9	10
8R-7, 49	87.049	105.01	N	4			359.3	3.4	2.15E–02	2.2	4	240	270	300	350	Org	Tied				
9R-1, 64	91.064	106.58	N	4			181.6	–3.9	2.70E–02	2.6	7	50	150	200	240	270	300	350	Org	Tied	
9R-3, 78	93.078	109.72	N	4			204.5	–2.4	2.37E–02	2.5	7	50	150	200	240	270	300	350	Org	Tied	
9R-5, 11	95.011	112.05	NP	3			200.8	5.1	4.06E–03	10.9	5	200	240	240	270	270	Org	Tied			
9R-7, 4	97.004	114.98	N	4			178.5	2.6	1.42E–02	3.5	6	150	200	240	270	300	350	Org	Tied		
10R-1, 34	101.034	115.38	N	4			220.5	–3.0	1.24E–02	2.6	4	240	270	300	350	Org	Tied				
10R-3, 32	103.032	118.34	N	4			236.5	1.4	1.26E–02	2.4	4	240	270	300	350	Org	Tied				
10R-5, 18	105.018	121.20	N	4			160.6	–2.9	1.18E–02	2.5	4	240	270	300	350	Org	Tied				
11R-1, 70	111.070	125.04	R	–4		C20r	226.1	9.8	1.12E–02	3.3	4	240	270	300	350	Org	Tied				
11R-3, 3	113.003	127.37	RP	–3			289.8	8.1	1.05E–02	2.9	5	240	270	270	300	350	Org	Tied			
11R-5, 3	115.003	130.37	RPP	–2			260.4	–9.8	8.52E–03	7.3	6	240	270	300	300	350	350	Org	Tied		
12R-1, 5	121.005	228.72	R	–4		C23r	138.5	2.4	2.89E–01	1.2	4	250	300	350	350	Org	Tied				
12R-3, 19	123.019	231.86	N	4		C24n	15.9	16.5	1.21E+00	1.7	4	200	250	300	350	Org	Tied				
12R-5, 13	125.013	234.80	NP	3			230.0	4.2	2.94E–01	2.9	4	200	250	300	350	Org	Tied				
13R-1, 14	131.014	237.08	N	4			28.2	–0.7	1.31E+00	1.1	4	200	250	300	350	Org	Tied				
13R-3, 12	133.012	240.06	N	4			359.2	7.3	3.25E–01	2.0	4	200	250	300	350	Org	Tied				
13R-5, 37	135.037	243.29	RP	–1		C24r	222.4	–3.1	1.11E–02	4.7	4	200	250	300	350	Org	Tied				
13R-7, 12	137.012	245.75	R	–4			232.6	–13.5	1.91E–02	2.7	5	150	200	250	300	350	Org	Tied			
14R-1, 45	141.045	247.44	RP	–3			240.1	–0.8	3.23E–02	3.5	4	200	250	300	350	Org	Tied				
14R-3, 18	143.018	250.12	RP	–3			80.1	1.6	1.09E–02	5.3	5	150	200	250	300	350	Org	Tied			
15R-1, 7	151.007	251.65	RP	–3			88.1	–8.9	2.23E–02	2.4	5	150	200	250	300	350	Org	Tied			
15R-3, 3	153.003	254.61	RP	–3			125.2	7.9	9.66E–03	4.8	5	150	200	250	300	350	Org	Tied			
15R-5, 8	155.008	257.66	RP	–3			119.6	–1.9	1.04E–02	5.7	5	200	250	300	350	400	Org	Tied			
16R-1, 9	161.009	261.37	RP	–3			324.4	–2.6	7.92E–03	3.8	3	250	300	350	Org	Tied					
16R-3, 3	163.003	264.31	R	–4			317.4	–5.5	9.94E–03	3.1	4	250	300	350	400	Org	Tied				
17R-1, 4	171.004	267.07	RP	–3			14.2	–7.2	9.52E–03	4.6	5	200	250	300	350	400	Org	Tied			
18R-5, 4	185.004	285.35	RPP	–2			167.0	59.5	4.44E–03	5.6	4	250	250	300	300	Org	Tied				
18R-9, 3	189.003	287.80	N?	1			320.8	64.1	1.24E–02	8.8	2	NRM	50	Org	Tied						
19R-1, 83	191.083	289.71	NPP	2		C25n	3.0	–56.2	5.44E–03	8.7	6	200	200	250	250	300	300	Org	Tied		
19R-9, 14	199.014	292.59	RP	–3		C25r	159.6	6.5	4.18E–03	6.0	4	250	250	300	300	Org	Tied				
20R-1, 74	201.074	298.86	RPP	–2			12.3	–27.3	6.17E–03	4.6	4	250	250	300	300	Org	Tied				
20R-3, 44	203.044	301.56	R	–4			179.6	9.8	2.44E–02	4.1	3	250	300	350	Org	Tied					
20R-5, 109	205.109	305.19	NP	3		C26n	99.2	6.8	3.48E–02	5.9	5	150	200	250	300	350	Org	Tied			
21R-1, 101	211.101	308.38	R	–4			204.4	11.6	1.31E–01	1.9	3	250	300	350	Org	Tied					
21R-2, 131	212.131	310.18	NP	3			41.3	22.8	1.81E–01	2.5	3	250	300	350	Org	Tied					
21R-3, 19	213.019	310.56	N?	1			355.2	80.2	5.94E–03	3.5	2	150	200	Org	Tied						
21R-4, 124	214.124	313.13	NP	3			85.2	23.6	3.29E–02	5.4	4	250	300	350	400	Org	Tied				
21R-5, 58	215.058	313.97	NP	3			351.2	26.2	1.64E–02	10.8	3	50	150	200	Org	Tied					
21R-6, 61	216.061	315.50	N	4			6.4	7.5	2.35E–01	0.6	3	250	300	350	Org	Tied					
21R-7, 59	217.059	317.00	R	–4		?	273.8	–1.2	9.53E–03	3.6	5	250	300	350	400	400	Org	Tied			
						Gap in coverage															
23R-1, 51	231.051	329.21	R	–4		?	343.7	10.2	1.47E–02	2.6	4	250	300	350	400	Org	Tied				
23R-4, 5	234.005	333.55	RP	–3		C29r	289.5	3.1	4.31E–02	3.6	5	250	300	350	400	450	Org	Tied			
23R-4, 77	234.077	334.27	R	–4			259.4	–1.4	1.84E–01	2.5	6	200	250	300	350	400	450	Org	Tied		
23R-4, 122	234.122	334.72	RP	–3			257.8	6.8	4.93E–02	1.7	2	350	400	Org	Tied						
23R-5, 35	235.035	335.35	R	–4			324.6	13.1	3.07E–01	2.0	5	150	200	250	300	350	Org	Tied			
23R-7, 72	237.072	338.72	RPP	–2			91.5	28.9	3.98E–03	5.4	3	250	250	250	Org	Tied					

Table T10 (continued).

Core, section, interval (cm)	PMAG code	Depth (mcd)	Polarity			Chron/ subchron	Declination (°)	Inclination (°)	Intensity (mA/m)	MAD (°)	*N*	Temperature steps used in least square analysis (°C)									
			Label	Code								1	2	3	4	5	6	7	8	9	10
24R-1, 5	241.005	338.95	NP	3		C30n	259.0	16.9	5.90E–03	4.1	5	150	200	200	250	250	Org	Tied			
24R-3, 4	243.004	341.94	R?	–1		to	170.1	2.6	3.35E–03	8.9	4	200	200	250	250	Org	Tied				
25R-1, 111	251.111	345.97	NPP	2		C31n	0.5	25.4	4.47E–03	4.1	2	150	150	Org	Tied						
25R-3, 66	253.066	348.50	NP	3			36.1	5.1	4.70E–03	9.5	4	150	150	200	200	Org	Tied				
25R-5, 68	255.068	351.54	NP	3			231.1	21.5	5.44E–03	2.6	6	150	150	200	200	250	250	Org	Tied		
25R-7, 5	257.005	353.91	R?	–1			288.7	63.9	2.12E–03	0.0	1	250									
26R-1, 119	261.119	360.45	RPP	–2		C31r?	334.2	61.0	5.56E–03	20.7	6	250	250	300	300	350	350	Org	Tied		
26R-3, 89	263.089	363.15	N?	1			266.3	–5.0	9.56E–03	1.5	2	350	350	Org	Tied						
26R-5, 114	265.114	366.40	RPP	–2			301.2	36.9	4.92E–03	6.1	6	200	200	250	250	300	300	Org	Tied		
26R-7, 44	267.044	368.70	NPP	2			122.9	33.5	6.32E–03	9.3	7	150	200	200	250	250	300	300	Org	Tied	
27R-1, 9	271.009	368.90	RPP	–2			284.9	11.8	4.83E–03	2.6	4	200	200	250	250	Org	Tied				
27R-3, 39	273.039	372.20	RPP	–2			46.4	75.5	3.94E–03	9.0	4	250	250	300	300	Org	Tied				
27R-5, 53	275.053	375.34	INT	0			163.7	71.2	9.00E–03	10.8	4	200	250	300	300	Org	Tied				
28R-1, 19	281.019	379.40	RP	–3			30.5	–0.9	3.48E–03	1.9	2	350	350	Org	Tied						
28R-2, 89	282.089	381.60	NPP	2		?	333.0	26.9	5.13E–03	9.3	4	150	150	200	200	Org	Tied				
29R-1, 7	291.007	383.51	RPP	–2			273.3	10.4	7.05E–03	5.8	4	250	250	300	300	Org	Tied				
29R-3, 42	293.042	386.86	NP	3		?	224.4	1.0	4.79E–03	10.5	6	250	250	300	300	350	350	Org	Tied		
30R-1, 11	301.011	388.82	NP	3			287.7	30.3	6.92E–03	9.3	6	200	200	250	250	300	300	Org	Tied		
30R-3, 16	303.016	391.87	INT	0			134.4	69.2	2.41E–02	4.8	4	150	200	250	300	Org	Tied				
41R-1, 108	411.108	477.94	N	4		C34n	191.8	31.0	1.90E–01	2.8	4	250	300	350	400	Org	Tied				
41R-2, 61	412.061	478.97	NP	3			72.1	7.9	4.11E–01	3.2	6	150	200	250	300	350	400	Org	Tied		
41R-3, 66	413.066	480.51	NP	3			297.9	2.9	2.10E–01	4.1	2	350	400	Org	Tied						
43R-1, 91	431.091	491.49	N?	1			299.8	3.0	4.40E–01	3.1	4	150	200	250	300	Org	Tied				
43R-2, 117	432.117	493.25	N	4			195.0	17.5	3.96E–01	1.4	4	250	300	350	400	Org	Tied				
43R-3, 5	433.005	493.38	N	4			58.5	47.6	7.14E–01	4.0	5	150	200	250	300	350	Org	Tied			
44R-1, 71	441.071	495.29	N	4			145.9	34.9	2.41E–01	5.5	5	200	250	300	350	400	Org	Tied			
44R-9, 3	449.003	496.89	N	4			291.5	45.4	1.85E–01	3.7	5	200	250	300	350	400	Org	Tied			
45R-2, 127	452.127	501.95	NP	3			179.6	13.7	1.44E–01	8.2	3	250	300	350	Org	Tied					
46R-2, 123	462.123	506.91	NP	3			213.2	23.2	9.11E–02	4.7	2	250	300	Org	Tied						
46R-3, 120	463.120	508.38	NPP	2			175.1	64.9	3.90E–01	2.9	6	150	200	250	300	350	400	Org	Tied		
46R-4, 13	464.013	508.81	INT	0			316.9	78.1	2.58E–01	4.4	5	200	250	300	350	400	Org	Tied			

Note: PMAG = paleomagnetism, MAD = maximum angular deviation. R = reversed polarity, N = normal polarity. RP and NP = less precise reversed and normal polarity assignments, respectively. RPP and NPP = sample did not achieve adequate cleaning during demagnetization but polarity was obviously reversed or normal, respectively. Orig. = origin. Black = normal polarity, white = reversed polarity, gray = intermediate or questionable polarity, yellow = gap in coverage or hiatus. Examples of interpretation of progressive demagnetization plots and methods of computation of the characteristic directions are given in **"Paleomagnetism,"** p. 16, in the "Explanatory Notes" chapter.

Table T11. Composite depth, Site 1260.

Core	Depth (mbsf)	Offset (m)	Depth (mcd)	Depth shifted
207-1260A-				
1R	0.0	0.00	0.00	N
2R	1.0	0.00	1.00	N
3R	10.3	0.00	10.30	N
4R	19.5	0.00	19.50	N
5R	28.8	0.00	28.80	N
6R	38.2	0.00	38.20	N
7R	47.5	0.10	47.60	Y
8R	57.2	0.10	57.30	N
9R	66.9	–1.00	65.90	Y
10R	76.6	–0.90	75.70	Y
11R	86.3	–1.38	84.92	Y
12R	95.9	–1.38	94.52	N
13R	105.6	–1.98	103.62	Y
14R	115.3	–1.68	113.62	Y
15R	124.9	–1.81	123.09	Y
16R	134.5	–1.81	132.69	N
17R	144.2	–1.81	142.39	N
18R	153.5	–1.81	151.69	N
19R	163.2	–1.81	161.39	N
20R	172.8	–1.81	170.99	N
21R	182.5	–1.81	180.69	N
22R	192.1	–1.81	190.29	N
23R	201.4	–1.81	199.59	N
24R	211.1	–1.81	209.29	N
25R	220.7	–1.81	218.89	N
26R	230.3	–1.81	228.49	N
27R	240.0	–1.51	238.49	Y
28R	249.6	–1.47	248.13	Y
29R	259.2	–0.77	258.43	Y
30R	268.9	–0.77	268.13	N
31R	278.5	–0.77	277.73	N
32R	288.2	–0.77	287.43	N
33R	297.8	–0.77	297.03	N
34R	307.4	–1.08	306.32	Y
35R	317.1	–1.08	316.02	N
36R	326.7	0.72	327.42	Y
37R	336.4	0.25	336.65	Y
38R	346.0	0.74	346.74	Y
39R	355.6	0.74	356.34	N
40R	365.3	2.66	367.96	Y
41R	374.9	2.66	377.56	N
42R	384.5	3.12	387.62	Y
43R	394.1	3.12	397.22	N
44R	403.7	3.12	406.82	N
45R	408.7	3.12	411.82	N
46R	414.3	3.07	417.37	Y
47R	423.9	3.59	427.49	Y
48R	433.5	3.59	437.09	N
49R	443.1	2.87	445.97	Y
50R	452.7	2.98	455.68	Y
51R	462.0	3.65	465.65	Y
52R	471.6	3.41	475.01	Y
53R	481.3	3.41	484.71	N
54R	487.9	2.48	490.38	Y
207-1260B-				
1R	40.2	0.00	40.20	Y
2R	49.7	–0.67	49.03	Y
3R	59.4	–1.50	57.90	Y
4R	64.4	–1.17	63.23	Y
5R	73.8	–0.53	73.27	Y
6R	78.8	–1.18	77.62	Y
7R	88.4	–0.97	87.43	Y
8R	98.0	–1.98	96.02	Y
9R	107.6	–1.66	105.94	Y
10R	117.2	–2.16	115.04	Y
11R	126.9	–2.56	124.34	Y
12R	235.0	–6.33	228.67	Y
13R	242.0	–5.06	236.94	Y
14R	251.6	–4.61	246.99	Y
15R	256.2	–4.62	251.58	Y
16R	265.9	–4.62	261.28	N
17R	270.9	–3.87	267.03	Y
18R	280.5	–1.19	279.31	Y
19R	290.1	–1.22	288.88	Y
20R	299.8	–1.68	298.12	Y
21R	309.4	–2.03	307.37	Y
22R	319.1	0.55	319.65	Y
23R	328.7	0.50	329.20	Y
24R	338.4	0.50	338.90	N
25R	348.0	–3.14	344.86	Y
26R	357.7	1.56	359.26	Y
27R	367.3	1.51	368.81	Y
28R	376.9	2.31	379.21	Y
29R	381.5	1.94	383.44	Y
30R	386.5	2.21	388.71	Y
31R	391.1	2.21	393.31	N
32R	396.1	2.21	398.31	N
33R	400.7	2.21	402.91	N
34R	405.7	2.70	408.40	Y
35R	415.3	4.54	419.84	Y
36R	424.9	3.35	428.25	Y
37R	434.5	2.42	436.92	Y
38R	444.1	4.07	448.17	Y
39R	453.7	2.78	456.48	Y
40R	463.1	4.58	467.68	Y
41R	472.7	4.16	476.86	Y
42R	482.3	2.68	484.98	Y
43R	487.9	2.68	490.58	N
44R	491.9	2.68	494.58	N
45R	496.5	2.68	499.18	N
46R	501.5	2.68	504.18	N

Note: N = no, Y = yes.

Table T12. Splice tie points, Site 1260.

Hole, core, section, interval (cm)	Depth (mbsf)	Depth (mcd)		Hole, core, section, interval (cm)	Depth (mbsf)	Depth (mcd)
207-				207-		
1260A-6R-5, 47.5	44.68	44.68	Tie to	1260B-1R-3, 147.5	44.68	44.68
1260B-1R-6, 55	48.25	48.25	Tie to	1260A-7R-1, 65	48.15	48.25
1260A-7R-6, 112.5	56.13	56.23	Append to	1260A-8R-1, 0	57.20	57.30
1260A-8R-6, 27.5	64.98	65.08	Tie to	1260B-4R-2, 35	66.25	65.08
1260B-4R-3, 2.5	67.43	66.26	Tie to	1260A-9R-1, 34.5	67.26	66.26
1260A-9R-6, 142.5	75.83	74.83	Tie to	1260B-5R-2, 4.5	75.36	74.83
1260B-5R-3, 25	77.05	76.52	Tie to	1260A-10R-1, 81	77.42	76.52
1260A-10R-6, 110	85.20	84.30	Tie to	1260B-6R-5, 67.5	85.48	84.30
1260B-6R-6, 77.5	87.08	85.90	Tie to	1260A-11R-1, 97.5	87.28	85.90
1260A-11R-7, 72.5	96.03	94.65	Tie to	1260A-12R-1, 12.5	96.03	94.65
1260A-12R-6, 17.5	103.58	102.20	Tie to	1260B-8R-5, 17.5	104.18	102.20
1260B-8R-6, 57.5	106.08	104.10	Tie to	1260A-13R-1, 47.5	106.08	104.10
1260A-13R-6, 72.5	113.83	111.85	Tie to	1260B-9R-4, 139.5	113.51	111.85
1260B-9R-6, 142.5	116.53	114.87	Tie to	1260A-14R-1, 125	116.55	114.87
1260A-14R-6, 100	123.80	122.12	Tie to	1260B-10R-5, 110	124.28	122.12
1260B-10R-6, 125	125.93	123.77	Tie to	1260A-15R-1, 67.5	125.58	123.77
1260A-15R-4, 40	129.80	127.99	Tie to	1260B-11R-3, 65	130.55	127.99
1260B-11R-6, 92.5	135.33	132.77				
207-				207-		
1260A-26R-7, 52.5	239.33	237.52	Tie to	1260B-13R-1, 57.5	242.58	237.52
1260B-13R-3, 62.5	245.63	240.57	Tie to	1260A-27R-2, 57.5	242.08	240.57
1260A-27R-7, 7.5	248.78	247.27	Tie to	1260B-14R-1, 27.5	251.88	247.27
1260B-14R-2, 7.5	253.18	248.57	Tie to	1260A-28R-1, 43.5	250.04	248.57
1260A-28R-5, 102.5	255.89	254.42	Tie to	1260B-15R-2, 133.5	259.04	254.42
1260B-15R-6, 17.5	263.88	259.26	Tie to	1260A-29R-1, 82.5	260.03	259.26
1260A-29R-6, 65	266.15	265.38	Append to	1260A-30R-1, 0	268.90	268.13
1260A-30R-8, 85	278.35	277.58	Append to	1260A-31R-1, 0	278.50	277.73
1260A-31R-6, 27.5	285.86	285.09	Tie to	1260B-18R-4, 127.5	286.28	285.09
1260B-18R-6, 75	288.75	287.56	Tie to	1260A-32R-1, 12.5	288.33	287.56
1260A-32R-2, 47.5	290.18	289.41	Tie to	1260B-19R-1, 52.5	290.63	289.41
1260B-19R-3, 55	293.65	292.43	Append to	1260A-33R-1, 0	297.80	297.03
1260A-33R-6, 17.5	305.44	304.67	Tie to	1260B-20R-5, 56	306.35	304.67
1260B-20R-7, 7.5	308.55	306.87	Tie to	1260A-34R-1, 55	307.95	306.87
1260A-34R-7, 65	317.05	315.97	Append to	1260A-35R-1, 0	317.10	316.02
1260A-35R-5, 87.5	323.98	322.90	Tie to	1260B-22R-3, 23	322.35	322.90
1260B-22R-7, 7.5	327.86	328.41	Tie to	1260A-36R-1, 98.5	327.69	328.41
1260A-36R-5, 17.5	332.88	333.60	Tie to	1260B-23R-4, 10	333.10	333.60
1260B-23R-6, 105	337.05	337.55	Tie to	1260A-37R-1, 90	337.30	337.55
1260A-37R-7, 82.5	345.54	345.79	Tie to	1260B-25R-1, 92	348.93	345.79
1260B-25R-2, 97.5	350.48	347.34	Tie to	1260A-38R-1, 60	346.60	347.34
1260A-38R-6, 92.5	354.43	355.17	Append to	1260A-39R-1, 0	355.60	356.34
1260A-39R-6, 135	364.45	365.19	Tie to	1260B-26R-4, 142.5	363.63	365.19
1260B-26R-7, 30	367.00	368.56	Tie to	1260A-40R-1, 60	365.90	368.56
1260A-40R-7, 55	374.35	377.01	Append to	1260A-41R-1, 0	374.90	377.56
1260A-41R-5, 142.5	382.33	384.99	Tie to	1260B-29R-2, 5	383.05	384.99
1260B-29R-4, 62.5	386.13	388.07	Tie to	1260A-42R-1, 45	384.95	388.07
1260A-42R-4, 147.5	390.48	393.60				
207-				207-		
1260A-46R-6, 20	421.27	424.34	Tie to	1260B-35R-4, 5	419.80	424.34
1260B-35R-6, 57.5	423.33	427.87	Tie to	1260A-47R-1, 37.5	424.28	427.87
1260A-47R-7, 82.5	432.96	436.55	Append to	1260A-48R-1, 0	433.50	437.09
1260A-48R-6, 37.5	441.06	444.65	Tie to	1260B-37R-6, 22.5	442.23	444.65
1260B-37R-7, 25	443.75	446.17	Tie to	1260A-49R-1, 20	443.30	446.17
1260A-49R-5, 15	449.10	451.97	Tie to	1260B-38R-3, 80	447.90	451.97
1260B-38R-6, 52.5	451.99	456.06	Tie to	1260A-50R-1, 37.5	453.08	456.06
1260A-50R-6, 42.5	460.63	463.61	Tie to	1260B-39R-5, 112	460.83	463.61
1260B-39R-7, 55	463.25	466.03	Tie to	1260A-51R-1, 37.5	462.38	466.03
1260A-51R-5, 67.5	468.66	472.31	Tie to	1260B-40R-4, 12.5	467.73	472.31
1260B-40R-6, 57.5	470.68	475.26	Tie to	1260A-52R-1, 25	471.85	475.26
1260A-52R-3, 145	476.03	479.44	Tie to	1260B-41R-2, 107.5	475.28	479.44
1260B-41R-5, 62.5	479.27	483.43				

Table T13. Planktonic foraminiferal and calcareous nannofossil datums used in the preliminary age-depth model, Hole 1260A. (See table notes. Continued on next page.)

Core, section, interval (cm)	Depth (mbsf)	Foraminifer age (Ma)		Foraminifer zone	Nannofossil age (Ma)	Nannofossil zone	Epoch
		Minimum	Maximum				
207-1260A-							
1R-CC, 12–18	0.75	0	1.92	PT1			Holocene–Pleistocene
2R-CC, 8–14	3.85	28.5	29.4	P21a			early Oligocene
3R-1, 50–54	10.80	32	33.8	P18			early Oligocene
3R-2, 50–54	12.30	33.8	35.2	P16			late Eocene
3R-3, 50–54	13.80	32	33.8	P18			early Oligocene
3R-CC, 13–18	14.51	32	33.8	P18			early Oligocene
4R-1, 50–54	20.00	32	33.8	P18			early Oligocene
4R-2, 50–54	21.50	32	33.8	P18			early Oligocene
4R-3, 50–54	23.00	29.4	30.3	P20			early Oligocene
4R-4, 50–53	24.50	29.4	30.3	P20			early Oligocene
4R-5, 50–53	26.00	30.3	32	P19			early Oligocene
4R-6, 43–45	27.43	30.3	32	P19			early Oligocene
4R-CC, 0–5	27.50	30.3	32	P19			early Oligocene
5R-CC, 19–24	36.10	33.8	35.2	P16			late Eocene
6R-1, 50–54	38.70	40.1	40.5	P13			middle Eocene
6R-5, 50–54	44.70	40.1	40.5	P13			middle Eocene
6R-CC, 0–5	45.79	40.1	40.5	P13			middle Eocene
7R-CC, 0–5	56.19	40.1	40.5	P13	40.4	NP16	middle Eocene
8R-1, 50–54	57.70	40.1	40.5	P13			middle Eocene
8R-2, 50–54	59.20	40.5	43.6	P12			middle Eocene
8R-3, 50–54	60.70	40.5	43.6	P12			middle Eocene
8R-4, 50–54	62.20	40.5	43.6	P12			middle Eocene
8R-5, 50–54	63.70	40.5	43.6	P12			middle Eocene
8R-CC, 0–5	65.71	40.5	43.6	P12			middle Eocene
9R-CC, 0–5	76.61	40.5	43.6	P12			middle Eocene
10R-CC, 8–13	85.45	40.5	43.6	P12	42.5	NP16	middle Eocene
11R-CC, 11–16	96.15	40.5	43.6	P12			middle Eocene
12R-CC, 15–22	104.96	40.5	43.6	P12			middle Eocene
13R-CC, 15–21	114.67	40.5	43.6	P12			middle Eocene
14R-CC, 19–24	124.79	40.5	43.6	P12	43.5	NP15	middle Eocene
15R-1, 50–54	125.40	43.6	45.8	P11			middle Eocene
15R-CC, 6–12	130.56	43.6	45.8	P11			middle Eocene
16R-1, 0–3	134.50	43.6	45.8	P11			middle Eocene
17R-CC, 13–19	148.84	43.6	45.8	P11	44	NP15	middle Eocene
18R-CC, 11–17	163.31	43.6	45.8	P11	46.1	NP15	middle Eocene
19R-CC, 0–7	171.95	43.6	45.8	P11			middle Eocene
20R-CC, 0–4	179.62	45.8	49	P10?			middle Eocene
21R-2, 71–76	184.61	45.8	49	P10?			middle Eocene
22R-CC, 0–5	192.10	45.8	49	P10	47.2	NP14	middle Eocene
23R-CC, 6–10	206.66	45.8	49	P10			middle Eocene
24R-CC, 13–18	217.93	45.8	49	P10	48	NP14	middle Eocene
25R-1, 50–54	221.20	50.4	50.8	P8			early Eocene
25R-2, 50–54	222.70	50.4	50.8	P8			early Eocene
25R-3, 50–54	224.20	50.4	50.8	P8			early Eocene
25R-4, 50–54	225.70	50.4	50.8	P8			early Eocene
25R-5, 50–54	227.00	50.8	52.3	P7			early Eocene
25R-7, 48–52	229.68	50.8	52.3	P7			early Eocene
25R-CC, 16–21	229.89	50.8	52.3	P7			early Eocene
26R-CC, 10–15	239.50	50.8	52.3	P7	53.3	NP11	early Eocene
27R-1, 50–54	240.50	52.3	54.7	P6			early Eocene
27R-2, 50–54	242.00	52.3	54.7	P6			early Eocene
27R-CC, 9–15	249.46	52.3	54.7	P6	54.1	NP9	early Eocene
28R-CC, 18–24	259.35	52.3	54.7	P6			early Eocene
29R-1, 0–1	259.20	52.3	54.7	P6			early Eocene
29R-CC, 0–3	266.16	52.3	54.7	P6			early Eocene
30R-1, 50–54	269.40	54.7	55.9	P5			early Eocene
30R-2, 50–54	270.82	54.7	55.9	P5			early Eocene
30R-3, 50–54	272.32	54.7	55.9	P5			early Eocene
30R-4, 50–54	273.82	54.7	55.9	P5			early Eocene
30R-5, 50–54	274.93	54.7	55.9	P5			early Eocene
30R-6, 50–54	275.93	54.7	55.9	P5			early Eocene
30R-8, 50–54	278.00	54.7	55.9	P5			late Paleocene
30R-CC, 0–4	278.35	54.7	55.9	P5			late Paleocene
31R-CC, 16–23	287.67	54.7	55.9	P5			late Paleocene
32R-1, 50–53	288.70	54.7	55.9	P5			late Paleocene
32R-2, 44–47	290.14			Barren			

Table T13 (continued).

Core, section, interval (cm)	Depth (mbsf)	Foraminifer age (Ma)		Foraminifer zone	Nannofossil age (Ma)	Nannofossil zone	Epoch
		Minimum	Maximum				
32R-3, 45–48	291.65	57.1	59.2	P4			late Paleocene
32R-CC, 22–25	292.35	57.1	59.2	P4	56.2	NP9	late Paleocene
33R-2, 50–54	299.80	57.1	59.2	P4			late Paleocene
33R-CC, 16–19	307.01	57.1	59.2	P4			late Paleocene
34R-CC, 20–22	317.30	57.1	59.2	P4	57.5	NP7	late Paleocene
35R-1, 50–54	317.60	57.1	59.2	P4			late Paleocene
35R-3, 50–54	320.60	57.1	59.2	P4			late Paleocene
35R-4, 50–54	322.10	57.1	59.2	P4?			late Paleocene
35R-5, 50–54	323.60	57.1	59.2	P4?			late Paleocene
35R-6, 50–54	325.10	60	61	P3a			late Paleocene
35R-7, 18–22	326.28	60	61	P3a			late Paleocene
35R-CC, 34–37	327.00	61	61.2	P2			early Paleocene
36R-1, 73–74	327.43	61	61.2	P2			early Paleocene
36R-2, 53–55	328.73	61	61.2	P2			early Paleocene
36R-3, 28–29	329.98	61	61.2	P2			early Paleocene
36R-4, 0–1	331.20	61.2	63	P1c			early Paleocene
36R-4, 80–81	332.00	64.8	65	Pa	65	NP1	early Paleocene
36R-CC, 6–9	336.09	65	68.6	KS31			Maastrichtian
37R-CC, 24–27	346.38	65	68.6	KS31	66.2	CC26	Maastrichtian
38R-1, 49–52	346.49	65	68.6	KS31			Maastrichtian
38R-2, 49–53	347.99	68.6	69.6	KS30a			Maastrichtian
38R-3, 49–52	349.49	68.6	69.6	KS30a			Maastrichtian
38R-4, 49–51	350.99	68.6	69.6	KS30a			Maastrichtian
38R-5, 49–52	352.49	68.6	69.6	KS30a			Maastrichtian
38R-6, 49–52	353.99	68.6	69.6	KS30a			Maastrichtian
38R-CC, 5–8	354.50	69.6	72.8	KS30b			late Campanian–Maastrichtian
39R-CC, 0–5	365.38	72.8	73.8	KS29			late Campanian
40R-CC, 17–22	374.56	72.8	73.8	KS29	71.3	CC23	late Campanian
41R-2, 147–150	377.87	72.8	73.8	KS29			late Campanian
41R-CC, 0–7	382.96			Barren			
42R-4, 0–5	389.00			Barren			
42R-CC, 20–22	390.70			Not defined	89.3	CC12	Unknown
43R-1, 68–71	394.78			Barren			
43R-2, 78–80	396.16			Not defined			Coniacian?
43R-2, 109–111	396.47	85.4	89.5	KS23			Coniacian
44R-3, 31–33	407.01			Not defined			Turonian?
44R-CC, 12–18	408.62			Not defined			Turonian
45R-3, 55–56	411.75			Not defined			Turonian?
45R-CC, 21–27	411.97			Not defined	93.2	CC11	Turonian?
46R-1, 54–56	414.84			Not defined			Turonian?
46R-4, 67–69	418.95			Not defined			Unknown
46R-6, 67–69	421.74			Not defined			Turonian?
46R-CC, 12–17	422.05			Barren			
47R-7, 0–4	432.13			Not defined			late Cenomanian–Turonian
48R-2, 60–62	435.60			Not defined			Unknown
48R-5, 146–150	440.64			Not defined	94	CC10a	late Cenomanian–Turonian
48R-6, 96–98	441.64			Not defined			Unknown
49R-2, 42–44	444.95	94	99.1	KS19-17			Cenomanian
49R-3, 16–18	446.11	94	99.1	KS19-17			Cenomanian
49R-CC, 0–7	450.82	94	99.1	KS19-17			Cenomanian
50R-1, 17–19	452.87			Not defined			late Albian–Cenomanian
50R-5, 0–2	458.70	94	99.1	KS19-17			Cenomanian
50R-CC, 16–21	462.11	94	99.1	KS19-17			Cenomanian
51R-3, 133–134	466.31			Not defined			late Albian–Cenomanian
51R-5, 52–55	468.50	94	100.4	KS19-16			late Albian–Cenomanian
51R-7, 50–51	471.06	94	100.4	KS19-16			late Albian–Cenomanian
51R-CC, 24–29	471.52			Not defined			late Albian–Cenomanian
52R-2, 99–101	474.09	94	100.4	KS19-16			late Albian–Cenomanian
52R-3, 115–116	475.73			Not defined			Unknown
52R-4, 66–68	476.74			Not defined			Unknown
52R-CC, 7–11	477.63			Not defined	101.7	NC10a	Unknown
53R-1, 24–26	481.54	105	109.5	KS13			early Albian
53R-1, 115–117	482.45	105	109.5	KS13			early Albian
53R-2, 129–130	484.09	105	109.5	KS13			early Albian
54R-CC, 6–11	491.36	105	109.5	KS13			Albian

Note: Both minimal and maximal assigned ages (Ma) are given for the planktonic foraminiferal datums in each sample analyzed.

Table T14. Magnetostratigraphic datums used in the preliminary age-depth model, Hole 1260A.

Core, section, interval (cm)	Depth (mbsf)	Age (Ma)	Polarity chron	Epoch
207-1260A-				
8R-3, 15	60.35	41.521	C19n (base)	middle Eocene
20R-2, 75	175.05	46.264	C20r (base)	middle Eocene
37R-5, 145	343.85	68.737	C31n (base)	Maastrichtian
38R-3, 45	349.45	71.071	C31r (base)	Maastrichtian
40R-6, 85	373.65	73.004	C32n (base)	late Campanian

Table T15. Linear sedimentation rates and mass accumulation rates, Hole 1260A.

Epoch (zone)	Core, section interval (cm)	Top		Bottom		Thickness (m)	Duration (m.y.)	LSR		DBD (g/cm^3)	MAR ($g/cm^2/k.y.$)	Main lithology
		Depth (mbsf)	Age (Ma)	Depth (mbsf)	Age (Ma)			(m/m.y.)	(cm/k.y.)			
	207-1260A-											
early Oligocene (reworking)	2R-1, 1 to 5R-1, 1	1.0	28.5	28.8	32.0	28.8	—	—	—	1.16	—	Nannofossil chalk
late Eocene (P16)	5R-1, 1 to 6R-1, 1	28.8	33.8	38.2	35.2	9.4	1.4	6.7	0.67	1.09	0.73	Nannofossil chalk
middle Eocene (P13–P10)	6R-1, 1 to 25R-1, 1	38.2	40.1	220.7	49.0	182.5	8.9	20.5	2.05	1.02	2.09	Nannofossil chalk
early Eocene–late Paleocene (P8–P4)	25R-1, 1 to 35R-6, 1	220.7	50.4	324.6	59.2	103.9	8.6	12.1	1.12	1.39	1.56	Nannofossil chalk
late Paleocene–late Campanian (P3a–KS29)	35R-6, 1 to 42R-1, 1	324.6	60.0	384.5	73.8	59.9	13.8	4.3	0.43	1.62	0.70	Nannofossil chalk
Coniacian–Albian (CC12–KS16)	42R-1, 1 to 53R-1, 1	384.5	89.3	481.3	100.4	93.3	11.1	8.4	0.84	1.42	1.19	Calc claystone with C_{org}
early Albian (KS13)	53R-1, 1 to 54R-CC, 11	481.3	105.0	491.4	109.5	13.6	4.5	3.0	0.30	1.80	0.54	Quartz siltstone

Notes: Average dry bulk densities (DBD) of major lithologies per studied interval were used (see **"Physical Properties,"** p. 30) to calculate mass accumulation rate (MAR) values. — = not assigned.

Table T16. Total carbon, inorganic carbon, carbonate, total organic carbon, and total nitrogen concentrations and carbon/nitrogen ratios, Site 1260. (See table notes. Continued on next two pages.)

Hole, core, section, interval (cm)	Depth (mbsf)	TC (wt%)	IC (wt%)	$CaCO_3$ (wt%)	TOC (wt%)	N (wt%)	C/N (atomic)
207-							
Unit I (nannofossil clay):							
1260A-1R-1, 15–16	0.15	1.32	1.24	10.3	0.08	0.04	2.4
Unit II (nannofossil chalk):							
1260A-2R-1, 68–69	1.68		5.21	43.4			
1260A-2R-2, 9–10	2.59	7.45	7.50	62.5	0.00	0.01	0.0
1260A-2R-2, 113–114	3.63		9.26	77.1			
1260A-3R-1, 11–12	10.41		9.06	75.5			
1260A-3R-2, 10–11	11.90	8.64	8.73	72.7	0.00	0.02	0.0
1260A-3R-3, 92–93	14.22		7.79	64.9			
1260A-4R-3, 73–74	23.23		8.57	71.4			
1260A-4R-5, 73–74	26.23	8.67	8.44	70.3	0.23	0.02	12.7
1260A-6R-1, 62–63	38.82		9.24	77.0			
1260A-6R-3, 137–138	42.57	7.07	7.01	58.4	0.06	0.01	6.2
1260A-6R-6, 23–24	45.43		8.66	72.1			
1260A-7R-2, 16–17	49.16		9.35	77.9			
1260A-7R-4, 20–21	52.20	9.91	9.87	82.2	0.04	0.01	4.4
1260A-8R-1, 49–50	57.69		9.82	81.8			
1260A-8R-6, 26–27	64.96	8.73	8.60	71.6	0.13	0.01	10.9
1260A-9R-1, 82–83	67.72		9.95	82.9			
1260A-9R-3, 89–90	70.79		9.30	77.5			
1260A-9R-5, 86–87	73.76	9.16	8.93	74.4	0.23	0.02	14.5
1260A-9R-7, 66–67	76.56		8.85	73.8			
1260A-10R-1, 83–84	77.43		8.39	69.9			
1260A-10R-3, 48–49	80.08		9.00	75.0			
1260A-10R-5, 72–73	83.32	9.07	8.98	74.8	0.09	0.01	9.3
1260A-11R-2, 80–81	88.60		9.93	82.7			
1260A-11R-4, 78–79	91.58		9.43	78.6			
1260A-11R-6, 84–85	94.64	9.06	9.02	75.1	0.04	0.01	5.4
1260A-12R-1, 62–63	96.52		8.69	72.4			
1260A-12R-3, 99–100	99.89		7.90	65.8			
1260A-12R-5, 60–61	102.50	8.45	8.47	70.6	0.00	0.01	0.0
1260A-13R-2, 64–64	107.74		8.19	68.2			
1260A-13R-4, 64–64	110.74		8.68	72.3			
1260A-13R-6, 64–64	113.74	8.75	8.69	72.4	0.06	0.01	5.2
1260A-14R-2, 75–76	117.55		8.54	71.1			
1260A-14R-4, 73–74	120.53		8.77	73.1			
1260A-14R-6, 75–76	123.55	8.44	8.37	69.8	0.07	0.01	12.5
1260A-15R-1, 70–71	125.60		9.14	76.2			
1260A-15R-3, 69–70	128.59	8.92	8.82	73.5	0.10	0.01	14.0
1260A-16R-1, 42–43	134.92	9.49	9.45	78.7	0.04	0.01	3.5
1260A-17R-2, 69–70	146.39	9.51	9.56	79.6	0.00	0.00	0.0
1260A-18R-1, 69–70	154.19		8.81	73.4			
1260A-18R-5, 70–71	160.20	9.16	9.14	76.1	0.02	0.01	2.1
1260A-19R-1, 70–71	163.90		8.27	68.9			
1260A-19R-5, 70–71	169.90	8.23	8.45	70.4	0.00	0.02	0.0
1260A-20R-2, 76–77	175.06		8.63	71.9			
1260A-20R-5, 77–78	179.57	8.49	8.50	70.8	0.00	0.02	0.0
1260A-21R-1, 7–8	182.57	7.53	7.54	62.8	0.00	0.02	0.0
1260A-23R-1, 92–93	202.32		7.62	63.5			
1260A-23R-3, 69–71	205.09	8.23	8.09	67.4	0.14	0.03	5.7
1260A-24R-1, 110–111	212.20		7.66	63.9			
1260A-24R-3, 63–64	214.53		6.16	51.3			
1260A-24R-5, 88–89	217.67	7.83	7.74	64.5	0.09	0.23	0.4
1260A-25R-1, 127–128	221.97		8.18	68.2			
1260A-25R-4, 1–2	225.21		5.79	48.2			
1260A-25R-6, 71–72	228.71	7.33	7.34	61.2	0.00	0.03	0.0
1260A-26R-1, 120–121	231.50		6.35	52.9			
1260A-26R-5, 19–20	236.49	6.65	6.59	54.9	0.06	0.03	2.7
1260A-26R-7, 59–60	239.39		6.72	56.0			
1260A-27R-1, 75–76	240.75		7.15	59.5			
1260A-27R-3, 74–75	243.74		7.54	62.8			
1260A-27R-5, 71–72	246.71		7.08	59.0			
1260A-27R-7, 19–20	248.89	7.50	7.41	61.7	0.09	0.03	3.8
1260A-28R-2, 75–76	251.66		6.04	50.3			

Table T16 (continued).

Hole, core, section, interval (cm)	Depth (mbsf)	TC (wt%)	IC (wt%)	$CaCO_3$ (wt%)	TOC (wt%)	N (wt%)	C/N (atomic)
1260A-28R-4, 75–76	254.62		7.48	62.3			
1260A-28R-6, 75–75	256.93	7.28	7.17	59.7	0.11	0.03	4.2
1260A-28R-8, 50–51	259.14		7.19	59.9			
1260A-29R-2, 69–70	260.88		7.23	60.2			
1260A-29R-4, 75–76	263.84		6.59	54.9			
1260A-29R-6, 14–15	265.64	6.60	6.43	53.6	0.17	0.03	7.2
1260A-30R-1, 67–68	269.57		7.59	63.2			
1260A-30R-3, 67–68	272.49		5.84	48.7			
1260A-30R-5, 59–60	275.02	6.80	6.74	56.1	0.06	0.00	15.6
Unit III (foraminifer to clayey nannofossil chalk):							
1260A-30R-8, 72–73	278.22		4.92	41.0			
1260B-17R-7, 69–69.1	279.84	0.18	0.10	0.9	0.08	0.03	2.9
1260A-31R-2, 49–50	280.28		6.48	54.0			
1260A-31R-4, 64–65	283.22	6.59	6.57	54.7	0.02	0.05	0.5
1260A-31R-6, 66–67	286.24		6.51	54.2			
1260A-32R-1, 68–69	288.88		5.01	41.7			
1260B-19R-1, 138–139	291.48	0.00	6.56	54.7			
1260A-32R-3, 29–30	291.49	6.52	6.35	52.9	0.17		
1260B-19R-3, 52–53	293.62	7.14	6.98	58.2	0.16	0.02	8.4
1260B-20R-1, 29–30	300.09	0.00	3.21	26.7			
1260B-20R-1, 135–136	301.15	0.00	4.52	37.6			
1260B-20R-3, 59–60	303.39	6.21	6.03	50.3	0.18	0.27	0.8
1260B-20R-6, 66–67	307.94	0.00	6.42	53.5			
1260B-21R-2, 94–95	311.84	0.00	5.33	44.4			
1260B-21R-4, 13–14	314.05	6.11	5.91	49.3	0.20	0.03	7.4
1260A-35R-1, 78–79	317.88		5.38	44.8			
1260B-21R-7, 1–2	318.45	0.00	6.72	56.0			
1260A-35R-3, 86–87	320.96	6.46	6.56	54.6	0.00	0.01	
1260B-22R-4, 2–3	323.62	9.42	9.28	77.3	0.14	0.01	11.3
1260A-35R-5, 116–117	324.26		10.30	85.8			
1260A-35R-7, 30–31	326.40		9.09	75.7			
1260B-23R-1, 110–111	329.80	0.00	6.77	56.4			
1260B-23R-6, 63–64	336.63	8.95	8.83	73.6	0.12	0.01	13.4
1260B-24R-3, 116–117	342.56	9.26	9.12	75.9	0.14	0.01	13.6
1260A-37R-5, 90–91	343.30	9.32	9.38	78.1	0.00	0.00	
1260A-37R-5, 109–110	343.49		6.75	56.2			
1260A-38R-1, 114–115	347.14		9.47	78.9			
1260A-38R-4, 70–71	351.20	6.10	6.05	50.4	0.05	0.01	4.8
1260A-38R-6, 10–11	353.60		6.29	52.4			
1260A-39R-1, 2–3	355.62		6.11	50.9			
1260A-39R-3, 73–74	359.33	5.72	5.51	45.9	0.21	0.01	17.7
1260A-39R-5, 115–116	362.75		5.44	45.3			
1260A-39R-6, 88–89	363.98		6.89	57.4			
1260B-27R-1, 8–9	367.38	0.00	7.36	61.3			
1260A-40R-3, 40–41	368.70	9.30	9.27	77.2	0.03	0.00	8.9
1260A-40R-4, 0–5	369.80	6.16	6.18	51.5	0.00	0.01	
1260B-27R-5, 107–108	374.37	7.40	7.27	60.5	0.13	0.02	9.0
1260A-41R-1, 67–68	375.57	8.39	8.37	69.7	0.02	0.01	3.5
1260B-28R-1, 72–72	377.62	5.49	5.31	44.3	0.18	0.02	9.9
1260B-28R-1, 149–150	378.39	5.50	5.34	44.5	0.16	0.03	6.7
1260A-41R-4, 0–5	379.40	3.95	3.94	32.8	0.01	0.01	1.3
1260B-29R-2, 0–1	383.00	3.91	3.71	30.9	0.20	0.05	5.1
1260B-29R-2, 0–1	383.00	4.04	3.71	30.9	0.33	0.04	9.4
1260B-29R-2, 49–50	383.49	0.00	3.60	30.0			
1260B-29R-3, 59–60	385.09	4.60	4.21	35.0	0.39	0.04	11.8
1260A-42R-1, 73–74	385.23		3.94	32.9			
1260A-42R-2, 0–5	386.00	3.50	3.43	28.5	0.07	0.00	
1260B-30R-1, 72–73	387.22	3.35	3.17	26.4	0.18	0.02	11.9
1260A-42R-2, 127–128	387.27		4.18	34.8			
1260B-30R-1, 145–150	387.95	4.06	3.93	32.7	0.13	0.02	6.2
1260A-42R-4, 55–56	389.55	5.39	5.15	42.9	0.24	0.02	15.1
Unit IV (laminated black shale):							
1260B-31R-1, 145–150	392.55	14.47	6.48	53.9	7.99	0.30	31.0
1260A-43R-1, 62–63	394.72	9.02	3.20	26.7	5.82	0.20	34.5
1260A-43R-2, 0–5	395.38	19.94	6.02	50.1	13.92	0.43	37.7
1260A-43R-2, 95–96	396.33	15.57	6.36	53.0	9.21	0.29	37.5
1260B-32R-2, 90–93	398.44	13.79	7.23	60.2	6.56	0.24	31.5
1260B-33R-1, 145–150	402.15	16.99	5.50	45.8	11.49	0.40	33.9

Table T16 (continued).

Hole, core, section, interval (cm)	Depth (mbsf)	TC (wt%)	IC (wt%)	$CaCO_3$ (wt%)	TOC (wt%)	N (wt%)	C/N (atomic)
1260B-33R-2, 56–57	402.76	14.98	5.00	41.7	9.98	0.37	31.4
1260A-44R-2, 0–5	405.20	11.77	5.49	45.7	6.28	0.22	34.1
1260A-44R-3, 32–33	407.02	15.16	4.50	37.5	10.66	0.40	30.9
1260A-44R-4, 88–89	408.38	13.86	5.63	46.9	8.23	0.30	31.5
1260B-34R-3, 0–5	408.70	15.13	2.26	18.9	12.87	0.53	28.2
1260A-45R-1, 107–108	409.77	12.74	10.94	91.2	1.80	0.05	42.3
1260A-45R-1, 148–150	410.18	10.18	5.75	47.9	4.43	0.16	33.1
1260A-45R-2, 10–11	410.30	12.42	4.80	40.0	7.62	0.30	30.1
1260B-34R-5, 25–26	411.95	11.53	1.28	10.7	10.25	0.39	30.5
1260A-46R-1, 38–39	414.68	14.82	3.58	29.8	11.24	0.43	30.6
1260A-46R-3, 118–119	418.12	13.35	0.46	3.8	12.89	0.52	28.9
1260A-46R-4, 0–5	418.28	13.77	0.78	6.5	12.99	0.54	28.2
1260B-35R-3, 0–5	418.30	11.97	9.00	75.0	2.97	0.16	21.4
1260A-46R-4, 66–67	418.94	14.75	2.29	19.1	12.46	0.50	29.3
1260B-35R-5, 16–16	421.41	14.40	1.25	10.4	13.15	0.41	37.3
1260A-46R-6, 43–44	421.50	14.35	3.36	28.0	10.99	0.42	30.2
1260B-36R-1, 61–62	425.51	15.75	7.53	62.7	8.22	0.31	31.0
1260B-36R-3, 0–5	427.90	14.65	6.25	52.1	8.40	0.34	29.0
1260A-47R-5, 143–145	431.31	15.75	5.26	43.8	10.49	0.39	31.7
1260B-36R-6, 14–15	432.54	15.41	5.33	44.4	10.08	0.40	29.2
1260B-36R-6, 91–92	433.31	12.35	11.58	96.4	0.77	0.03	35.6
1260A-48R-1, 2–3	433.52	15.56	4.81	40.1	10.75	0.41	30.3
1260A-48R-3, 0–2	436.40	13.06	10.31	85.9	2.75	0.12	27.0
1260A-48R-3, 111–112	437.51	14.48	5.50	45.8	8.98	0.35	30.2
1260B-37R-5, 0–5	440.50	15.13	6.11	50.9	9.02	0.35	29.6
1260A-48R-6, 99–100	441.67	18.05	6.37	53.1	11.68	0.41	33.0
1260A-49R-2, 39–40	444.92	13.80	5.39	44.9	8.41	0.28	35.7
1260B-38R-2, 0–2	445.60	15.99	7.05	58.7	8.94	0.29	35.6
1260A-49R-4, 0–2	447.45	12.88	10.75	89.5	2.13	0.07	38.2
1260A-49R-5, 82–83	449.77	12.91	10.36	86.3	2.55	0.06	50.0
1260B-38R-CC, 4–5	452.33	16.76	5.72	47.6	11.04	0.39	33.4
1260A-50R-1, 43–44	453.13	17.77	7.19	59.9	10.58	0.33	37.1
1260B-39R-2, 0–2	455.20	16.28	8.18	68.2	8.10	0.26	35.9
1260A-50R-4, 68–69	457.88	12.30	10.68	89.0	1.62	0.04	52.0
1260A-50R-5, 0–2	458.70	15.07	8.96	74.7	6.11	0.20	36.6
1260A-50R-7, 29–30	461.49	14.41	8.85	73.7	5.56	0.23	28.1
1260B-39R-7, 7–8	462.77	56.69	0.79	6.6	55.90	0.80	81.5
1260A-51R-4, 12–13	466.60	12.55	5.15	42.9	7.40	0.26	33.3
1260A-51R-5, 4–5	468.02	12.53	10.36	86.3	2.17	0.05	47.8
1260A-51R-5, 146–148	469.44	15.79	8.04	66.9	7.75	0.26	35.5
1260B-40R-CC, 15–16	470.90	14.61	10.03	83.5	4.58	0.12	44.7
1260A-52R-2, 29–30	473.39	12.46	10.55	87.9	1.91	0.05	43.8
1260B-41R-2, 0–2	474.20	14.02	5.18	43.1	8.84	0.27	38.4
1260A-52R-4, 0–2	476.08	13.08	9.74	81.1	3.34	0.17	23.1
1260A-52R-4, 50–51	476.58	16.09	7.01	58.4	9.08	0.31	34.3
1260B-41R-4, 18–19	477.38	16.11	7.16	59.7	8.95	0.32	33.0
1260B-42R-1, 29–30	482.59	7.06	5.44	45.3	1.62	0.06	29.5
1260A-53R-1, 143–145	482.73	7.23	5.19	43.2	2.04	0.06	41.8
1260A-53R-1, 145–146	482.75	6.84	5.38	44.9	1.46	0.04	40.7
Unit V (silty calcareous claystone):							
1260A-53R-2, 66–67	483.46	1.51	1.06	8.8	0.45	0.01	37.2
1260B-42R-2, 138–139	484.96	1.59	1.03	8.6	0.56	0.03	20.3
1260B-42R-3, 21–22	485.18	1.43	0.93	7.8	0.50	0.03	21.1
1260A-54R-1, 149–150	489.39	1.57	1.09	9.1	0.48	0.02	29.5
1260B-43R-2, 0–2	489.40	1.65	0.01	0.1	1.64	0.03	56.2
1260A-54R-2, 70–71	490.10	1.47	1.01	8.4	0.46	0.01	44.7
1260B-44R-1, 88–89	492.78	1.80	1.32	11.0	0.48	0.03	19.1
1260B-44R-2, 0–2	493.37	1.43	1.02	8.5	0.41	0.02	19.5
1260B-45R-1, 80–81	497.30	1.68	1.07	8.9	0.61	0.03	21.5
1260B-45R-1, 148–150	497.98	1.41	1.00	8.4	0.41	0.03	17.6
1260B-46R-2, 80–81	503.80	1.53	1.11	9.3	0.42	0.03	18.4
1260B-46R-2, 145–150	504.45	1.68	1.02	8.5	0.66	0.04	20.3
1260B-46R-4, 60–61	506.60	1.95	1.29	10.8	0.66	0.04	20.6

Notes: TC = total carbon, IC = inorganic carbon, TOC = total organic carbon. Atomic C/N ratios are calculated from concentrations of organic carbon and total nitrogen.

Table T17. Rock-Eval pyrolysis analyses of sediment samples, Site 1260.

Hole, core, section, interval (cm)	Depth (mbsf)	TOC (wt%)	T_{max} (°C)	S_1	S_2	S_3	HI	OI
207-								
Unit IV (laminated black shale):								
1260A-43R-1, 62–63	394.72	5.82	400	3.56	37.26	4.52	640	77
1260A-43R-2, 95–96	396.33	9.21	394	6.20	46.67	9.59	506	104
1260B-33R-2, 56–57	402.76	9.98	394	7.91	59.94		600	
1260A-44R-3, 32–33	407.02	10.66	404	4.94	65.99	9.41	619	88
1260A-44R-4, 88–89	408.38	8.23	392	6.21	47.80	10.43	580	126
1260A-45R-1, 107–108	409.77	1.80	378	1.58	11.55	1.59	641	88
1260A-45R-2, 10–11	410.30	7.62	393	4.78	46.29	7.64	607	102
1260B-34R-5, 25–26	411.95	10.25	398	7.79	57.98		565	
1260A-46R-1, 38–39	414.68	11.24	387	10.44	63.93	12.36	568	110
1260A-46R-3, 118–119	418.12	12.89	393	6.66	70.33	7.02	545	54
1260A-46R-4, 66–67	418.94	12.46	395	7.86	67.49	9.91	541	79
1260B-35R-5, 16–16	421.41	13.15	405	7.79	81.28		618	
1260A-46R-6, 43–44	421.50	10.99	396	5.43	66.73	9.11	607	82
1260B-36R-1, 61–62	425.51	8.22	404	4.54	47.22		574	
1260B-36R-6, 14–15	432.54	10.08	402	7.31	65.05		645	
1260A-48R-1, 2–3	433.52	10.75	402	5.16	69.09	10.30	642	95
1260A-48R-3, 111–112	437.51	8.98	396	4.83	53.50	8.63	595	96
1260A-48R-6, 99–100	441.67	11.68	401	5.12	74.52	8.67	636	74
1260A-49R-2, 39–40	444.92	8.41	400	2.71	55.36	8.82	658	104
1260A-49R-5, 82–83	449.77	2.55	394	0.90	15.58	3.65	610	143
1260B-38R-CC, 4–5	452.33	11.04	400	6.48	68.38		619	
1260A-50R-1, 43–44	453.13	10.58	400	6.23	69.06	6.34	652	59
1260A-50R-4, 68–69	457.88	1.62	409	0.56	8.75	2.51	540	154
1260A-50R-7, 29–30	461.49	5.56	402	3.05	40.16	6.68	722	120
1260B-39R-7, 7–8	462.77	55.90	375	16.84	172.96		309	
1260A-51R-4, 12–13	466.60	7.40	401	2.81	42.67	4.69	644	63
1260A-51R-5, 4–5	468.02	2.17	391	0.57	7.44	4.86	342	223
1260B-40R-CC, 15–16	470.90	4.58	414	1.87	22.19		484	
1260A-52R-2, 29–30	473.39	1.91	385	0.30	2.11	4.86	110	254
1260A-52R-4, 50–51	476.58	9.08	394	5.04	61.19	10.03	673	110
1260B-41R-4, 18–19	477.38	8.95	403	4.38	58.61		654	
1260A-53R-1, 145–146	482.75	1.46	406	0.38	7.32	1.67	501	114
Unit V (silty calcareous claystone):								
1260A-53R-2, 66–67	483.46	0.45	404	0.05	0.33	0.80	73	177
1260A-54R-2, 70–71	490.10	0.46	404	0.01	0.32	0.54	69	117
1260B-45R-1, 80–81	497.30	0.61	409	0.01	0.02		3	
1260B-46R-4, 60–61	506.60	0.66	413	0.03	0.43		65	

Note: TOC = total organic carbon. HI = milligrams of hydrocarbon-like material released by pyrolysis (S_2) per gram of organic carbon, OI = milligrams of CO_2 (S_3) per gram of organic carbon. See **"Organic Geochemistry,"** p. 27, in the "Explanatory Notes" chapter for definitions of T_{max}, S_1, S_2, and S_3.

Table T18. Headspace analyses of interstitial and microbial gases, Site 1260. (See table note. Continued on next page.)

Hole, core, section, interval (cm)	Depth (mbsf)	Routine safety monitoring				Microbial study			
		C_1 (ppmv)	C_2 (ppmv)	C_3 (ppmv)	C_1/C_2	C_1 (ppmv)	C_2 (ppmv)	C_3 (ppmv)	C_1/C_2
207-									
Unit II:									
1260A-2R-1, 145–150	2.45	2				8			
1260A-3R-1, 145–150	11.75	2				4			
1260A-4R-4, 0–5	24.00	3				5			
1260A-5R-4, 0–5	33.30	4				4			
1260A-6R-4, 0–5	42.70	4				23	0		55
1260A-7R-4, 0–5	52.00	3				5			
1260A-8R-4, 0–5	61.70	4				6			
1260A-9R-4, 0–5	71.40	4				23	0		47
1260A-10R-4, 0–5	81.10	4				7			
1260A-11R-4, 0–5	90.80	5				7	0		29
1260A-12R-4, 0–5	100.40	5				6			
1260A-13R-4, 0–5	110.10	3				13			
1260A-14R-4, 0–5	119.80	7				20			
1260A-15R-2, 0–5	126.40	3				8	1		13
1260A-16R-1, 3–5	134.53	2							
1260A-17R-2, 0–5	145.70	4				5			
1260A-18R-4, 0–5	158.00	3				5			
1260A-19R-4, 0–5	167.70	3				5	1		6
1260A-20R-4, 0–5	177.30	3				5	0		11
1260A-21R-1, 129–130	183.79	2							
1260A-23R-3, 0–5	204.40	3				4			
1260A-24R-3, 137–139	215.27	4				3			
1260A-25R-3, 0–2	223.70	4				4			
1260A-26R-2, 148–150	233.28	3				4			
1260A-27R-3, 148–150	244.48	3				2			
1260A-28R-5, 0–2	254.86	3				4			
1260A-29R-5, 98–100	265.48	4				5			
1260A-30R-4, 0–2	273.32	17				19			
Unit III:									
1260A-31R-4, 0–5	282.58	133				260			
1260A-32R-1, 145–150	289.65	236				451	1		609
1260A-33R-4, 0–5	302.26	569				776	1		872
1260A-34R-4, 0–5	311.90	1,414	1		1,088	1,432	2		930
1260A-35R-5, 0–5	323.10	1,455	1		1,119	1,226	1		943
1260A-36R-2, 0–5	328.20	2,246	2		1,248	2,208	2		1,110
1260A-37R-2, 0–5	337.90	2,741	2		1,371	2,047	2		1,329
1260B-24R-3, 0–2	341.40	1,125	1		1,293				
1260A-38R-4, 0–5	350.50	1,258	1		968	3,872	3		1,237
1260B-25R-3, 145–150	352.45	1,508	1		1,371				
1260A-39R-4, 0–5	360.10	747	1		1,493	682			
1260B-26R-5, 0–5	363.70	481			1,203				
1260A-40R-4, 0–5	369.80	1,291	1		1,435	2,507	2		1,441
1260B-27R-3, 0–5	370.30	600							
1260B-28R-1, 149–150	378.39	1,091	1		1,213				
1260A-41R-4, 0–5	379.40	3,511	3		1,351	2,392	2		1,367
1260B-29R-2, 0–1	383.00	1,880	2		1,106				
1260A-42R-2, 0–5	386.00	4,014	3		1,434	2,105	1		1,537
1260B-30R-1, 145–150	387.95	1,067							
Unit IV:									
1260B-31R-1, 145–150	392.55	16,596	29		574				
1260A-43R-2, 0–5	395.38	17,840	39		457	10,112	18		562
1260B-32R-2, 90–93	398.44	15,556	28		560				
1260B-33R-1, 145–150	402.15	9,885	11		899				
1260A-44R-2, 0–5	405.20	17,995	11		1,578	10,240	5		1,907
1260B-34R-3, 0–5	408.70	13,149	17		778				
1260A-45R-1, 148–150	410.18	8,333	11		744	6,427	7		980
1260A-46R-4, 0–5	418.28	15,565	34		463	9,101	16		555
1260B-35R-3, 0–5	418.30	6,355	12		512				
1260B-36R-3, 0–5	427.90	34,665	108	11	322				
1260A-47R-5, 143–145	431.31	16,025	50	5	319	15,861	40	2	398
1260A-48R-3, 0–2	436.40	8,000	23	2	351	6,552	14		462
1260B-37R-5, 0–5	440.50	22,539	63	6	360				
1260B-38R-2, 0–2	445.60	48,558	123	16	396				
1260A-49R-4, 0–2	447.45	12,783	34	5	378	5,989	15		387

Table T18 (continued).

Hole, core, section, interval (cm)	Depth (mbsf)	Routine safety monitoring C_1 (ppmv)	C_2 (ppmv)	C_3 (ppmv)	C_1/C_2	Microbial study C_1 (ppmv)	C_2 (ppmv)	C_3 (ppmv)	C_1/C_2
1260B-39R-2, 0–2	455.20	68,266	190	27	359				
1260A-50R-5, 0–2	458.70	18,102	58	9	313	21,045	80	11	263
1260B-40R-2, 0–2	464.60	3,941	13		301				
1260A-51R-5, 146–148	469.44	16,567	53	6	313	35,955	117	12	307
1260B-41R-2, 0–2	474.20	17,337	64	6	270				
1260A-52R-4, 0–2	476.08	8,843	26		336	10,200	44	5	234
1260A-53R-1, 143–145	482.73	4,109	20		206		8		
Unit V:									
1260B-42R-2, 138–139	484.96	3,910	10		407				
1260A-54R-1, 149–150	489.39	4,260	10		435	2,834		1	
1260B-43R-2, 0–2	489.40	6,973	17		418				
1260B-44R-2, 0–2	493.37	2,179	4		559				
1260B-45R-1, 148–150	497.98	7,827	14		547				
1260B-46R-2, 145–150	504.45	6,275	13		486				

Note: C_1 = methane, C_2 = ethane, C_3 = propane.

Table T19. Interstitial water analyses, Site 1260.

Core, section, interval (cm)	Depth (mbsf)	Depth (mcd)	Salinity	Alkalinity (mM)	pH	Cl^- (mM)	$*SO_4^{2-}$ (mM)	NH_4^+ (μM)	$*H_4SiO_4$ (μM)	B (mM)	Li^+ (μM)	Sr^{2+} (μM)	Ca^{2+} (mM)	K^+ (mM)	Mg^{2+} (mM)	Ba^{2+} (μM)	Fe^{2+} (μM)	Mn^{2+} (μM)	Na^+ (mM)	Na^+ diff
207-1260A-																				
1R-1, 58–63	0.58	0.58	35.5	3.53	7.46	558	28.7	35	230	0.61	31	99	10.9	11.0	51.5	7	53.0	11.2	477	483
2R-1, 145–150	2.45	2.45	35.5	4.17	7.24	564	27.9	65	222	0.63	38	113	11.4	10.9	52.2	7	14.0	9.5	476	485
3R-1, 145–150	11.75	11.75	35.5	3.00	7.48	560	25.4	95	206	0.50	38	112	10.7	11.3	49.5	7	5.7	4.1	481	482
4R-3, 145–150	23.95	23.95	35.0	3.92	7.29	561	24.6	155	342	0.52	50	141	12.3	11.4	51.1	7	3.8	2.0	490	476
6R-5, 90–100	45.10	45.10	35.3	5.61	7.21	563	24.0	210	669	0.44	62	179	15.0	10.8	49.4	7	35.2	1.5	485	476
7R-5, 145–150	54.95	55.05	35.0	5.89	7.11	560	23.5	245	671	0.45	65	185	14.4	10.9	48.3	7	25.1	1.6	478	475
8R-5, 142–150	64.62	64.72	35.3	5.60	7.14	563	21.9	255	686	0.45	72	193	15.0	10.5	50.4	7	35.9	1.2	467	470
9R-5, 142–150	74.32	73.32	35.0	5.60	7.04	563	22.4	280	650	0.45	75	209	15.4	10.5	48.6	7	30.9	1.1	473	474
10R-5, 142–150	84.02	83.12	35.3	6.17	7.20	562	20.9	310	712	0.45	79	222	16.1	10.3	49.0	7	24.8	1.1	479	468
12R-4, 140–150	101.80	100.42	35.7	6.47	7.02	565	20.4	335	715	0.46	86	243	16.5	9.3	47.2	7	37.8	1.1	493	474
14R-6, 105–110	123.85	122.17	35.5	5.87	7.24	567	20.3	415	693	0.46	92	256	16.2	10.1	47.3	7	14.8	1.0	482	475
17R-1, 145–150	145.65	143.84	35.0	6.53	7.17	567	18.1	525	714	0.46	101	292	17.0	9.5	46.2	7	14.6	1.0	486	472
19R-5, 143–150	170.63	168.82	35.0	6.27	7.25	569	17.2	615	723	0.45	112	333	16.7	8.9	45.3	7	21.1	1.1	488	475
21R-1, 130–140	183.80	181.99	34.7	7.35	7.03	570	15.7	685	664	0.45	115	368	17.9	8.5	45.4	7	33.3	1.4	471	473
23R-2, 140–150	204.30	202.49	34.7	7.55	7.09	572	14.7	770	563	0.45	121	385	17.4	8.3	40.9	7	31.9	1.8	472	482
25R-2, 141–150	223.61	221.80	35.0	7.29	7.11	570	13.2	795	540	0.45	120	408	18.0	8.1	41.6	7	19.1	1.6	475	475
27R-4, 140–150	245.90	244.39	35.0	6.55	7.13	570	11.5	900	651	0.45	123	421	17.1	7.4	41.0	7	3.9	1.5	472	474
29R-3, 130–140	262.99	262.22	34.7	6.76	7.02	568	9.4	915	652	0.43	127	461	16.8	6.9	39.7	8	1.6	1.5	474	471
31R-4, 140–150	283.98	283.21	34.5	5.10	7.30	567	7.4	955	721	0.37	130	477	16.9	6.3	38.7	8	1.5	1.6	476	468
33R-3, 0–12	300.76	299.99	34.3	ND	ND	574	6.3	1070	685	0.35	131	498	16.8	6.4	37.3	8	1.0	2.1	477	470
35R-1, 135–150	318.45	317.37	33.3	6.39	7.13	556	4.6	1045	650	0.40	136	541	17.0	5.7	37.4	8	2.7	1.9	464	455
37R-3, 135–150	340.75	341.00	34.3	5.96	6.99	582	3.1	1285	409	0.43	146	581	15.7	6.0	35.0	9	1.6	1.2	482	484
39R-4, 135–150	361.45	362.19	32.5	3.12	7.69	574	2.0	1420	316	0.31	141	624	14.2	5.8	33.9	10	0.9	0.8	475	476
41R-1, 140–150	376.30	378.96	32.3	4.71	7.26	558	1.7	1380	567	0.46	140	605	14.9	5.5	33.7	13	1.1	0.8	458	461
54R-2, 110–120	490.50	492.98	33.7	8.71	7.37	577	0.5	2070	149	0.34	181	988	15.7	4.3	29.8	29	7.1	1.3	480	487
207-1260B-																				
38R-5, 140–150	451.36	455.43	33.7	8.14	7.10	582	0.3	1770	315	0.58	175	836	16.5	5.0	31.9	56	15.5	0.0	489	485
40R-4, 140–150	469.00	473.58	34.0	7.92	7.35	582	0.3	1900	215	0.52	176	911	16.4	4.8	32.1	53	0.3	0.1	484	485
46R-3, 140–150	505.90	508.58	34.3	7.32	7.49	579	1.0	2060	143	0.29	186	1022	16.2	4.3	29.6	18	1.5	0.7	482	488

Note: * = ICP-AES. ND = not determined.

Table T20. Index properties of discrete samples, Holes 1260A and 1260B. (See table notes. Continued on next three pages.)

Core, section, interval (cm)	Depth (mbsf)	Depth (mcd)	Water content (%) Wet	Water content (%) Dry	Density (g/cm³) Bulk	Density (g/cm³) Dry	Density (g/cm³) Grain	Porosity (%)	Void ratio
207-1260A-									
2R-1, 28–30	1.28	1.28	38.2	61.7	1.638	1.013	2.601	61.1	1.568
2R-2, 60–62	3.10	3.10	31.3	45.5	1.663	1.143	2.323	50.8	1.033
2R-2, 88–90	3.38	3.38	34.5	52.7	1.652	1.082	2.441	55.7	1.257
3R-1, 13–15	10.43	10.43	27.9	38.7	1.709	1.232	2.306	46.6	0.872
3R-2, 18–20	11.98	11.98	27.9	38.8	1.794	1.292	2.532	49.0	0.959
4R-2, 19–21	21.19	21.19	30.4	43.6	1.693	1.179	2.367	50.2	1.008
4R-3, 25–27	22.75	22.75	31.9	46.8	1.729	1.178	2.550	53.8	1.165
4R-4, 76–78	24.76	24.76	35.6	55.3	1.672	1.077	2.573	58.2	1.390
4R-5, 24–26	25.74	25.74	28.6	40.0	1.710	1.221	2.335	47.7	0.912
5R-1, 25–27	29.05	29.05	38.2	61.8	1.650	1.019	2.651	61.5	1.600
5R-2, 62–65	30.92	30.92	34.5	52.6	1.709	1.120	2.637	57.5	1.354
5R-3, 89–91	32.69	32.69	35.1	54.1	1.695	1.100	2.624	58.1	1.387
5R-4, 100–102	34.30	34.30	35.4	54.9	1.711	1.104	2.709	59.2	1.453
6R-1, 24–26	38.44	38.44	45.1	82.1	1.559	0.856	2.732	68.7	2.191
6R-2, 53–55	40.23	40.23	47.9	92.0	1.508	0.786	2.670	70.6	2.399
6R-3, 56–58	41.76	41.76	54.3	118.8	1.389	0.635	2.410	73.7	2.796
6R-4, 48–50	43.18	43.18	45.1	82.0	1.537	0.844	2.608	67.6	2.089
6R-5, 60–62	44.80	44.80	49.2	97.0	1.492	0.757	2.678	71.7	2.535
7R-1, 38–40	47.88	47.98	43.0	75.5	1.584	0.903	2.697	66.5	1.988
7R-2, 22–24	49.22	49.32	41.9	72.3	1.587	0.921	2.631	65.0	1.856
7R-3, 30–32	50.80	50.90	40.0	66.6	1.634	0.981	2.708	63.8	1.760
7R-4, 28–30	52.28	52.38	32.1	47.2	1.759	1.195	2.661	55.1	1.226
7R-5, 85–87	54.35	54.45	36.2	56.6	1.687	1.077	2.665	59.6	1.474
8R-1, 74–76	57.94	58.04	42.3	73.2	1.597	0.922	2.703	65.9	1.932
8R-2, 78–80	59.48	59.58	39.0	63.9	1.656	1.010	2.732	63.0	1.705
8R-3, 77–79	60.97	61.07	41.2	70.1	1.590	0.935	2.594	64.0	1.776
8R-4, 20–22	61.90	62.00	44.0	78.6	1.574	0.881	2.724	67.7	2.091
8R-5, 19–21	63.39	63.49	40.9	69.2	1.597	0.944	2.608	63.8	1.763
9R-1, 80–82	67.70	66.70	37.1	59.0	1.662	1.045	2.629	60.2	1.516
9R-2, 67–69	69.07	68.07	40.0	66.8	1.601	0.960	2.564	62.6	1.672
9R-3, 92–94	70.82	69.82	39.1	64.3	1.617	0.984	2.575	61.8	1.616
9R-4, 90–92	72.30	71.30	34.1	51.7	1.639	1.081	2.378	54.5	1.199
9R-6, 93–95	75.33	74.33	34.3	52.1	1.600	1.052	2.265	53.5	1.153
10R-1, 81–83	77.41	76.51	37.2	59.3	1.560	0.979	2.264	56.8	1.312
10R-2, 58–60	78.68	77.78	32.5	48.1	1.621	1.094	2.254	51.4	1.060
10R-3, 44–46	80.04	79.14	39.1	64.2	1.609	0.980	2.542	61.5	1.595
10R-4, 77–79	81.87	80.97	38.9	63.7	1.561	0.954	2.346	59.3	1.460
10R-5, 69–71	83.29	82.39	34.0	51.4	1.643	1.085	2.385	54.5	1.197
10R-6, 63–65	84.73	83.83	42.2	73.1	1.582	0.914	2.629	65.2	1.877
11R-1, 80–82	87.10	85.72	37.5	60.0	1.639	1.024	2.562	60.0	1.501
11R-2, 78–80	88.58	87.20	32.6	48.3	1.641	1.106	2.314	52.2	1.092
11R-3, 65–67	89.95	88.57	36.0	56.3	1.661	1.062	2.556	58.4	1.406
11R-4, 75–77	91.55	90.17	33.7	50.9	1.628	1.079	2.324	53.6	1.155
11R-5, 70–72	93.00	91.62	41.0	69.6	1.582	0.933	2.547	63.4	1.731
11R-6, 85–87	94.65	93.27	33.3	50.0	1.630	1.086	2.314	53.1	1.130
12R-1, 61–63	96.51	95.13	39.0	63.9	1.554	0.948	2.324	59.2	1.451
12R-2, 69–71	98.09	96.71	43.8	78.0	1.518	0.853	2.434	65.0	1.855
12R-3, 85–87	99.75	98.37	39.9	66.3	1.526	0.917	2.260	59.4	1.464
12R-4, 85–87	101.25	99.87	36.8	58.2	1.601	1.012	2.380	57.5	1.352
12R-5, 65–67	102.55	101.17	46.4	86.6	1.538	0.824	2.722	69.7	2.303
12R-6, 65–67	104.05	102.67	42.1	72.7	1.504	0.871	2.281	61.8	1.620
13R-1, 78–80	106.38	104.40	42.3	73.4	1.558	0.898	2.522	64.4	1.808
13R-2, 101–103	108.11	106.13	43.0	75.4	1.566	0.893	2.607	65.8	1.920
13R-3, 75–77	109.35	107.37	45.7	84.2	1.540	0.836	2.677	68.8	2.201
13R-4, 89–91	110.99	109.01	38.9	63.7	1.633	0.997	2.630	62.1	1.637
13R-5, 73–75	112.33	110.35	40.4	67.9	1.595	0.950	2.565	63.0	1.700
13R-6, 82–84	113.92	111.94	41.4	70.6	1.580	0.926	2.564	63.9	1.768
14R-1, 71–73	116.01	114.33	44.1	78.9	1.569	0.877	2.706	67.6	2.086
14R-2, 73–75	117.53	115.85	43.1	75.7	1.602	0.912	2.799	67.4	2.069
14R-3, 70–72	119.00	117.32	42.5	74.0	1.578	0.907	2.633	65.5	1.903
14R-4, 75–77	120.55	118.87	40.7	68.5	1.635	0.971	2.768	64.9	1.852
14R-5, 69–71	121.99	120.31	42.2	73.0	1.596	0.923	2.698	65.8	1.925
14R-6, 77–79	123.57	121.89	40.9	69.2	1.584	0.936	2.550	63.3	1.724
15R-1, 66–68	125.56	123.75	35.7	55.6	1.604	1.031	2.341	56.0	1.271
15R-2, 136–138	127.76	125.95	34.1	51.7	1.662	1.096	2.450	55.3	1.236
15R-3, 70–72	128.60	126.79	39.6	65.6	1.620	0.979	2.621	62.7	1.679

Table T20 (continued).

Core, section, interval (cm)	Depth (mbsf)	Depth (mcd)	Water content (%) Wet	Water content (%) Dry	Density (g/cm³) Bulk	Density (g/cm³) Dry	Density (g/cm³) Grain	Porosity (%)	Void ratio
15R-4, 87–89	130.27	128.46	37.8	60.7	1.680	1.045	2.752	62.0	1.632
16R-1, 38–40	134.88	133.07	30.3	43.5	1.691	1.178	2.361	50.1	1.004
17R-1, 76–78	144.96	143.15	35.5	55.1	1.715	1.106	2.733	59.5	1.472
17R-2, 68–70	146.38	144.57	36.3	57.0	1.725	1.099	2.829	61.2	1.576
18R-1, 53–55	154.03	152.22	39.4	65.0	1.626	0.985	2.634	62.6	1.673
18R-2, 40–42	155.40	153.59	36.8	58.3	1.660	1.048	2.602	59.7	1.482
18R-3, 38–40	156.88	155.07	35.9	55.9	1.672	1.072	2.587	58.6	1.413
18R-4, 22–24	158.22	156.41	34.8	53.3	1.728	1.127	2.726	58.7	1.419
18R-5, 23–25	159.73	157.92	33.4	50.2	1.724	1.148	2.623	56.2	1.285
18R-6, 19–21	161.19	159.38	35.9	56.1	1.679	1.076	2.620	58.9	1.435
19R-1, 30–32	163.50	161.69	34.2	52.0	1.733	1.140	2.708	57.9	1.376
19R-2, 18–20	164.88	163.07	35.9	55.9	1.674	1.074	2.596	58.6	1.418
19R-3, 25–27	166.45	164.64	33.6	50.7	1.729	1.147	2.655	56.8	1.315
19R-4, 20–22	167.90	166.09	33.2	49.7	1.725	1.152	2.613	55.9	1.268
19R-5, 21–23	169.41	167.60	34.7	53.1	1.713	1.119	2.665	58.0	1.381
19R-6, 15–17	170.85	169.04	32.9	49.1	1.729	1.159	2.612	55.6	1.253
20R-1, 18–20	172.98	171.17	34.5	52.7	1.690	1.106	2.570	57.0	1.323
20R-2, 41–43	174.71	172.90	37.0	58.9	1.668	1.050	2.647	60.3	1.522
20R-3, 22–24	176.02	174.21	36.1	56.6	1.673	1.068	2.608	59.0	1.441
20R-4, 16–18	177.46	175.65	35.8	55.7	1.678	1.078	2.604	58.6	1.417
21R-1, 35–37	182.85	181.04	30.7	44.3	1.797	1.246	2.700	53.9	1.167
21R-2, 37–39	184.27	182.46	27.3	37.5	1.861	1.353	2.682	49.5	0.982
23R-1, 74–76	202.14	200.33	34.2	52.1	1.710	1.125	2.627	57.2	1.335
23R-2, 66–68	203.56	201.75	34.3	52.3	1.706	1.120	2.617	57.2	1.336
23R-3, 81–83	205.21	203.40	39.4	65.2	1.620	0.981	2.609	62.4	1.660
24R-1, 46–48	211.56	209.75	33.8	51.0	1.721	1.139	2.636	56.8	1.314
24R-2, 63–65	213.13	211.32	34.5	52.6	1.707	1.119	2.631	57.5	1.352
24R-3, 73–75	214.63	212.82	29.7	42.3	2.603	1.829	7.496	75.6	3.098
24R-4, 64–66	215.93	214.12	33.3	50.0	1.728	1.152	2.634	56.2	1.286
25R-1, 27–29	220.97	219.16	33.6	50.7	1.733	1.150	2.672	56.9	1.323
25R-2, 16–18	222.36	220.55	33.3	50.0	1.735	1.157	2.658	56.5	1.298
25R-3, 17–19	223.87	222.06	34.0	51.5	1.716	1.132	2.631	57.0	1.324
25R-4, 20–22	225.40	223.59	29.7	42.3	1.779	1.250	2.585	51.6	1.068
25R-5, 22–24	226.72	224.91	29.5	41.8	1.768	1.247	2.542	51.0	1.039
25R-6, 17–19	228.17	226.36	33.2	49.6	1.723	1.152	2.605	55.8	1.262
26R-1, 22–24	230.52	228.71	28.5	39.9	1.799	1.286	2.577	50.1	1.003
26R-2, 25–27	232.05	230.24	29.1	41.0	1.781	1.263	2.556	50.6	1.024
26R-3, 86–89	234.16	232.35	28.4	39.7	1.809	1.295	2.601	50.2	1.008
26R-4, 69–71	235.49	233.68	29.5	41.8	1.770	1.248	2.544	50.9	1.038
26R-5, 73–75	237.03	235.22	26.6	36.2	1.842	1.352	2.594	47.9	0.918
26R-7, 44–46	239.24	237.43	26.9	36.9	1.833	1.339	2.586	48.2	0.931
27R-1, 77–79	240.77	239.26	28.1	39.0	1.803	1.297	2.565	49.4	0.977
27R-2, 78–80	242.28	240.77	27.5	37.9	1.810	1.313	2.554	48.6	0.945
27R-3, 72–74	243.72	242.21	27.1	37.3	1.837	1.338	2.609	48.7	0.949
27R-4, 62–64	245.12	243.61	28.2	39.2	1.811	1.301	2.593	49.8	0.993
27R-5, 67–69	246.67	245.16	27.4	37.8	1.822	1.322	2.581	48.8	0.953
27R-6, 103–105	248.48	246.97	26.2	35.5	1.873	1.382	2.653	47.9	0.919
28R-1, 77–79	250.37	248.90	27.5	38.0	1.824	1.322	2.592	49.0	0.962
28R-2, 83–85	251.74	250.27	26.2	35.6	1.855	1.369	2.608	47.5	0.906
28R-3, 75–77	253.16	251.69	26.3	35.7	1.873	1.380	2.661	48.1	0.928
28R-4, 94–96	254.81	253.34	28.7	40.3	1.810	1.290	2.623	50.8	1.033
28R-5, 59–61	255.45	253.98	26.1	35.3	1.876	1.386	2.656	47.8	0.916
28R-6, 64–66	256.82	255.35	26.8	36.6	1.854	1.357	2.634	48.5	0.941
28R-7, 58–60	257.88	256.41	27.3	37.5	1.817	1.322	2.559	48.4	0.936
29R-1, 87–89	260.07	259.30	25.6	34.3	1.871	1.393	2.613	46.7	0.876
29R-2, 89–91	261.08	260.31	26.4	35.8	1.841	1.356	2.576	47.4	0.900
29R-3, 57–59	262.26	261.49	24.8	33.0	1.900	1.428	2.647	46.0	0.853
29R-4, 66–68	263.75	262.98	25.0	33.3	1.883	1.413	2.613	45.9	0.849
29R-5, 86–88	265.36	264.59	25.9	35.0	1.865	1.382	2.618	47.2	0.894
29R-6, 57–59	266.07	265.30	27.9	38.7	1.832	1.321	2.639	50.0	0.999
30R-1, 65–67	269.55	268.78	27.8	38.5	1.824	1.317	2.611	49.6	0.983
30R-2, 75–77	271.07	270.30	29.8	42.4	1.798	1.262	2.646	52.3	1.096
30R-3, 65–67	272.47	271.70	29.8	42.5	1.780	1.249	2.595	51.8	1.077
30R-4, 97–99	274.29	273.52	26.8	36.6	1.857	1.359	2.646	48.6	0.946
31R-1, 56–58	279.06	278.29	25.5	34.3	1.879	1.399	2.632	46.9	0.882
31R-2, 108–110	280.87	280.10	23.3	30.4	1.909	1.464	2.591	43.5	0.770
31R-3, 59–61	281.67	280.90	26.3	35.8	1.829	1.347	2.544	47.0	0.888
31R-4, 65–67	283.23	282.46	21.9	28.1	1.935	1.511	2.580	41.4	0.708
31R-5, 92–94	285.00	284.23	20.2	25.4	1.940	1.548	2.510	38.3	0.622

Table T20 (continued).

Core, section, interval (cm)	Depth (mbsf)	Depth (mcd)	Water content (%) Wet	Water content (%) Dry	Density (g/cm³) Bulk	Density (g/cm³) Dry	Density (g/cm³) Grain	Porosity (%)	Void ratio
31R-6, 67–69	286.25	285.48	21.0	26.5	1.975	1.561	2.619	40.4	0.678
32R-1, 69–71	288.89	288.12	26.6	36.2	1.828	1.343	2.552	47.4	0.901
32R-2, 85–87	290.55	289.78	22.8	29.5	1.912	1.477	2.568	42.5	0.739
33R-1, 59–61	298.39	297.62	19.3	23.9	2.020	1.630	2.633	38.1	0.615
33R-2, 70–72	300.00	299.23	22.7	29.4	1.923	1.486	2.591	42.6	0.743
33R-3, 80–82	301.56	300.79	18.6	22.9	2.012	1.637	2.580	36.5	0.576
33R-4, 61–63	302.87	302.10	22.5	29.0	1.934	1.499	2.607	42.5	0.739
33R-5, 84–86	304.60	303.83	25.7	34.5	1.888	1.404	2.665	47.3	0.899
33R-6, 77–79	306.03	305.26	24.7	32.8	1.897	1.428	2.635	45.8	0.845
34R-1, 69–71	308.09	307.01	21.5	27.5	1.965	1.542	2.628	41.3	0.705
34R-2, 83–85	309.73	308.65	24.3	32.2	1.899	1.437	2.619	45.1	0.822
34R-3, 68–70	311.08	310.00	25.0	33.3	1.886	1.415	2.621	46.0	0.852
34R-4, 86–88	312.76	311.68	21.8	28.0	1.967	1.537	2.649	42.0	0.723
34R-5, 80–82	314.20	313.12	19.1	23.6	2.048	1.657	2.680	38.2	0.618
34R-6, 90–92	315.80	314.72	19.7	24.6	2.046	1.643	2.711	39.4	0.650
35R-1, 77–79	317.87	316.79	24.9	33.1	1.891	1.421	2.627	45.9	0.849
35R-2, 74–76	319.34	318.26	18.7	23.0	2.033	1.652	2.628	37.1	0.591
35R-3, 74–76	320.84	319.76	20.8	26.2	2.001	1.585	2.668	40.6	0.683
35R-4, 84–86	322.44	321.36	20.6	25.9	2.008	1.595	2.674	40.4	0.677
35R-5, 77–79	323.87	322.79	18.9	23.2	2.066	1.676	2.706	38.1	0.614
37R-1, 23–25	336.63	336.88	17.1	20.6	2.114	1.752	2.709	35.3	0.546
37R-2, 26–28	338.16	338.41	16.9	20.4	2.115	1.757	2.702	35.0	0.537
37R-3, 20–22	339.60	339.85	18.6	22.9	2.098	1.707	2.760	38.2	0.617
37R-4, 65–67	341.55	341.80	17.1	20.6	2.136	1.772	2.751	35.6	0.553
37R-5, 56–58	342.96	343.21	18.7	22.9	2.109	1.716	2.786	38.4	0.624
37R-6, 13–15	344.03	344.28	21.2	26.9	2.003	1.578	2.696	41.5	0.709
38R-1, 68–70	346.68	347.42	24.7	32.7	1.915	1.443	2.678	46.1	0.856
38R-2, 33–35	347.83	348.57	13.8	16.0	2.208	1.904	2.710	29.7	0.423
38R-3, 74–76	349.74	350.48	19.9	24.8	2.035	1.631	2.693	39.5	0.652
38R-4, 84–86	351.34	352.08	26.0	35.2	1.882	1.392	2.669	47.9	0.918
38R-5, 21–23	352.21	352.95	18.0	22.0	2.096	1.718	2.721	36.9	0.584
39R-1, 24–26	355.84	356.58	16.1	19.1	2.156	1.810	2.733	33.8	0.511
39R-2, 68–70	357.78	358.52	25.5	34.3	1.935	1.441	2.785	48.2	0.932
39R-3, 15–17	358.75	359.49	23.3	30.4	1.948	1.494	2.684	44.3	0.796
39R-4, 79–81	360.89	361.63	17.8	21.7	2.125	1.746	2.770	37.0	0.587
39R-5, 21–23	361.81	362.55	18.1	22.0	2.076	1.701	2.684	36.6	0.578
39R-6, 64–66	363.74	364.48	21.8	27.9	1.961	1.533	2.633	41.8	0.718
40R-1, 17–19	365.47	368.13	25.8	34.7	1.883	1.398	2.658	47.4	0.901
40R-2, 21–23	367.01	369.67	14.5	17.0	2.175	1.859	2.689	30.9	0.447
40R-3, 23–25	368.53	371.19	15.7	18.6	2.161	1.823	2.722	33.0	0.493
40R-4, 16–18	369.96	372.62	24.9	33.1	1.879	1.412	2.597	45.6	0.839
41R-1, 17–19	375.07	377.73	20.6	25.9	2.034	1.615	2.732	40.9	0.691
41R-2, 30–32	376.70	379.36	24.0	31.6	1.907	1.449	2.622	44.7	0.809
41R-3, 15–17	378.05	380.71	22.9	29.6	1.908	1.472	2.564	42.6	0.742
41R-4, 22–24	379.62	382.28	27.0	37.0	1.809	1.321	2.523	47.7	0.911
207-1260B-									
1R-2, 59–61	42.29	42.29	52.8	112.0	1.414	0.667	2.468	73.0	2.700
2R-2, 136–138	52.56	51.89	38.0	61.3	1.659	1.029	2.677	61.6	1.602
2R-4, 118–120	55.38	54.71	39.3	64.6	1.636	0.994	2.665	62.7	1.682
3R-1, 138–140	60.78	59.28	42.8	74.9	1.578	0.902	2.656	66.0	1.944
3R-3, 53–55	62.43	60.93	42.3	73.2	1.579	0.912	2.616	65.2	1.870
4R-2, 61–63	66.51	65.34	44.7	80.9	1.549	0.856	2.647	67.6	2.091
4R-4, 8–10	68.98	67.81	38.0	61.2	1.669	1.035	2.714	61.8	1.621
5R-1, 70–72	74.50	73.97	40.6	68.4	1.622	0.963	2.704	64.4	1.807
5R-3, 69–71	77.49	76.96	43.6	77.4	1.558	0.878	2.614	66.4	1.976
6R-2, 86–88	81.16	79.98	44.3	79.5	1.577	0.879	2.761	68.2	2.143
6R-4, 3–5	83.33	82.15	40.0	66.8	1.619	0.971	2.644	63.3	1.724
7R-2, 146–148	91.36	90.39	43.0	75.5	1.583	0.902	2.691	66.5	1.984
7R-4, 118–120	94.08	93.11	44.7	80.8	1.571	0.869	2.762	68.5	2.179
8R-2, 106–108	100.56	98.58	47.1	89.0	1.503	0.795	2.575	69.1	2.238
8R-4, 93–95	103.43	101.45	45.9	84.8	1.505	0.815	2.502	67.4	2.071
9R-2, 41–43	109.51	107.85	46.7	87.7	1.511	0.805	2.594	69.0	2.221
9R-4, 20–22	112.30	110.64	45.5	83.6	1.514	0.825	2.522	67.3	2.059
10R-2, 128–130	119.96	117.80	41.6	71.4	1.601	0.934	2.676	65.1	1.865
10R-4, 9–11	121.77	119.61	40.9	69.2	1.613	0.953	2.678	64.4	1.809
11R-2, 70–72	129.10	126.54	36.4	57.2	1.638	1.042	2.493	58.2	1.392
11R-4, 70–72	132.10	129.54	34.3	52.1	1.649	1.084	2.417	55.2	1.230
11R-6, 70–72	135.10	132.54	41.6	71.3	1.578	0.921	2.570	64.2	1.790

Table T20 (continued).

Core, section, interval (cm)	Depth (mbsf)	Depth (mcd)	Water content (%) Wet	Water content (%) Dry	Density (g/cm³) Bulk	Density (g/cm³) Dry	Density (g/cm³) Grain	Porosity (%)	Void ratio
13R-2, 10–12	243.60	238.54	29.6	42.1	1.799	1.266	2.638	52.0	1.083
13R-4, 10–12	246.58	241.52	28.9	40.6	1.800	1.280	2.600	50.8	1.031
19R-1, 91–93	291.01	289.79	23.2	30.2	1.928	1.481	2.627	43.6	0.774
20R-2, 131–133	302.61	300.93	20.0	25.0	2.004	1.604	2.634	39.1	0.642
20R-4, 30–32	304.58	302.90	24.5	32.5	1.895	1.431	2.617	45.3	0.829
20R-6, 56–58	307.84	306.16	23.6	30.8	1.926	1.472	2.643	44.3	0.795
21R-2, 22–24	311.12	309.09	22.7	29.4	1.963	1.518	2.687	43.5	0.771
21R-6, 24–26	317.16	315.13	25.1	33.5	1.889	1.415	2.636	46.3	0.863
23R-1, 47–50	329.17	329.67	19.8	24.7	2.045	1.640	2.713	39.6	0.655
23R-5, 18–20	334.68	335.18	23.5	30.7	1.956	1.497	2.713	44.8	0.813
23R-7, 16–19	337.66	338.16	16.6	19.9	2.130	1.777	2.712	34.5	0.526
24R-2, 9–11	339.99	340.49	15.2	17.9	2.179	1.848	2.729	32.3	0.476
24R-4, 9–11	342.99	343.49	17.7	21.5	2.155	1.773	2.826	37.3	0.594
25R-3, 70–72	351.70	348.56	17.1	20.6	2.133	1.769	2.744	35.5	0.551
25R-5, 72–74	354.72	351.58	18.1	22.1	2.113	1.731	2.761	37.3	0.595
26R-3, 94–96	361.64	363.20	24.6	32.7	1.914	1.443	2.675	46.1	0.854
32R-1, 41–42	396.51	398.72	32.0	47.1	1.630	1.108	2.259	51.0	1.039
34R-6, 42–44	413.12	415.82	36.7	57.9	1.610	1.020	2.407	57.6	1.361
35R-2, 47–48	417.27	421.81	33.7	50.9	1.562	1.035	2.132	51.5	1.060
36R-3, 107–109	428.97	432.32	31.7	46.4	1.657	1.132	2.323	51.3	1.052
36R-6, 91–92	433.31	436.66	6.2	6.6	2.467	2.313	2.722	15.0	0.177
37R-5, 50–52	441.00	443.42	34.8	53.3	1.633	1.065	2.391	55.5	1.245
37R-6, 20–22	442.20	444.62	36.3	57.0	1.640	1.045	2.497	58.2	1.391
38R-1, 88–90	444.98	449.05	37.3	59.5	1.467	0.920	1.975	53.4	1.147
38R-1, 90–92	445.00	449.07	37.3	59.6	1.506	0.944	2.094	54.9	1.218
39R-1, 122–124	454.92	457.70	31.8	46.7	1.706	1.162	2.475	53.0	1.129
39R-3, 38–40	457.08	459.86	15.6	18.5	2.107	1.778	2.620	32.1	0.474
39R-4, 37–39	458.57	461.35	32.2	47.5	1.701	1.153	2.479	53.5	1.150
40R-2, 45–47	465.05	469.63	12.6	14.4	2.256	1.971	2.729	27.8	0.384
40R-6, 60–62	470.70	475.28	23.6	30.8	1.936	1.480	2.670	44.6	0.804
40R-CC, 15–17	470.90	475.48	23.1	30.0	1.938	1.491	2.648	43.7	0.776
41R-1, 94–96	473.64	477.80	29.3	41.4	1.722	1.218	2.398	49.2	0.969
41R-3, 90–92	476.60	480.76	23.9	31.3	1.961	1.493	2.749	45.7	0.841
41R-4, 24–26	477.44	481.60	30.5	44.0	1.691	1.175	2.371	50.5	1.019
41R-5, 42–44	479.06	483.22	5.0	5.3	2.497	2.372	2.701	12.2	0.139
42R-1, 90–92	483.20	485.88	18.3	22.4	2.031	1.660	2.605	36.3	0.570
42R-2, 65–67	484.23	486.91	14.7	17.3	2.211	1.885	2.766	31.8	0.467
42R-3, 26–28	485.23	487.91	17.1	20.6	2.108	1.747	2.697	35.2	0.543
43R-1, 83–85	488.73	491.41	17.4	21.1	2.106	1.738	2.711	35.9	0.560
43R-2, 90–92	490.30	492.98	15.1	17.8	2.171	1.843	2.713	32.1	0.472
44R-1, 100–102	492.90	495.58	17.3	21.0	2.093	1.730	2.679	35.4	0.548
45R-2, 74–76	498.74	501.42	16.5	19.8	2.125	1.774	2.701	34.3	0.523
46R-3, 58–60	505.08	507.76	14.3	16.7	2.170	1.860	2.670	30.4	0.436
46R-4, 50–52	506.50	509.18	14.4	16.8	2.187	1.872	2.704	30.8	0.444

Note: This table is also available in **ASCII.**

Table T21. Discrete measurements of *P*-wave velocity, Site 1260.

Core, section, interval (cm)	Depth (mbsf)	Depth (mcd)	Velocity (m/s) x	Velocity (m/s) y	Velocity (m/s) z
207-1260A-					
2R-1, 9.8	1.10	1.10	1489.3		
2R-1, 29	1.29	1.29	1526.5		
2R-1, 55	1.55	1.55	1523.6		
2R-1, 88.6	1.89	1.89	1533.6		
2R-1, 108.5	2.09	2.09	1595.6		
2R-1, 129.5	2.30	2.30	1595.1		
2R-2, 10.3	2.60	2.60	1589.4		
2R-2, 61	3.11	3.11	1615.8		
2R-2, 85	3.35	3.35	1664.2		
2R-2, 109.7	3.60	3.60	1596.1		
3R-1, 14.6	10.45	10.45	1623.3		
3R-1, 81.3	11.11	11.11	1647.9		
3R-1, 131.7	11.62	11.62	1667.5		
3R-2, 18.8	11.99	11.99	1765.1		
3R-2, 112.2	12.92	12.92	1680.5		
4R-1, 30.8	19.81	19.81	1811.4		
4R-1, 69.6	20.20	20.20	1719.7		
4R-1, 125	20.75	20.75	1637.0		
4R-2, 19.9	21.20	21.20	1626.2		
4R-3, 25.2	22.75	22.75	1641.0		
4R-3, 60.7	23.11	23.11	1714.4		
4R-3, 117.3	23.67	23.67	1734.8		
4R-4, 24.5	24.25	24.25	1694.1		
4R-4, 76	24.76	24.76	1743.0		
4R-4, 128.3	25.28	25.28	1759.1		
4R-5, 25.1	25.75	25.75	1747.7		
4R-5, 76.7	26.27	26.27	1733.5		
4R-5, 127.5	26.77	26.77	1770.5		
5R-1, 32	29.12	29.12	1835.0		
5R-1, 92	29.72	29.72	1807.0		
5R-1, 129.9	30.10	30.10	1792.2		
5R-2, 35.3	30.65	30.65	1826.1		
5R-2, 79.1	31.09	31.09	1787.3		
5R-2, 133.5	31.64	31.64	1864.2		
5R-3, 29.7	32.10	32.10	1791.3		
5R-3, 84.7	32.65	32.65	1824.8		
5R-3, 130	33.10	33.10	1833.0		
5R-4, 30	33.60	33.60	1776.2		
5R-4, 87.3	34.17	34.17	1910.9		
5R-4, 119.9	34.50	34.50	1818.3		
5R-5, 24.5	35.04	35.04	1887.8		
5R-5, 77.1	35.57	35.57	1818.0		
5R-5, 99.6	35.80	35.80	1749.8		
6R-1, 24.7	38.45	38.45	1553.6		
6R-1, 69	38.89	38.89	1552.7		
6R-1, 125.7	39.46	39.46	1559.6		
6R-2, 12.5	39.83	39.83	1550.3		
6R-2, 54.8	40.25	40.25	1542.3		
6R-2, 99.8	40.70	40.70	1538.8		
6R-2, 125.8	40.96	40.96	1566.2		
6R-2, 143.6	41.14	41.14	1526.1		
6R-3, 15.1	41.35	41.35	1525.1		
6R-3, 56.8	41.77	41.77	1530.6		
6R-3, 92.7	42.13	42.13	1567.5		
6R-3, 139.3	42.59	42.59	1541.2		
6R-4, 15.7	42.86	42.86	1560.6		
6R-4, 48.5	43.19	43.19	1578.4		
6R-4, 102.7	43.73	43.73	1529.1		
6R-4, 136.2	44.06	44.06	1567.0		
6R-5, 19.6	44.40	44.40	1599.6		
6R-5, 60.7	44.81	44.81	1600.0		
6R-6, 33.1	45.53	45.53	1596.3		
7R-1, 37.6	47.88	47.98	1586.5		
7R-1, 124.4	48.74	48.84	1582.7		
7R-2, 23.4	49.23	49.33	1623.0		
7R-2, 77.6	49.78	49.88	1592.2		
7R-2, 130.4	50.30	50.40	1569.0		
7R-3, 30.5	50.81	50.90	1611.4		
7R-3, 90.8	51.41	51.51	1591.5		
7R-3, 135.4	51.85	51.95	1618.4		
7R-4, 28.4	52.28	52.38	1723.1		
7R-4, 86	52.86	52.96	1596.7		
7R-4, 136.7	53.37	53.47	1559.3		
7R-5, 25.7	53.76	53.86	1579.6		
7R-5, 86.5	54.37	54.47	1573.5		
7R-5, 131.1	54.81	54.91	1603.7		
7R-6, 29.7	55.30	55.40	1592.2		
7R-6, 57.8	55.58	55.68	1596.9		
7R-6, 96.9	55.97	56.07	1591.6		
8R-1, 31.2	57.51	57.61	1588.6		
8R-1, 74.2	57.94	58.04	1607.9		
8R-1, 120.9	58.41	58.51	1590.9		
8R-2, 26.2	58.96	59.06	1615.7		
8R-2, 77.6	59.48	59.58	1616.7		
8R-2, 131.3	60.01	60.11	1594.0		
8R-3, 31.6	60.52	60.62	1634.8		
8R-3, 77.4	60.97	61.07	1593.6		
8R-3, 131.4	61.51	61.61	1583.3		
8R-4, 21.1	61.91	62.01	1596.2		
8R-4, 82	62.52	62.62	1599.2		
8R-4, 127.5	62.97	63.08	1611.1		
8R-5, 15.7	63.36	63.46	1603.9		
8R-5, 19.5	63.40	63.49	1619.4		
8R-5, 53.1	63.73	63.83	1590.1		
8R-5, 61.5	63.81	63.92	1602.8		
8R-5, 92	64.12	64.22	1612.8		
8R-5, 119.3	64.39	64.49	1569.0		
9R-1, 37.3	67.27	66.27	1589.4		
9R-1, 80.1	67.70	66.70	1563.6		
9R-1, 125.2	68.15	67.15	1611.8		
9R-2, 13.3	68.53	67.53	1592.1		
9R-2, 67.3	69.07	68.07	1590.2		
9R-2, 117.2	69.57	68.57	1587.3		
9R-3, 11.1	70.01	69.01	1606.4		
9R-3, 47.3	70.37	69.37	1590.3		
9R-3, 92.2	70.82	69.82	1615.2		
9R-3, 121.4	71.11	70.11	1593.9		
9R-4, 18.5	71.58	70.58	1559.1		
9R-4, 50	71.90	70.90	1630.4		
9R-4, 89.6	72.30	71.30	1597.0		
9R-4, 131.4	72.71	71.71	1574.3		
9R-5, 17.9	73.08	72.08	1620.5		
9R-5, 54.3	73.44	72.44	1609.8		
9R-5, 88.4	73.78	72.78	1576.1		
9R-5, 115.9	74.06	73.06	1577.5		
9R-6, 16.1	74.56	73.56	1613.8		
9R-6, 54.4	74.94	73.94	1647.6		
9R-6, 93.2	75.33	74.33	1620.7		
9R-6, 124.4	75.64	74.64	1562.2		
9R-7, 17.5	76.07	75.07	1543.5		
9R-7, 53.4	76.43	75.43	1564.6		
10R-1, 19.6	76.80	75.90	1615.6		
10R-1, 48.9	77.09	76.19	1614.7		
10R-1, 80.7	77.41	76.51	1608.1		
10R-1, 130.4	77.90	77.00	1599.2		
10R-2, 20.9	78.31	77.41	1620.9		
10R-2, 58.4	78.68	77.78	1618.4		
10R-2, 97.5	79.07	78.18	1593.5		
10R-2, 136.9	79.47	78.57	1611.3		

Notes: Multiple axis measurements were performed on 2-cm^3 samples. X-direction is perpendicular to the surface of a split core, y-direction is parallel to the surface of a split core, and z-direction is perpendicular to the top of the core. Only a portion of this table appears here. The complete table is available in **ASCII.**

Table T22. Checkshot survey data, Site 1260.

Checkshot station	Depth (mbrf)	Depth (mbsf)	Traveltime (s one way)	Traveltime (sbsf 2 way)	Interval time (s)	RMS velocity (m/s)	Interval velocity (m/s)
1	2553.0	0.0	1.699		1.699	1495.0	1495.0
2	2660.0	107.0	1.765	0.132	0.066	1499.6	1612.7
3	2690.0	137.0	1.783	0.168	0.018	1501.2	1654.2
4	2720.0	167.0	1.798	0.199	0.015	1505.1	1897.6
5	2749.0	196.0	1.814	0.230	0.015	1508.3	1848.1
6	2797.0	244.0	1.837	0.276	0.023	1515.6	2008.2
7	2827.0	274.0	1.853	0.308	0.016	1518.8	1855.1
8	2857.0	304.0	1.869	0.340	0.016	1521.6	1812.4
9	2887.0	334.0	1.885	0.372	0.016	1524.7	1850.4
10	2917.0	364.0	1.896	0.395	0.012	1531.1	2346.8
11	2947.0	394.0	1.911	0.425	0.015	1534.8	1950.0
12	2977.0	424.0	1.928	0.458	0.017	1537.2	1791.4
13	3007.0	454.0	1.943	0.488	0.015	1541.1	1989.0
14	3037.0	484.0	1.958	0.518	0.015	1544.3	1904.4
15	3067.0	514.0	1.970	0.543	0.012	1549.8	2267.4

Note: sbsf = seconds below seafloor. RMS = root mean square. Rig floor (including Kelly Bushing) to sea level = 11.5 m. Auger depth = 2 mbsl.